12-9-2011

Studies on Hexahapto-Dibenzo[A,E]Cyclooctatetraene Complexes of Chromiumtricarbonyl and Cationic Manganesetricarbonyl

Nilantha Bandara

STUDIES ON HEXAHAPTO-DIBENZO[*a*,*e*]CYCLOOCTATETRAENE COMPLEXES OF CHROMIUMTRICARBONYL AND CATIONIC MANGANESETRICARBONYL

By

Nilantha Bandara

A Dissertation
Submitted to the Faculty of
Mississippi State University
in Partial Fulfillment of the Requirements
for the Degree of Doctor of Philosophy
in Chemistry
in the Department of Chemistry

Mississippi State, Mississippi

December 2011

STUDIES ON HEXAHAPTO-DIBENZO[*a*,*e*]CYCLOOCTATETRAENE

COMPLEXES OF CHROMIUMTRICARBONYL AND

CATIONIC MANGANESETRICARBONYL

By

Nilantha Bandara

Approved:

William P. Henry Associate Professor of Chemistry (Director of Dissertation)	Steven R. Gwaltney Associate Professor of Chemistry (Committee Member)
David O. Wipf Professor of Chemistry (Committee Member)	Andrzej Sygula Professor of Chemistry (Committee Member)
Stephen C. Foster Associate Professor of Chemistry (Graduate Coordinator and Committee Member)	Gary Myers Professor Dean, College of Arts & Sciences

Name: Nilantha Bandara

Date of Degree: December 9, 2011

Institution: Mississippi State University

Major Field: Chemistry

Major Professor: Dr. William P. Henry

Title of Study: STUDIES ON HEXAHAPTO-DIBENZO[*a*,*e*]CYCLOOCTATETRA-ENE COMPLEXES OF CHROMIUMTRICARBONYL AND CATIONIC MANGANESETRICARBONYL

Pages in Study: 195

Candidate for Degree of Doctor of Philosophy

Mono- and dinuclear chromiumtricarbonyl and manganesetricarbonyl complexes of dibenzo[*a*,*e*]cyclooctatetraene (DBCOT) were synthesized and characterized. In the bis(chromiumtricarbonyl)DBCOT synthesis, the main product was the *syn*,*anti* isomer where the two $Cr(CO)_3$ moieties coordinate to opposite faces of the DBCOT backbone. This complex exhibits three dynamic processes in solution. A ring inversion of the organic skeleton occurs while the two chromiumtricarbonyl moieties undergo tripod rotation.

This is the first study where eight-membered ring inversion is studied for a pi-coordinated metallic system. The rate of inversion at various temperatures was determined by ^{1}H NMR line shape analysis at two different field strengths (300 and 600 MHz). Compared with other cyclooctatetraene compounds reported, there is a large positive entropy of activation and a relatively high enthalpy of activation in this system. DFT calculations, using the B3LYP/6-31G** basis set, were performed to gain a better understanding of the experimental results. It is proposed that free rotation of both

$Cr(CO)_3$ groups in the planar transition state are responsible for the large entropy of activation for ring inversion in hexahapto,hexahapto-dibenzo[*a*,*e*]cyclooctatetraene-*syn*,*anti*-bis(tricarbonylchromium). The relatively large enthalpy of activation is due to a stabilizing interaction between the *endo* carbonyl groups on the *syn*-$Cr(CO)_3$ and the remote arene.

In the monometallic DBCOT complexes, the metal can either be inside or outside the tub conformation. Interestingly, the crystal structures show opposite orientations for the isoelectronic chromium and manganese systems. The $Cr(CO)_3$ group is positioned *anti* relative to the DBCOT backbone while the $Mn(CO)_3^+$ is *syn*. It should be noted that the optimized gas phase geometries obtained through DFT calculations agree with the crystallographic results. Electrochemical studies were performed to investigate the change in redox behavior associated with coordination of mono and bis-chromium units to the DBCOT backbone.

Four new organometallic crystal structures are reported in this dissertation. Different tripod orientations, DBCOT backbone angles, and metal orientation relative to the interior of the organic skeleton are found. C-H…O, C-H…pi, and charge assisted C-H…F hydrogen bonding interactions were observed in the solid state packing. The structural motifs found suggest these complexes could serve as organometallic synthons in supramolecular chemistry.

Keywords: Dibenzocyclooctatetraene, ring inversion, arenechromiumtricarbonyl, arenemanganesetricarbonyl, dynamic NMR, theoretical calculations, DFT, crystal structure, organometallic synthesis

DEDICATION

This research is dedicated to my family: to my loving wife Indika and precious son Hesara, to my parents, Silmon and Kamala, and to my brothers Gaya, Kapila, Chula, Nalaka and sister Devika Bandara.

ACKNOWLEDGEMENTS

I wish to express my sincere appreciation to all who dedicated their time and support for the success of this dissertation. My utmost gratitude goes to Dr. William P. Henry, for granting the opportunity to do research under his direction and for his continuing guidance, support and encouragement throughout the work. I would like to thank my committee members, Dr. Stephen C. Foster, Dr. Steven R. Gwaltney, Dr. Andrzej Sygula, and Dr. David O. Wipf for their support, guidance and feedback. I also thank all the lecturers and staff members in the Department of Chemistry for their kindness and encouragement. Special thanks must go to Dr. Steven R. Gwaltney and Dr. Debbie J. Beard for the research collaborations on this project. The GAANN scholarship from the US Department of Education and the teaching assistantship from Department of Chemistry are greatly appreciated.

I would like to remember my late father, where I know he would be the proudest person in the whole world if he was to witness my success. Whole hearted thanks go to my mother for her unconditional love and faith shown me throughout my life. Education was the number one priority in my family. I greatly appreciate my elder brothers and sister for pointing me towards the right direction. I thank my loving wife for the devotion and encouragement given to me. I would also like to thank my little bundle of joy for fulfilling our lives with happiness.

I like to thank all my friends who have supported me intellectually and emotionally throughout my student life. Special thanks go to Bryan, David, Jehan, Nuwan, Samantha, Shamitha, and Whitnee for their comments and contributions towards the success of this dissertation. All my former teachers are remembered at this point with the highest respect. Mrs. Kannangara and Mr. Sirisena, thanks for introducing me to the world of science and the inspiration provided. Finally, I would like to thank my alma mater Royal College, Colombo and the Free Education System of Sri Lanka for providing the best academic foundation.

TABLE OF CONTENTS

LIST OF TABLES

LIST OF FIGURES

LIST OF SCHEMES

LIST OF ABBREVIATIONS

$\Delta G^{\ddagger}$	Free energy of activation
$\Delta H^{\ddagger}$	Free energy of enthalpy
$\Delta S^{\ddagger}$	Free energy of entropy
Δv	Frequency difference
ATR	Attenuated total reflectance
BCOT	Benzo[*a*,*e*]cyclooctatetraene
BS	Bond shift
CCD	Charge couple device
COSY	Correlation spectroscopy
COT	Cyclooctatetraene
CV	Cyclic voltammetry
DBCOD	5,6,11,12-Tetrahydrodibenzo[*a*,*e*]cyclooctadiene
DBCOT	Dibenzo[*a*,*e*]cyclooctatetraene
DFT	Density functional theory
DMA	*N*,*N*-Dimethylacetamide
DMF	*N*,*N*-Dimethylformamide
E_a	Activation energy
h	Planck constant

HMBC	Heteronuclear multiple-bond correlation
HMQC	Heteronuclear multiple-quantum correlation
IR	Infrared spectroscopy
k	Rate constant
k_B	Boltzmann constant
MTT	Manganese tricarbonyl transfer
NBS	*N*-Bromosuccinimide
NMR	Nuclear magnetic resonance
PC	Propylene carbonate
R	Universal gas constant
RB flask	Round bottom flask
RI	Ring inversion
TBAHFP	Tetrabutylammonium hexafluorophosphate
TBAP	Tetrabutylammonium perchlorate
T_c	Coalescence temperature
TEAP	Tetraethylammonium perchlorate
THF	Tetrahydrofuran
TLC	Thin layer chromatography
TMS	Tetramethylsilane
TS	Transition state
VI	Valence isomerization
VT	Variable temperature

XRD	X-ray diffraction
δ_A	Chemical shift
ν_A	Frequency of species A
τ_A	Lifetime of species A

CHAPTER I

INTRODUCTION

1.1 Introduction

This dissertation focuses on η^6 metalcarbonyl complexes of the ligand dibenzo[*a*,*e*]cyclooctatetraene (DBCOT, **1**) with particular attention to their dynamic behavior in solution. DBCOT is a cyclooctatetraene (COT) derivative with two fused benzene rings on opposite sides of the eight-membered COT (Figure 1.1).[1] The dynamic behavior of some derivatives of DBCOT and COT have been studied.[2-6] This work is the first attempt at studying the dynamics of an η^6 metal coordinated system, where a ring inversion of the eight-membered carbon skeleton occurs. The activation parameters for ring inversion and interesting organometallic compounds studied will be highlighted in the following chapters. A brief introduction on previous work providing the basis for the current study is presented in this chapter.

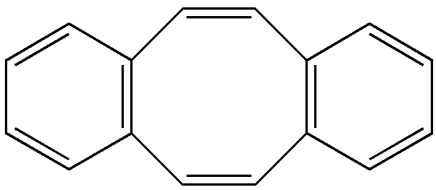

Figure 1.1 Dibenzo[*a*,*e*]cyclooctatetraene, **1**

1.2 Cyclooctatetraene (COT)

Many studies have concerned COT and its derivatives.[4-6] This compound has been the subject of much controversy due to its unique structure,[7-9] the question of aromaticity,[6, 10] its fluxional properties[4, 6, 11] and its use in metal coordination.[12-14] The synthesis, structure, reactivity, and dynamic behavior of COT will be discussed in this section.

1.2.1 Synthesis of COT

The first synthesis of 1,3,5,7-cyclooctatetraene (**2**) was reported by Richard Willstätter and coworkers in 1911.[10, 15] Starting with pseudo-pelletierine (**3**), an alkaloid extracted from the bark of the pomegranate tree,[16] Willstätter, Waser, and Heidelberger produced **2** in a multi-step process (Scheme 1.1).[17] Their synthetic route contained a series of Hoffmann elimination[18] steps to create alternating double bonds resulting in a poor overall yield.[19] Richard Willstätter's choice for the starting material was unique because it was only available as a natural product. He was the recipient of the 1915 Nobel Prize in chemistry because of his contributions to the field of plant pigments including chlorophyll.[20] Due to the difficulties in obtaining **3**, alternative routes were evaluated for the synthesis of **2** and its derivatives.[21-23] However, Willstätter's synthesis of **2** was the only successful attempt for several decades. Therefore, a controversy emerged concerning whether Willstätter and coworkers had actually made the product or whether they only obtained an isomer of COT (styrene).[24] Attempts to discredit Willstätter's synthesis was pointless as reduction of their compound produced cyclooctane (C_8H_{16}).[15] In 1947, using chemically-synthesized **3**,[25] Cope and Overberger were able to

successfully reproduce Willstätter's work and also isolate most of the intermediate products.[26]

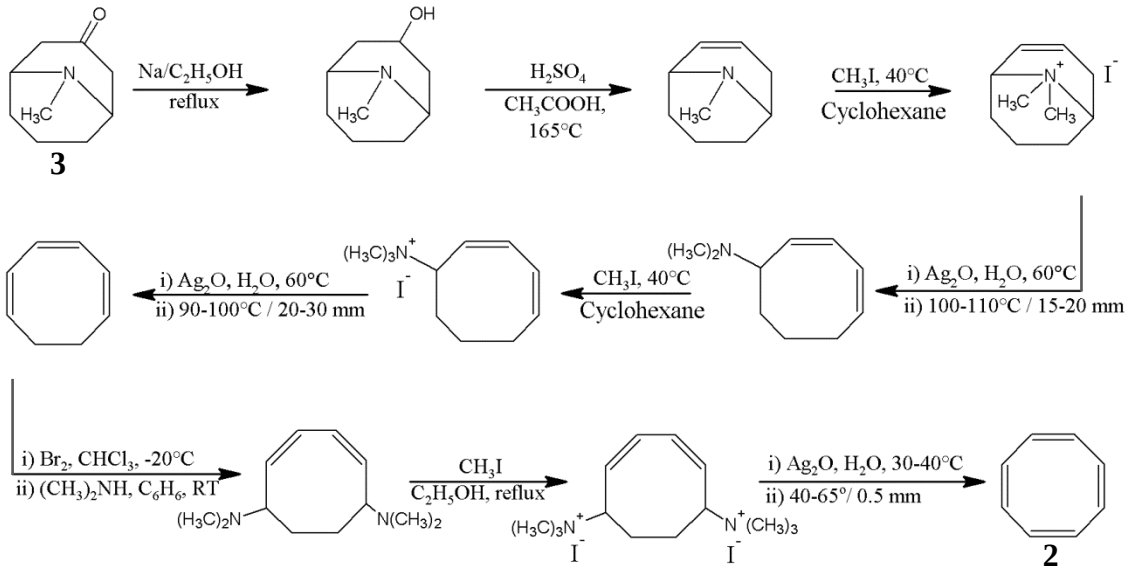

Scheme 1.1 Synthetic route for **2** starting with **3**[10, 15, 17, 26]

In 1948, Reppe *et al.* successfully achieved **2** in a single step (Scheme 1.2) with their patented method for oligomerization of acetylene (**4**).[27] This has become a useful method to generate COT in high yield due to the vast availability of **4**. As the commercial production of **2** increased based on Reppe's finding, research on COT became more popular.[6, 17]

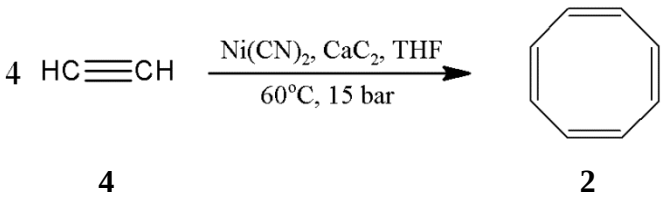

Scheme 1.2 Walter Reppe's synthesis of **2**[27]

1.2.2 Structure of COT

COT is the next annulene[28] ($C_{2m}H_{2m}$ where m = 2, 3, 4..) species found after benzene.[4, 29] Therefore, **2** is also named as [8]annulene.[6] Apart from the similarity in the chemical formula, COT and benzene do not fall into the same category regarding structure or properties. This led to COT being the subject of many investigations.[4, 6, 30]

Based on extensive studies with infrared (IR) spectroscopy,[31] Raman spectroscopy,[7] X-ray diffraction (XRD),[9, 32] and electron diffraction,[33, 34] the non-planarity in the ground state of **2** has been well established. However, according to the pioneering investigators, there was extensive debate about the correct structure (Figure 1.2). Early IR and Raman spectroscopic studies suggested that COT is in a crown conformation.[7, 35] Based on vibrational spectra, Lippincott and coworkers speculated that both COT and C_8D_8 favor the crown conformation (D_4) over the tub conformation (D_{2d}).[31] From electron diffraction, Bastiansen and Hassel reported that **2** could be categorized as "octa-benzene" where C-C bond distances are similar to benzene and the C-C-C angles are 120°.[8] The authors suggested a crown shaped carbon skeleton having equivalent C-C bond distances (D_{4d}).[8] In 1947, Kaufman was the first to report the structure of **2** in the tub conformation[9, 32] with C=C-C and C=C-H angles of 126.1° and 117.6°, respectively, using X-ray crystallography. However, Kaufman's structure was challenged by other researchers as their spectroscopic results supported a crown conformation.[33, 35, 36] Based on Raman and IR studies, Saksena and Narain supported a D_{4d} crown structure with all C-C bonds being equal.[36] Even as late as 1984, Dewar and Merz predicted that the chair conformation of COT was preferred using semi-empirical

calculation.[37] Later, Bastiansen and coworkers accepted that COT is in the tub conformation (D_{2d}) after a series of electron diffraction studies.[33, 38] Based on potential energy calculations, Pearson *et al.* also reported that COT favored the tub conformation.[39] Traetteberg used the sector electron diffraction method to determine the structure of COT conclusively in 1966.[34] The crystal structure of **2** at 129 K was reported by Claus and Krüger in 1988, where it was found in a tub conformation with alternating single and double bonds (1.47 Å and 1.33 Å).[40]

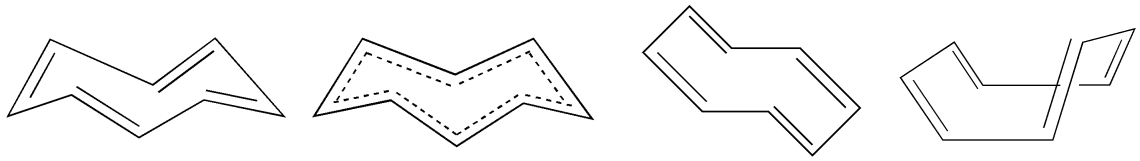

Figure 1.2 Structural possibilities for COT; (a) crown (D_4),[31, 35] (b) crown (D_{4d}),[8, 36] (c) chair (C_{2h}),[37] and (d) tub (D_{2d}).[32, 34, 40]

1.2.3 Aromaticity and reactivity of COT

Being the next higher vinylogue of benzene, the aromaticity of COT was an interesting research topic.[8, 41] With the introduction of the Hückel rule,[42, 43] methodology was developed to determine the aromaticity of cyclic compounds. Although **2** contains 8 π electrons (4n system, n = 2), it is a non-aromatic compound due to its non-planarity.[44, 45] COT is the smallest non-planar annulene.[4, 29]

Thomas J. Katz, was the first to study the reduction of **2**. COT is easily reduced in the presence of alkali metals to produce the planar dianion[46, 47] as well as the radical anion.[48] The planar COT dianion (D_{8h}) was observed as a monocyclic aromatic species

containing 10 π electrons. Conrow and Bak reported alkylation of the dianion to produce 1,2 and 1,4 COT derivatives.[49] Goldberg *et al.* reported the crystal structure of the first COT^{2-} complex as they were successful in crystallizing air-sensitive crystals of the potassium diglyme derivative.[50] A dication of COT also should be planar and aromatic. Unsubstituted COT^{2+} has not been reported yet. Olah *et al.* have reported several dication derivatives with all of them being planar aromatics.[51, 52] However, Nishinaga *et al.* reported that the tetrakis(bicyclo[2,2,2]octeno)cyclooctatetraene dication exists in the tub geometry due to the presence of bulky substituents attached to the COT ring.[53]

The X-ray crystal data for COT indicate that the dihedral angle between vicinal double bonds is 56^{o}.[40] Therefore, π bonds do not conjugate extensively in the ground state of **2** due to the poor overlap of neighboring *p* orbitals.[54] COT also shows a higher reactivity to electrophilic attack than arenes. These results indicate that the chemistry of **2** is much closer to that of alkenes than aromatic compounds.[41]

The COT structural skeleton is closely related to several noteworthy organic cyclic structures. Direct protonation of **2** results in the homoaromatic[55] homotropylium cation (**5**).[56, 57] Schröder synthesized bullvalene (**6**) in 1963 via the photolysis of COT.[58] Avram and coworkers reported a synthesis of an isomer of COT as a dimer of cyclobutadiene (**7**).[59] Zimmerman and coworkers reported that photochemical isomerization of barrelene[60] (**8**) produces **2** and semibullvalene.[61] Basketene (**9**)[62] is another interesting compound which can be obtained from **2**.[17]

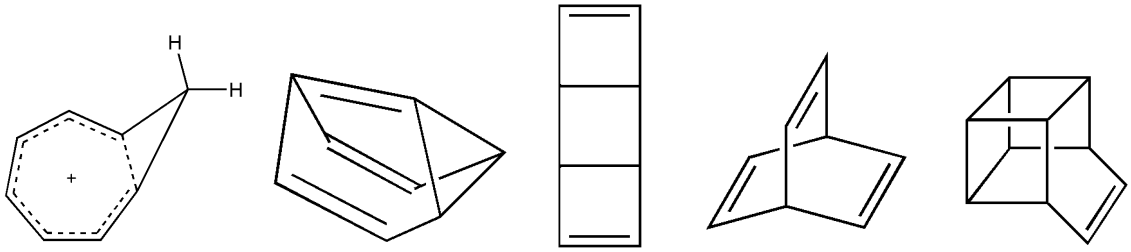

5 **6** **7** **8** **9**

Figure 1.3 Several interesting cyclic molecules which are closely related to the COT skeleton; **5**, **6**, **7**, **8** and **9**.

1.2.4 Dynamic behavior of COT

The ground state tub-shaped COT ring is capable of three important fundamental structural changes identified as ring inversion (RI), bond shift (BS), and valence isomerization (VI).[4-6, 11, 29, 63] The first two occur through a planar transition state (TS).[6, 17] There have been both experimental[4-6, 11] and theoretical studies[64] focused on these dynamic processes to estimate the barriers.

All protons in the COT ring are magnetically equivalent. Therefore, they give a single peak in the NMR spectrum (4.32 ppm),[17] and no further experimental information can be obtained by ^{1}H NMR regarding the dynamic behavior of the molecule.[4] Anet was a pioneer in attempting to overcome this problem with the use of ^{13}C satellite peaks[11, 65] and COT derivatives.[5] When a functional group is introduced on the COT ring, the hydrogen atom environments change, and they become distinguishable by NMR.[4, 6] Currently, this is the commonly accepted method for investigating RI and BS using different derivatives.[3, 66] Due to the nonplanarity of **2**, substituted derivatives can be chiral and, therefore, racemization can take place with the dynamic processes.[29]

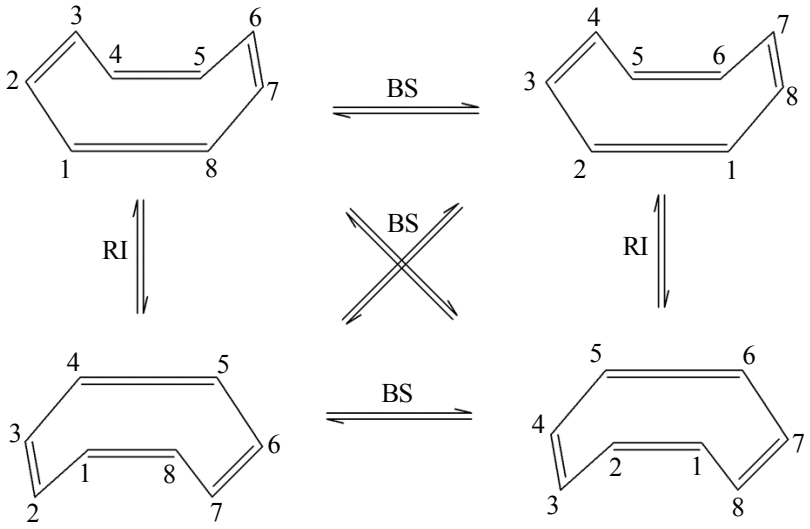

Scheme 1.3 Ring inversion (RI) and bond shift (BS) in **2**[4, 6]

Ring inversion occurs through a conformation mobility (rotation around single bonds).[4] It is also isodynamical [67] (reversible structural change where two structures are superimposable or become enantiomers).[4] The parent COT regenerates a similar conformation after the planar TS (D_{4h} symmetry, **2a**) with alternate single and double bonds.[29] The C=C-C bond angle changes from 126° to 135° and then back to 126°. It is important to note that although the transition state is planar (D_{4h}), due to the length difference of bonds, it remains non-aromatic.[17] The activation energy for COT ring inversion is in the range of 10-13 kcal mol^{-1}.[54, 68] Arguably, RI can be identified as the lowest energy pathway for the COT dynamic processes as only C-C single bond rotation is needed for the conformation change.[63] Mislow and Perlmutter reported the first isolation of an optically active COT derivative, a diacid (**1a**, Figure 1.4), where the barrier to inversion was found to be the highest recorded for a RI process in COT with 27 kcal mol^{-1}.[2]

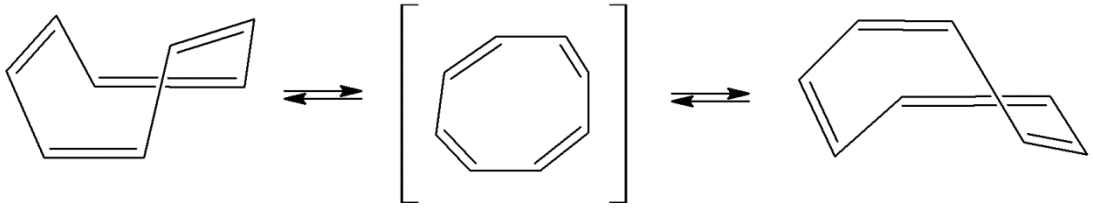

Scheme 1.4 Ring inversion of COT via **2a** (D_{4h} symmetry)[6]

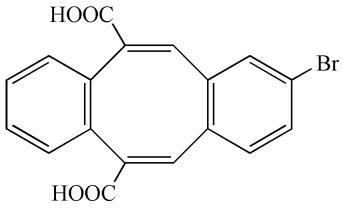

1a

Figure 1.4 The optically active COT derivative studied by Mislow[2, 3]

The bond shift process can be viewed as a migration of π electrons in the octagonal ring.[63] This process also occurs through a planar TS, but here the main difference from ring inversion is that all bonds become equal in the planar transition state (D_{8h} symmetry, **2b**).[6] Anet was the first to estimate an activation value (~13.7 kcal mol^{-1}) for this process.[11] As opposed to the TS in RI, here it was deemed as anti-aromatic due to delocalization of π bonds with all C-C bonds being equal. Therefore, bond shift requires a higher energy compared to ring inversion (1- 4 kcal mol^{-1} more).[4-6, 11, 17, 63] However, from their dynamic NMR study with nematic solvents, Luz and Meiboom claim a 10.9 kcal mol^{-1} barrier for COT BS.[64]

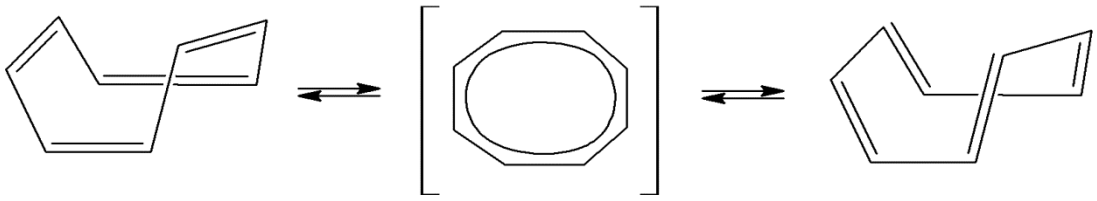

2b

Scheme 1.5 Bond shift of COT via **2b** (D_{8h} symmetry)[6]

The valence isomerization process occurring in **2** is not related to the bond shift or bond inversion, and it does not occur through a planar transition state.[6, 63] VI is the process where the eight-member ring changes into a bicyclic product (bicyclo[4.2.0]octa-2,4,7-triene, **2c**).[6, 69] **2c** is achieved through thermally allowed 6π disrotatory[70] electrocyclization.[17] Huisgen and Mietzsch reported that the **2** to **2c** activation barrier is much higher than for the RI and BS processes.[71] It was reported that at 100°C only 0.01% of **2c** was found in an equilibrium mixture.[69] Interestingly, **2c** shows more tendency towards Diels-Alder cycloaddition reactions than **2**.[29]

Alkyl substitution on the COT ring seems to increase the thermodynamic stability of the bicyclic tautomer.[29] Paquette and coworkers reported that the 1,2,3,4-tetramethyl COT derivative exhibits 25% isomeric tautomerization (**2d**) at RT.[72] Opposite to what is shown in Scheme 1.6, the fully methylated COT species is less stable than its bicyclic counterpart (**2e**).[29, 73]

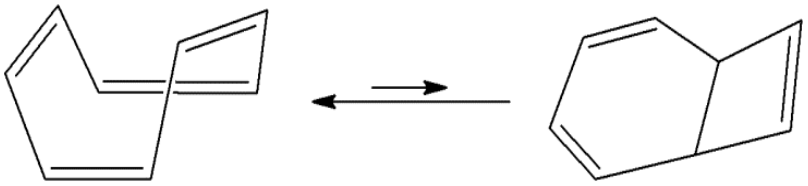

2 **2c**

Scheme 1.6 Valence isomerization in COT[6]

2d **2e**

Figure 1.5 Bicyclic tautomers of methyl substituted derivatives; **2d**[72] and **2e**[73]

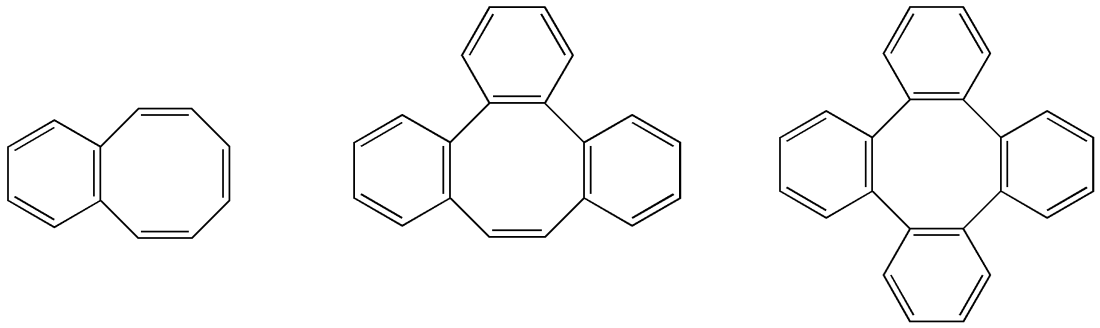

10 **11** **12**

Figure 1.6 Besides **1**, other fused benzo derivatives of COT; **10**,[74] **11**,[75] and **12**.[76]

1.3 Fused benzo derivatives of COT

Early researchers who attempted to synthesize COT believed that the fused derivatives of COT were more stable than **2**.[21-23] Therefore, synthesis of fused-ring derivatives was attempted before that of COT itself. Wawzonek[21] and Bachman[23] tried to synthesize the dibenzo derivative while Rapson[22] attempted making the benzo derivative (BCOT, **10**) of COT. Rapson and coworkers were the first to synthesize both the tribenzo (**11**) and tetrabenzo (*o*-tetraphenylene**, 12**) derivatives of COT.[75, 76] The dibenzo derivative of the COT is the main ligand in this study. Therefore, synthesis, structure and properties of DBCOT are discussed in the following sections.

1.3.1 Dibenzo[*a,e*]cyclooctatetraene

The introduction of the aromatic rings to the COT structure changes the chemistry of the overall molecule with the extension of conjugation. The two fused rings force the molecule to keep the carbon skeleton intact and therefore only ring inversion can occur in **1**. DBCOT became the ideal candidate for this work due to the above reasons and also because of its ability for η^6 coordination of two metals.

1.3.1.1 Synthesis of 1

The first successful synthesis of **1** was reported in 1946 by Fieser and Pechet from the reaction of *o*-phthaldehyde with *o*-phenylenediacetonitrile in the presence of sodium ethoxide.[77] In 1951, Cope and Fenton reported a synthetic route for **1** via 5,6,11,12-tetrahydrodibenzo[*a*,*e*]cyclooctadiene (DBCOD, **13**).[78] Cope *et al.* incorporated a specialized bromination agent, *N*-bromosuccinimide (NBS, **14**) to functionalize the

benzylic positions of saturated **13**, and achieved the unsaturated product through pyrolysis.

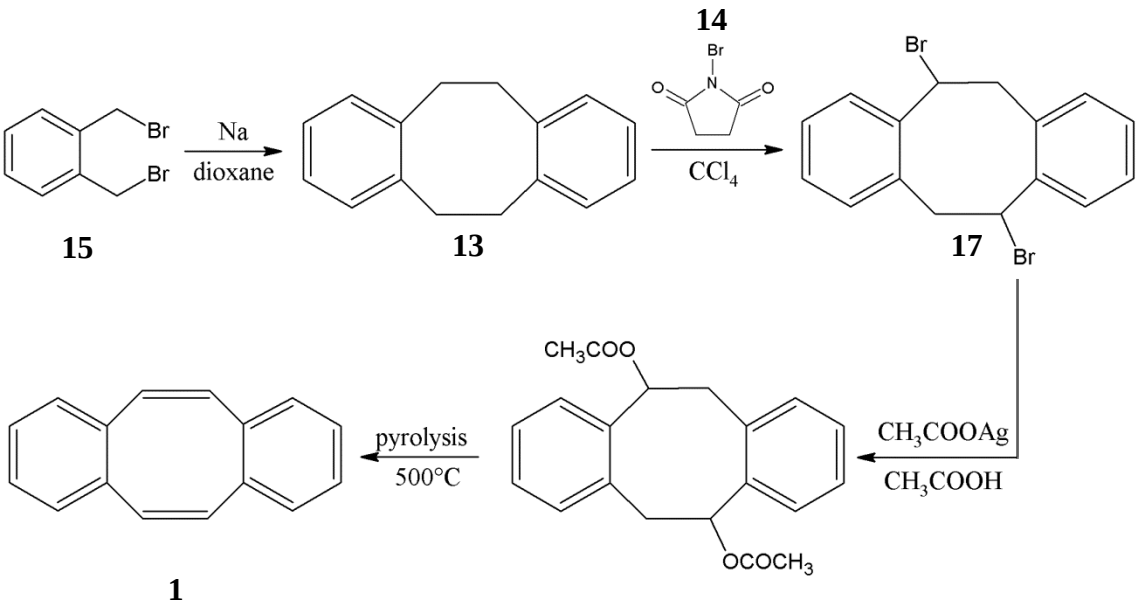

Scheme 1.7 Cope and Fenton's synthesis of DBCOT[78]

The chemistry of DBCOD was studied by Baker, Banks, Lyon, and Mann in 1945 where it was synthesized using the Wurtz reaction[18] starting with α,α′-dibromo-*o*-xylene (**15**) in the presence of sodium in dry dioxane.[79] Cope and Fenton improved the yield of **13** to 30 - 46%[78] compared to the 6% reported by Baker *et al.*[79] Boudjouk *et al.* reported the importance of the metal used in the coupling reaction of **15** and improved the yield of **13** to 80% using an ultrasonic-accelerated reaction with Li sand.[80] Domiano[81] and Stroddart[82] pointed out that the mechanism for the coupling reaction is a complex one and a series of cyclic and acyclic biproducts can be observed from the coupling reaction.

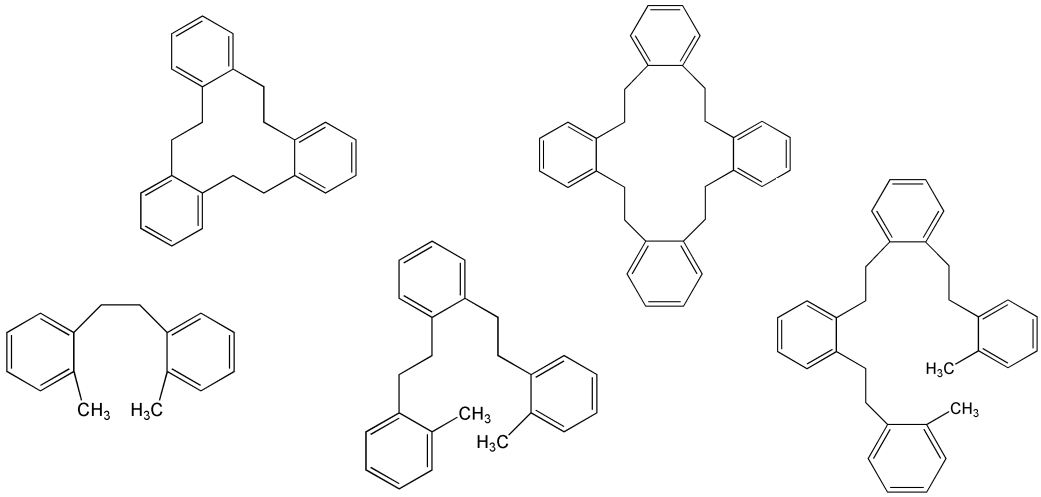

Figure 1.7 A few of the byproducts isolated from the coupling reaction of **15**[81]

Over the years, several other synthetic routes appeared in the literature which can produce **1**.[83-86] Wittig and coworkers[83, 87] and Griffin *et al.*[88] preferred the Wittig reaction.[18] Avram *et al.*[84, 89] and Nozaki *et al.*[90] obtained **1** through debromination. Oth and coworkers preferred a photochemical reaction with [16]annulene.[85] Rabideau *et al.* reported that **1** can be achieved by photoisomerization of dibenzobarrelene.[86] From their study of DBCOT, Griffin,[88] Nozaki,[90] and Rabideau[86] reported that the IR spectrum for **1** was not identical to the spectrum reported by Cope and coworkers. Later, Cutshall and Rabideau clarified this discrepancy[91] as it was pointed out that the synthesis routes were accurate but the IR spectra for **1** and another product (5-methylenedibenzo[*a,d*]cycloheptatriene, **16**) had been interchanged in back to back publications by Cope and Fenton in 1951.[78, 92]

During their synthesis of DBCOT, Cope *et al.* made an important observation in that 5,11-dibromo-5,6,11,12-tetrahydrodibenzo[*a,e*]cyclooctadiene (**17**) cannot be

directly converted to **1**.[78] It was reported that debromination of **17** would facilitate a rearrangement reaction (Cope rearrangement) producing **16** in the presence of a base.[78, 92] Dimethylamine, triethylamine, diethylaniline, 2-methylpyridine, 2,6-dimethylpyridine, and quinoline bases were tested by Cope and Fenton, and the highest yield of **16** was observed with 2-methylpyridine.[92] Therefore, Cope and Fenton opted to undergo an extra step to produce **1** through a diacetate derivative. In 2002, Chaffins, Brettreich, and Wuld modified the above synthesis, showing that **1** can be achieved with direct debromination of **17** in the presence of a stronger base, potassium *tert*-butoxide (**18**).[93] The synthesis route reported by Chaffins *et al.* is currently identified as one of the most economical and efficient ways of achieving **1**.[94]

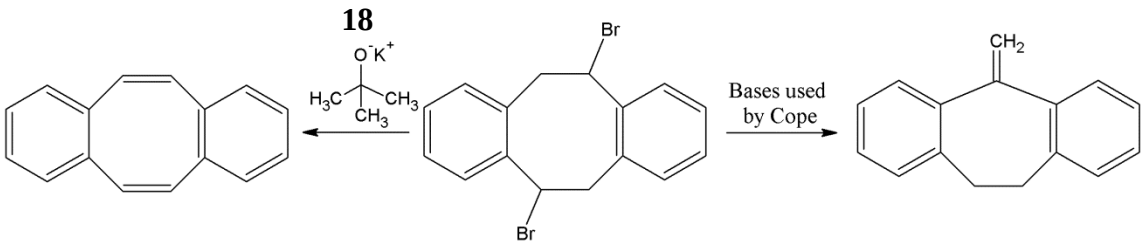

1 **17** **16**

Scheme 1.8 Attempted debromination of **17** and the resulting products[92, 93]

1.3.1.2 Structure and properties of 1

From the first synthesis of **1**, Fisher and Pechet predicted that DBCOT is non-planar and not capable of resonance stabilization.[77] These assertions were due to an interesting UV study where **1** and its derivatives were compared with ethylene, styrene and *cis*-stilbene derivatives (Figure 1.8). According to the authors, DBCOT derivatives showed only partial conjugation between aromatic rings. The crystal structures of **1** and

12 were reported in 1981, by Irngartinger and Reibel.[1] Similar to COT and most of its derivatives, **1** adopts a tub conformation (Figure 1.9).[1]

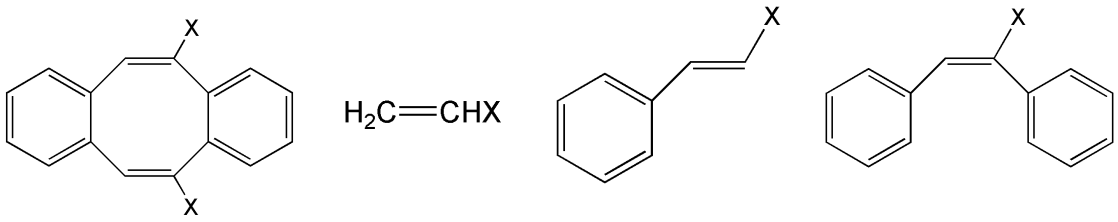

Figure 1.8 Compounds studied by UV-vis spectroscopy by Fisher and Pechet;[77] (a) **1**, (b) ethylene, (c) styrene, and (d) *cis*-stilbene; Where X = H, COOH, and CN.

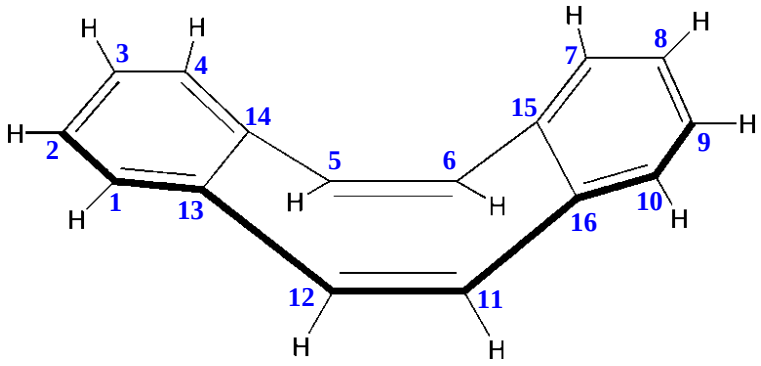

Figure 1.9 Structure of **1**[1]

In 1964, Stiles and Burchardt reported an interesting reaction of the DBCOT structural framework, where a 5,6-disubstituted derivative rearranged into a 5,11-isomer upon heating.[95] In 1978, Salisbury further investigated the kinetics of racemization with several 5,6- and 5,11-substituted DBCOT species.[96] As in COT, Katz and coworkers found that DBCOT is also much easier to reduce than unconjugated alkenes. Using alkali metals, both the DBCOT anion and dianion have been produced with both showing

planar geometry.[97] The DBCOT dication was obtained by Olah *et al.* in 1977 as a 16 carbon system with 14 π electrons in a planar aromatic system.[52] A helical version of DBCOT (5Z, 11E) has been reported recently by Carnes *et al.*[98]

1.3.1.3 Structure and properties of DBCOD

DBCOD is the saturated bridge analogue of **1**. DBCOD can also be considered as a dibenzo derivative of 1,5-cyclooctadiene (**19**). Interest in DBCOD was increased with the work of Cope and Fenton when they used it as an intermediate to synthesize **1**. From the initial work on **13,** Baker *et al.* reported that DBCOD adopts three different conformations, namely chair (C_{2h}, **13a**), boat (C_{2V}, **13b**), and twisted boat (D_2, **13c**).[79, 99] However, these conformations were reinvestigated by Allinger *et al.* and Jimeno *et al.*[100, 101] According to Jimeno *et al.* the four conformations identified for DBCOD were chair (C_{2h}), boat (C_{2V}), twisted boat (C_2, **13d**), and twist (D_2, similar to the twisted boat structure of Baker *et al.*) In the crystal lattice it was found to be in the chair conformation. The initial structural work was reported by Baker *et al.*,[79] and the structure was redetermined by Elguero and coworkers in 1992.[81]

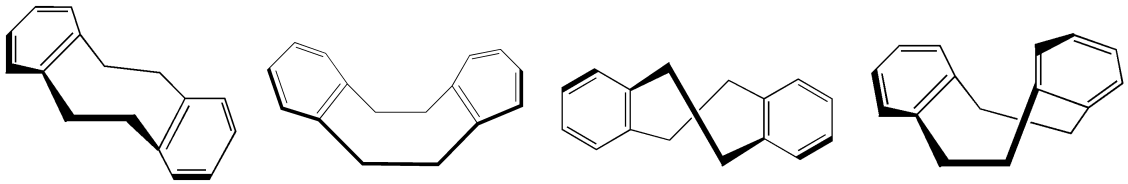

13a **13b** **13c** **13d**

Figure 1.10 Possible conformations of DBCOD; **13a**, **13b**, **13c**, and **13d**.[99, 100]

The dynamic behavior of **13** is much more complex than in derivatives of **1** or **2** as there are angular strains due to the C-C single bonds in an eight-membered ring. St-Jacques,[102, 103] Allinger,[100] and Jimeno[101] conducted investigations on inversion and twist processes occurring in **13**.[100, 101] Some of these processes occur very fast on the NMR time scale.[101]

1.3.2 Ring inversion studies of 1 and other benzo fused COT derivatives

The ring inversion of the dibenzo COT derivative was first reported by Mislow and Perlmutter in 1962 with a racemization study of **1a**.[2] The non-bonded interactions from carboxylic groups to the benzene hydrogen atoms in the transition state significantly contributes to the large value of $\Delta G^{\ddagger}$ (27 kcal mol^{-1}) observed for inversion barrier.[3] In 1971, Figeys and Dralants reported the lowest inversion barrier associated with a fused COT system, where 5.7 kcal mol^{-1} was given for a teraphenylene derivative (**12a**).[104] The authors rationalized this unusually small energy barrier with the postulate that benzene substitution decreases the anti-aromaticity in the predicted planar transition state.[104]

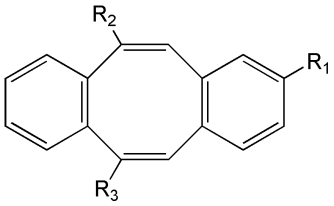

1a: R_1 = Br; R_2 = R_3 = COOH

1b: R_1 = CF_2; R_2 = R_3 = H

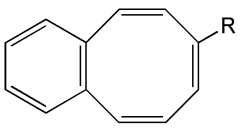

10a: R = $(CH_3)_2H$

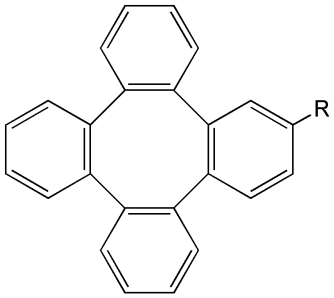

12a: R = $(CH_3)_2OH$

12b: R = $CH(OH)CH_3$

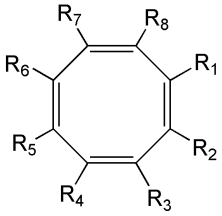

2f: R_1 = $(CH_3)_2H$; R_2-R_8 = H

2g: R_1 = $(CH_3)_2OH$; R_2-R_8 = D

2h: R_1- R_3 = $(CH_2)_8$; R_2=H, R_4-R_8 = H

2i: R_1 = OH; R_2-R_8 = H

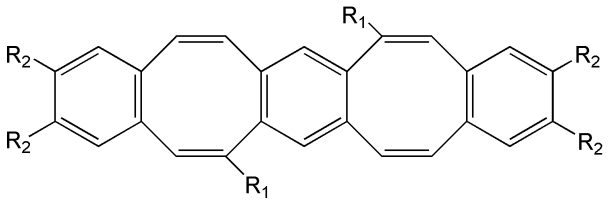

20a: R_1 = CN; R_2 = OCH_3

20b: R_1 = CN; R_2 = OC_2H_5

20c: R_1 = CHO; R_2 = OCH_3

20d: R_1 = CHO; R_2 = OC_2H_5

Figure 1.11 Some COT derivatives where RI was investigated

The low barrier to inversion reported by Figeys *et al.* was questioned by other researchers as there is a significantly larger steric factor involved with the closeness of α-hydrogen atoms in the adjacent benzene rings.[3, 105, 106] A year later, Mislow and coworkers reported 67 kcal mol^{-1} as the lower limit for the inversion barrier in **12b**.[3] A CNDO/2 calculation conducted by Allinger and coworkers predicted 222 kcal mol^{-1} as the inversion barrier for **12**.[105]

Mislow and coworkers reported a RI study of **1b** in 1972, where they found a 12.3 kcal mol^{-1} for $\Delta G^{\ddagger}$ at the coalescence temperature -5°C.[3] Buchanan reported the barriers

for **2f** and **10a** were 14.8 and 13.4 kcal mol^{-1} at coalescence temperatures of -25 and -30°C, respectively.[107] The activation energy for **2f** agrees with the earlier report concerning COT (**2g**) studied by Anet *et al.*[5] The latest RI study for the tetrabenzene derivative was conducted in 2009 by Huang *et al*.[106] Experimentally, the evidence for RI was not observed even at 600°C.[106] The energy barrier for **12** was calculated as 135 kcal mol^{-1} using the B3LYP/6-31G(d,p) basis set.[106]

In 2009, Bachrach reported relative energies for the ring inversion processes in **1**, **2**, **10**, **11**, and **12** systems using B3LYP/6-13G(d,p) and MP2/6-13G(d,p) calculations.[108] Interestingly, according to Bachrach, only **1** (D_{2h}), **2** (D_{4h}), and **10** (C_{2v}) have a planar TS in RI with barriers of 9.22, 10.55, and 9.06 kcal mol^{-1}, respectively. It was found that in **11** and **12**, the planar systems C_{2v} and D_{4h} contained more than one imaginary frequency. The lowest energies found in non-planar TS's were for **11** (C_2) and **12** (D_4), with values of 39.13 and 76.48 kcal mol^{-1}, respectively.[108]

Iyoda and coworkers reported the dynamics of molecular tweezer derivatives (**20a** - **20d**) containing DBCOT dimers.[109] These belt-like molecules undergo ring inversions due to the presence of a COT ring in the skeleton. The inversion barriers were found for each derivative (16.5, 16.5, 21.2, and 20.8 kcal mol^{-1}) and they have also reported the calculated values using planar transition states (14.1 kcal mol^{-1} for **12a**, **12b**; 20.1 kcal mol^{-1} for **12c**, **12d**).[109]

1.4 Organometallic chemistry

Since our main focus is to study metal carbonyl complexes of DBCOT, a brief introduction to organometallic chemistry is appropriate at this time. The first

organometallic compound was reported by Danish chemist William C. Zeise in 1827.[110-112] Zeise claimed his platinum compound contained a coordinated ethylene. Unfortunately, he was unable to convince the scientific community in that era. After three decades, Griess and Martius confirmed that Zeise's interpretation was correct. Even now, scientists generally call this product ($K[PtCl_3(C_2H_4)].H_2O$, **21**) Zeise's salt.[113, 114]

The term organometallic was coined by Sir Edward Frankland in 1852 when reporting his novel organozinc compounds.[115] These compounds were widely employed in organic synthesis until Victor Grignard discovered alkylmagnesium halide reagents (RMgX) in 1900.[116, 117] The first metal carbonyl complex $[PtCl_2(CO)_2]$ was reported by Schutzenberger in 1868.[112, 118] Alfred Werner revolutionized the field of coordination chemistry with his postulation of octahedral configuration.[117, 119, 120] He was awarded the 1913[121] Nobel prize in chemistry, and it was the first time an inorganic chemist won this prestigious title.

(a) (b)

Figure 1.12 Important discoveries in the history of organometallics; (a) Zeise's salt[113] and (b) ferrocene.[122, 123]

The first π-arene metal complexes were discovered by Franz Hein in 1919.[124] Hein was not able to describe his products because the concept of metal π-coordination

was unknown at that time.[125] The work of two independent research groups led to the discovery of ferrocene, a novel organo-iron compound,[126, 127] which signaled the origin of modern organometallic chemistry.[128] The concept of back-bonding in a metallic complex was also reported during this time by Orgel, Pauling, and Zeiss.[112] In 1952, in independent work, Wilkinson *et al.* and Fischer *et al.* corrected the structure of ferrocene (iron biscyclopentadienyl, **22**) to the well-known "sandwich" structure having π-back donation.[122, 123] Fischer and Wilkinson were awarded the 1973 Nobel prize for their contributions to the field of organometallic chemistry.[112, 129] After four decades, Zeiss and coworkers[130, 131] were able to confirm Hein's results based on the ferrocene research.[124, 125]

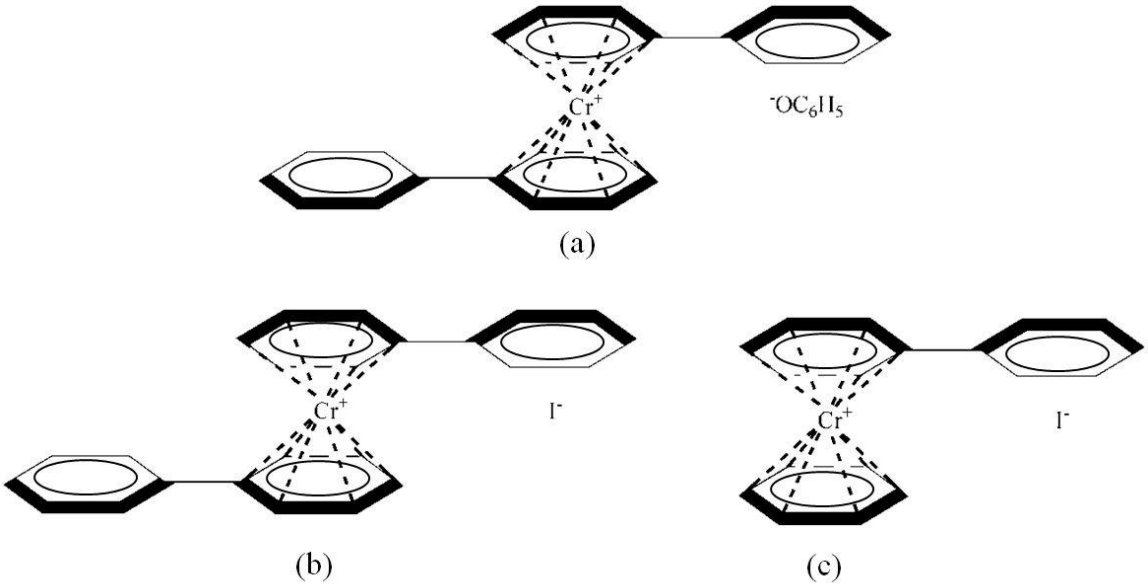

Figure 1.13 Hein's organometallic compounds; (a) pentaphenylchromium hydroxide, (b) teraphenylchromuim iodide, and (c) triphenylchromium iodide[131]

1.4.1 η^6-Arene chromium complexes

The first synthesis of η^6-bisbenzenechromium was reported by Fischer and coworkers in 1955.[132] This was achieved under drastic conditions using an autoclave reactor.[128] The crystal structure was reported the following year and confirmed this compound to be a "sandwich" structure.[133] In 1957, Fischer and coworkers used $(C_6H_6)_2Cr$ to prepare the "half sandwich" η^6-benzenetricarbonylchromium complex.[134] In $(C_6H_6)Cr(CO)_3$ (**23**), a d^6 chromium metal coordinates to the arene and the three carbonyl groups to achieve an 18 electron complex. Currently, these are generally known as "piano stool" complexes.[112] The synthesis of **23** was improved in 1958 by heating chromiumhexacarbonyl in the presence of benzene.[135, 136] The solvated $Cr(CO)_3$ species generated by reflux with a high boiling solvent was used as an intermediate in making **23**.[137] This method became the widely accepted synthetic route to produce arene chromium complexes. The arene exchange reaction is another popular method for making arene chromium complexes. A common example for this would be treating different organic ligands with the labile (naphthalene)$Cr(CO)_3$ (**24**) complex.[138] The first synthesis of **24** was reported by Fischer and coworkers in 1958, where they synthesized a series of novel chromium, molybdenum, and tungsten carbonyl complexes along with **24**.[139, 140]

1.4.1.1 Reactivity of arene chromium complexes

Upon chromiumtricarbonyl coordination, the chemistry of the aromatic ring is changed dramatically.[141] Unsaturated hydrocarbons tend to resist nucleophilic attack.[112] Generally, nucleophilic substitutions in aromatics are achieved only after functionalizing with an electron withdrawing group and adding a leaving group in a favorable position

(*ortho* or *para*) on the ring.[18] However, by coordinating electron deficient metal centers, which can act as electron withdrawing groups, benzene can be subjected to nucleophilic attack.[112, 114, 142] A nucleophilic attack on **23** would yield an η^5-cyclohexadienyltricarbonylchromium (**25**) species.[142-145] Semmelhack *et al.* were the first to isolate **25**.[143, 144] The stabilization associated with the η^5-cyclohexadienyl structure can also be used to further extend the conjugation when a benzylic hydrogen is present. The deprotonation of the benzylic position has been well utilized in organic synthesis to introduce electrophiles as in Scheme 1.10.[146, 147]

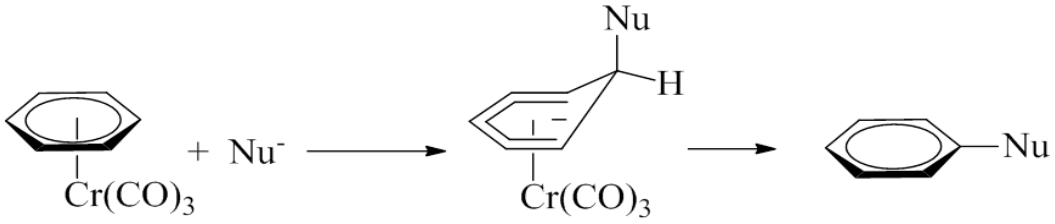

23 **25**

Scheme 1.9 Nucleophilic attack on unsubstituted benzene via η^5-cyclohexadienyltricarbonylchromium species[142]

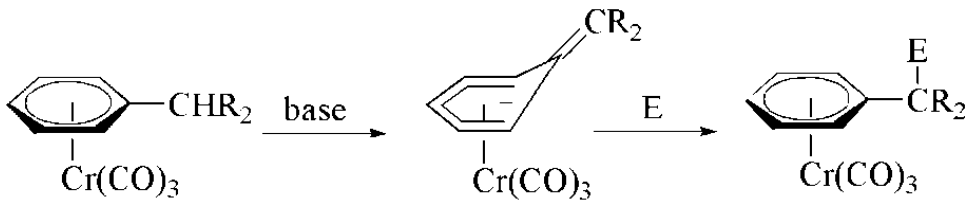

Scheme 1.10 Electrophilic attack on benzylic carbon via deprotonation.[146, 147]

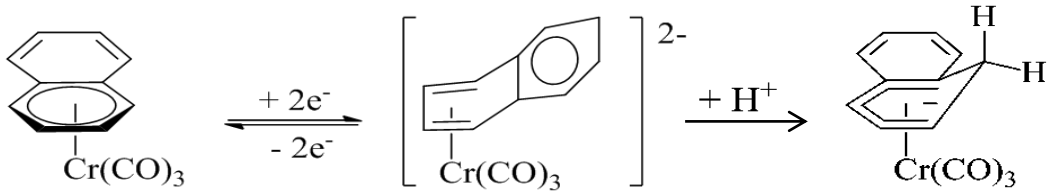

24 **26** **25a**

Scheme 1.11 Haptotropic rearrangement of **24**[148] to the η^4-dianion and the formation of a stable η^5-cyclohexadineyltricarbonylchromium species (**25a**) with the addition of a proton[149]

Metaltricarbonyl units can significantly affect the electrochemical properties of organic compounds.[141, 149-151] Benzene- and naphthalenechromiumtricarbonyl complexes are good examples of this behavior. The electrochemical studies reported by Henry and coworkers elaborated that **24** displays a considerable difference to **23** in reduction chemistry.[148, 149, 152] When **23** was reduced in a cyclic voltammogram (CV) experiment, the dianion indicated very little reoxidation. However, when **24** was reduced, a reversible two electron process was observed, showing that the dianion is stable.[148, 149, 152]

In **24**, six π electrons are localized in the ring coordinated to the chromium metal, and the naphthalene fragment is planar. The aromaticity varies in the two fused rings of naphthalene. The coordinated ring is fully aromatic, while the other ring resembles a diene. With reduction, the properties of the two rings are changed dramatically. The non-coordinated ring can acquire full aromaticity with 6 π electrons while chromium coordinated carbons changed to a butadiene system. This process is known as "haptotropic rearrangement".[148, 153] The η^4-naphthalenetricarbonylchromium dianion (**26**) was observed as a stable product and reaction with protons generated **25a**.[149]

1.4.1.2 Bimetallic chromium complexes

The earliest reports of bimetallic complexes involving transition metals were made in 1961 by Semenov *et al.*[154] Arene bimetallic complexes were first reported by Fischer and coworkers.[128] Rieke and coworkers conducted an interesting electrochemical analysis on a series of conjugated bimetallic chromium carbonyl complexes.[151, 155] Upon a two electron reduction, the dianions readily convert to stable η^5-cyclohexadineyltricarbonylchromium species.[155]

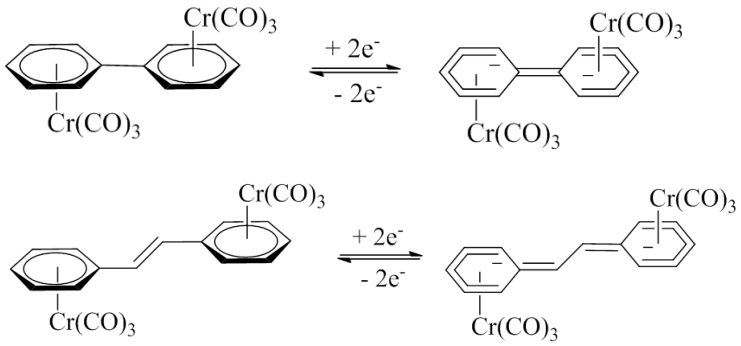

Scheme 1.12 Reduction of conjugated bimetallic $Cr(CO)_3$ complexes[155]

1.4.2 Manganese complexes

Manganese carbonyls were first discovered by Brimm *et al.* in 1954.[156] Wilson reported the synthesis of pentacarbonylmanganese complexes,[157] specifically $Mn(CO)_5Br$ (**27**), which played a vital role in arenemanganese synthesis. Fischer and Hafner proved that under reducing conditions, π aromatic compounds can be prepared in the presence of strong Lewis acids.[132] Later, this method was developed into a general route for the synthesis of Mn[158-161] and Fe[162] complexes.

Subsequently, two other methods were developed to prepare η^6-arenemanganese cations with a better yield.[161] The method introduced by Rybinskaya *et al.* dealt with drastic conditions where $Mn(CO)_5X$ (X = Cl, Br) were subjected to a strongly acidic medium to prepare $[Mn(CO)_5]^+$.[163] The synthetic route which produced $[Mn(CO)_5]^+$ in the presence of a silver(I) ion[164, 165] became the most popular method as it required relatively mild conditions.[161] The main advantage of the Ag(I) method is that, due to the less reactive conditions, partial hydrogenation of hydrocarbons does not occur. Therefore, this synthesis can be widely used in labile polyarene systems.

The first η^6-naphthalenetricarbonylmanganese complex (**28**) was reported by the Wilkinson group in 1961.[158] Sun *et al.* reported a series of well-characterized naphthalene complexes synthesized in the presence of $AgBF_4$ in dichloromethane.[166] Sun *et al.* developed an efficient method for making a range of new $(arene)Mn(CO)_3^+$ complexes using the high lability of naphthalene complexes.[166] These exchange reactions were termed the manganese tricarbonyl transfer (MTT) process. The $Mn(CO)_3^+$ moiety is transferred to a new arene ligand in solution at close to room temperature.[166, 167] The synthesis of a variety of bi- and polymetallic compounds which use the MTT method can be found.[168-172]

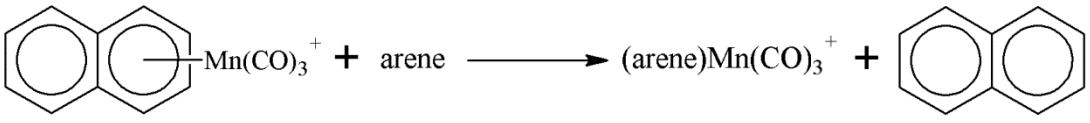

28

Scheme 1.13 MTT from naphthalene complex to another arene[166]

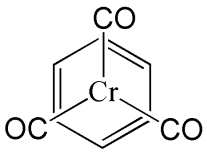

Eclipsed

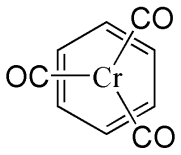

Staggered

Figure 1.14 Possible conformations of arene chromiumtricarbonyl complexes

1.4.3 Tripod orientations in metal carbonyl complexes

With the continuing growth of ML_3 type complexes, there was interest in establishing a set of guidelines to predict the tripod orientation with respect to the arene ring.[173, 174] When benzene is coordinated with $Cr(CO)_3$, two possibilities exist for the tricarbonyl orientation (Figure 1.14). In benzene- and hexamethylbenzenechromiumtricarbonyl complexes, a staggered orientation is preferred. For anisole derivatives an eclipsed orientation was observed.[175, 176] The major contributing factor for these tricarbonyl orientations are electronics in nature.[176, 177]

Metal complexes of the fused ring derivatives can be identified as an important subgroup in studying tricarbonyl orientations. It was noticed that the tricarbonyl orientations for 1,2-substituted arene complexes mainly fell into two eclipsed extremes: *exo* and *endo* conformations (Figure 1.14). In 1984, Rogers *et al.* established a theoretical strategy to predict conformational preferences for ML_3 groups in bicyclic polyene complexes.[173] The simplified version prediction is that whenever the second ring has 4n electrons, the *exo* conformation is favored and, when there are 4n+2 electrons in the noncoordinated ring, the *endo* conformation is favored. The π electrons that do not contribute to the coordination are counted in this system, and therefore, complex **24** is

considered a 4n system with only four electrons in the neighboring ring. Rogers' prediction method has been widely accepted as a generalized method for predicting metalcarbonyl orientations.[74]

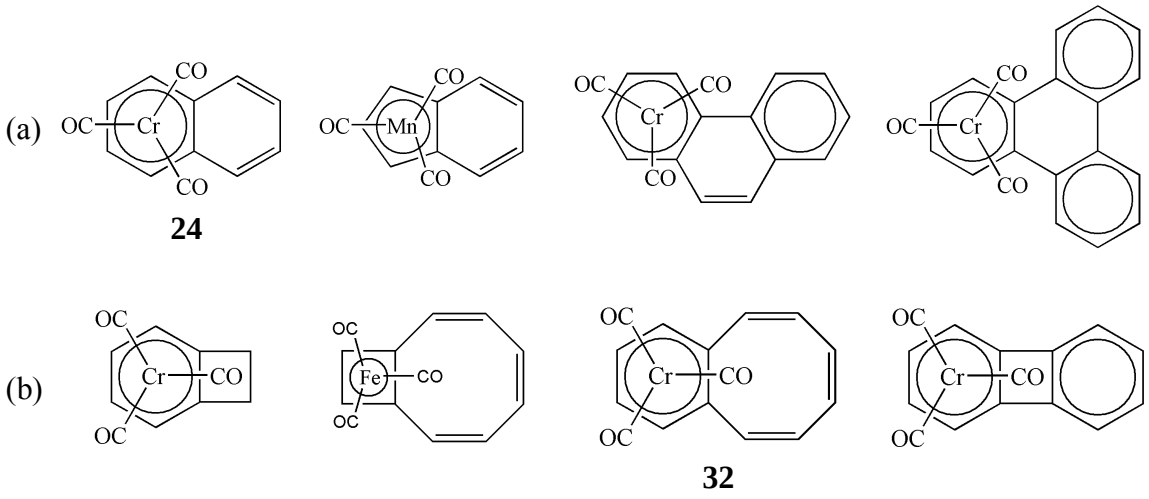

Figure 1.15 Tricarbonyl orientations in several organometallic complexes**; (**a) *exo* complexes, (b) *endo* complexes.[74, 173]

1.4.4 Organometallic complexes containing COT

With the ability to act as a variable hapticity ligand, COT complexes have been extensively studied.[114] Even in Walter Reppe's initial synthesis of **2**, the product was achieved through a nickel-catalyzed tetramerization reaction.[27] The mechanism of the above synthesis remained unclear until 1964. Schrauzer *et al.* postulated that the reaction proceeded through a pseudo-octahedral nickel(II) complex where four acetylene molecules were π-bound to the nickel atom.[178]

The first evidence of a COT metal complex was reported by Cope and Hochstein in 1950 when a crystalline silver nitrate adduct of COT was prepared.[179] Mathews and

Lipscomb solved the crystal structure of the above complex ($Ag(COT)NO_3$) in 1958. The $Ag(COT)^+$ units were weakly connected to form an infinite chain.[180] In 1959, the first COT metal carbonyl derivatives were synthesized independently by three research groups.[181-183] These iron carbonyl products include mononuclear η^4-$C_8H_8Fe(CO)_3$ and two other binuclear derivatives. In 1961, Dickens and Lipscomb reported the crystal structure of one of the bimetallic derivatives ($\eta^4,\eta^{4'}$-COT)$Fe_2(CO)_6$ (Figure 1.16c) where the COT was in a "chair" conformation.[12, 114, 184] Fritz *et al.* reported a cobalt carbonyl complex where COT was observed with η^4-hapticity in a boat conformation (Figure 1.16b).[185] Hughes *et al.*, reported several η^1-FeCp type complexes where the inversion barrier of the COT ring was studied.[186]

The crystal structure of a novel "sandwich" type complex was reported by Kroon *et al.* in 1970.[14] Titanium(II) was bond to η^8-COT and η^5-cyclopentadienyl rings to make an 18 electron complex. The planar COT^{2-} acted as a 10 π electron donor showing equal C-C distances in the crystal structure (Figure 1.16d).[14] COT is known to act as a simple η^2 ligand as in (η^2-COT)(η^5-Cp)$Mn(CO)_2$ (Figure 1.16a) or as a more complex bridging ligand as shown in [Ti(η^8-COT)]$_2\mu$-(η^4, η^4-COT) (Figure 1.16e).[187]

Uranocene [bis(cyclooctatetraenyl)uranium] (Figure 1.16f) was prepared by Streitwieser and Müller-Westerhoff in 1968.[13] This is one of the earliest *f*-block organometallic compounds. The uranium(IV) combines with two planar COT^{2-} rings to form a stable "sandwich" complex having D_{8h} symmetry. Following this work a number of articles reported the complexation of lanthanides and actinides with COT and its derivatives.[188] COT complexes of all lanthanides ($[Ln^{III}(\eta^8\text{-}COT)_2]^-$) and thorium,

protactinium, neptunium and plutonium COT complexes have been developed so far.[114, 187]

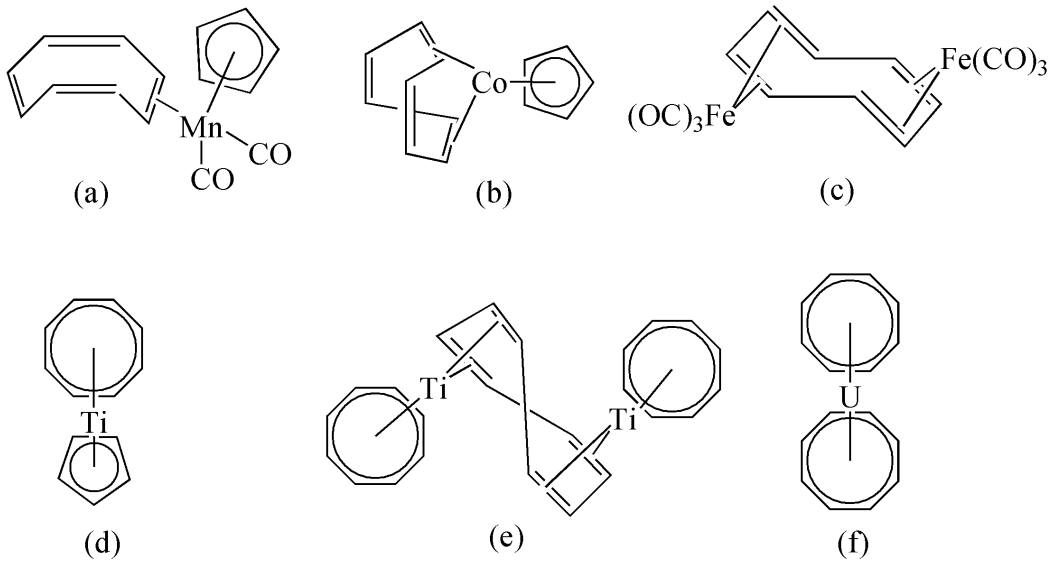

Figure 1.16 Several COT complexes found in literature (a) (η^2-C_8H_8)(η^5-C_5H_5)$Mn(CO)_2$,[187] (b) (η^4- C_8H_8)(η^5- C_5H_5)Co,[185] (c) (η^4,$\eta^{4'}$-C_8H_8)$Fe_2(CO)_6$,[12] (d) (η^8- C_8H_8)(η^5- C_5H_5)Ti,[14] (e) [Ti(η^8-COT)]$_2\mu$-(η^4,$\eta^{4'}$-C_8H_8),[187] and (f) U(η^8-COT)$_2$.[13]

1.4.5 Chromium complexes of ligands BCOT, DBCOT and DBCOD

Coordination chemistry of **1**, **10**, and **13** is interesting as these ligands can produce complexes not achievable with their monocyclic counterparts. The synthesis of η^6-dibenzo[*a*,*e*]cyclooctatetraene(tricarbonylchromium) (**29**) and η^6,η^6-dibenzo[*a*,*e*]-cyclooctatetraenebis(tricarbonylchromium) (**30**) were reported prior to this work. In 1969, Müller and coworkers investigated the stability and preference of the π aromatic organometallic system compared to the π alkene system.[189] Ligand **1** offered an ideal platform for their study as the extended conjugation allowed for the possibility of having both η^6-arene and η^4-diolefin structures of chromiumtricarbonyl.

Müller synthesized the η^4-DBCOTCr(CO)$_4$ (**31**) complex by treating **1** with excess tris(acetonitrile)tricarbonylchromium at low temperature (40^{o}C). **31** was converted to an η^6-monochromium complex by heating it to 140^{o}C in dibutylether. The bimetallic product was achieved by reflux of **29** with additional hexacarbonylchromium at 140^{o}C (Scheme 1.14).[189]

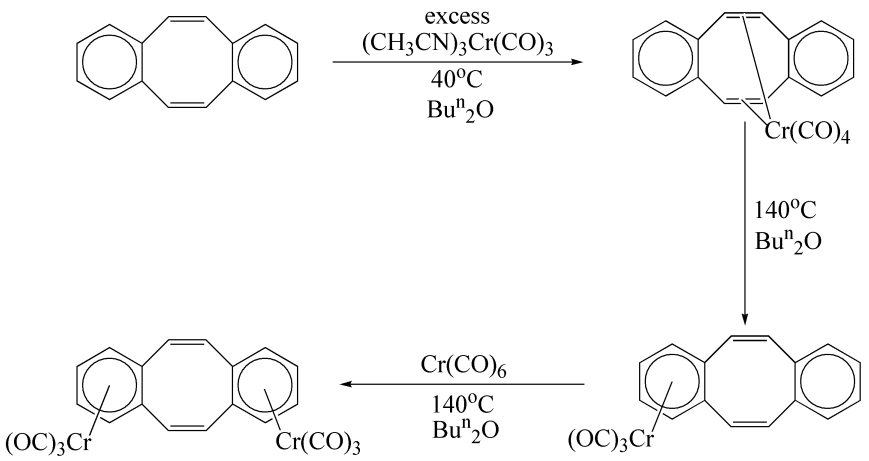

Scheme 1.14 Synthesis of Cr(CO)$_3$ complexes of DBCOT by Müller and coworkers[189]

In 2000, Henry and coworkers reported the crystal structure of **30** with detailed information about the Cr(CO)$_3$ orientation and the chromium coordination.[190] It was found that in the preferred configuration of **30**, Cr(CO)$_3$ moieties bind to the DBCOT tub on opposite sides producing a *syn*,*anti* structure (Figure 1.17). It was important to note that in the crystal lattice of **30**, four independent molecules having different Cr(CO)$_3$ orientations were found.[190] It was postulated that these variable tripodal rotations resulted from a series of intermolecular C-H···O hydrogen bonds.

In 1987, Berno *et al.*[74] reported two chromium complexes of **10**, similar to the work of Müller *et al.*[189] The η^6-chromiumtricarbonyl derivative (**32**) showed an *anti* configuration with respect to the BCOT tub with the carbonyls in the *endo* conformation (Figure 1.15b). When the chromium is coordinated to the eight-membered ring, an 18 electron complex was achieved with the π-donation of six COT carbons (η^6 hapticity). From the crystal structure, the $Cr(CO)_3$ moiety was shifted towards the triene bonds.[74] The only other BCOT metal complex reported so far is the silver perchlorate adduct by Mark *et al.* where they observed η^4 metal coordination of the COT ring.[191]

A monometallic complex for the ligand DBCOD was found in 1978 by Benedikt *et al.*[192] Fakhri and coworkers reported the crystal structures of $C_{16}H_{16}Cr(CO)_3$ (**33**) and *cis*-$C_{16}H_{16}[Cr(CO)_3]_2$ (**34**) in 2000.[193] As opposed to the behavior for the complex with the unsaturated ligand, the crystallography of **34** showed an *anti*,*anti* configuration.

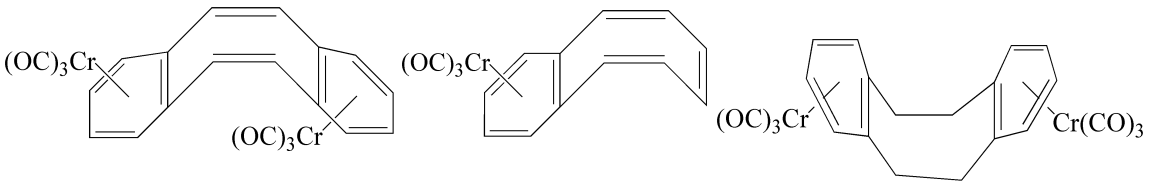

30 **32** **34**

Figure 1.17 Chromium carbonyl complexes of ligands **1**, **10** and **13**; **30**,[190] **32**,[74] and **34**.[193]

1.4.6 DBCOT metallic complexes other than chromium

The first DBCOT metal complexes containing silver and lead metals were reported by Avram *et al.* in 1960.[84] Müller *et al.* also reported a few molybdenum complexes in 1969.[189] However, apart from Müller's chromium complexes, no other π

arene coordinated DBCOT systems have been reported. However, as a fused derivative of COT, the coordination ability of the eight-membered ring in DBCOT has been thoroughly investigated.

Crabtree and coworkers studied complexes of molybdenum, rhodium, iridium, and palladium, where **1** was used as a poison for homogeneous catalysts.[194, 195] A tetrameric copper η^2-DBCOT structure (Figure 1.18a) was reported by Book and coworkers in 1983.[196] Sygula *et al.* reported a crystal structure of the planar η^8-dilithium DBCOT complex (Figure 1.18b) containing the aromatic COT^{2-} dianion at room temperature.[197] Läng *et al.* synthesized several η^4 iridium(I) and rhodium(I) complexes containing chiral DBCOT (Figure 1.18c).[94] Following their previous work with1,5-cyclooctadiene (**19**) metal complexes,[198] Sharp and coworkers reported a series of η^4-DBCOT complexes in 2006[199] and 2008[200] (Figure 1.18d). Interestingly, Sharp and coworkers opposed[199, 200] the idea stated by Crabtree and coworkers that **1** is bound more strongly to metal centers than **19**.[194, 195] Carnes *et al.* recently reported a propeller type nickel complex containing three η^2-helical DBCOT ligands.[201]

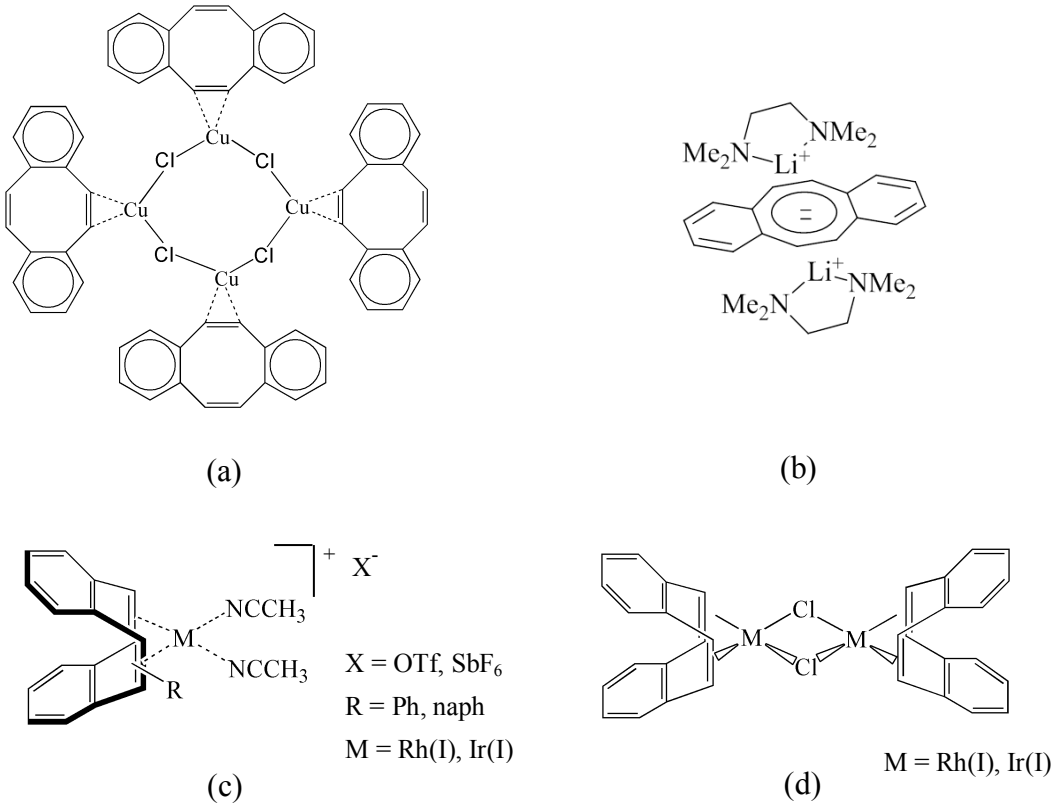

Figure 1.18 Various DBCOT metal complexes found in literature; (a) η^2 Cu(I),[196] (b) η^8 Li(I),[197] (c) η^4 Rh(I) and Ir(I),[94] (d) η^4 Rh(I) and Ir(I)[200]

1.5 Studying the dynamic processes with variable temperature NMR spectroscopy

In the current study, variable temperature (VT) NMR line shape analysis is conducted to determine accurate activation parameters for the fluxional process. Computational calculations are used to assist in understanding the chemistry of these organometallic compounds. Significant contributions made throughout history in terms of VT NMR analysis are briefly summarized in this section.

The fundamental concept of NMR was first reported by Isidor I. Rabi in 1938.[202] The practical aspects on reporting magnetic resonance of a bulk sample was initiated

from the work of Felix Bloch and Edward M. Purcell in 1946.[203] Bloch, Hansen, and Packard successfully studied proton signals in a water sample doped with a paramagnetic salt at RT.[204, 205] Purcell, Torrey, and Pound independently reported the proton resonance of a paraffin sample. For their significant contributions, Rabi (1944) and Bloch and Purcell (1952) were awarded Noble Prizes in physics.[206, 207] In 1951, Packard and coworkers reported that the position of the proton resonance for the hydroxyl group is dependent on temperature and concentration.[208] Methanol and ethanol samples were also studied, and in a parallel work, Liddel and Ramsey stated that the temperature dependence of ethyl alcohol was associated with the hydrogen bonding of the hydroxyl group.[209] Anthony Van Geet innovated temperature calibration techniques increasing the accuracy of the temperature readings for VT studies.[210, 211] Currently, the "methanol thermometer" is widely accepted as an accurate temperature calibration method for modern NMR spectrometers.[212]

The aspect of molecular motion with respect to nuclear magnetic relaxation was first investigated by Bloembergen *et al.* in 1948.[213] Gutowsky and coworkers suggested that the chemical exchange averages chemical shifts in the proton resonance spectrum.[214, 215] Therefore, a rate constant for exchange can be derived using NMR spectroscopy.[203] Following this work, Gutowsky and coworkers reported the first dynamic study using a variable temperature NMR experiment.[216] The barrier to internal rotation of *N*,*N*-dimethylformamide (DMF) and *N*,*N*-dimethyl-acetamide (DMA) were examined using variable temperature NMR spectroscopy. Anet and coworkers pioneered the ring

inversion studies in cyclic carbon skeletons using VT NMR experiments.[11, 217] In 1968, Kessler *et al.* studied the ring inversion of a *tert*-butyl derivative of cyclohexane.[218]

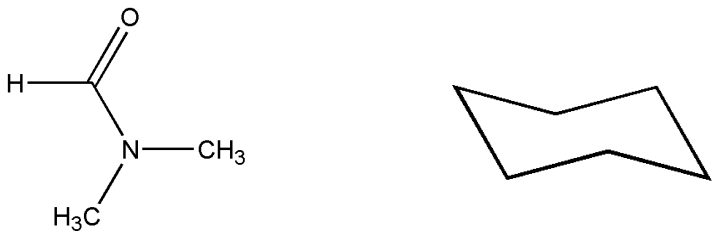

(a) (b)

Figure 1.19 Classical systems where dynamics have been studied using VT NMR; (a) DMF and (b) cyclohexane

In 1968, Lambert *et al.* pointed out the need of a change in terminology for inversions.[219] Separate terms were suggested for "ring flip" or "reversal" as opposed to "atom inversion".[219] However, due to the fact that in most systems both ring flip and atom inversion can occur simultaneously, the term "ring inversion" is retained as the popular term. The established definition for ring inversion is the change in the signs of the all ring dihedral angles (the magnitude does not change) except the ones close to 0^{o} or 180^{o}.[30]

When interconversion of structures occurs rapidly (fast exchange), only an average of chemical shifts and coupling constants is observed on the NMR time scale.[220] When the structural changes occur at a slower rate (slow exchange), each conformation exhibits characteristic peaks in the NMR spectrum.[220-222] The rate of exchange can be controlled by changing the temperature of the sample.[30] Using the spectral line shapes in the intermediate region, thermodynamic information such as the rate constant (k) and

Gibbs free energy of activation ($\Delta G^{\ddagger}$) can be deduced.[222] Depending on the accuracy of the NMR data, the enthalpy and entropy of activation can also be evaluated.[30]

1.6 Research objectives to be addressed

From the detailed investigations of Oth, Anet, and Paquette, it was determined that increasing the substitution on the COT ring slows BS and RI.[4-6, 29, 30, 63] The effect of benzo annulation on RI rates have been studied by Mislow, Buchanan, and Figeys.[2, 104, 107] Very little work has been done regarding eight-membered RI in a metal coordinated system. Only monocyclic compounds with the metal sigma bonded to the COT ring have been studied so far.[186] As summarized above, only two η^6 DBCOT metal systems are known and RI has not been studied in either of them.[189] In this study, the main focus is to determine the barrier to inversion in an η^6-arene coordinated DBCOT complex for the first time. It is of interest to know whether the electron withdrawing effect of the metal has any effect on the dynamic process, as in the reduction studies for conjugated bimetallic systems.[155]

Since the chromium bimetallic complex favors the *syn*,*anti* configuration in the solid state, the all-important question concerns the preferred configuration for the monometallic complex. Since only the chromium carbonyl chemistry of DBCOT was studied, the investigation of the isoelectronic Mn(I) system is of interest. Synthetic methods for generating mono- and bimanganese complexes were evaluated in this work, and the direction of coordination with respect to the DBCOT tub is examined.

The synthesis, purification, and characterization of the metal DBCOT compounds are described in the next chapter. Detailed experimental procedures are given for the

dynamic NMR and electrochemistry studies. The results and discussion of the experiments are provided in Chapter 3. Finally, the overall conclusions are discussed in Chapter 4.

CHAPTER II

EXPERIMENTAL DETAILS

This chapter is divided into three sections; synthesis and characterization, variable temperature NMR studies, and electrochemical experiments. The synthesis and characterization section includes the preparation of organic compounds, preparation of metal carbonyl complexes, and the characterization of all products. Sample preparation, calibration of the NMR spectrometer temperature control unit, and obtaining NMR spectra at a series of temperatures are described in section 2.2. The experimental procedure to evaluate the electrochemical properties of the products is reported in section 2.3.

2.1 Synthesis and characterization

2.1.1 Materials and methods

Dichloromethane (CH_2Cl_2), hexanes (C_6H_{14}), diethyl ether ($C_2H_5OC_2H_5$), tetrahydrofuran (THF, C_4H_8O), acetone (CH_3COCH_3), chloroform ($CHCl_3$), ethanol (C_2H_5OH), propylene carbonate (PC, $C_4H_6O_3$), Celite (diatomaceous earth) and chromatographic silica gel were purchased from Fisher Scientific. α,α′-Dibromo-*o*-xylene [**15**, $C_6H_4(CH_2Br)_2$], *n*-butyl ether ($C_4H_9OC_4H_9$), potassium *tert*-butoxide (**18**, C_4H_9OK), nitromethane (CH_3NO_2), carbon disulfide (CS_2), molecular sieves (4A), tetraethylammonium perchlorate [TEAP, $(C_2H_5)_4N(ClO_4)$], tetrabutylammonium

perchlorate [TBAP, $(C_4H_9)_4N(ClO_4)$], tetrabutylammonium hexafluorophosphate [TBAHFP, $(C_4H_9)_4N(PF_6)$], deuterated chloroform ($CDCl_3$), acetone-d_6 (CD_3COCD_3), dichloromethane-d_2 (CD_2Cl_2), methanol-d_4 (CD_3OD) and tetramethylsilane [TMS, $Si(CH_3)_4$] were obtained from Sigma-Aldrich. Chromium carbonyl [$Cr(CO)_6$], manganese carbonyl [$Mn_2(CO)_{10}$], ferrocene [**22**, $Fe(C_5H_5)_2$], and silver tetrafluoroborate ($AgBF_4$) were purchased from Strem Chemicals. Naphthalene ($C_{10}H_8$) and *N*-bromosuccinimide (**14**, $C_4H_4BrNO_2$) were obtained from Baker Chemicals. Drierite ($CaSO_4$) was purchased from Acros Organics, and ultra-high purity argon gas was purchased from Airgas, Inc.

All manipulations of air-sensitive materials were performed under purified ultra-pure argon using a gas vacuum double manifold and standard Schlenk techniques.[223] For all air-sensitive materials, solid transfers and storage for prolonged period were conducted in a glove box. The Ar used in Schlenk lines was purified by passing it through a copper catalyst and phosphorous pentoxide columns to remove oxygen and moisture. Commercial grade solvents were dried and freshly distilled under argon prior to use. Hexanes, THF, and *n*-butyl ether were distilled from Na/K amalgam, while dichloromethane was distilled from P_2O_5. Carbon disulfide was distilled from and stored over activated molecular sieves. Anhydrous diethyl ether was bubbled with Ar prior to use. PC used in electrochemical experiments was purified by vacuum distillation. TEAP, TBAP, and TBAHFP salts were recrystallized twice and vacuum dried at 110^{o}C prior to use. Silica gel was dried and activated under vacuum with heating at 120^{o}C overnight. Deuterated solvents used for NMR experiments of air-sensitive compounds were degassed with freeze-pump-thaw cycles and pot-to-pot distilled using a high vacuum line

equipped with a diffusion pump. Chromium carbonyl and **22** were purified by sublimation before use. NBS, **15**, and naphthalene were recrystallized prior to use from distilled water, hexanes, and methanol solvents, respectively.

^{1}H and ^{13}C NMR spectra were obtained using Bruker Avance III 300 MHz and 600 MHz spectrometers. The chemical shifts of the peaks were reported versus TMS as the internal reference.[224] The 2D NMR experiments were performed using the 600 MHz broad band fluorine observation (BBFO) probe with standard parameter files. Non-diagonal cross-peaks from ^{1}H-^{1}H correlation spectroscopy (COSY)[225] are listed as (^{1}H, ^{1}H) in the following sections. The couplings from ^{1}H-^{13}C heteronuclear multiple-quantum correlation (HMQC)[226] and heteronuclear multiple-bond correlation (HMBC)[227] experiments are reported as (^{1}H, ^{13}C). NMR spectra were simulated using gNMR software (Version 4.1.0).[228] Structural assignments and coupling constants were determined based on 1D and 2D experimental data, spectra simulations, and theoretical calculations. Assignments are discussed in Chapter 3. To gain an insight into experimental results, in collaboration with Dr. Gwaltney's group a theoretical study was undertaken. Calculations were performed using Spartan (2010, V 1.0.1)[229] and Q-Chem[230] quantum mechanics programs by Dr. Steven R. Gwaltney and Chinthaka N. Ratnaweera. Density functional theory (DFT/B3LYP)[231, 232] coupled with the 6-31G(d,p) basis set[233] were used to optimize geometries and calculate vibrational frequencies.

Infrared spectroscopy of the solid products was performed using a single-bounce diamond attenuated total reflectance (ATR) accessory on a Thermo Nicolet 6700 FT-IR spectrometer at RT. The vibrational spectra for liquid samples were analyzed with a thin

liquid film cell in a suitable solvent. Melting points were obtained using a Mel-Temp melting point apparatus, and the readings obtained are uncorrected.

The single crystal X-ray diffraction (XRD) data were obtained on a Bruker Smart 1000 diffractometer equipped with a molybdenum X-ray source (Mo-Kα, λ = 0.71073 Å), upgraded with an APEX II charge couple device (CCD) area detector, a monocap beam collimator, and a 3-circle goniometer. All data were collected at 100 K using an Oxford cryostream accessory. Data collection was controlled by the Bruker APEX II crystallographic software package[234] that incorporates many aspects of the SHELXTL (2008/ 3) program suite for solving, refining, and analyzing crystal data.[235]

Cyclic voltammetry was performed using a Princeton Applied Research (PAR) model 273A Potentiostat/Galvanostat with positive feedback iR compensation. Data collection and processing was conducted using M270 software.[236] A standard three-electrode electrochemical cell was used with a platinum disk as the working electrode.[237] Silver and platinum wires were used as reference and counter electrodes, respectively. All experiments were carried out under a blanket of argon. Ar was bubbled through the solvent between scans to keep the solvent oxygen free. Tetraalkylammonium salts (TEAP, TBAP, and TBAHFP) were used as supporting electrolytes. Ferrocene was added as an internal standard.

2.1.2 Organic ligand synthesis

Synthesis of **1** was achieved in a three step process (Scheme 2.1) according to the most recent synthetic methodology found in the literature.[93] Slight modifications were made to the literature preparation to accommodate current laboratory settings. The

changes include prolong sonication (> 6 h), introduction of sublimation instead of chromatography, conducting bromination under inert conditions, and extending the reflux time for the final step (continued overnight).

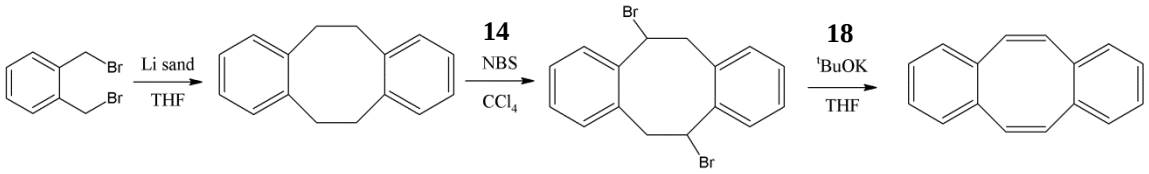

15 **13** **17** **1**

Scheme 2.1 Synthesis of **1**[93]

Preparation of lithium sand:[93] About 8 g of Li wire was rapidly stirred in 200 mL of silicon oil at 210^{o}C in a 1 L three-neck round bottom (RB) flask with a mechanical stirrer. Stirring was continued for 2-4 h, until Li particles achieved the desired size (2-4 mm in diameter). The suspension was cooled and stored under argon. Prior to use in the synthesis, the silicon oil was removed using a cannula. Lithium sand was then washed with dry hexanes under inert atmosphere.

5,6,11,12-Tetrahydrodibenzo[*a*,*e*]cyclooctadiene (**13**): 50.0 g (0.189 mol) of **15** was carefully added to 7.70 g (1.10 mol) of lithium sand suspended in anhydrous THF (225 mL) in a 1 L three-neck round bottom flask equipped with a reflux condenser. The system was maintained at 0^{o}C during the solid transfer, then degassed with argon, and brought to room temperature. The reaction was facilitated by sonication for 6-8 h until a red solution was observed. The solution containing crude product was separated from the unreacted lithium using a cannula. Excess lithium was discarded after slowly reacting it

with isopropanol. Solvent evaporation from the solution produced a gummy solid. Sublimation of the crude mixture at 110°C yielded 13.6 g (68.7%, lit[93] 63%) of needle-like white crystalline product.

Melting point: 107-108°C, lit. 108.5°C[79] and 108.5-109.0°C;[78] ^{1}H NMR (300 MHz; $CDCl_3$): δ = 7.00 (8H, br s, H1, H2, H3, H4, H7, H8, H9, H10), 3.07 (8H, s, H5, H6, H11, H12). ^{1}H NMR chemical shifts agree with values reported in the literature.[93] ^{13}C NMR (300 MHz; $CDCl_3$): δ = 140.60 (C13, C14, C15, C16), 129.66 (C1, C4, C7, C10), 126.09 (C2, C3, C8, C9), 35.13 (C5, C6, C11, C12).

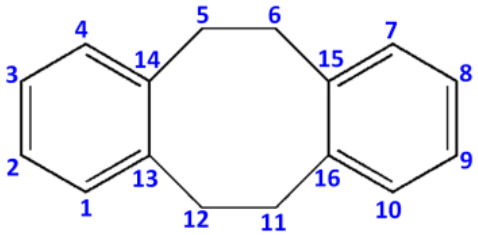

Figure 2.1 Numbering scheme for **13**

5,11-Dibromo-5,6,11,12-tetrahydrodibenzo[*a*,*e*]cyclooctadiene (**17**): A 200 ml Schlenk flask was vacuum dried, and 3.12 g (15.0 mmol) of freshly sublimed **13** and 5.50 g (31.0 mmol) of recrystallized NBS were added. 60 mL of anhydrous CCl_4 was added using a cannula under argon pressure and the solution was refluxed for 2-3 h. The completion of the reaction was determined by thin layer chromatography (TLC) using silica as the solid phase with hexanes as eluent. The cooled mixture was filtered with a Buchner funnel to remove solid succinimide. The residue was washed with CCl_4, and upon evaporation of the combined solutions a white solid was obtained. The crude

product was washed with distilled water and recrystallized using 95% ethanol. The mass of **17** obtained was 4.72 g (yield 86%, lit. (crude) 95%[93] and 98%[238]). XRD quality single crystals were obtained by sublimation of the product at 185°C under vacuum. The crystallographic data and structure refinement information are summarized in table 2.1.

Table 2.1 Crystallographic parameters for **17**

empirical formula	$C_{16}H_{14}Br_2$	color	colorless
formula weight	366.09	density (g cm^{-3})	1.77
crystal system	orthorhombic	temperature (K)	100
space group	$P2_12_12_1$	wavelength (Å)	0.71073
final indices R_1, wR_2	0.0297, 0.0695	all data R_1, wR_2	0.0328, 0.0707
unit cell parameters			
a (Å)	7.6248(10)	α (deg)	90°
b (Å)	8.6601(11)	β (deg)	90°
c (Å)	20.770(3)	γ (deg)	90°
V ($Å^3$)	1371.5(3)	Z	4

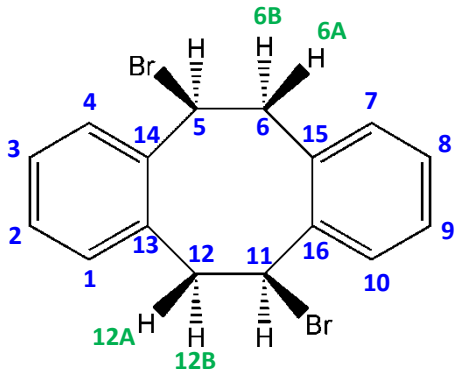

Figure 2.2 Numbering scheme for **17**

Melting point: 185-187°C, lit. 181-183°C,[238] 185-186°C,[44] and 188.1-189.0°C;[78] ^{1}H NMR (300 MHz; $CDCl_3$): δ = 6.90-7.20 (8H, m, H1, H2, H3, H4, H7, H8, H9, H10), 5.34 (2H, dd, ^{3}J = 11.2 Hz, ^{3}J = 8.5 Hz, H5, H11), 4.29 (2H, dd, ^{2}J =14.2, ^{3}J = 11.2, H6A, H12A), 3.66 (2H, dd, ^{2}J =14.2 Hz, ^{3}J = 8.5 Hz, H6B, H12B). Chemical shifts agree with those reported by Moore *et al.*;[238] however, the coupling values differ from the ones reported by Chaffins *et al.*[93] ^{1}H NMR (600 MHz; acetone-d_6): δ = 7.25 (2H, d, ^{3}J = 7.2 Hz, H1, H7), 7.15 (2H, dd, ^{3}J = 7.2 Hz, ^{4}J = 1.7 Hz, H3, H9), 6.98-7.11 (4H, m, H2, H4, H8, H10), 5.64 (2H, dd, ^{3}J = 11.0 Hz, ^{3}J = 8.6 Hz, H5, H11), 4.23 (2H, dd, ^{2}J =13.9, ^{3}J = 11.0, H6A, H12A), 3.78 (2H, dd, ^{2}J = 13.9 Hz, ^{3}J = 8.6 Hz, H6B, H12B). ^{13}C NMR (600 MHz; acetone-d_6): δ = 139.58 (C13, C15), 137.58 (C14, C16), 131.88 (C4, C10), 131.80 (C1, C7), 129.86 (C3, C9), 128.65 (C2, C8), 54.30 (C5, C11), 44.25 (C6, C12).

2D NMR (600 MHz; Acetone-d_6): Non-diagonal peaks were found in the COSY spectrum (Figure 2.3) at (5.64, 4.23) and (5.64, 3.78). HMQC peaks were identified at (7.25, 131.80), (7.15, 129.86), (7.07, 131.88), (7.07, 128.65), (5.64, 54.30), (4.23, 44.25) and (3.78, 44.25). Long range couplings were observed in the HMBC spectrum (7.25,

139.58), (7.25, 128.65), (7.25, 44.25), (7.15, 137.58), (7.15, 131.88), (7.07, 139.58), (7.07, 137.58), (7.07, 131.80), (7.07, 129.86), (7.07, 54.30), (5.64, 139.58), (5.64, 137.58), (5.64, 131.88), (5.64, 44.25), (4.23, 139.58), (4.23, 137.58), (4.23, 131.80), (4.23, 54.30), (3.78, 139.58), (3.78, 137.58), (3.78, 131.80), and (3.78, 54.30).

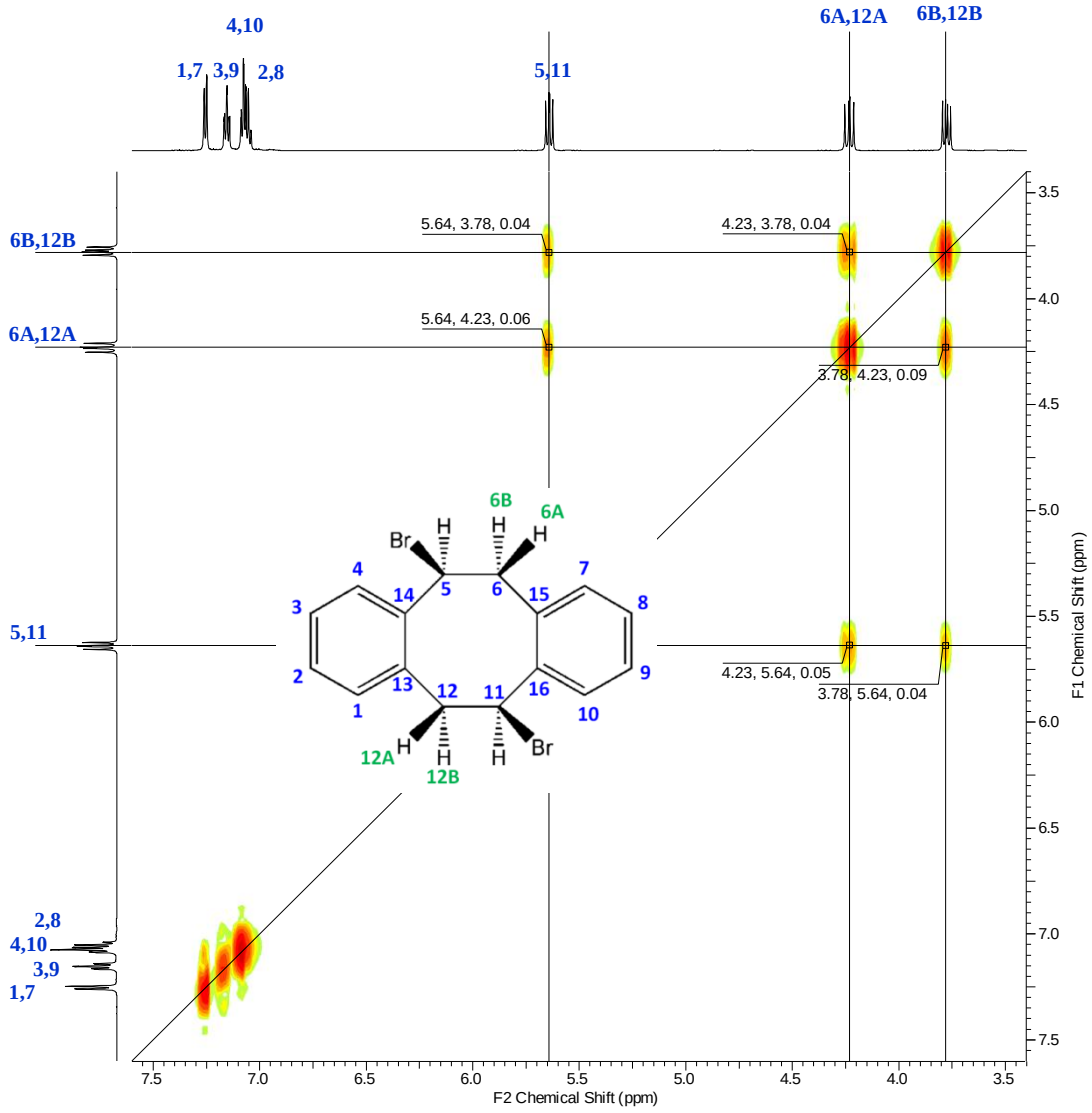

Figure 2.3 COSY spectrum of **17**; 600 MHz, RT, acetone-d_6

Dibenzo[*a*,*e*]cyclooctatetraene (**1**): 0.95 g (2.6 mmol) of **17** was dissolved in 20 mL of THF in a dry 200 mL Schlenk flask. The flask was cooled to 0^{o}C using an ice bath. 42 mL (16 equiv.) of 1 M *t*-BuOK solution in THF was slowly introduced to the reaction flask with the addition of another 16 mL of THF under an inert atmosphere. A moisture trap containing Drierite was connected to the Schlenk flask. The system was allowed to warm to RT slowly and continued to stir overnight. Completion of the reaction was determined by TLC. Distilled water was added to quench the reaction, and the contents were transferred to a separation funnel. The product was extracted three times with $CHCl_3$. The solid, obtained after evaporating the solvent, was purified by recrystallization with 95% ethanol. 0.39 g (73% yield, lit. 79%[93]) of needle-like colorless crystals was obtained.

Melting point: 107-109^{o}C, lit. 108.5-110.0^{o}C,[77] 106.5-107.0^{o}C,[78] 109.2-109.4^{o}C;[88] ^{1}H NMR (300 MHz; $CDCl_3$): δ = 7.11-7.21 (4H, m, H2, H3, H8, H9), 7.01-7.10 (4H, m, H1, H4, H7, H10), 6.75 (4H, s, H5, H6, H11, H12). Chemical shifts agree with those reported in the literature.[93] ^{1}H NMR (600 MHz; acetone-d_6): δ = 7.13-7.20 (4H, m, H2, H3, H8, H9), 7.03-7.10 (4H, m, 4H, m, H1, H4, H7, H10), 6.77 (4H, s, H5, H6, H11, H12). ^{13}C NMR (600 MHz; acetone-d_6): δ = 138.09 (C13, C14, C15, C16), 134.08 (C5, C6, C11, C12), 130.00 (C1, C4, C7, C10), 127.80 (C2, C3, C8, C9). These assignments are discussed in the next chapter.

2D NMR (600 MHz; Acetone-d_6): Non-diagonal peaks were found in COSY spectrum at (7.15, 7.07) and (7.07, 6.77). HMQC (Figure 2.4) peaks were identified at (7.16, 127.80), (7.07, 130.01), and (6.77, 134.08). Long range couplings were observed

from the HMBC (Figure 3.1) experiment at (7.15, 138.09), (7.15, 130.00), (7.07, 138.09), (7.07, 134.08), (7.07, 127.80), (6.77, 138.09), (6.77, 134.08), and (6.77, 130.00).

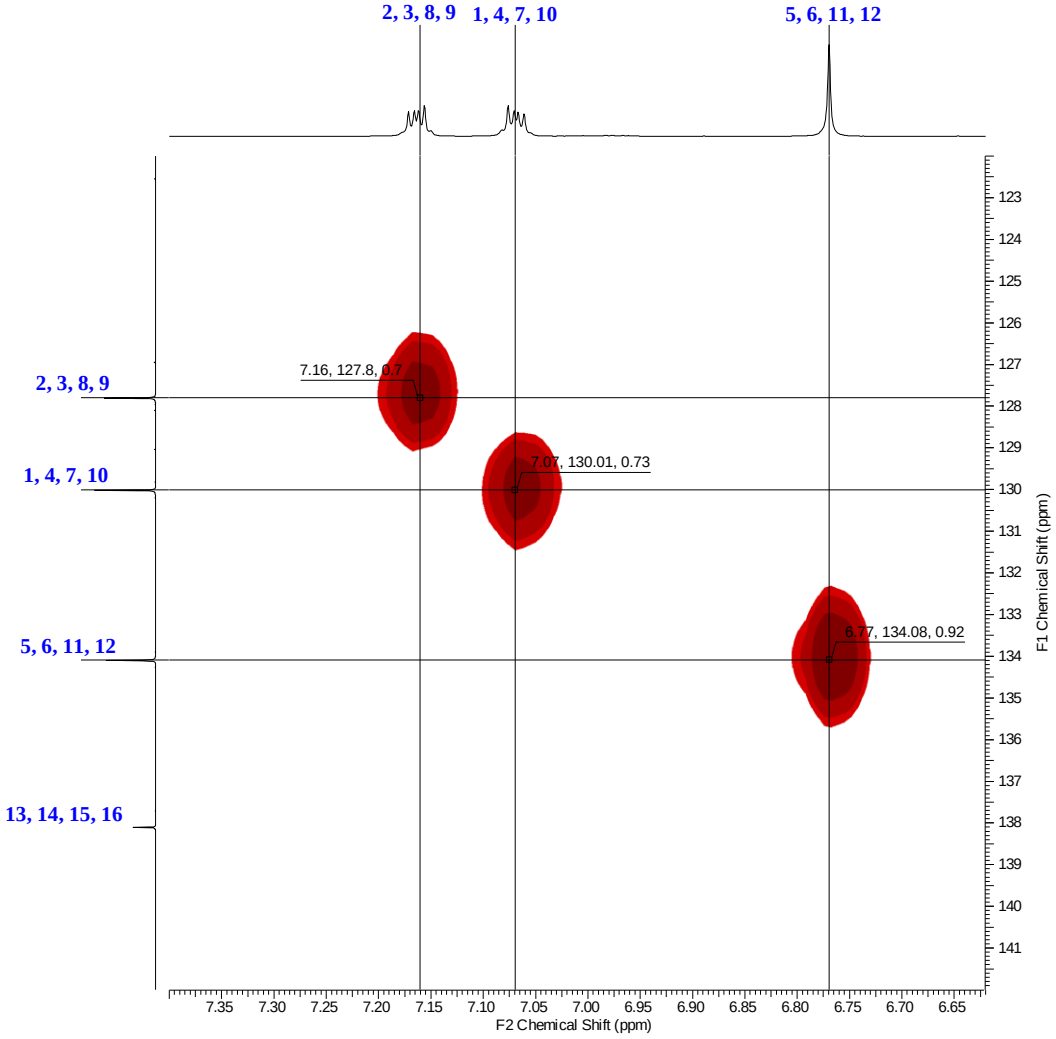

Figure 2.4 HMQC spectrum of **1**; 600 MHz, RT, acetone-d_6

2.1.3 Chromium(0) carbonyl complexes

Chromium metal complexes are highly sensitive to air and moisture in solution. In the presence of air, yellowish chromium(0) compounds are readily oxidized to a green

colored product containing Cr(III). The above oxidation is a self-catalytic reaction continuing in rapid phase. Therefore, a reaction mixture had to be discarded if any Cr(III) was observed. It is vital to maintain strictly inert conditions throughout the synthesis of these reactive materials.

η^6-Dibenzo[*a*,*e*]cyclooctatetraene(tricarbonyl)chromium (**29**): Freshly sublimed $Cr(CO)_6$ (0.484 g, 2.20 mmol) and **1** (0.408 g, 2.00 mmol) were added to a 100 mL Schlenk flask. The flask was cooled to 0^oC in an ice bath. Five short cycles of evacuation and filling were performed. Freshly distilled dry *n*-dibutyl ether (18 mL) and THF (2 mL) were added and the reaction mixture was refluxed for three days, keeping the oil bath temperature at 140^oC. Dry argon was purged through a bubbler attached above the reflux condenser. A schematic diagram for the experimental setup is displayed in Figure 2.6a. After reflux, the reaction was allowed to cool to RT slowly, and the solvent was evaporated under vacuum to obtain a yellowish solid. This crude product was purified using a long silica column under inert atmosphere (Figure 2.6b). Hexane was used as the primary solvent with increasing amounts of diethyl ether (1% - 20%). Three different bands were eluted from the column. Fraction I was the unreacted ligand (**1**), fraction II was the desired product (**29**) and fraction III was a mixture of *syn*,*anti* and *anti*,*anti* bimetallic chromium complexes (**30** and **35**). 0.41 g (yield 60%) of **29** was isolated by solvent evaporation. XRD quality single crystals were grown by slow cooling of a concentrated hexane solution. Crystallographic parameters are listed in Table 2.2. NMR samples were prepared using Schlenk techniques with deoxygenated acetone-d_6.

Table 2.2 Crystallographic parameters for **29**

empirical formula	$C_{19}H_{12}CrO_3$	color	yellow translucent
formula weight	340.29	density (g cm^{-3})	1.50
crystal system	triclinic	temperature (K)	100
space group	$P\bar{1}$	wavelength (Å)	0.71073
final indices R_1, wR_2	0.0333, 0.0781	all data R_1, wR_2	0.0404, 0.0818
unit cell parameters			
a (Å)	8.3782(17)	α (deg)	99.107(2)°
b (Å)	8.4005(17)	β (deg)	106.551(2)°
c (Å)	11.369(2)	γ (deg)	92.880(2)°
V ($Å^3$)	753.5(3)	Z	2

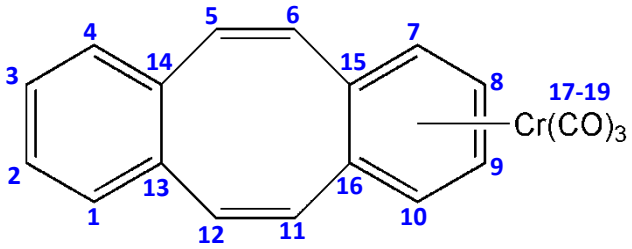

Figure 2.5 Numbering scheme for **29**

Melting point: 167-169°C (decomp.), lit. 168-170;[189] IR (hexanes): 1977 and 1914 cm^{-1}, lit. 1980, 1913 cm^{-1} (ν_{CO});[189] IR (CH_2Cl_2): 1967 and 1893 cm^{-1} (ν_{CO}); ^1H NMR (300 MHz; acetone-d_6): δ = 7.25-7.33 (2H, m, H2, H3), 7.13-7.22 (2H, m, H1, H4), 6.87 (2H, d, ^3J =11.9, H5, H12), 6.53 (2H, d, ^3J =11.9, H6, H11), 5.52-5.63 (4H, m, H7, H8, H9, H10). ^1H NMR (600 MHz; acetone-d_6): δ = 7.24-7.36 (2H, m, H2, H3), 7.10-7.23 (2H, m, H1, H4), 6.86 (2H, d, ^3J =12.0, H5, H12), 6.53 (2H, d, ^3J =12.0, H6, H11), 5.48-5.64 (4H, m, H7, H8, H9, H10). Chemical shifts agree with those reported in the literature.[189]

^{13}C NMR (600 MHz; acetone-d_6): δ = 234.20 (C17, C18, C19), 136.36 (C5, C12), 136.19 (C13, C14), 130.14 (C6, C11), 130.04 (C1, C4), 128.33 (C2, C3), 109.03 (C15, C16), 94.54 (C7, C10), 94.02 (C8, C9). 2D NMR (600 MHz; acetone-d_6); In the ^1H-^1H COSY spectrum a non-diagonal peak was found at (6.86, 6.53). ^1H-^{13}C HMQC and HMBC experiments were also performed. (7.28, 128.33), (7.17, 130.04), (6.86, 136.36), (6.53, 130.14), (5.58, 94.02), and (5.55. 94.54) peaks were observed by HMQC (Figure 3.39). The HMBC spectrum (Figure 3.40) gave cross peaks at (7.28, 130.04), (7.17, 136.36), (7.17, 136.19), (7.17, 128.33), (6.86, 136.19), (6.86, 130.14), (6.86, 130.04), (6.86, 109.03), (6.53, 136.36), (6.53, 136.19), (6.53, 109.03), (6.53, 94.54), (5.58, 94.54), and (5.55, 94.02).

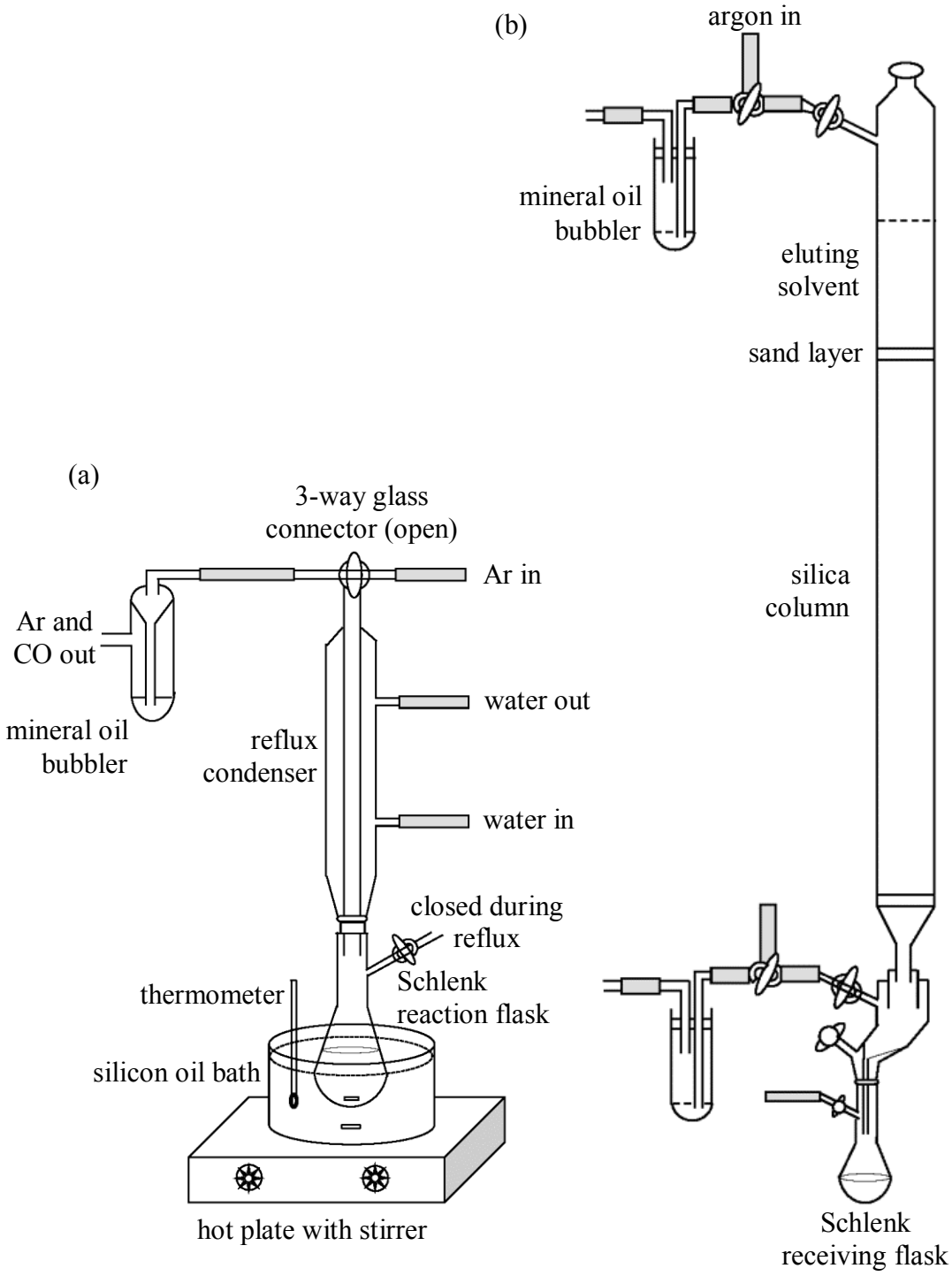

Figure 2.6 (a) Experimental setup for extended reflux in the preparation of DBCOT complexes, (b) Silica gel column for chromatography under inert gas.

η^6,η^6-Dibenzo[*a*,*e*]cyclooctatetraene-*syn*,*anti*-bis(tricarbonyl)chromium (**30**): Synthesis and purification were conducted similarly to **29**. 0.44 g (2.0 mmol) of $Cr(CO)_6$ was allowed to react with 0.11 g (0.50 mmol) of **1** in a mixture of *n*-dibutyl ether (18 mL) and THF (2 mL). The reaction mixture was refluxed for 7 days at 130°C, with a continuous flow of argon above the reflux condenser as shown in Figure 2.6a. A yellow solid was obtained after evaporation of solvent. This crude product also contained small amounts of uncoordinated ligand and the metallic complexes **29** and **35**. Chromatographic purification using an inert atmosphere silica column (Figure 2.6b) with hexane and diethyl ether (1% - 40%) yielded 0.17 g (yield 71%) of **30**.

Melting point: 169-170°C (decomp.), lit. 170 °C (decomp.);[189] IR (hexanes): 1977 and 1915 cm^{-1}, lit. 1980, 1913 cm^{-1} (ν_{CO});[189] IR (CH_2Cl_2): 1967 and 1895 cm^{-1} (ν_{CO}); ^1H NMR (300 MHz; acetone-d_6): δ = 6.66 (4H, s, H5, H6, H11, H12), 5.68-5.74 (4H, m, H2, H3, H8, H9), 5.58 (4H, br s, H1, H4, H7, H10). ^1H NMR (600 MHz; acetone-d_6): δ = 6.65 (4H, s, H5, H6, H11, H12), 5.67-5.78 (4H, m, H2, H3, H8, H9), 5.46-5.65 (4H, m, H1, H4, H7, H10). ^{13}C NMR (600 MHz; acetone-d_6): δ = 234.06 (C17, C18, C19, C20, C21, C22), 130.20 (C5, C6, C11, C12), 107.42 (C13, C14, C15, C16), 95.01 (C1, C4, C7, C10), 93.94 (C2, C3, C8, C9).

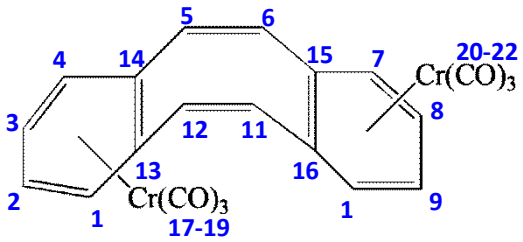

Figure 2.7 The geometry and numbering scheme for **30**

2D NMR (600 MHz; acetone-d_6); ^{1}H-^{1}H COSY, ^{1}H-^{13}C HMQC and HMBC experiments were performed. Non-diagonal peaks were not found by COSY. HMQC (Figure 3.3a) direct coupling peaks were found at (6.65, 130.20), (5.71, 93.94), and (5.57, 95.01). The HMBC spectrum (Figure 3.3b) gave couplings of (6.65, 107.42), (6.65, 95.01), (5.71, 107.42), (5.71, 95.01), and (5.56, 93.94).

Reduction of **30** was attempted in using of a couple of the alkali metals as reductants. In separate experiments, 1 mmol of **30** was stirred with excess Na and K in THF under dry, inert conditions. No color change was observed and no significant change was observed in the liquid IR spectra.

η^6,η^6-Dibenzo[*a*,*e*]cyclooctatetraene-*anti*,*anti*-bis(tricarbonyl)chromium (**35**): During column chromatography in the synthesis of **30**, a small amount of **35** (0.014 g, yield 5.7%) was isolated. A small band of **35** can be observed coming off the column before **30**, with the introduction of diethyl ether (20%-30%). Melting point: 169-170^{o}C (decomp.); IR (hexanes): 1981 and 1914 cm^{-1} (ν_{CO}); IR (CH_2Cl_2): 1969 and 1895 cm^{-1} (ν_{CO}); NMR (300 MHz; acetone-d_6): δ = 6.60 (4 H, s, H5, H6, H11, H12), 5.68 (8 H, br s, H1, H2, H3, H4, H7, H8, H9, H10). All attempts to obtain an XRD quality crystal were unsuccessful.

2.1.4 Manganese(I) carbonyl complexes

$Mn(CO)_5Br$ and MTT transfer agent were synthesized according to the reported procedures.[166, 239] The following section illustrates the first synthesis attempts for complexes **36-39**. Manganese(I) complexes are sensitive to air, moisture, and light. Therefore, all work described in this section was conducted under an inert environment

with minimum light exposure. The reactions were done in a darkened fume hood, and reaction flasks were covered with aluminum foil at all times.

Manganese(pentacarbonyl)bromide (**27**): 2.23 g (5.72 mmol) of dimanganese decacarbonyl [$Mn_2(CO)_{10}$] was added to 50 mL of distilled CS_2 in a 200 mL Schlenk flask. After stirring for 10 minutes, a solution of 0.35 mL (6.8 mmol) Br_2 in 10 mL CS_2 was slowly added using a dropping funnel. Stirring was continued for 3 h, and evaporation of solvent under vacuum gave an orange colored solid. The crude product was dissolved in 150 mL of CH_2Cl_2 and filtered using a Schlenk filter under argon. Hexanes (60 mL) were added to the orange solution, and the solvents were evaporated until the total volume was reduced to 1/10. An orange crystalline product precipitated. Solvent evaporation was conducted under reduced pressure using a secondary solvent trap. The remaining supernatant was removed by a cannula. The crude product was washed several times with dry hexanes, while cooling the flask using an ice bath. 2.52 g (80%, lit 90%[239]) of orange product was obtained. Melting point 177-178^oC; IR (in CCl_4, cm^{-1}): 2137(v), 2050(s), 2000(m), lit. 2134(w), 2051(s), 2020(vw), 2000(m).[239]

η^6-Naphthalene(tricarbonyl)manganese(I) tetrafluoroborate (**28**): 1.00 g (3.64 mmol) of **27** was mixed with $AgBF_4$ (0.78 g, 4.0 mmol) in a 100 mL three-neck RB flask equipped with a vacuum adaptor and reflux condenser. After three quick evacuation-fill cycles at 0^oC, 50 mL of CH_2Cl_2 was added to the flask and the mixture was refluxed for 1 h in the dark. 0.94 g (7.3 mmol) of naphthalene was dissolved in 10 mL of CH_2Cl_2 in a 50 mL Schlenk flask and transferred to the RB flask using a cannula. The reaction mixture was allowed to reflux overnight under an inert atmosphere. After cooling to RT, the

reaction mixture was filtered through a Schlenk filter packed with a 1 cm Celite layer. The solution was concentrated to 20 mL under reduced pressure. Anhydrous diethyl ether was added to obtain a yellow precipitate. The crude product was washed several times with 0°C diethyl ether and then vacuum dried to obtain 1.12 g (yield 87%, lit 86%[166]) of **28**.

IR (CH_2Cl_2): 2078 and 2024 cm^{-1}, lit. 2077, 2022 cm^{-1} (ν_{CO});[189] ^1H NMR (300 MHz; CD_2Cl_2): δ = 8.07 (4H, br s, H1, H2, H3, H4), 7.35-7.49 (2H, m, H5, H8), 6.64-6.78 (2H, m, H6, H7). Chemical shifts agree with the values reported in the literature.[166, 167]

η^6-Dibenzo[*a*,*e*]cyclooctatetraene(tricarbonyl)manganese tetrafluoroborate (**36**): 0.41 g (2.0 mmol) of **1** and 0.78 g (2.2 mmol) of **28** were placed in a 100 mL Schlenk flask and three quick evacuation-fill cycles were performed. CH_2Cl_2 (50 mL) was added and the reaction was refluxed overnight. Upon cooling to RT, the solvent was evaporated under vacuum until the total volume was reduced to 10 mL. Cold anhydrous diethyl ether was added to the solution to obtain a yellow precipitate. The crude product was washed with cold diethyl ether several times to remove any unreacted ligands. 0.65 g (75%) of the yellow solid was obtained. XRD quality crystals were grown from solvent diffusion of diethyl ether into a concentrated solution of **36** in CH_2Cl_2. The crystallographic data for **36** are summarized in Table 2.3. NMR samples were prepared using Schlenk techniques with deoxygenated dichloromethane-d_2 as solvent.

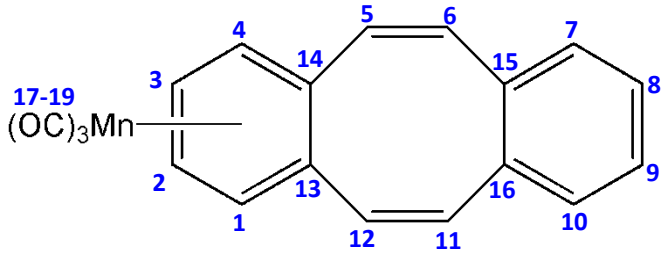

Figure 2.8 Numbering scheme for **36**

Melting point: 180-181°C (decomp.); IR (CH_2Cl_2): 2078 and 2022 cm^{-1} (ν_{CO}); ^1H NMR (600 MHz; CD_2Cl_2): δ = 7.44 (2H, br s, H8, H9), 7.25 (2H, br s, H7, H10), 7.17 (2H, d, ^3J =12.4, H6, H11), 6.47-6.64 (4H, m, H2, H3, H5, H12), 6.27 (2H, br s., H1, H4). ^{13}C NMR (600 MHz; CD_2Cl_2): δ = 214.06 (C17, C18, C19), 142.17 (C6, C11), 134.30 (C15, C16), 130.90 (C7, C10), 129.32 (C8, C9), 124.44 (C5, C12), 116.71 (C13, C14), 101.39 (C1, C4), 99.48 (C2, C3).

2D NMR (600 MHz; CD_2Cl_2); ^1H-^1H COSY cross peaks were found at (7.17, 6.54) and (6.57, 6.27). ^1H-^{13}C HMQC (Figure3.43) peaks found at (7.44, 129.32), (7.25, 130.90), (7.17, 142.17), (6.57, 99.48), (6.54, 124.44), and (6.27, 101.39). The HMBC spectrum (Figure3.44) gave peaks at (7.25, 129.32), (7.17, 134.30), (7.17, 130.90), (7.17, 124.44), (7.17, 116.71), (6.57, 101.39), (6.54, 142.17), (6.54, 134.30), (6.54, 116.71), (6.54, 101.39).

Table 2.3 Crystallographic parameters for **36**

empirical formula	$C_{19}H_{12}BF_4MnO_3$	Color	yellow translucent
formula weight	430.04	density (g cm^{-3})	1.62
crystal system	tetragonal	temperature (K)	100
space group	$P4_12_12$	wavelength (Å)	0.71073
final indices R_1, wR_2	0.0183, 0.0489	all data R_1, wR_2	0.0188, 0.0491
unit cell parameters			
a (Å)	11.5181(5)	α (deg)	90°
b (Å)	11.5181(5)	β (deg)	90°
c (Å)	26.5388(14)	γ (deg)	90°
V ($Å^3$)	3520.8(3)	Z	4

Attempted synthesis of η^6,η^6-Dibenzo[*a*,*e*]cyclooctatetraenebis(tricarbonyl)-manganese tetrafluoroborate (**37**): 0.020 g (0.10 mmol) of **1** and 0.14 g (0.40 mmol) of **28** were dissolved in 30 mL of CH_2Cl_2. The solution was refluxed for three days under an inert atmosphere using the experimental setup as shown in Figure 2.6a. Precipitation occurred during the reflux. After cooling to RT, the solids were isolated by carefully removing the solvent using a cannula. To remove any unreacted ligands, the product was washed with diethyl ether. The precipitate was vacuum dried to give 0.036 g of yellow solid. The supernatant removed from the reaction mixture was placed under vacuum and then diethyl ether was added to precipitate products. A minute amount of solid (< 0.010

g) was obtained from this process. The solid postulated to be a mixture of **36** and **37**. Monomanganese product was removed by washing with CH_2Cl_2.

Melting point: 185-187°C (decomp.); IR (ATR): 2072 and 2007 cm^{-1} (ν_{CO}). The solubility in a variety of organic solvents was evaluated. The product was not soluble in CH_2Cl_2, acetone, THF, MeOH, EtOH, toluene, or acetonitrile (either cold or hot) solvents. In H_2O, DMSO, and nitromethane solvents, **21** showed partial solubility in hot solutions. The failure to obtain a satisfactory NMR spectrum indicates that the product may have decomposed in these solvent systems. All attempts to obtain crystals were unsuccessful.

η^6-5,6,11,12-Tetrahydrodibenzo[*a*,*e*]cyclooctadiene(tricarbonyl)manganese tetrafluoroborate (**38**): Synthesis of this complex was similar to **36**. 0.42 g (2.0 mmol) of **13** and 0.78 g (2.2 mmol) of **28** was refluxed overnight in 50 mL of CH_2Cl_2 in a dry 100 mL Schlenk flask. A light yellow solid was isolated by filtration, washed with diethyl ether, and dried under vacuum. The yellow solid collected had a mass of 0.74 g (78%). Translucent yellow crystals were grown from diffusion of diethyl ether into a concentrated solution of acetone. Crystal data is given in Table 2.4. NMR samples were prepared using Schlenk techniques in deoxygenated dichloromethane-d_2.

Table 2.4 Crystallographic parameters for **38**

empirical formula	$C_{19}H_{16}BF_4MnO_3 \cdot {}^1/_2CH_2Cl_2$	color	light yellow translucent
formula weight	476.54	density (g cm^{-3})	1.63
crystal system	orthorhombic	Temperature (K)	100(2)
space group	$Pna2_1$	wavelength (Å)	0.71073
final indices R_1, wR_2	0.0263, 0.0647	all data R_1, wR_2	0.0280, 0.0658
unit cell parameters			
a (Å)	11.886(2)	α (deg)	90°
b (Å)	30.000(6)	β (deg)	90°
c (Å)	10.872(2)	γ (deg)	90°
V ($Å^3$)	3876.7(14)	Z	6

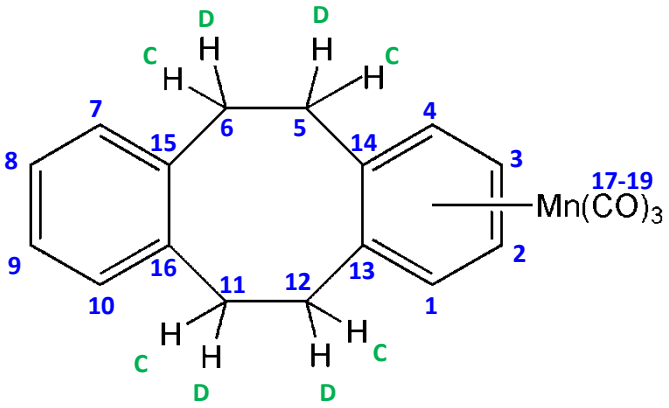

Figure 2.9 Numbering scheme for **38**

Melting point: 179.0-179.5°C (decomp.); IR (CH_2Cl_2): 2078 and 2028 cm^{-1} (ν_{CO}); ^1H NMR (600 MHz; CD_2Cl_2): δ = 6.90-7.22 (4H, m, H7, H8, H9, H10), 6.32 (2H, br s, H2, H3), 6.22 (2H, br s, H1, H4), 3.43 (2H, br s, H6C, H11C), 3.25 (2H, br s, H6D, H11D), 3.03 (4H, br s, H5C, H5D, H12C, H12D). ^{13}C NMR (600 MHz; CD_2Cl_2): δ = 214.98 (C17, C18, C19), 137.89 (C15, C16), 130.85 (C7, C10), 128.35 (C8, C9), 120.43 (C13, C14), 101.75 (C1, C4), 99.51 (C2, C3), 33.62 (C5, C6, C11, C12).

2D NMR (600 MHz; CD_2Cl_2); Non-diagonal cross peaks were found in the ^1H-^1H COSY (Figure 3.45) spectrum at (6.32, 6.22), (3.43, 3.03), and (3.25, 3.03). Direct couplings for ^1H-^{13}C HMQC (Figure 3.46) were found at (7.10, 128.35), (7.07, 130.85), (6.32, 99.51), (6.22, 101.75), (3.43, 33.62), (3.25, 33.62), and (3.03, 33.62). HMBC spectra (figure 2.10) indicated long range couplings at (7.10, 130.87), (7.07, 137.89), (7.07, 128.35), (7.07, 33.62), (6.32, 120.43), (6.32, 101.75), (6.22, 120.43), (6.22, 99.51), (6.22, 33.62), (3.43, 137.89), (3.43, 130.85), (3.43, 120.43), (3.43, 101.75), (3.43, 33.62), (3.25, 137.89), (3.25, 120.43), (3.25, 101.75), (3.25, 33.62), (3.03, 137.89), (3.03, 130.85), (3.03, 120.43), (3.03, 101.75), (3.03, 33.62).

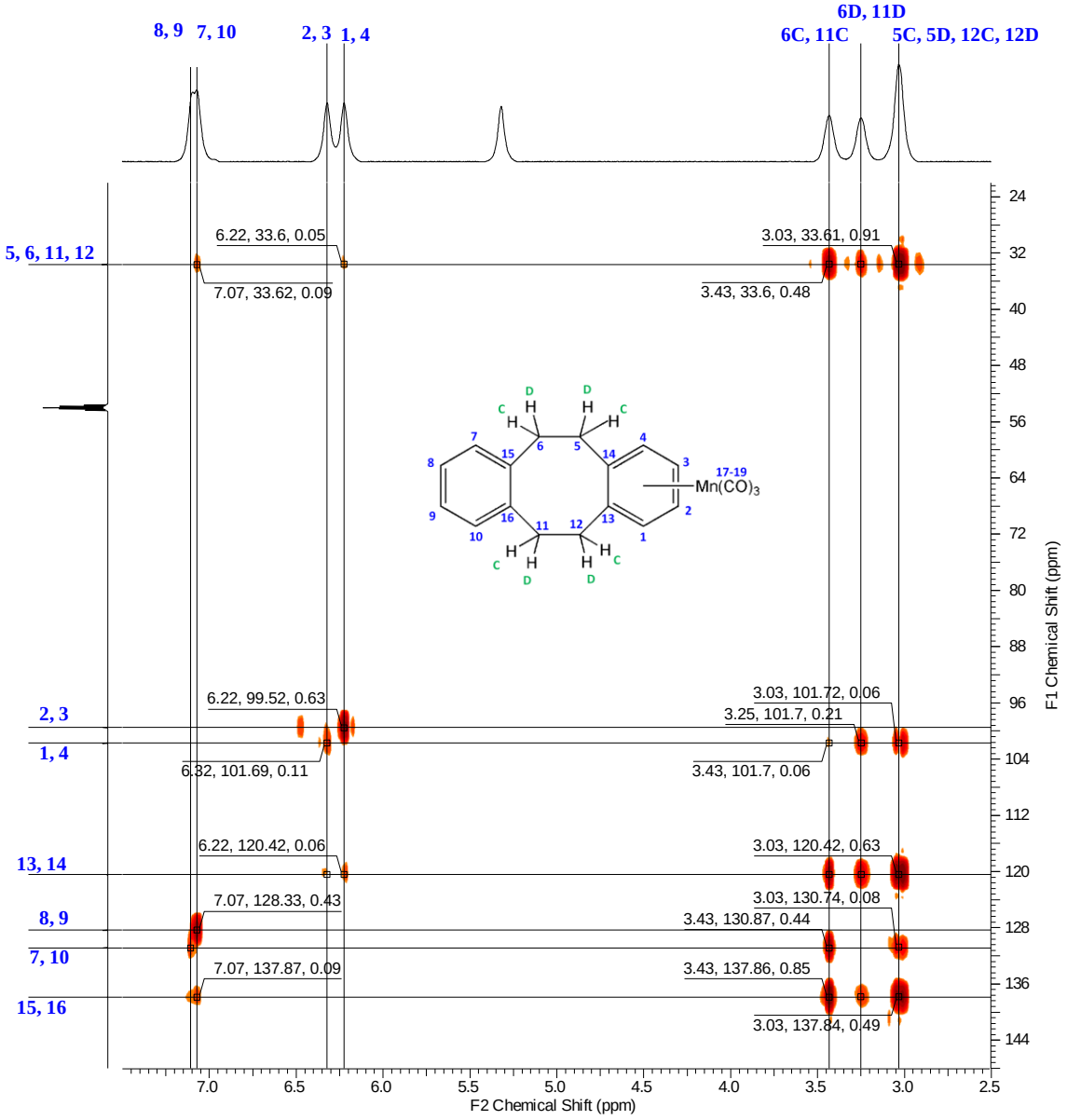

Figure 2.10 HMBC spectrum of **38**; 600 MHz, RT, CD_2Cl_2

Attempted synthesis of η^6,η^6-5,6,11,12-tetrahydrodibenzo[*a*,*e*]cycloocta-dienebis(tricarbonyl)manganese tetrafluoroborate (**39**): The attempted synthesis was carried out using a similar method to that for **37**. 0.021 g (0.10 mmol) of **13** and 0.14 g (0.40 mmol) of **28** were refluxed in 30 mL of CH_2Cl_2 for three days. A solid precipitated

during the reflux. After cooling to RT, precipitates in the flask were isolated by carefully removing the solvent using a cannula. Unreacted ligands were removed by washing with diethyl ether. The yellow solid was vacuum dried to yield 0.041 g.

Melting point: 187-189°C (decomp.); IR (ATR): 2074 and 2017 cm^{-1} (ν_{CO}). The solubility was tested for **39** and results show that it was not soluble in CH_2Cl_2, acetone, THF, MeOH, EtOH, toluene, or acetonitrile. All attempts to obtain crystals were unsuccessful.

Attempted synthesis of η^6,η^6-dibenzo[*a*,*e*]cyclooctatetraene-*anti*-(tricarbonyl)chromium(0)-*syn*-(tricarbonyl)manganese(I) tetrafluoroborate (**40**): 0.034 g (0.10 mmol) of **29** and 0.036 g (0.10 mmol) of **28** were added to a 50 mL Schlenk flask. Three evacuation-fill cycles were performed at 0°C. 20 mL of freshly distilled CH_2Cl_2 was added and the solution was refluxed for two days with argon purge above the condenser. During reflux, the solution's color changed from yellow to orange. An orange color precipitate was observed after 20 h of reflux. After 2 days of reflux, the solid precipitate on the bottom of the flask was isolated by carefully removing the solvent using a cannula. The product was washed with cold diethyl ether, and dried under vacuum to obtain 0.031 g of product. Similar to the solubilities of **37** and **39**, **40** was also not soluble in most solvents. IR (ATR): 2074, 2022, and 1931 (br) cm^{-1} (ν_{CO}).

Crystallization of η^6-dibenzo[*a*,*e*]cyclooctatetraene-*anti*-(tricarbonyl)chromium ·0.5naphthalene (**41**): During the initial attempt to synthesize **40**, product **41** was obtained. 0.034 g (0.10 mmol) of **29** and 0.039 g (0.11 mmol) of **28** was refluxed in 20 mL of freshly distilled CH_2Cl_2 for two days with argon purge above the condenser.

During the reflux, a precipitate was not observed as expected, and no color change was observed. After two days of reflux, the reaction was allowed to cool to RT and the solvent was evaporated under vacuum until the total volume was reduced to 10 mL. Anhydrous diethyl ether was added to the solution to obtain a yellow colored solid. The crude product was carefully washed with cold diethyl ether to remove any ligands present. After drying under vacuum, 0.018 g (yield 45%) of product was obtained. ATR 1950 and 1855 cm^{-1} (ν_{CO}).

The product was partially soluble in CH_2Cl_2. The solid was dissolved in about 20 ml of CH_2Cl_2 at RT. Using a vacuum pump, the solvent was reduced to 12 mL without any precipitation. Two separate systems were set up to grow crystals. One was by slow cooling and the other by slow solvent diffusion with diethyl ether under an inert atmosphere. After three weeks, translucent needle-like crystals were found in the low temperature system. Crystallographic parameters are listed in Table 2.5. All attempts to synthesize the product using **29** with different ratios (1:0.5, 1:1, 1:2, 1:3, and 1:4) of naphthalene failed.

Table 2.5 Crystallographic parameters for **41**

empirical formula	$C_{16}H_{12}CrO_3 \cdot {}^1/_2C_{10}H_8$	color	light yellow translucent
formula weight	404.37	density (g cm^{-3})	1.37
crystal system	triclinic	Temperature (K)	100(2)
space group	$P\bar{1}$	wavelength (Å)	0.71073
final indices R_1, wR_2	0.0854, 0.1812	all data R_1, wR_2	0.2235, 0.2445
unit cell parameters			
a (Å)	11.524(5)	α (deg)	83.998(5)°
b (Å)	12.141(5)	β (deg)	74.506(5)°
c (Å)	16.278(6)	γ (deg)	62.988(4)°
V ($Å^3$)	1954.9(13)	Z	4

2.2 Variable temperature NMR experiments

2.2.1 Sample preparation

All metallic complexes were highly air sensitive in solution. Degassed deuterated solvents were used at all times and samples were prepared under inert conditions. Septum-sealed NMR tubes were dried under vacuum for 1 h and flushed with Ar. The product was dissolved in 0.6-0.8 mL of deuterated solvent in a dry 5 mL Schlenk flask with continuous stirring. The sample was transferred to the NMR tube using a cannula with filtering through a 1 mL syringe packed with a thin glass wool layer. Acetone-d_6 was used as the solvent for chromium complexes and dichloromethane-d_2 was used as the

solvent for the manganese complexes. Due to light sensitivity, the manganese samples were prepared in the dark and kept covered with aluminum foil until the NMR analysis was performed. Commercial deuterated methanol without further purification was used for the temperature calibrations.

2.2.2 Temperature calibration of NMR spectrometers

^{1}H NMR spectra were taken at varying temperatures ranging from 300 to 200 K. The thermocouple was calibrated using methanol thermometer. The chemical shifts from residual peaks of methanol in deuterated methanol are known for their temperature dependence due to intermolecular hydrogen bonding.[211] The temperature was lowered in 5^{o}C steps, allowed to stabilize for approximately 10 min, and the ^{1}H NMR spectrum was obtained. The chemical shift difference ($\Delta\delta$) between the OH and CHD_2 at each set temperature (T_{set}) was determined, and the actual temperature of the sample was calculated (T_{cal}) according to the quadratic equation established by Findeisen *et al.*[212] The temperature calibration plot for the 600 MHz field strength is shown in Figure 2.12. The relationships determined for temperature corrections for the two field strengths are listed in Table 2.5.

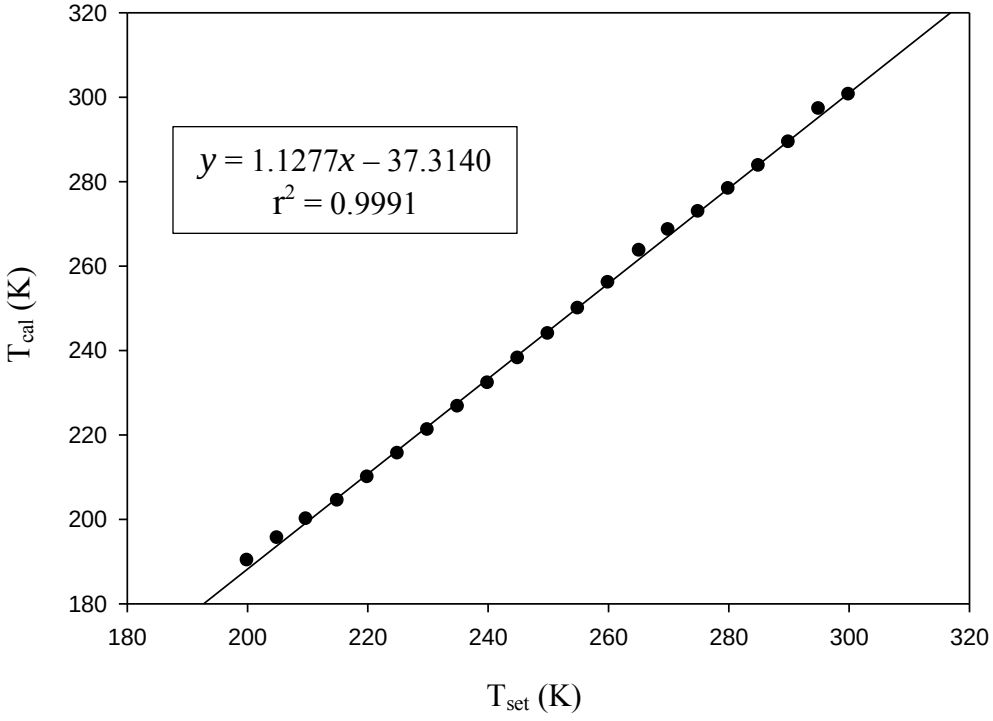

Figure 2.11 Temperature calibration plot, 600 MHz, 300 K to 200K

Table 2.6 Formulas from temperature calibration for field strengths of 300 and 600 MHz

Field strength	Temperature correction
600 MHz	$T_{cal} = 1.1277T_{set} - 37.3140$
300 MHz	$T_{cal} = 0.9878T_{set} + 2.9378$

2.2.3 NMR at varying temperatures

Dynamic ^{1}H NMR studies were conducted for samples **29**, **30** and **36**, at temperatures varying from 300 K to 180 K at field strengths of 300 MHz and 600 MHz. The temperature was reduced in 5^{o}C steps, and around important temperature regions, the NMR spectra were obtained at every 1^{o}C change. Once the desired temperature was reached, the sample was allowed to equilibrate for 10 min prior to the NMR spectral scan. ^{1}H NMR spectra for all temperature values and some ^{13}C NMR spectra were obtained. Experimental spectra are shown in Figures 3.4-3.5, followed by discussion in section 3.1.

2.2.4 Line shape analysis

Spectral simulations were performed using gNMR simulation software for field strengths of both 300 MHz and 600 MHz.[228] By comparison of experimental spectra and simulated spectra, rate constants at the various temperatures were obtained (Figure 3.15). The thermodynamic parameters for the ring inversion process of **30** were calculated for both field strengths (Table 3.3) and are discussed in chapter 3.

2.3 Electrochemical studies

CV experiments were conducted in three stages. Initially, supporting electrolyte was dissolved in 10 mL of solvent under argon and scanned for background signals. Then, 1.0 mmol of the analyte was introduced to the cell and the voltage was swept. Finally, 1.0 mmol of ferrocene was added to the system and the CV obtained. TEAP (0.25 mol) was used as the supporting electrolyte for PC solvent systems. When THF was

used as the solvent, TBAP (0.2 mol) or TBAHFP (0.2 mol) was used as supporting electrolyte. A positive pressure of Ar was maintained throughout the study. The electrodes were polished with a sand paper (1000 grit) prior to use, maintaining a clean surface for electrochemical studies.

The sweeps were conducted in both positive and negative directions while varying scan rates from 0.01 mV s^{-1} to 5 mV s^{-1}. All E_p values were corrected to Fc/Fc^+ as 0.00 V. Simulations were attempted using BASi DigiSim software.[240] Products **29** and **30** were analyzed in the electrochemical study and the $(E_{pa}+E_{pc})/2$ values were calculated. $(E_{pa}+E_{pc})/2$ values for **29** and **30** were found to be at -2.17 V and -2.11 V with respect to the Fc/Fc^+.

The results and a detailed discussion of the above experiments will be presented in the next chapter. These discussions include the synthetic procedure, NMR results of the variable temperature study, and crystallography. The bond angles and the bond lengths of the crystal structures are listed in the appendix.

CHAPTER III

RESULTS & DISCUSSION

The results and discussion chapter of this dissertation is divided into five sections. The first part discusses the study of the ring inversion of **30**. The second section involves the synthesis of new organometallic complexes and their structures. NMR characterization of the monometallic complexes is discussed in the third section. The electrochemical studies are discussed in the fourth section. Finally, theoretical calculations are used to help explain the experimental results.

3.1 Ring inversion studies on the *syn,anti*-DBCOT[Cr(CO)$_3$]$_2$ complex

3.1.1 Spectral assignments and the evidence for dynamic process

At room temperature, the ^{1}H NMR spectrum of ligand **1** shows three peaks. A singlet is observed at 6.77 ppm for the alkene protons and multiplets were found at 7.07 and 7.15 ppm for the arene protons. The DBCOT molecule is known to have a tub conformation in the ground state with C_{2V} symmetry (Figure 1.9).[1] Therefore, three proton peaks are expected in the ^{1}H NMR spectrum as observed. Experimental 2D NMR spectroscopy was employed to identify the peaks associated with the α (H1, H4, H7, H10) and β (H2, H3, H8, H9) protons.

From the non-diagonal peak (6.77, 7.07) observed in the ^{1}H-^{1}H COSY 2D NMR spectrum (not shown), the arene proton peaks at 7.07 ppm can be identified as resulting

from the α protons. This is straightforward because the β protons are too far to correlate with the alkene protons. The above assignment can be verified from the results of ^{1}H-^{13}C HMBC experiment (Figure 3.1). The direct ^{1}H-^{13}C correlations observed from the HMQC spectrum were shown in Figure 2.4. The splitting pattern observed for the arene protons correspond to the AA′BB′ system in the Pople notation.[241, 242] Similar splitting can be observed in the ^{1}H NMR spectrum of naphthalene.[241]

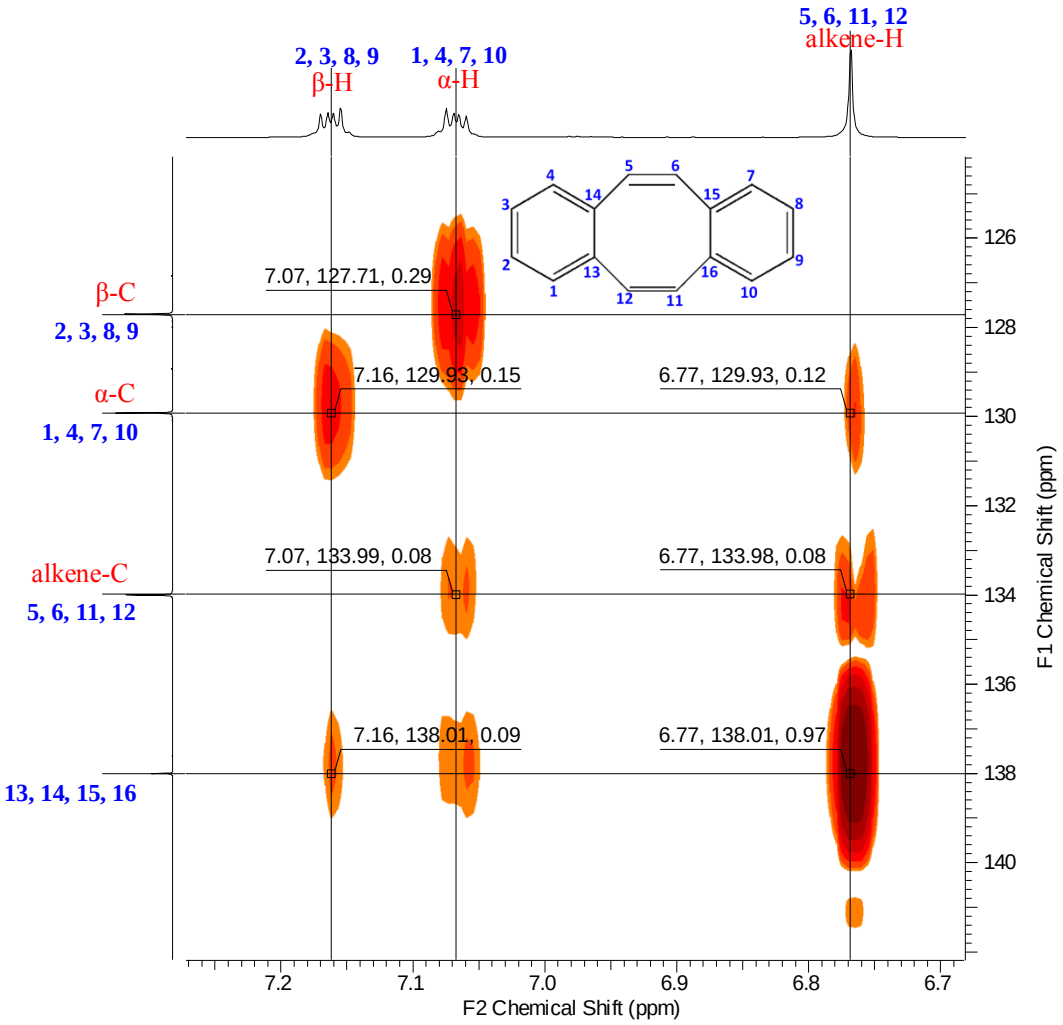

Figure 3.1 HMBC spectrum of **1**; 600 MHz, RT, acetone-d_6.

In the HMBC spectrum, the α carbons (130.00 ppm) show two bond correlation to the β protons (7.15 ppm) and three bond coupling to the alkene protons, where the β carbons (127.80 ppm) only show two bond correlation with the α protons (Figure 3.1). These assignments agree with the spectral assignments for **10** by Berno *et al.*[74] Therefore, the beta protons are deshielded compared to the alpha protons.

Interestingly, the metal complex of **30** at room temperature also shows only three ^{1}H NMR peaks with a singlet at 6.65 ppm, a multiplet at 5.71 ppm, and a broad singlet at 5.57 ppm (Figure 3.2b). With the coordination of electron withdrawing metal moieties, all protons are shifted upfield in the NMR spectrum with arene protons shifted about 1.5 ppm.[243-246] As in BCOT and DBCOT, the α protons appear to be more shielded relative to the β protons. However, in the ^{1}H NMR spectrum of **30**, the α protons show a broad singlet compared to the AA′BB′ multiplet of the β protons. The lack of fine structure for the α+α′ protons at RT is due to different coupling constants between the A+α and A′+α′ protons. This difference results in a broad peak when the proton resonances are averaged.

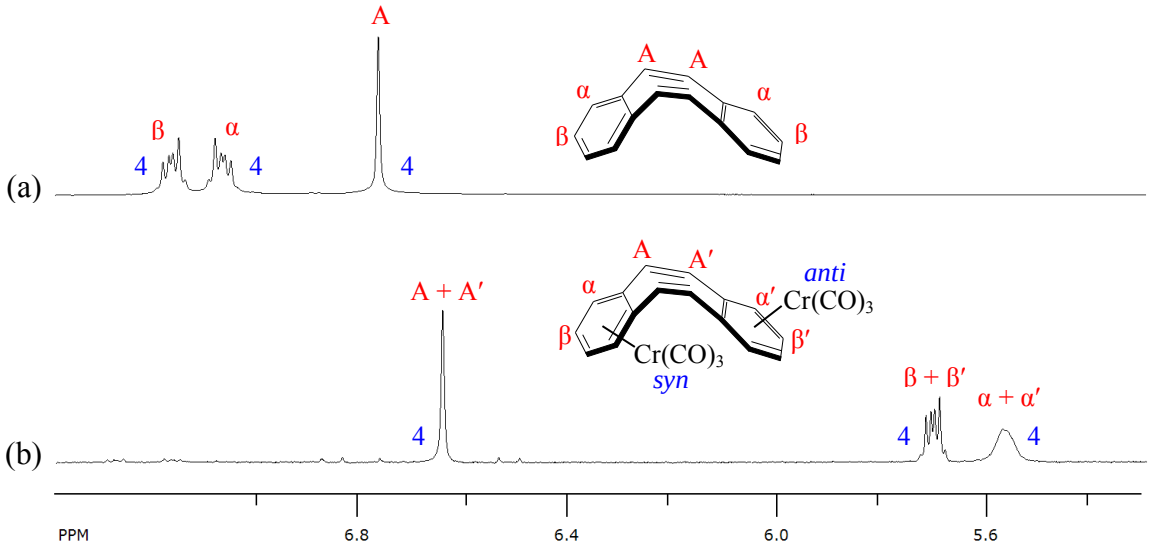

Figure 3.2 RT ^{1}H NMR spectra of (a) **1**, and (b) **30** in acetone-d_6 with 600 MHz. The proton assignments are given in red and the integrations are shown in blue.

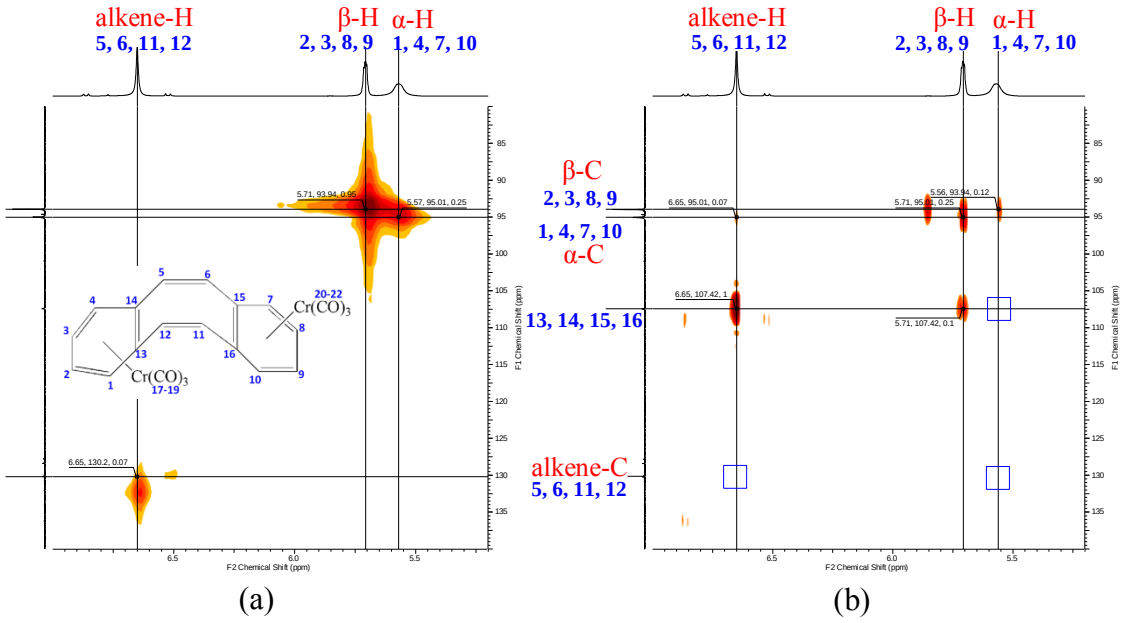

Figure 3.3 2D NMR spectra of **30**; 600 MHz, RT, acetone-d_6; (a) HMQC, and (b) HMBC; expected cross peaks missing in HMBC are indicated with blue squares.

Cross coupling peaks were not observed in the ^{1}H-^{1}H COSY spectrum (not shown) of **30**. In the HMBC spectrum, the cross peaks expected from the α protons to the carbons contained in both rings (5.57, 107.42), and coupling of the alkene protons and the α protons to the alkene carbons [(6.65, 130.20) and (5.57, 130.20)] were not observed (Figure 3.3b, indicated with blue squares). Therefore, the arene protons and the carbons were assigned with the aid of theoretical calculations and previous assignments for similar systems (Table 3.1).[74]

^{1}H NMR chemical shifts were calculated using the 6-31G**/B3LYP basis set. The calculated chemical shift values (ppm) are 7.66 (H6, H11), 7.52 (H5, H12), 6.40 (H8, H9), 6.38 (H7, H10), 6.28 (H2, H3), and 6.04 (H1, H4). The calculated ^{13}C NMR values are 228.94 (C20, unique CO, *endo*), 228.50 (C21, C22), 227. 95 (C19, unique CO), 227.15 (C17, C18), 131.94 (C6, C11), 126.96 (C5, C12), 105.94 (C13, C14), 103.48 (C15, C16), 93.36 (C7, C10), 90.65 (C1, C4), 90.13 (C8, C9) and 89.14 (C2, C3). These assignments correlate to the low temperature NMR results. In order to obtain calculated ^{1}H and ^{13}C chemical shifts at RT, the chemical shift values for exchanging centers were averaged. The average chemical shifts in the ^{1}H NMR spectrum calculated as 7.59 (H5, H6, H11, H12), 6.34 (H2, H3, H8, H9), and 6.21 (H1, H4, H7, H10). ^{13}C NMR chemical shifts at RT are 228.03 (C17, C18, C19, C20, C21, C22), 129.45 (C5, C6, C11, C12), 104.71 (C13, C14, C15, C16), 92.01 (C1, C4, C7, C10), 89.64 (C2, C3, C8, C9). The experimental chemical shifts for BCOT and its π-arene chromium complex reported by Berno *et al.* are summarized in Table 3.1 and the numbering scheme is shown in Figure 3.4.[74]

Table 3.1 NMR chemical shifts reported for BCOT and its π-arene chromium complex[74]

Position	BCOT		$BCOTCr(CO)_3$	
	^{1}H NMR	^{13}C NMR	^{1}H NMR	^{13}C NMR
1, 4	6.95	130.51	5.43	95.33
2, 3	7.20	127.76	5.63	93.90
5, 10	6.53	134.45	6.30	130.40
6, 9	6.01	131.93	6.11	133.76
7, 8	5.85	131.68	6.00	130.69
11, 12	-	138.98	-	109.38

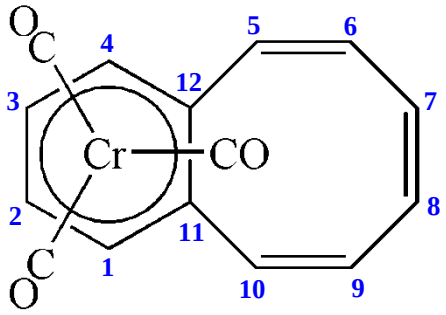

Figure 3.4 Numbering scheme for BCOT chromium complex

According to crystallographic results for complex **30**, the two chromiumtricarbonyl moieties coordinate to the DBCOT tub in both *syn* and *anti* orientations (Figure 1.17).[190] This orientation requires that the hydrogen atoms on different sides of the DBCOT backbone should result in separate NMR peaks. However,

the experimental NMR spectrum at RT clearly indicates only three peaks (Müller *et al.* in 1969 using 60 MHz field strength observed only two peaks, where all arene protons were seen as one multiplet at 5.74 ppm).[189] The four alkene protons (H5, H6, H11, H12) of the eight-membered ring averaged to a single peak in the ^{1}H NMR spectrum at RT. This observation clearly suggests a fluxional behavior for **30** in solution.

3.1.2 Low temperature NMR

In order to verify the fluxionality, the ^{1}H NMR spectrum of **30** was obtained using acetone-d_6 as the solvent at low temperature (Figure 3.5b). At 180 K, five proton peaks were observed with a relative integration of 2:2:4:2:2. The alkene protons appeared as two doublets at 6.82 and 6.67 ppm with a coupling of 12 Hz. The change from singlet to two doublets with the temperature reduction confirms that a ring inversion for the DBCOT organic backbone in the bischromium complex (Scheme 3.1) is occurring. The averaging of both A and A′ protons was observed as a peak at 6.65 ppm at room temperature.

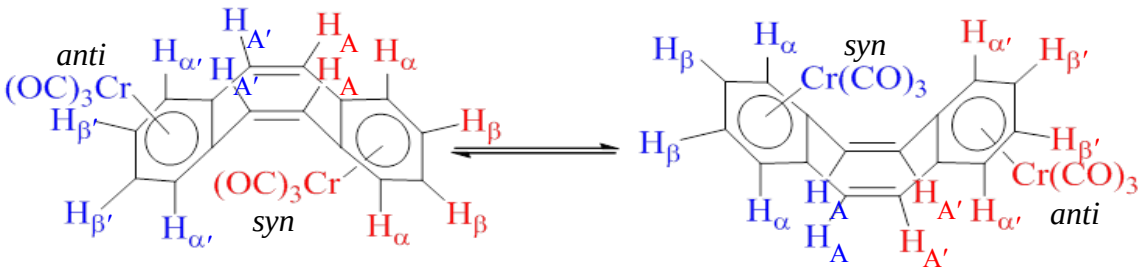

Scheme 3.1 Ring inversion of **30**

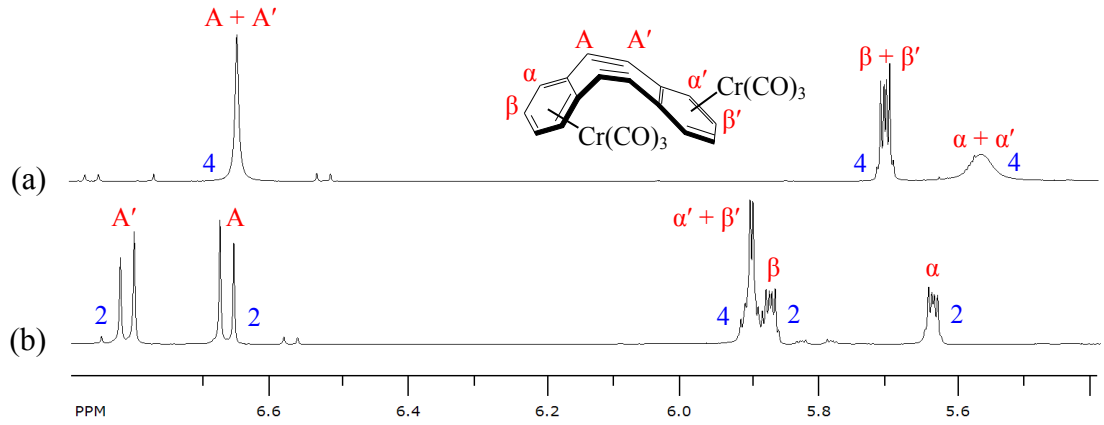

Figure 3.5 ^{1}H NMR spectra of **30** in acetone-d_6, 600 MHz; (a) 293 K, and (b) 180 K. The proton assignments are given in red and the integrations are shown in blue.

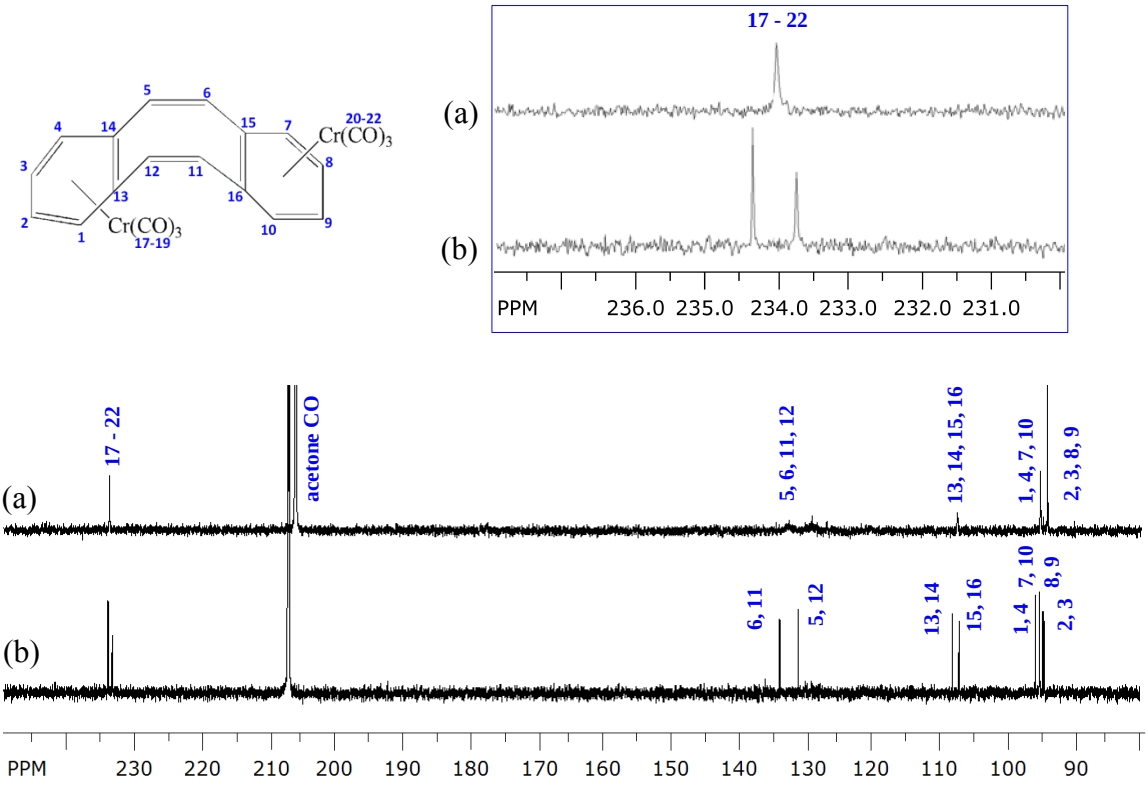

Figure 3.6 ^{13}C NMR spectra of **30** in acetone-d_6, 600 MHz; (a) 293 K and (b) 180 K; The carbonyl peaks are highlighted in the blue insert.

Likewise, in the ^{13}C NMR spectrum, the number of peaks doubled when going from RT to low temperature (Figure 3.6). The low temperature peaks were assigned based on the theoretical calculations. There are three separate dynamic processes that take place in solution for complex **30**. They are the ring inversion of the carbon skeleton, rotation of the *syn*-tricarbonylchromium group, and rotation of the *anti*-tricarbonylchromium group. By reducing the temperature, the possibility existed that the first two of these processes would become slow on the time frame of the experiment. However, the ^{13}C NMR spectrum indicated that the rotation of the *syn*-tricarbonyl chromium unit was not slowed significantly because only two carbonyl peaks were observed for the carbonyl carbons at 180 K (Figure 3.6). If the *syn*-carbonyl rotation is frozen out, three peaks with a 3:2:1 integration ratio should be observed in the ^{13}C NMR spectrum. A 1:2:1:2 carbonyl carbon ratio is predicted by theoretical calculations for the static molecule. From previous studies and calculations it is highly unlikely that the slowed rotation of the *anti*-chromiumtricarbonyl rotation would ever be observed by NMR in solution. As discussed later in this chapter the calculation of the barrier to rotation suggests *syn*-carbonyl rotation will not be slow under the experimental conditions. Tricarbonyl rotations are observed even in the solid state.[247-249] The carbonyl peaks in the solid state ^{13}C NMR spectrum of (η^6-$C_6H_5CH_3$)$M(CO)_3$; M = Cr and Mo) sharpened as the temeperature changed from RT.[247]

The primary objective of this research is to evaluate the ring inversion of **30**. A variable temperature NMR experiment can be used to study the ring inversion process. When performing a variable temperature NMR experiment, relevant spectral changes are

recorded as a function of their respective temperatures. Therefore, the accuracy of the temperature values plays a vital part in a dynamic study.[210, 212] It is important to perform a calibration of the temperature control unit prior to VT NMR analysis.

3.1.3 Temperature calibration for the NMR spectrometers

The temperature displayed by the NMR spectrometers may be different than the sample temperature. These temperature differences can result from poor thermocouple calibration, heat loss issues, and gas flow interferences between the thermocouple and sample. When a high degree of accuracy is desired, the best option is to directly measure the sample temperature using an external source. In 1968, Anthony van Geet developed a thermistor probe which gives an accurate temperature reading in a 5 mm NMR sample tube.[210] The use of a thermocouple is another popular method where small temperature changes can be measured from voltage changes.[211] An economical alternative to get accurate readings is to calibrate the sample temperature relative to the displayed temperature reading. Temperature calibration can be achieved using a sample with a temperature-dependent chemical shift. Generally, methanol and ethylene glycol samples are used for low temperature and high temperature NMR calibrations, respectively.[210, 212]

In early spectrometers, a mixture of methanol and deuterated methanol with a trace amount of HCl (0.03% v/v) was used for low temperature calibrations.[211] With the slow exchange of protons, a broadening can be observed at the OH peak in MeOH. When HCl is introduced, the peaks are sharpened by increasing the exchange rate.[211, 250] In 2007, Findeisen *et al*. reported that for modern NMR spectrometers, pure MeOD-d_4 can be used to obtain accurate temperature readings.[212]

Van Geet in 1968 established a quadratic relationship resulting from a chemical shift difference between the methanol peaks and temperature.[210] This relationship was further improved in 1970, covering a 175 K to 330 K temperature range (Equation 3.1).[211] In Equation 3.1, the chemical shift differences are recorded in Hz for a 60 MHz spectrometer and the conversion to ppm values are shown in Equation 3.2. In 1982, Amman *et al.* reported a slightly modified relationship (Equation 3.3) using a Pt resistor.[251] The most recent quadratic relationship for temperature calibrations was reported by Findeisen *et al.* in 2007 (Equation 3.4).[212]

$$T(K) = 403.0 - 0.491\Delta\nu - 66.2(10^{-2}\Delta\nu)^2 \quad (3.1)$$

$$T(K) = 403.0 - 29.46\Delta\delta - 23.832\Delta\delta^2 \quad (3.2)$$

$$T(K) = 409.0 - 36.54\Delta\delta - 21.85\Delta\delta^2 \quad (3.3)$$

$$T(K) = 419.1381 - 52.5130\Delta\delta - 16.7467\Delta\delta^2 \quad (3.4)$$

In this study, a neat methanol-d_4 sample was used, and the chemical shift difference between the OH and CHD_2 peaks was measured for temperatures ranging from 200 K to 300 K. The sample temperature was calculated (T_{cal}) using equation 3.4, and T_{cal} *vs* T_{set} (set temperature using the spectrometer's variable temperature unit) was plotted. The T_{cal} *vs* T_{set} plots resulting from both the 600 and 300 MHz instrument calibrations are displayed in Figures 2.12 and 3.7, respectively. Ordinary least squares analysis was used to calculate the slopes and intercepts for the data. The errors associated with the T_{cal} values were calculated as 1.1 and 0.7 K for 600 and 300 MHz field strengths,

respectively. Temperature corrections for both 600 and 300MHz field strengths were performed according to Equations 3.5 and 3.6, respectively.

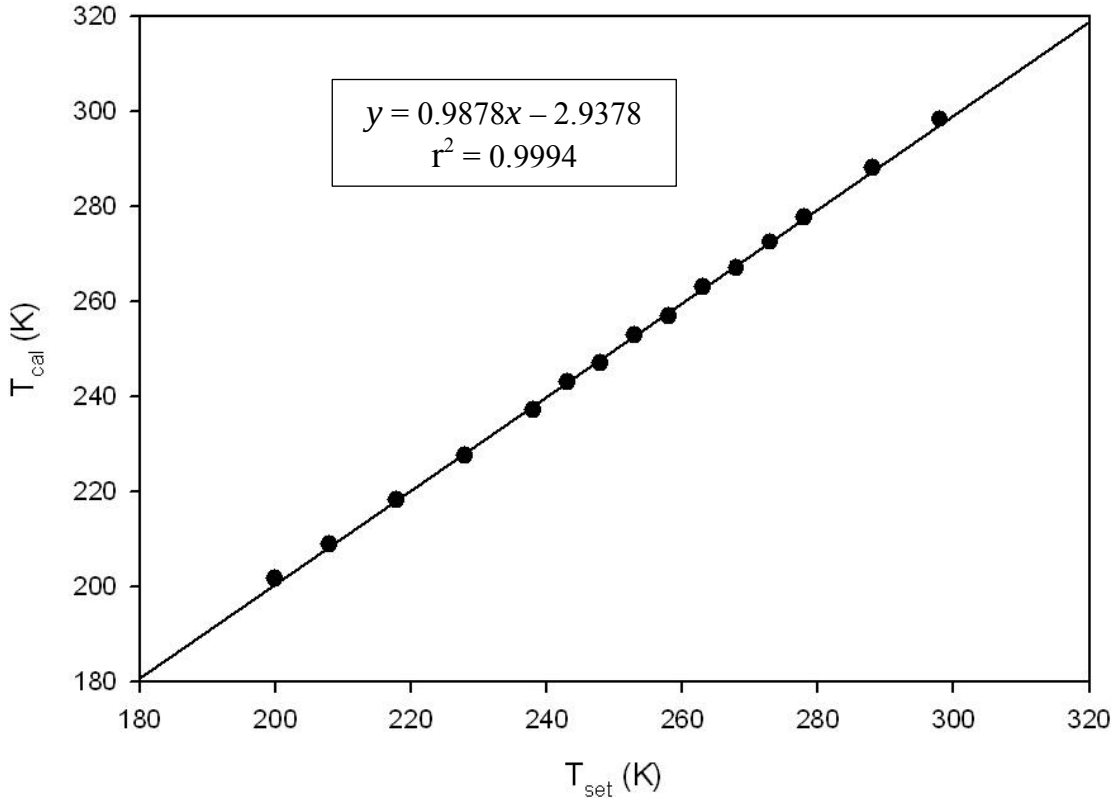

Figure 3.7 Temperature calibration plot, 300 MHz, temperature range 200 K to 300 K.

$$T_{cal} = 1.1277 \cdot T_{set} - 37.3140 \quad (3.5)$$

$$T_{cal} = 0.9878 \cdot T_{set} - 2.9378 \quad (3.6)$$

3.1.4 Spectral reference with TMS

The use of TMS in proton NMR spectra was introduced by Tiers in 1958.[224] The International Union of Pure and Applied Chemistry (IUPAC) recognizes TMS as the internal standard for ^{1}H, ^{13}C and ^{29}Si NMR experiments.[252] Generally, chemical shifts are reported downfield from the TMS signal, which is positioned at 0 ppm. However, it is known that TMS shows a temperature-dependent chemical shift.[253-258] In 1975, Jameson *et al.* reported a series of experiments where chemical shifts were measured relative to the ^{129}Xe resonance frequency.[255] The TMS chemical shift dependence in the ^{1}H NMR spectrum with respect to the temperature (range of 273 to 190 K) was derived as in Equation 3.7.

$$\delta_{TMS}(ppm) = -4.13 \times 10^{-5} - 5.14 \times 10^{-3} \cdot T(^{o}C) - 2.8 \times 10^{-5} \cdot [T(^{o}C)]^{2} \qquad (3.7)$$

During the variable temperature studies of **30** with TMS assigned at 0 ppm, a slight downfield shift was observed for all peaks which correlated to the lowering of the temperature (Figure 3.8). Therefore, Equation 3.7 was used to introduce a corrected TMS value associated with the change in temperature (Figure 3.9). However, the TMS corrections were not helpful in rectifying the temperature dependent shift observed for complex protons. Therefore, the use of correction of temperature dependence for TMS was ignored in this research, and at all temperatures, the TMS chemical shift was assigned as 0 ppm. However, in some figures for the clarity of analysis, the spectral series can be found vertically aligned to chemical shift positions for protons of the complex rather than the TMS reference.

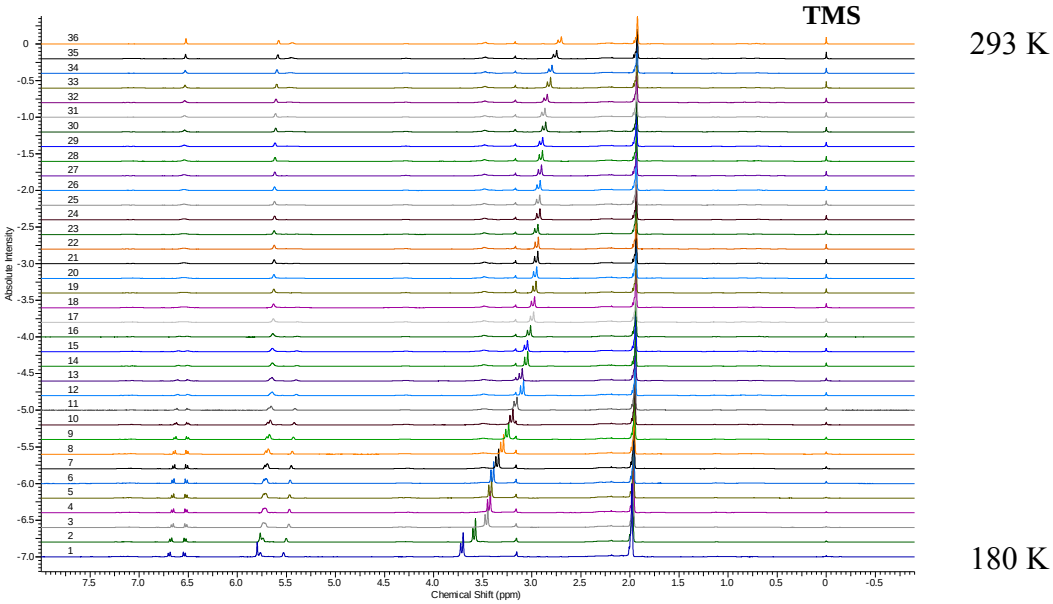

Figure 3.8 VT NMR spectra for **30**, 300 MHz, temperature range 180 K to 293 K, -1 to 8 ppm, TMS assigned at 0 ppm to all temperatures.

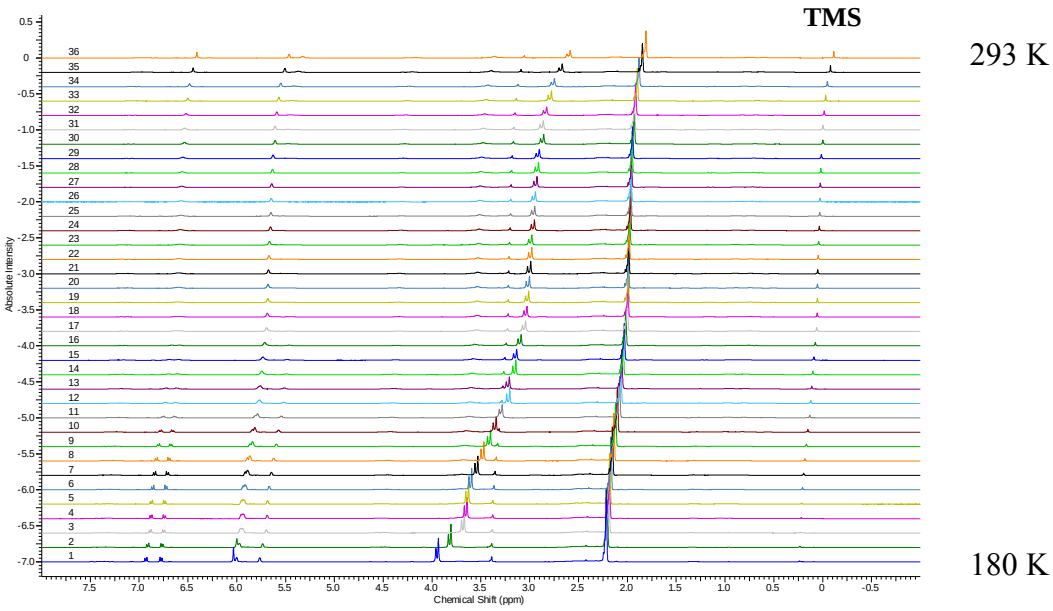

Figure 3.9 VT NMR spectra for **30**, 300 MHz, temperature range 180 K to 293 K, -1 to 8 ppm, TMS position was calculated and assigned according to Equation 3.7 for the respective temperatures.

3.1.5 Variable temperature NMR analysis

After temperature calibrations, a complete dynamic ^{1}H NMR study was conducted for **30** at temperatures varying from 293 K to 180 K using both the 300 and 600 MHz spectrometers. Some of the spectra obtained from the 600 MHz instrument are shown in Figure 3.10. When the temperature was lowered, the singlet observed for the alkene protons broadened and split into two doublets (for the A and A′ protons). The arene protons also changed from the integration ratio of 4:4 at RT to 4:2:2 at low temperature. These spectra were taken with the NMR spinner turned off because of condensation issues and it did not adversely effect on alkene proton resonance.

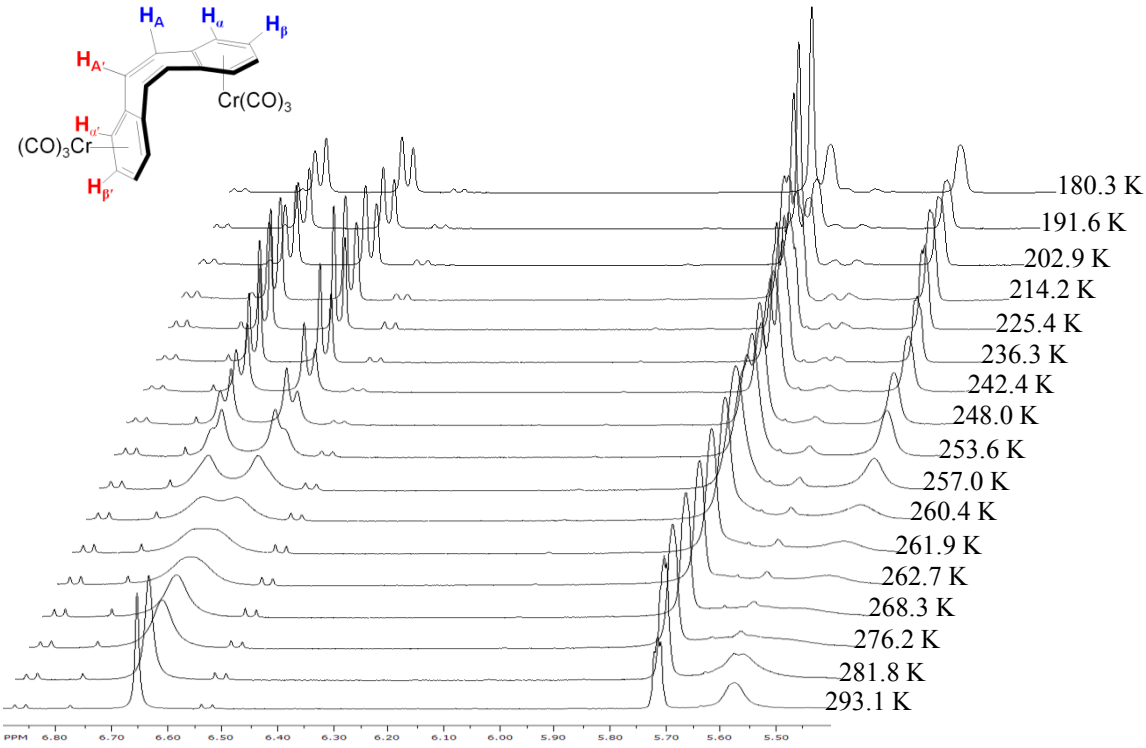

Figure 3.10 ^{1}H NMR spectra of **30** in acetone-d_6, 600 MHz, 293 to 180 K, 5.5 to 6.9 ppm, All spectra were aligned with the center of alkene proton peaks at 6.65 ppm.

The spectral changes occurring in the alkene proton region can be directly correlated to the reversible ring flip dynamic process occurring in the DBCOT backbone. The situation was complicated for the arene protons. At low temperatures, the hydrogens associated with the *syn* moiety split into α and β protons, and *anti* moiety arene protons (α′ + β′) appeared at the same chemical shift (Figures 3.5b, 3.10, and 3.11) giving a single peak. The arene proton assignments are based upon calculations. The α protons being the most shielded is reasonable, however the α′ protons located at the least shielded arene position creates some ambiguity. Then again, if both β and β′ protons were placed at the same position at low temperature, a line broadening should not be seen in the spectra with the averaging of β and β′ protons. Additionally, in the ^{1}H NMR spectrum of the *anti*-DBCOTCrCO_3 complex, both α′ and β′ appear at similar chemical shift positions.

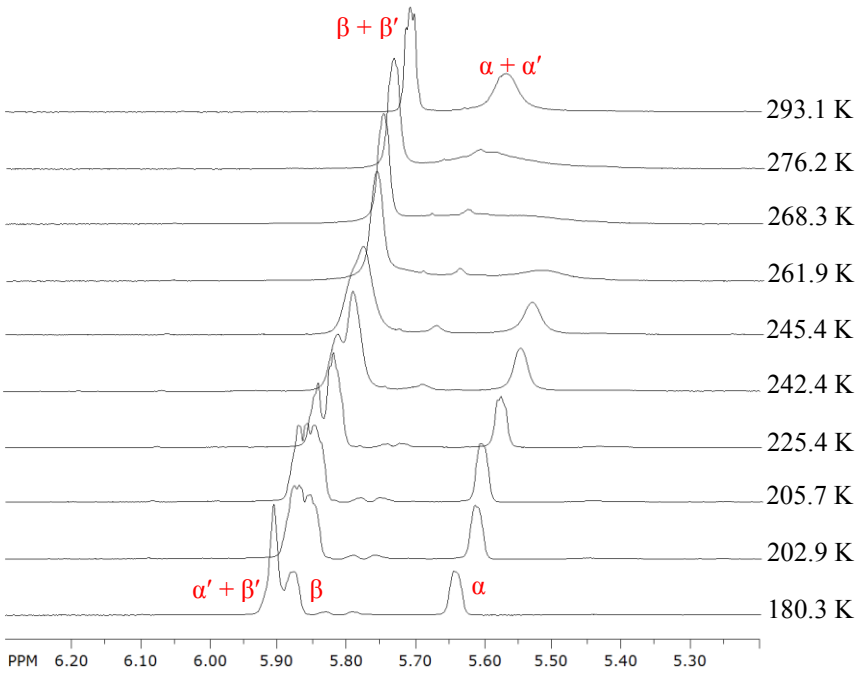

Figure 3.11 ^{1}H NMR spectra of **30** in acetone-d_6, 600 MHz, arene protons, 293 to 180 K

Most RI studies conducted for eight-membered rings have been done with a functional group present. For example, for **1b** (Figure 1.11), the DBCOT RI was studied using the CF_2 resonance exchange by ^{19}F NMR experiment. The two fluorine atom resonances changed from an A_2X to an ABX system upon slowing of the ring flip. The alkene protons in **30** provide a simple, straightforward system to study the eight-membered ring inversion by ^1H NMR spectroscopy. $Cr(CO)_3$ coordination to the opposite sides of the DBCOT backbone caused the chemical environments of the A and A′ protons to become distinctly different. As indicated in Scheme 3.1, DBCOT undergoes ring inversion causing the A and A′ protons to interchange. This means that one proton is exchanging between two different sites having different magnetic environments. On the NMR time scale, the lifetime (τ) of a chemically exchange nucleus is detectable only if it is in the range of 1 s to 10^{-6} s.[220] The lifetime in a dynamic exchange process and its rate constant (k) show an inverse relationship (Equation 3.8).[222, 259]

$$\tau = \frac{1}{k} \tag{3.8}$$

If τ is lower than the detectable level of the NMR experiment, it is termed as a fast exchange. The two proton sites involved in a fast exchange cannot be separately identified, because an average signal is produced for both proton environments. However, when the temperature is lowered, τ becomes long enough that separate peaks are observed and the system is known as undergoing slow exchange.[220, 221] Two distinguishable signals can then appear in the NMR spectrum corresponding to the proton sites involved in the chemical exchange. In the experimental spectrum of **30** at 180 K,

two doublets are observed at 6.82 (δ_A) and 6.67 (δ_B) ppm for the A′ and A proton positions, respectively (Figure 3.5b).

3.1.5.1 Coalescence temperature calculations

As discussed earlier, in a dynamic process with an exchange between two sites, two peaks are observed in the slow exchange regime, and one signal is observed in the fast exchange regime.[221, 259] The coalescence temperature (T_c) is the transition point where the two separate peaks become one.[221] T_c can be identified by its characteristic flat-topped peak (Figure 3.10). In this study, T_c was found for **30** at 255.8 K and 261.9 K at 300 and 600 MHz field strengths, respectively.

$$k_c = \frac{\pi \Delta \nu_c}{\sqrt{2}} \tag{3.9}$$

At T_c, the rate constant (k_c) can be calculated from the frequency difference ($\Delta \nu_c$) as described by Equation 3.9.[220, 259] Normally, in a dynamic process during the transition from slow exchange to coalescence, the isotropic chemical shift is expected to remain constant.[220] However, it has been reported that $\Delta \nu$ can also be temperature dependent.[259-264] According to the experimental spectra for **30**, it was clearly observed that the A and A′ proton peaks exhibit temperature dependence of their chemical shifts (Figure 3.12).

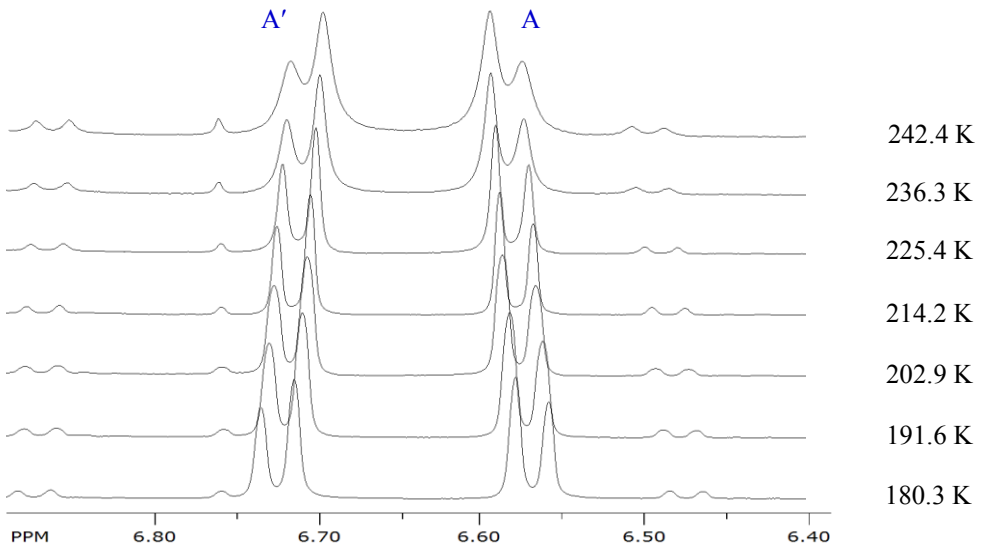

Figure 3.12 ^{1}H NMR spectra of **30** in acetone-d_6, 600 MHz, alkyl protons, 242 to 180K, 6.4 to 6.9 ppm; The average of all peaks aligned to 6.65 ppm.

When spin coupling between two protons has a large chemical shift difference relative to the coupling constant ($\Delta\nu$/J > 8), a simple two doublet pattern can be observed in the NMR spectra (Figure 3.13a).[241] This is denoted as an AX system in the Pople notation.[241, 242] When the chemical shifts difference between the doublets decreases relative to the coupling constant ($\Delta\nu$/J < 8), an AB type spectral pattern is observed. In the resulting doublet of doublets (Figure 3.13b), the inner two peaks (P_2 and P_3) increase and the outer two peaks (P_1 and P_4) decrease. One of the main dissimilarities between AX and AB systems is the position of the proton chemical shift. In the AX system, ν_A and ν_X are found in the center of the doublets, while ν_A and ν_B are found at the weighted average in the AB system.[241] Therefore, in order to find the $\Delta\nu_c$ for the alkene protons in **30**, a weighted average of P_1, P_2 and P_3, P_4 was calculated using peak separation plots displayed in Figure 3.14. By extrapolating the respective plots to the coalescence

temperature, $\Delta\nu_c$ values were obtained as 33.7 and 64.4 Hz at 300 and 600 MHz field strengths. From analysis of the plot obtained, errors associated with the $\Delta\nu_c$ values were deteremined as 0.09 and 0.91 Hz for 300 and 600 MHz field strengths, respectively.

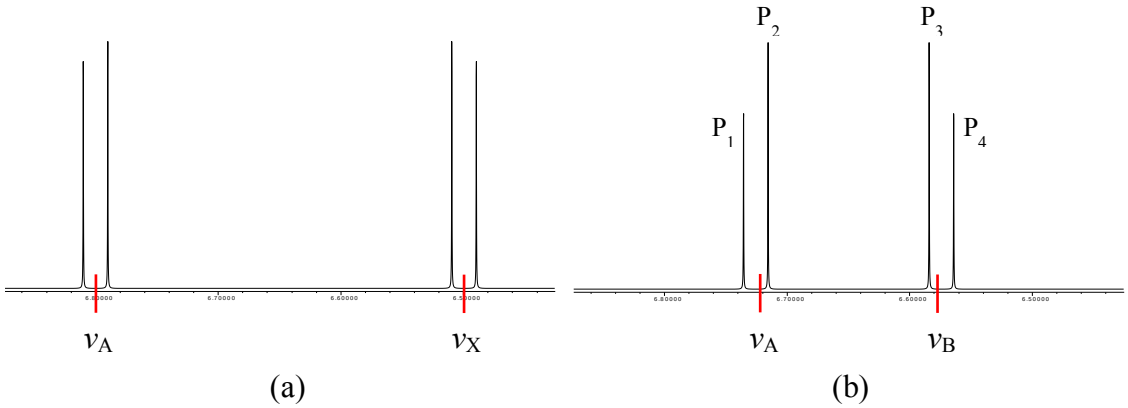

Figure 3.13 Spin coupling patterns (a) AX and (b) AB system; generated from gNMR; ν_A and ν_X are found at the center of the doublet; ν_A and ν_B are found at the center of gravity of the doublet.

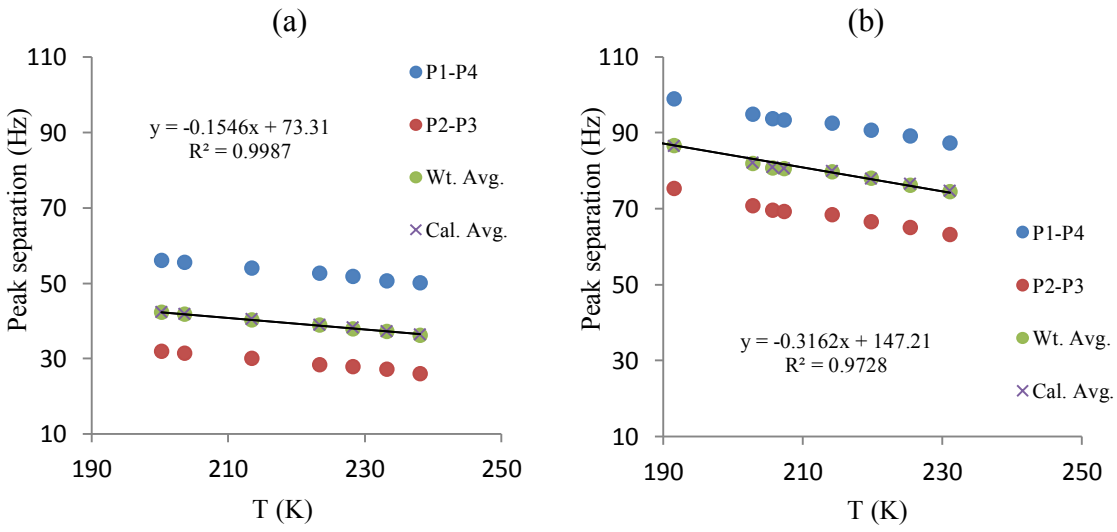

Figure 3.14 Peak separation and weighted average calculations for alkene protons in ^{1}H NMR spectra of **30**, (a) 300 MHz, (b) 600 MHz.

The relationship between rate constant, energy of activation (E_a), and the temperature in a chemical reaction can be found using the Arrhenius equation (Equation 3.10).[265] *A* is the pre-exponential term and R is the gas constant (R = 8.31451 J K^{-1} mol^{-1} = 1.98722 cal K^{-1} mol^{-1}).[265] The free energy of activation ($\Delta G^{\ddagger}$) is calculated using the Eyring equation (Equation 3.11).[220, 259, 265] The transmission coefficient (κ) depends on the nature of the process and is generally assumed to have a value of 1.[220] The Boltzmann constant (k_B) and the Planck constant (h) have values of 1.38065 x 10^{-23} J K^{-1} and 6.62608 x 10^{-34} J s, respectively.[265]

$$\mathrm{k} = Ae^{-\left(\frac{\mathrm{E}_a}{\mathrm{RT}}\right)} \tag{3.10}$$

$$\mathrm{k} = \kappa \frac{\mathrm{k}_B \mathrm{T}}{\mathrm{h}} e^{-\left(\frac{\Delta \mathrm{G}^{\ddagger}}{\mathrm{RT}}\right)} \tag{3.11}$$

By rearranging Equation 3.11 and applying the coalescence temperature conditions to it, Equation 3.12 can be derived. The free energy of activation at the coalescence temperature can be calculated if the values of T_c and k_c are known, and k_c can be calculated from Equation 3.9 when $\Delta\nu_c$ is known.[259]

$$\Delta \mathrm{G}_{\mathrm{c}}^{\ddagger} = -\mathrm{RT}_{\mathrm{c}} \ln\left(\frac{\mathrm{k}_{\mathrm{c}} \mathrm{h}}{\mathrm{k}_{\mathrm{B}} \mathrm{T}_{\mathrm{c}}}\right) \tag{3.12}$$

Using Equations 3.9 and 3.12, the barrier to inversion ($\Delta G^{\ddagger}$) in **30** was calculated as 12.71 ± 0.04 and 12.68 ± 0.05 kcal mol^{-1} for field strengths of 300 MHz and 600 MHz. The error estimations were generated from a propagation of uncertainty analysis using the division/multiplication and logarithmic propagation functions.[266] From the accuracy of the temperature measurements, the error values are given to one decimal place.

Therefore, the $\Delta G^{\ddagger}$ at coalescence temperature for both 300 and 600 MHz frequencies is 12.7 ± 0.1 kcal mol^{-1}. The results are summarized in Table 3.2.

Table 3.2 Rate constants and free energies of activation calculated at coalescence temperatures

Parameter	Field Strength	
	300 MHz	600 MHz
$\Delta\nu_c$	33.74 ± 0.09 Hz	64.4 ± 0.9 Hz
T_C	256.0 ± 0.7 K	262 ± 1 K
k_c	75.0 ± 0.2 Hz	143 ± 2 Hz
$\Delta G_c^{\ddagger}$	12.7 ± 0.1 kcal mol^{-1}	12.7 ± 0.1 kcal mol^{-1}

3.1.5.2 Line shape analysis

Line shape analysis is the most widely accepted procedure for determine the activation parameters of a dynamic process studied by NMR involving chemical exchange. The variation observed in NMR spectra for the alkene proton resonance was studied as a function of temperature to obtain the thermodynamic parameters associated with the inversion barrier. By using a simulation program such as gNMR,[228] experimental NMR spectra can be accurately simulated . The simulations provide the rates for the dynamic process for each experimental spectrum at the respective temperatures. A few of the 600 MHz field strength experimental spectra for **30** are shown in Figure 3.15 with the corresponding simulations.

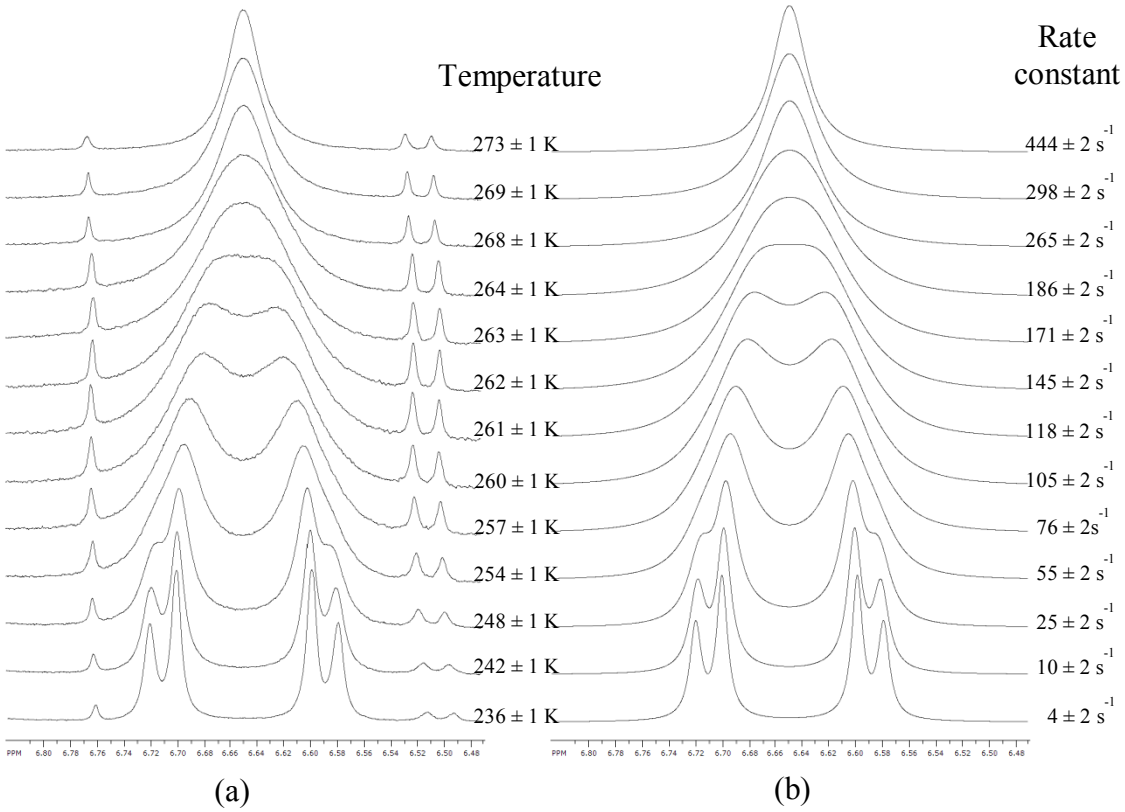

Figure 3.15 ^{1}H NMR of **30** at 600 MHz; (a) experimental spectra, and (b) simulated spectra using gNMR software; The average of all peaks aligned to 6.65 ppm.

The free energy of activation can be described as a function of the entropy of activation and enthalpy of activation (Equation 3.13).[265] By applying this relationship to the Eyring equation, where $\kappa = 1$, Equation 3.14 is obtained. Rearrangement gives Equation 3.15.

$$\Delta G^{\ddagger} = \Delta H^{\ddagger} - T\Delta S^{\ddagger} \tag{3.13}$$

$$\frac{k}{T} = \left(\frac{k_B}{h}\right) e^{-\left(\frac{\Delta H^{\ddagger}}{RT}\right)} e^{\left(\frac{\Delta S^{\ddagger}}{R}\right)} \tag{3.14}$$

$$\ln\left(\frac{k}{T}\right) = -\left(\frac{\Delta H^{\ddagger}}{R}\right)\frac{1}{T} + \left(\ln\frac{k_B}{h} + \frac{\Delta S^{\ddagger}}{R}\right) \quad (3.15)$$

From Equation 3.15, plotting ln (k/T) *vs* 1/T gives Eyring plots for the 300 MHz and 600 MHz data (Figure 3.16). Using the slope of the Eyring plot, $\Delta H^{\ddagger}$ was derived and $\Delta S^{\ddagger}$ can be calculated from the y-intercept. Errors associated with the slope and intercept of the line were obtained from the linear regression analysis.[267] The propagation of uncertainty was used for calculations of the standard errors for $\Delta H^{\ddagger}$ and $\Delta S^{\ddagger}$. Activation parameters obtained from the Eyring plots are summarized in Table 3.3. Using Equation 3.13, $\Delta G^{\ddagger}_{c}$ was calculated from the values obtained with the Eyring plot. The uncertainty was higher when $\Delta G^{\ddagger}_{c}$ was calculated from the Eyring plot results compared to the coalescence temperature as both $\Delta H^{\ddagger}$ and $\Delta S^{\ddagger}$ errors propagated to increase $\Delta G^{\ddagger}_{c}$ errors. However, the calculated $\Delta G^{\ddagger}_{c}$ values from both methods agree within the range of accuracy of temperature measurements. The $\Delta H^{\ddagger}$ and $\Delta S^{\ddagger}$ values for the two frequencies averaged to 15.9 ± 0.4 kcal mol^{-1} and 12 ± 2 cal mol^{-1} K^{-1}, after considering the propagation of the errors associated with the two individual values.

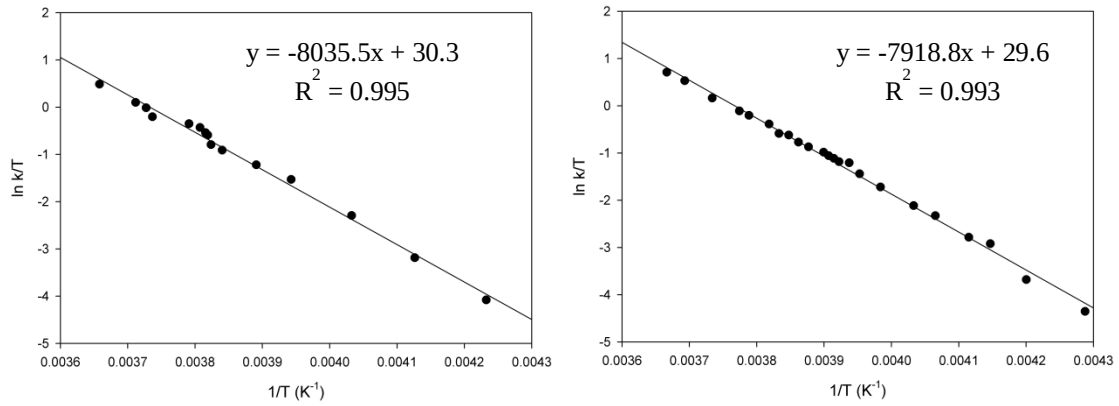

(a) (b)

Figure 3.16 Eyring plots [ln (k/T) *vs* 1/T]; (a) 300 MHz, and (b) 600 MHz field strength.

Table 3.3 Thermodynamic parameters obtained from Eyring plots.

Thermodynamic parameter	300 MHz	600 MHz
$\Delta H^{\ddagger}$	16.0 ± 0.2 kcal mol^{-1}	15.7 ± 0.4 kcal mol^{-1}
$\Delta S^{\ddagger}$	13 ± 1 cal mol^{-1} K^{-1}	12 ± 1 cal mol^{-1} K^{-1}
$\Delta G^{\ddagger}_{c}$	12.7 ± 0.3 kcal mol^{-1}	12.7 ± 0.5 kcal mol^{-1}

3.1.5.3 Comparison of the thermodynamic data

This is the first study where an eight-membered RI was evaluated for an η^6 metal coordinated system. Therefore, the above results are mainly compared with non-metallic examples. Interestingly, the experimentally-determined barrier to ring inversion for **30** is close to the value of $\Delta G^{\ddagger}$ published by Senkler *et al.* in 1972 for a substituted DBCOT

system.[3] For **1b** ($C_{16}H_{11}CF_2H$), a 12.3 kcal mol^{-1} barrier to ring inversion was reported at the coalescence temperature of -5°C.[3]

The similarity of $\Delta G^{\ddagger}$ values for **30** and **1b** was not anticipated. Metal coordination was expected to lower the RI barrier in DBCOT. Being a tub shaped molecule (C_{2v}), DBCOT is postulated to undergo RI through a planar transition state (D_{2h}). The presence of the electron withdrawing chromium tricarbonyl moieties were expected to stabilize the "anti-aromatic" transition state. From related COT studies, RI does not go through an anti-aromatic transition state (D_{4h}).[268] The bond shift processes for COT goes through a D_{8h} planar anti-aromatic transition. A bond shift does not occur in DBCOT because the fused benzene rings do not allow for it.

After a thorough inspection of RI in eight-membered systems, it was found that the experimental enthalpy and entropy of activation values for **30** were unique. This is the highest favorable entropy of activation reported for RI in a COT derivative. Most reported $\Delta S^{\ddagger}$ values observed are either negative or have low positive values.[186, 269-277] So far, the highest reported $\Delta S^{\ddagger}$ value is 2.2 ± 1.7 cal mol^{-1} K^{-1}, found in a chiral 1,3-bridged COT derivative (**2h**) reported by Paquette and coworkers in 1990.[277] Due to the low absolute values for $\Delta S^{\ddagger}$ in most reported COT derivatives, $\Delta G^{\ddagger}$ is essentially the same as the enthalpy of activation.[186, 269-277] The almost 16 kcal mol^{-1} observed in the system studied here can be considered a high value for $\Delta H^{\ddagger}$ for a ring inversion process.

As mentioned above, in most reported cases, the entropy of activation was considered as being slightly less than zero.[3-5] This means $\Delta G^{\ddagger}$ can be considered an upper limit for $\Delta H^{\ddagger}$. For all unsubstituted and monosubstituted COT derivatives reported in the

literature, the maximum $\Delta G^{\ddagger}$ is found for methoxycyclooctatetraene (**2i**) which has a value of 17.0 kcal mol^{-1}.[278] In all other cases, the energy barrier was found below 15.2 kcal mol^{-1}.[5, 107, 279-282] Apart from the 27 kcal mol^{-1} reported by Mislow *et al.* for the highly crowded **1a**,[2] the barrier to ring inversion for BCOT and DBCOT derivatives were found to be less than 13.4 kcal mol^{-1}.[3, 107] The high value for **1a** was caused by the carboxylic groups on the DBCOT backbone which leads to a huge "buttressing" effect.[2, 269]

It is well documented that increased substitution to the COT ring will lead to an increase in $\Delta G^{\ddagger}$.[2, 283-285] However, an increase in $\Delta H^{\ddagger}$ and $\Delta S^{\ddagger}$ due to metal coordination has not been observed before. Therefore, a theoretical study was undertaken in collaboration with Dr. Steven R. Gwaltney to help explain our experimental results. DFT calculations were conducted with the B3LYP/6-31G** basis sets. The results of these calculations are discussed in section 3.5.

3.2 Synthesis and structures

3.2.1 Stereochemistry and geometry of 17

The synthesis of **1** was carried out according to the route of Chaffins, Bretthreich and Wudl reported in 2002 (Scheme 2.1).[93] The unsaturation of **1** was achieved by the debromination of **17** in the presence of strong base **18**.[93] Compounds **13**[78-80, 101] and **1**[77, 84, 86-88] have been the subject of structural and reactivity studies, but little attention has been given to **17**. Although not a priority, a study of this compound's geometry and stereochemistry was undertaken.

During the first synthesis of **17**, Cope and Fenton established that the formation of dibromide is favored over monobromide.[78] For the dibromo product, four possible constitutional isomers were identified by Cope *et al.* (Figure 3.17).[78] Using a series of wet chemistry experiments, the authors determined that 5 and 11 are the correct skeletal positions for the two bromine atoms (Figure 3.17c).[78] Yet, the stereoisomers of the above product have not been subjected to discussion in literature.

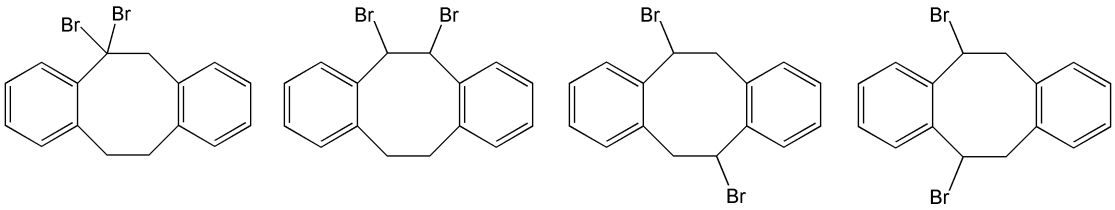

Figure 3.17 Constitutional isomers of dibromo-5,6,11,12-tetrahydrodibenzo[*a*,*e*]cyclooctadiene studied by Cope and Fenton.[78]

A theoretical calculation was used to evaluate which is the favorable structure for the two diastereomers of **17a** and **17b** (Figure 3.18). According to the DFT calculations, the *cis*-isomer produced the most stable structure. Interestingly, there were two other structural possibilities for **17** close in electronic energy to the *trans* isomer. All four structures are shown in Figure 3.19. The electronic energy values are compared relative to the energy of **17b**.

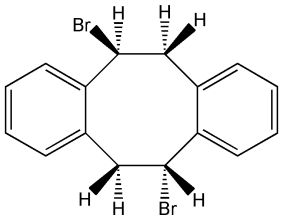

trans-isomer, **17a**

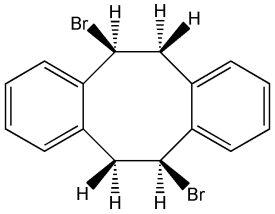

cis-isomer, **17b**

Figure 3.18 Stereoisomers of **17**

From the calculated structural possibilities, **17b** is clearly the most stable stereoisomer. While **17b** conformers contain *cis* bromine atoms, the two halogen atoms face away from the inside of the boat in boat, *exo*-**17b** unlike boat, *endo*-**17b** which places the bromine atoms closer to the concave side. The extra stability of the *cis-boat*, *exo* product appears to stem from the bulky bromine groups in the pseudo axial position and less ring strain from the higher boat angle. The angles between least square planes for the arene rings in boat, *exo*-**17b** and boat, *endo*-**17b** were calculated as 77.21^{o} and 65.65^{o}, respectively.

The crystal structures of **1** and **13** exhibit tub and chair conformations, respectively.[1, 79] The theoretical calculations indicate a twisted boat as the preferred configuration for **17a** or **17b**. It was interesting to study the solid state geometry of **17**. The crystal structure was determined using a single crystal isolated by sublimation. **17b** is found as the *cis* isomer in the boat conformation. The thermal ellipsoid (50% probability) drawing is shown in Figure 3.20. **17b** crystallizes in the $P2_12_12_1$ space group with four molecules per unit cell. The angle between least square planes for the arene rings is

measured to be 77.59°.The crystal structure indicated a single enantiomer (5*S*, 11*S*), although **17b** exist as a racemic mixture.

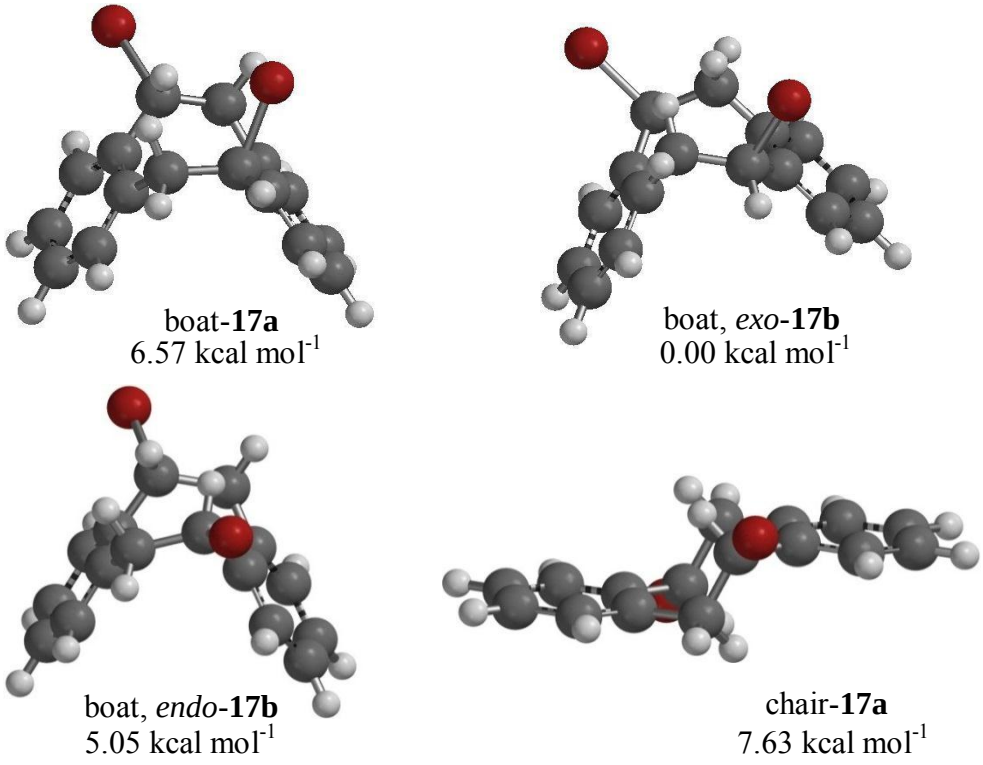

Figure 3.19 Calculated structures for **17**

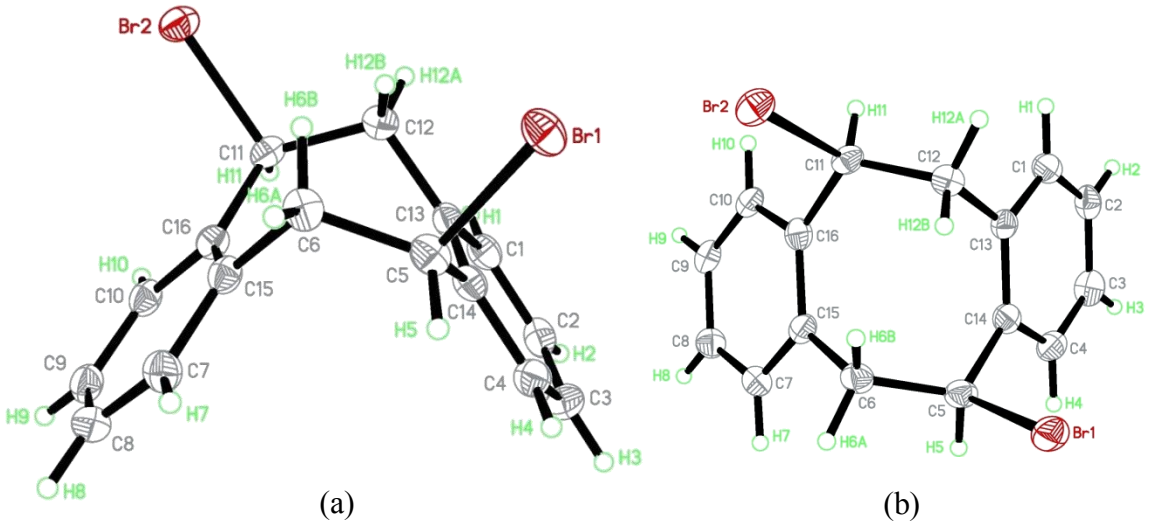

Figure 3.20 Thermal ellipsoid (50% probability) drawing of **17b** (a) side on view; (b) viewed from top, orthogonal to the eight-membered ring plane.

In the bromination of **13**, the dibromo species was formed with high selectivity. The mechanism for the bromination was discussed by Thaler *et al.* in 1963.[44, 286] It was predicted that the second bromine atom was introduced *via* the bridged intermediate product **42** (Figure 3.21). Yates *et al.* suggested that **42** can be achieved only if **17** is the *trans* stereoisomer.[44] But, according to the crystal data only the *cis* isomer is found in the solid state.

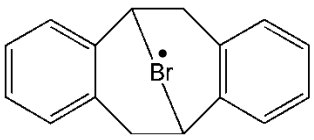

42

Figure 3.21 Postulated intermediate in the bromination of **13** by Thaller and Yates.[44]

Previously, only ^{1}H NMR and IR data were reported for **17**. In this study, ^{13}C NMR, COSY, HMQC and HMBC experiments were performed to identify all proton and carbon assignments in **17b**. Coupling values were determined using gNMR simulations. In the COSY spectrum (Figure 2.3), the cross couplings of eight-membered ring protons were observed. H6A, H6B, H12A and H12B are diastereotopic protons. The A and B assignments were given based on reported coupling values of *cis* and *trans* relationships in a vicinal proton system ($J_{trans} > J_{cis}$).[241] The HMQC and HMBC spectra are shown in Figure 3.22 and 3.23, where all proton-carbon correlations are assigned.

17 shows C_2 symmetry, and therefore four different signals are expected for arene protons in the ^{1}H NMR spectrum. However, using $CDCl_3$ as the solvent, previous work did not report any separation of peaks.[93, 238] Using acetone-d_6 at 600 MHz, separate signals for the arene protons were observed. However, the H4, H10 multiplet and the H2, H8 multiplet were found to be overlapped. The assignments are listed in the experimental chapter under Section 2.12. The regions for the arene protons in the HMBC and HMQC spectra are enlarged in Figure 13.24.

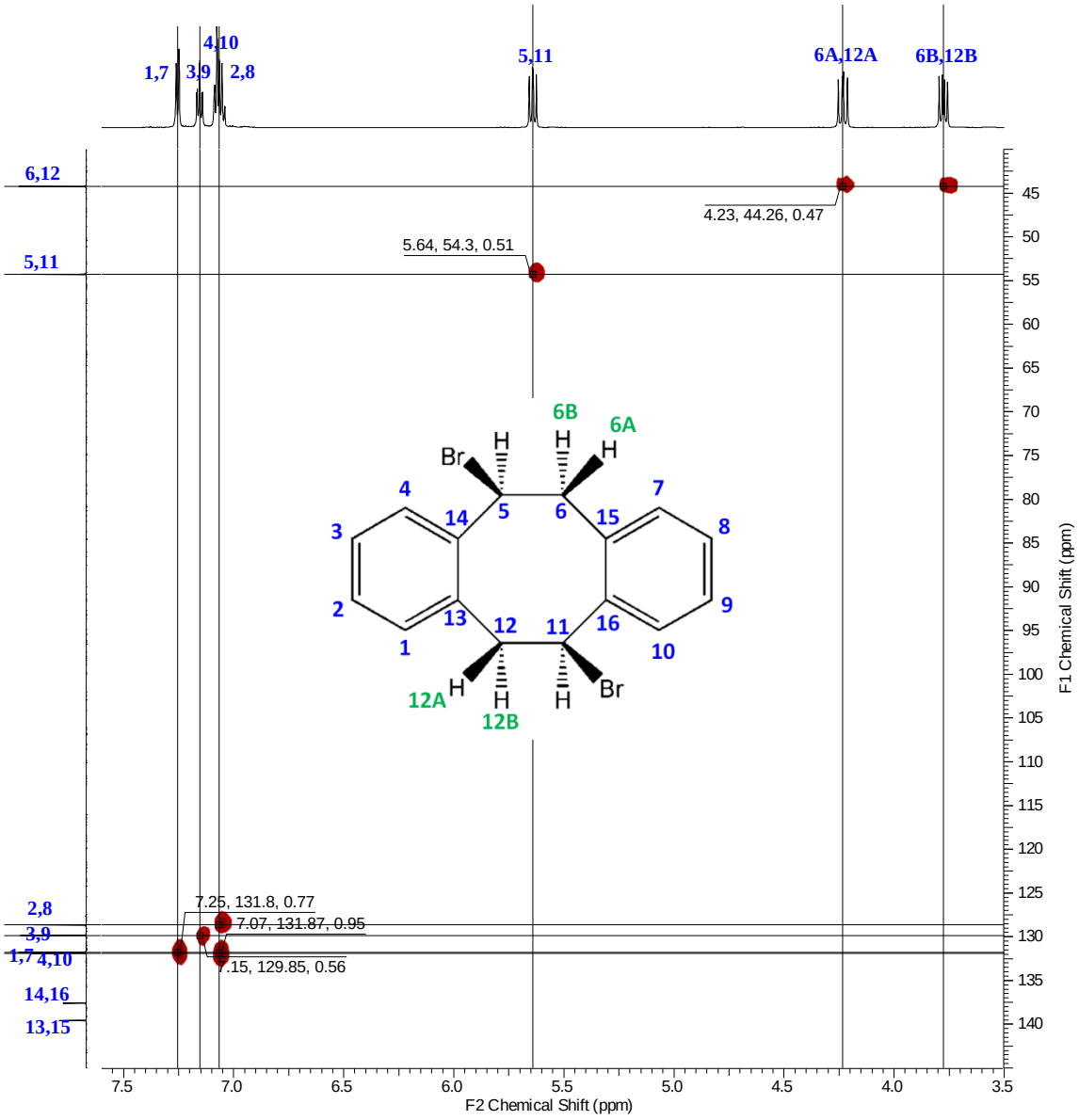

Figure 3.22 HMQC spectrum of **17b**, 600 MHz, RT, acetone-d_6

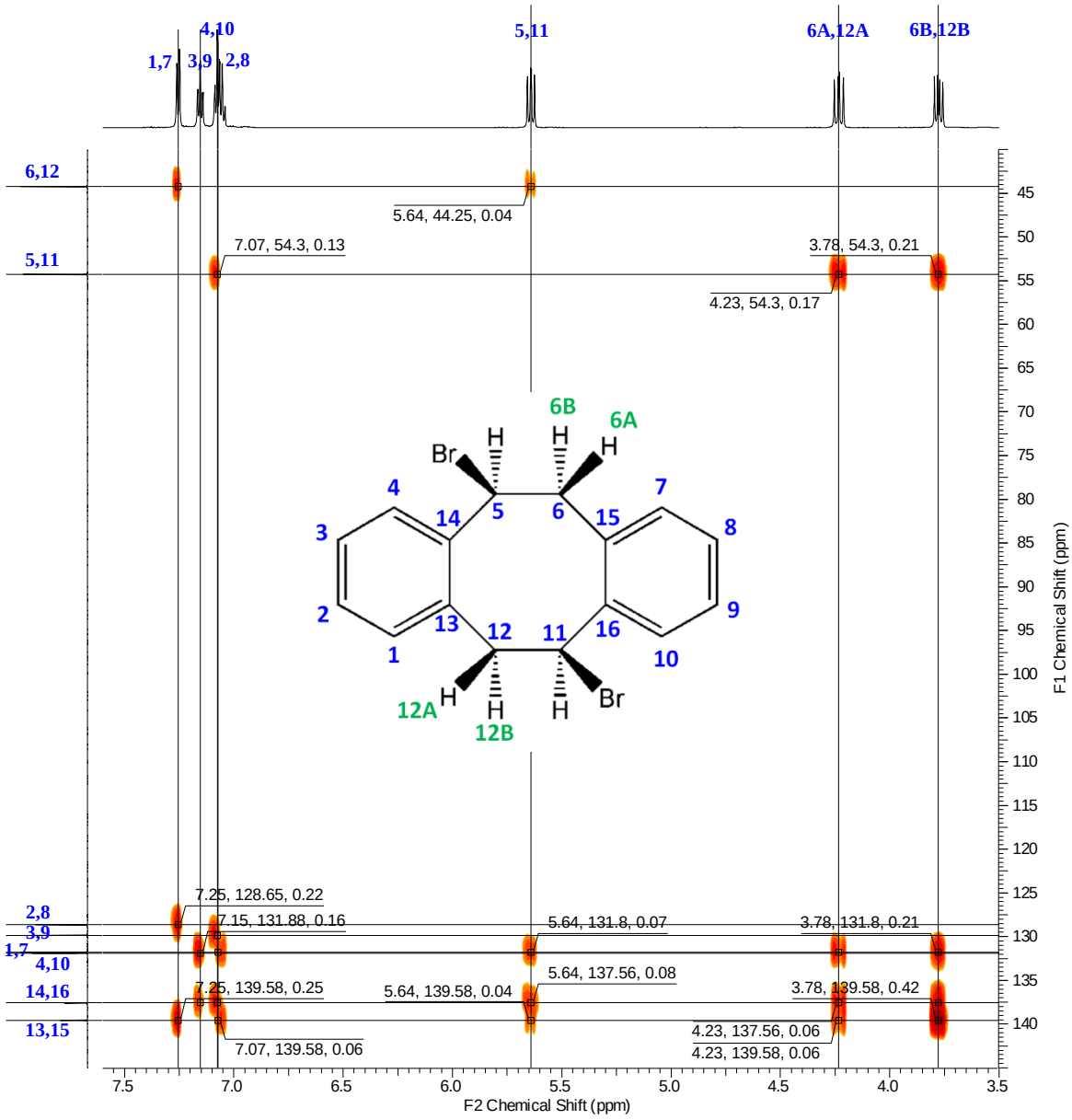

Figure 3.23 HMBC spectrum of **17b**, 600 MHz, RT, acetone-d_6

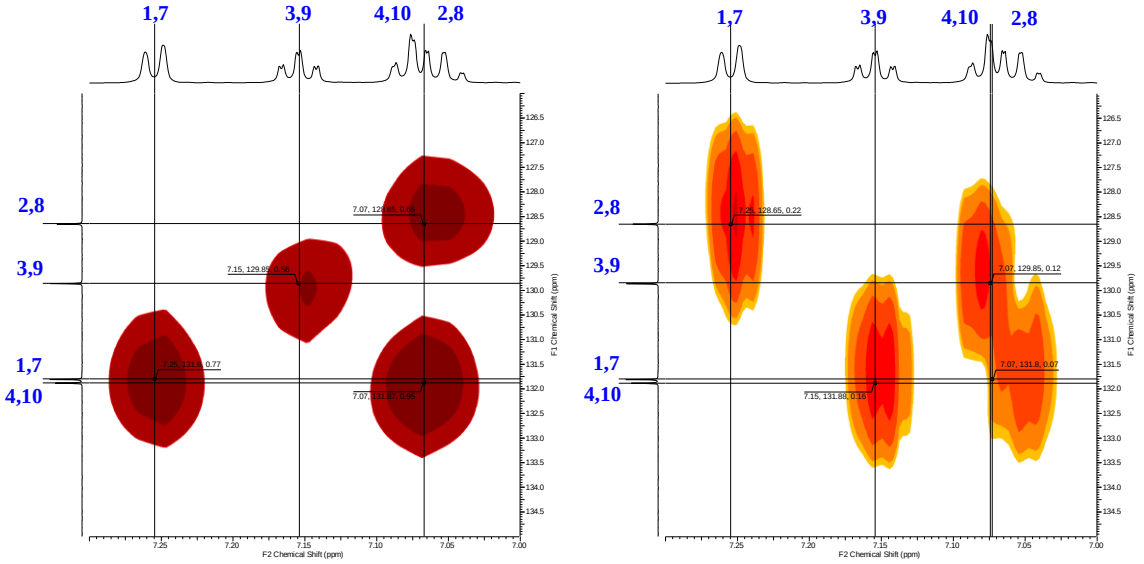

Figure 3.24 Enlarged view of the arene region for **17b**, 600 MHz, RT, acetone-d_6; (a) HMQC, and (b) HMBC.

3.2.2 Synthesis of chromium complexes

Müller and coworkers were the first to synthesize the η^6-DBCOT chromiumtricarbonyl complexes **29** and **30** during their study of π-aromatic metallic systems.[189] In this research, **29** and **30** were produced using a direct approach where the arenes were refluxed with excess chromiumhexacarbonyl. This is a commonly accepted method for making a range of arene compounds.[137] In the current work, a weeklong reflux under inert conditions produced **30** as the major product (Scheme 3.2). An argon stream was maintained throughout the reflux with a bubbler attached above the condenser as shown in Figure 2.6. The main purpose of this was to help flush out carbon monoxide from the system and keep positive pressure of argon in the reaction system. With prolonged heating of highly air sensitive products, it is important to maintain a positive

pressure of inert gas. The positive pressure prevents pressure drops during cold temperature periods.

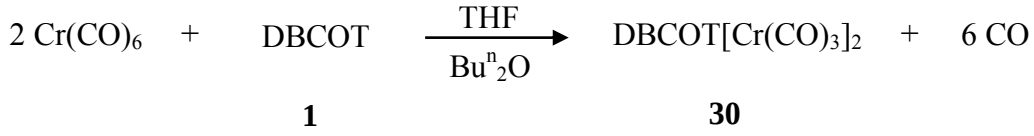

Scheme 3.2 Synthesis approach for **30**

According to the above reaction, three carbonyl groups will be removed from one chromiumhexacarbonyl unit. This process requires high temperatures.[134, 137] During the initial attempts for making π-arene chromium complexes, E. O. Fischer opted to heat the reaction at high temperatures (e.g: 220°C) in sealed vessels.[134] In recent synthetic routes, higher temperatures were achieved with the use of high boiling solvents.[137] Dibutyl ether (b.p. 142°C) is a common choice as a high boiling for synthesis of arenetricarbonylchromium. However, dibutyl ether is not used alone in a synthesis as it tends to react slowly because of its weak donor properties. Therefore, due to its high donor ability, THF is used as a catalyst for the reaction. THF is also useful as it washes back any sublimed $Cr(CO)_6$ into the reaction.[137] A straight reflux condenser was used (Figure 2.6) in this reaction to simplify the return of sublimed $Cr(CO)_6$.[137]

3.2.2.1 Crystal structure of 30 and tripod orientation

In 2000, Henry and coworkers reported the crystal structure of **30**, where it was observed as the *syn,anti* isomer (Figure 1.17).[190] The crystal lattice has four different molecules in the unit cell.[190] These molecules are different due to the *anti*-$Cr(CO)_3$

orientations which were controlled by a three-dimensional array of C-H···O (carbonyl) hydrogen bonds in the crystal lattice. There were 24 intermolecular O···H distances identified having less than a 2.7 Å separation, with the shortest being 2.29 Å.[190]

The tripod orientations of piano stool complexes have been discussed in the literature.[173, 174, 287, 288] When benzene is fused to another ring, the coordinated tricarbonyl units can be aligned into three limiting positions, named eclipsed, *endo* staggered, and *exo* staggered (Figure 3.25). These variations can be characterized using an angle (θ) starting from an imaginary center line perpendicular to the bond shared by the fused ring (Figure 3.25a).

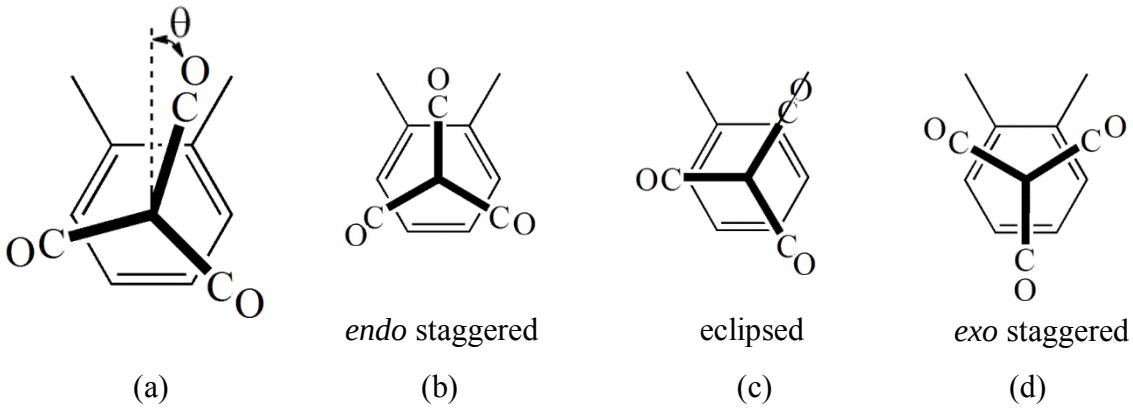

endo staggered eclipsed *exo* staggered

(a) (b) (c) (d)

Figure 3.25 Tripod orientations; (a) θ defined as the angle from the imaginary bisecting line, (b) θ = 0°, c) θ = 30°, d) θ = 60°.

In the crystal lattice of **30**, the four isomeric molecules were identified as A, B, C and D with θ angles of the *anti*-$Cr(CO)_3$ group at 53.8°, 29.2°, 21.0°, 9.5°, respectively.[190] Molecule A was *exo* staggered and D was in the *endo* staggered orientation. B was found in an eclipsed orientation, while C was intermediate between *endo* staggered and

eclipsed. All of the *syn*-$Cr(CO)_3$ groups were found to be in *exo* staggered orientations due to the steric restrictions from the DBCOT skeleton.[190]

Among the thousands of chromiumtricarbonyl complexes reported, there are only a few examples known to have different tripod orientations within the same crystal lattice. A dimeric $Cr(CO)_3(C_6H_5CH_2OCH_2C_6H_5)Cr(CO)_3$ complex (CSD ref code: KENQEZ) and a bimetallic complex of phenanthrene (WEDWAD), have two different tripod orientations in the same molecule.[289, 290] Chromiumtricarbonyl complexes of dibenzobicyclo[2,2,2]octadiene (KALVOI) and 1,2,3,4-tetrahydro-1-naphthalenol (ZOZMIK) show molecules with different orientations in the crystal lattice.[291, 292]

3.2.2.2 The mono chromiumtricarbonyl complex and hydrogen bonding in the solid state

With the crystallographic information on **30**, a number of interesting questions arose regarding the mononuclear complex. First, it was of interest to know the preferred orientation of a single $Cr(CO)_3$ group when attached to the DBCOT backbone. Will it prefer the *syn* or *anti* conformation? It was also reasonable to investigate the intermolecular interactions in the solid state. A determination as to whether a monometallic complex of DBCOT can also effectively participate in hydrogen bonding was needed.

Compound **29** was synthesized previously by Müller et al.[189] During their synthesis, a η^4-monochromiumtetracarbonyl complex (**31**) was achieved, and it was then converted to the η^6-arene-coordinated complex. In the present work, **29** was synthesized directly by refluxing **1** with chromiumhexacarbonyl in a 1:1 ratio with dibutylether and

THF as solvents. Products were separated using inert atmosphere column chromatography with silica as packing material and increasing concentrations of diethyl ether in hexanes as eluent. Yellow translucent crystals were achieved by slowly cooling a concentrated hexane solution of the complex.

The crystal structure of **29** indicates that the $Cr(CO)_3$ group is *anti* with respect to the interior of the DBCOT tub (Figure 3. 26a). **29** crystallizes in the $P\bar{1}$ space group with two molecules per unit cell. These molecule have the *endo*-staggered conformation (Figure 3.26b), which agrees with the predictions of Rogers *et al.*[173] The deviation from the perfect *endo* conformation is 2.1°, 0.7° and 1.0°.The crystal structure of **29** can be compared to a closely related system from the literature. The BCOT chromiumcarbonyl complex **32** also shows an *anti*- $Cr(CO)_3$ group where the unique carbonyl is in *endo* position.[74] However, **32** shows significant distortion from the *endo*-staggered conformation (~11°) while **29** is close to the perfect *endo* position.

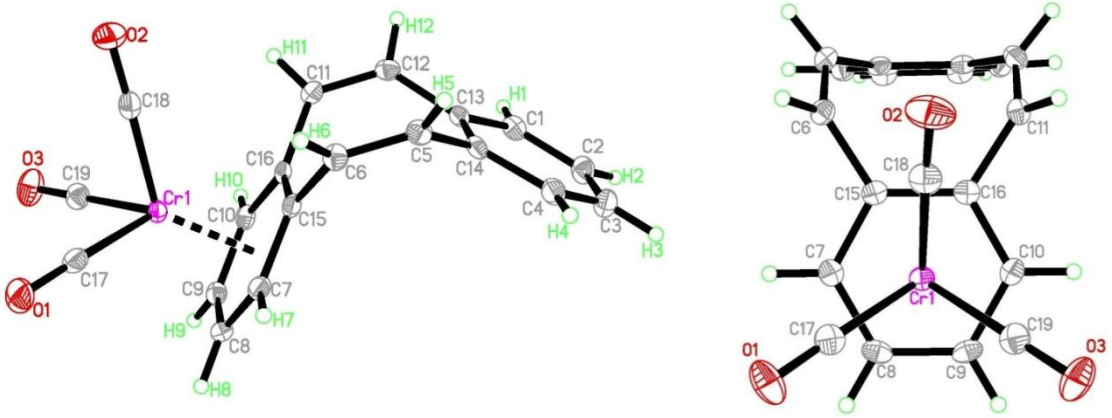

Figure 3.26 Crystal structure of **29** (thermal ellipsoid with 50% probability) (a) side view; (b) viewed from below the Cr atom orthogonal to the coordination plane.

C-H···O hydrogen bonding interactions were evaluated for the crystal structure. The commonly accepted criteria for C-H···O hydrogen bonding is an O···H distance less than or equal to 2.8 Å with the angle at the hydrogen atom greater than 110°.[293] C-H···O hydrogen bonds identified for **29** are listed in Table 3.4. All C-H bond distances are normalized to 1.08 Å.[294]

Many examples can be found where the oxygen atom of a metal carbonyl moiety acts as the hydrogen bond acceptor in a C-H···O hydrogen bond interaction.[293, 295-299] Likewise, the preference for coordinated arenes to act as the C-H hydrogen bond donors is also well known.[295, 296, 298, 300, 301] It is also known that metal coordination increases the acidity of the hydrogen atoms, thus increasing the strength of the hydrogen bonding interactions[298, 302-304] When compared with **30**, the C-H···O parameters for hydrogen bonding indicated weaker interactions in the solid state of **29**. Having only one molecule in **29** compared to four independent molecules in the crystal lattice of **30** might be indicative of the weaker hydrogen bonding. The stronger interactions in **30** are due to the presence of two $Cr(CO)_3$ moieties coordinated to the organic backbone. The effects of two electron withdrawing metal groups accepting electron density from the DBCOT increases the acidity of all hydrogen atoms in **30** and therefore increases the strength of the hydrogen bonding interactions.

Table 3.4 C-H···O hydrogen bonding observed in **29**, distances (Å) and angles (°)

H	O	O···H	O···C	C-O···H	C-H···O
2	3[a]	2.74	3.797(3)	95.7	166.7
3	1[a]	2.50	3.523(3)	107.5	157.6
6	2[b]	2.72	3.701(2)	152.1	151.6
7	3[c]	2.80	3.324(2)	149.6	110.0
8	1[d]	2.60	3.296(2)	111.9	121.6
10	1[e]	2.67	3.353(2)	163.7	120.9
10	3[f]	2.60	3.310(2)	122.0	123.3
12	2[g]	2.57	3.482(2)	104.1	141.9

[a] -1+x, 1+y, z
[b] 1-x, 1-y, 1-z
[c] -1+x, y, z
[d] 1-x, 1-y, 2-z
[e] x, 1+y, z
[f] 2-x, 2-y, 2-z
[g] 1-x, 2-y, 1-z

3.2.2.3 The angle between arene planes (ϕ)

In the ligand DBCOT and its metal complexes, the interior angle between the least square planes formed by the two arenes is an important structural feature to be considered. Figure 3.27 illustrates the way ϕ angle is measured between the planes of C(1)C(2)C(3)C(4)C(14)C(13) and C(7)C(8)C(9)C(10)C(16)C(15), as well as the numbering scheme used in the metal complexes with *syn* and *anti* units. It was discovered that in the bimetallic complex the organic framework was flattened in comparison to the parent hydrocarbon. The respective angles were 106.70° (average from all four

molecules) and 98.70° for **30** and **1**, respectively. For the monometallic complex, since the metal coordination is on the convex side of the DBCOT tub, one would assume that ϕ should not change significantly from the parent compound. However, the angle is actually lower than in the free ligand, measuring only 91.70 (0.06)°. It appears that in **29**, the two planes are aligned approximately into a right angle.

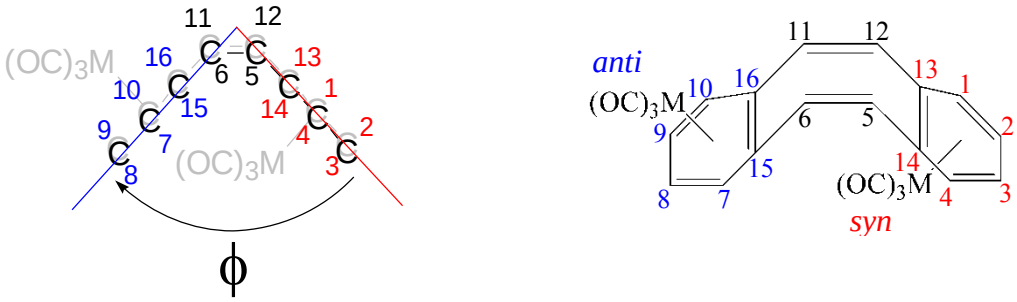

Figure 3.27 The angle between the arene ring planes and numbering scheme for DBCOT tub

The ϕ for the bimetallic complex, which is higher than for the monometallic complex, is understandable. In **30**, steric congestion is present inside the tub due to the presence of a *syn* $Cr(CO)_3$ group. However, the reason ϕ for **29** is smaller than for the parent compound is not clear if only intramolecular interactions are considered.

The reduced angle for **29** is due to the packing motif in the crystal lattice. β-Hydrogen atoms of the coordinated arene (H8 and H9) are directed toward the non-coordinated arene of another molecule (1-x, 2-y, 2-z). A dimer is formed due to these attractions (Figure 3.28). The distances between H8 and H9 and the centroid of the non-coordinated arene ring are 3.15 Å and 2.84 Å. C-H···centroid angles are 118.8° and

132.2°, respectively. This arrangement, in combination with the associated parameters, is clearly indicative of the existence of C-H···π interactions.[305]

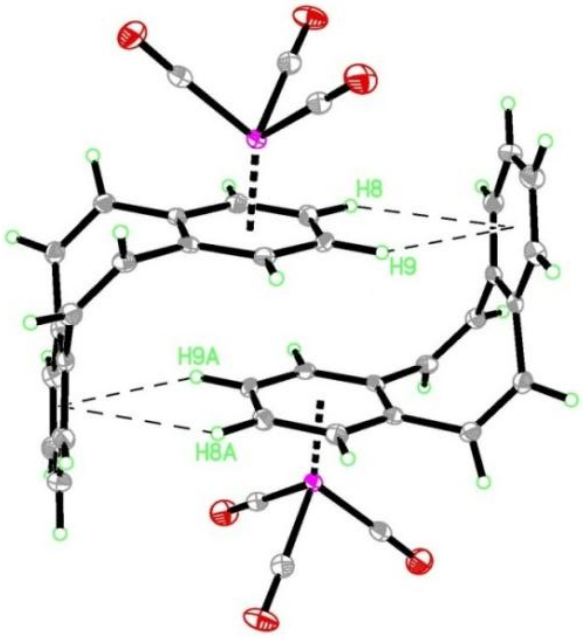

Figure 3.28 The dimer formed in **29**. C-H···π hydrogen bonds are indicated by dashed lines.

To date only one other arenetricarbonylchromium compound is reported to have C-H···π interactions in the solid state.[306] However, a Cambridge Structural Database (CSD)[307] search revealed 128 arenetricarbonylchromium compounds with a C-H···phenyl centroid distance less than or equal to 3.15 Å, the angle at H greater than 110,° and the C-H vector to the phenyl plane greater than 60°. In all of these compounds the hydrogen bond donor was on the coordinated arene. Out of 128, only 18 examples were found where the coordinated arene also served as a hydrogen bond acceptor. In all other cases, a non-coordinated ring or a solvent arene were the hydrogen bond acceptor.

Because of the interesting dimer observed in the crystal lattice for **29**, a search for similar structural patterns was undertaken from the 128 compounds found with a C-H···π interaction. Only five examples were found with dimers having a non-coordinated arene ring approximately perpendicular to the coordinated arene. These examples include ligand systems triptycene (Ref code: AYOCUM, DEYPUS and NOGWAH),[308-310] anthracene (PASSOR),[311] and indene (RIVBIH).[312] Therefore, it should be mentioned that **29** is the first example found for a COT derivative to form a dimer with C-H···π interactions. Furthermore, **29** could serve as a model for developing organometallic synthons in supramolecule chemistry.

3.2.3 Synthesis of manganese complexes

3.2.3.1 η^6 Monomanganesetricarbonyl complex of ligand 1

Being an isoelectronic counterpart of $Cr(CO)_3$ and with its greater electron withdrawing capabilities,[313] it was of interest to make a monometallic complex of **1** with the $Mn(CO)_3^+$ group. It is of interest to know whether the increase in electron withdrawing capability would enhance hydrogen bonding in the crystal. The type of hydrogen bonding preferred in the structure was also a question as mono- and bimetallic complexes of chromiumtricarbonyl favored C-H···π and C-H···O interactions, respectively. The position that the metal is coordinated with respect to the DBCOT backbone was also an interest. One would expect the same conformation in $Mn(CO)_3^+$ as the isoelectronic chromium derivative.

To address the above questions, the monomanganesetricarbonyl derivative of **1** was prepared for the first time. It is well known that the MTT approach is the most suitable for making manganesetricarbonyl complexes with unsaturated ligands.[168] In the synthetic route, the MTT agent **28** was prepared using established literature procedures,[168, 239] (Scheme 3.3a) and the ligand exchange reaction was conducted to make **36** (Scheme 3.3b). It should be noted that by changing the metal to ligand ratio, the synthesis of a bimetallic complex was also attempted. Due to low solubility, all crystallization attempts for **37** were unsuccessful. However, XRD quality yellow translucent crystals of **36** were readily achieved by slow vapor diffusion of diethyl ether into a concentrated solution of CH_2Cl_2.

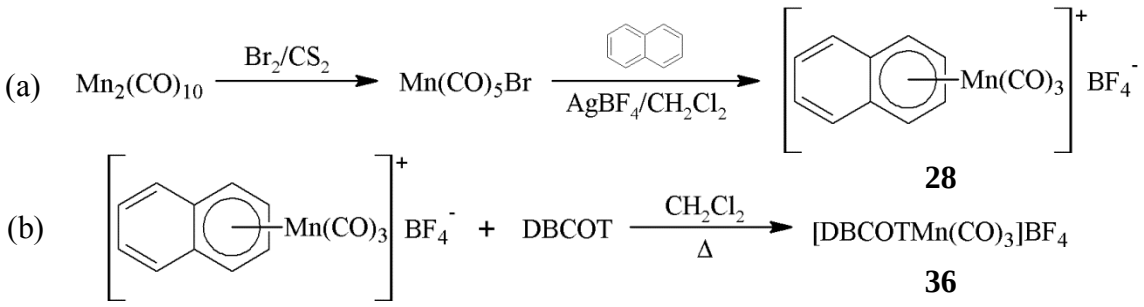

Scheme 3.3 Synthesis of **36**: (a) preparation of MTT agent; (b) ligand exchange reaction.

The crystal structure of **36** indicates that the $Mn(CO)_3^+$ group is in the *syn* conformation (Figure 3.29), opposite to the orientation of **29** in the crystal. **36** crystallizes in the $P4_12_12$ space group with four molecules per unit cell. As seen in the crystal

structure of **30**, the metal carbonyl in **36** also shows an *exo*-staggered orientation. This is mainly due to the steric effects imposed by the DBCOT tub.

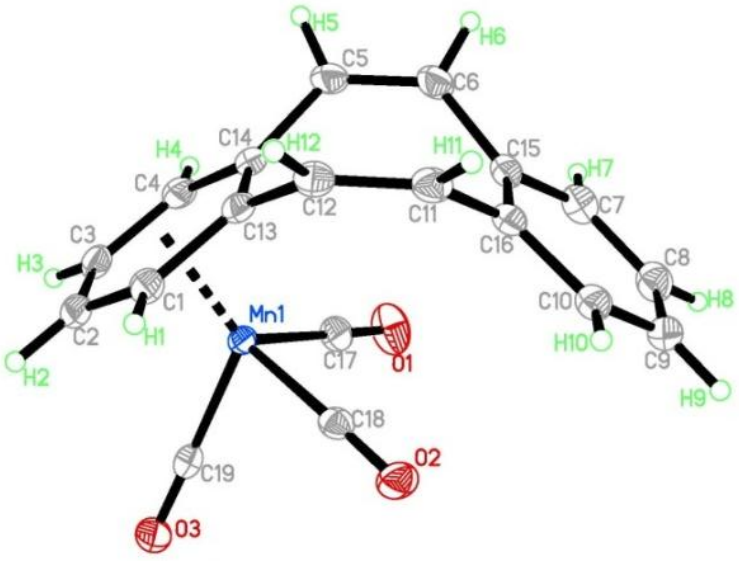

Figure 3.29 Thermal ellipsoid (50% probability) drawing of **36**; BF_4^- unit is not shown.

The angle between the least squares planes for the arene rings of the DBCOT backbone is 106.91 (0.03)^o. This angle is significantly larger than for the monochromium complex as well as the free ligand. This larger ϕ value is caused by the *syn*-metaltricarbonyl moiety interacting with the DBCOT backbone. For obvious reasons, the ϕ for **36** is almost the same as **29**. The ϕ values for DBCOT and its metallic complexes are summarized in Figure 3.30.

Regarding the barrier to inversion of these complexes, the ϕ angle could play a vital role. Compared to the free ligand, ϕ is 8^o larger in complexes **30** and **36**. Therefore, it would be expected that the planar transition state should be more easily achieved for **30** and **36** in comparison to DBCOT.

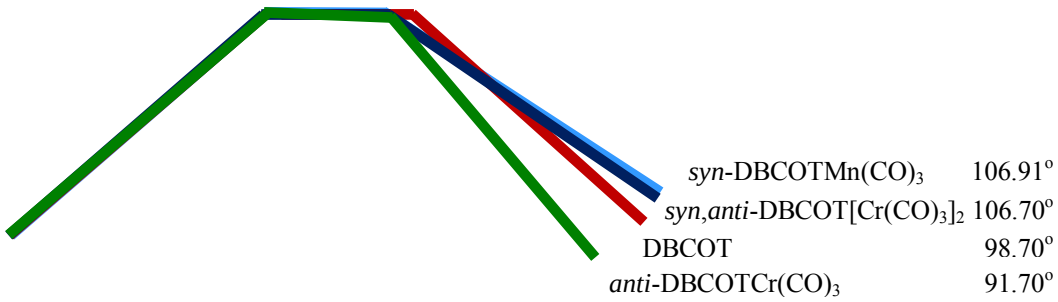

Figure 3.30 Comparison of the ϕ for DBCOT and its metal complexes. The organic framework for products **1**, **29**, **30** and **36** are overlaid on top of each other.

Both C-H···O and C-H···F hydrogen bonds are found in the crystal structure of **36** (Table 3.5). However, there were no C-H···π interactions observed. The accepted criteria for assigning C-H···F hydrogen bonding is that the H···F distance is less than or equal to 2.60 Å and the angle at H must be greater than 90°.[314] The C-H bond lengths are normalized to 1.08 Å.[294] With the manganese complexes having the BF_4^- counter anion, the possibility of having charge assisted C-H···F hydrogen bonds exists. Similar situations have been reported with BF_4^- [300, 315-322] and PF_6^- [314, 315, 323-327] counter anions involved in charge assisted C-H hydrogen bonding interactions.

Interestingly, it was observed that the distances for the C-H···O interactions in **36** were shorter than the distances found in the crystal of **29**. The average distances for the C···O interactions were 3.30 Å for **36** and 3.47 Å for **29**. This clearly indicates that in the manganese complex, hydrogen bonding is much stronger when compared to the chromium complex. The above results are due to the increased electron withdrawing effect of the Mn cation on the arene ring. The coordinated arene hydrogen atoms become

more acidic with the increased electron withdrawing capabilities of manganese and became better hydrogen bond donors.[313]

Table 3.5 Distances (Å) and angles (°) for C-H···X-Y (C-H···O-C and C-H···F-B) hydrogen bonds in **36** (All C-H bonds normalized to 1.08 Å)

H	X	Y	X···H	X···C	Y-X···H	C-H···X
2	O2[a]	C18	2.52	3.1821(15)	172.6	118.5
3	O2[a]	C18	2.55	3.1938(15)	114.8	117.6
8	O1[b]	C17	2.71	3.3775(17)	120.5	120.0
9	O1[b]	C17	2.66	3.3609(16)	171.3	121.9
11	O3[c]	C19	2.66	3.3986(15)	92.4	125.0
12	O3[c]	C19	2.50	3.3199(15)	87.1	132.1
1	F2[d]	B1	2.47	3.4674(16)	91.0	152.8
2	F4[d]	B1	2.47	3.2392(16)	114.7	126.9
3	F3[e]	B1	2.32	3.2461(16)	115.3	142.5
4	F1[f]	B1	2.56	3.1162(15)	146.8	111.3
5	F1[f]	B1	2.36	3.2081(15)	141.8	134.5
8	F2[g]	B1	2.55	3.5387(18)	91.3	151.6
9	F4[h]	B1	2.49	3.2365(16)	120.4	125.4

[a] 1.5-x, 0.5-y, 0.25-z
[b] 2.5-x, 0.5+y, 0.25-z
[c] 0.5+y, 1.5-x, -0.25+z
[d] y, x, 1-z
[e] 1.5-y, -0.5+x, -0.75+z
[f] 0.5+x, 0.5-y, 0.75-z
[g] 1+y, x, 1-z
[h] 1.5-y, 0.5+x, -0.75+z

A dimeric packing motif was not observed in the manganese complex since there were no C-H···π interactions. However, another interesting packing situation was seen in the crystal structure of **36** as the coordinated arene of one molecule was arranged parallel to the non-coordinated arene of the adjacent molecule (Figure 3.31). The distance between the two centroids was 3.64 Å and the angle between the least square planes of the arenes was 12.9°. The nearest non-bonded C-C distances are 3.378 and 3.388 Å between C2-C15 (y, -1+x, -z) and C3-C16 (y, -1+x, -z), respectively. This kind of packing can be identified as π-π stacking.[328-330] A linear chain is formed when a stack of coordinated arenes are placed in an alternating manner with the non-coordinated arenes. The metal moiety coordinated to the concave side of the tub also played an important role to allow this packing formation.

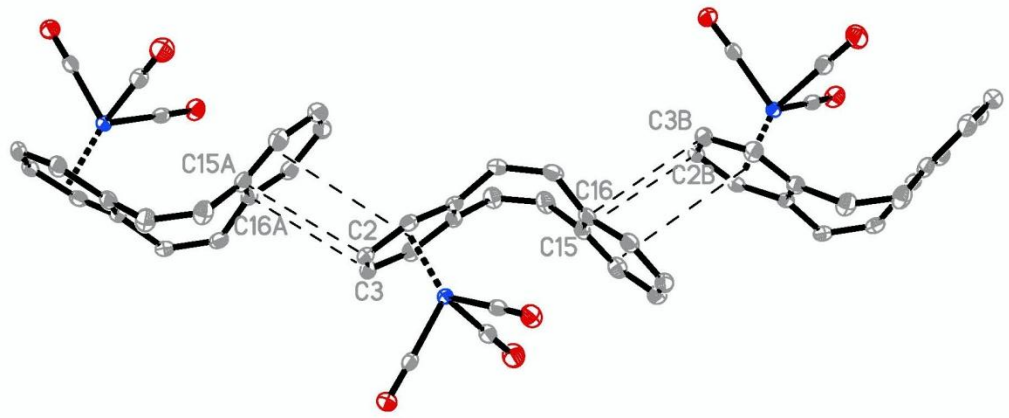

Figure 3.31 π-π Stacking interactions in **36** (H atoms are omitted for clarity). The centroid-centroid and shortest intermolecular C-C distances are shown in dashed lines.

A literature search was conducted for similar packing systems. Only four other structures were found in the CSD for arenetricarbonylmanganese compounds with intermolecular arene centroid distances less than or equal to 3.65 Å. Three of the structures involved with coordinated ring to non-coordinated ring interactions. These were composed of fluorenyl (BODNIR; 3.57 Å),[331] pyrene (WASMAF; 3.60 Å avg.),[332] and biphenylene (REVJIL; 3.62 Å)[333] ligand systems. The fourth example was a bimetallic compound where one metal coordinated as a piano stool complex and the other one connected to the second ring with thiolate and ethenyl groups (PAYGUR; 3.46 Å).[334] All of the above systems are planar and therefore, π-π stacking interactions produced only dimers. Due to the non-planarity having the two arene rings almost perpendicular to each other, the $DBCOTMn(CO)_3^+$ fragments favor a linear expansion. It should be pointed out that **36** is the first example found of an arenetricarbonylmanganese complex showing a linear continuous packing arrangement having π-π stacking interactions.

3.2.3.2 η^6 Monomanganesetricarbonyl complex of ligand 13

During the synthesis of ligand **1**, DBCOD was formed in the second step. From the coupling reaction of **15**, **13** was obtained on a gram scale. Although chromium complexes of **13** have been studied, no research has been reported for the manganese analogues. The crystal structures of both the mononuclear (**33**) and the *cis* isomer of binuclear (**34**) $Cr(CO)_3$ complexes of DBCOD were reported by Fakhri *et al.* in 2000.[193]

Interestingly, in both **33** and **34**, the organic backbone preferred the boat conformation, and the tricarbonylchromium groups preferred *anti* coordination with respect to the interior of the tub. Considering the direction of metal coordination, the

monometallic structure **33** was similar to **29**, but the bimetallic complex preferred the *anti*,*anti* configuration which is different than in **30**. The boat conformation achieved for DBCOD complexes were interesting, as the ligand alone crystalizes in a chair conformation.[79, 81] Fakhri *et al.* attempted to crystallize a *trans*-DBCOD[$Cr(CO)_3$]$_2$ complex, where they assumed the organic framework will be in the chair conformation, but a crystal structure was not obtained.[193] The $Cr(CO)_3$ orientations in **33** were found to exist in the *endo* conformation. In **34**, one carbonyl orientation was found to be *endo*-staggered while the other was *exo*.[193] Although, the two metal bonding environments appeared to be equivalent in **34**, a clear difference between the two carbonyl orientations has not been investigated by the authors.

Because of the interesting crystal structures of **29**, **30** and **36** with respect to the packing forces observed, there was a desire to determine the structures of the manganese complexes of ligand **13**. Using the well-established MTT method, the synthesis of **38** and **39** was attempted for the first time. Due to the low solubility of the bimetallic complex, a crystal structure was not achieved. However, XRD quality crystals for the monometallic species were achieved using slow vapor diffusion of diethyl ether into a concentrated solution of acetone.

38 crystallizes in the $Pna2_1$ space group with six molecules per unit cell. One CH_2Cl_2 was found for every two $[DBCODMn(CO)_3]^+$ and BF_4^- units. Similar to **33**, the $[Mn(CO)_3]^+$ moiety was *anti* to the interior of the DBCOD backbone (Figure 3.32). Interestingly, in **38** two independent molecules were observed in the crystal each with different tripod orientations. As shown in Figure 3.33, the two molecules were named A

and B, where A consisted of a manganesetricarbonyl unit being in the *endo*-staggered conformation and B consisted of a manganesetricarbonyl unit in the *exo*-staggered conformation.

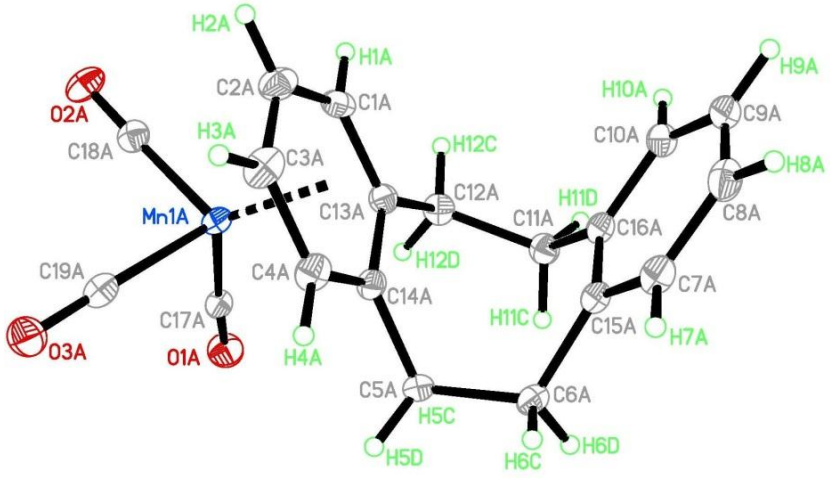

Figure 3.32 Crystal structure of **38** (thermal ellipsoid with 50% probability)

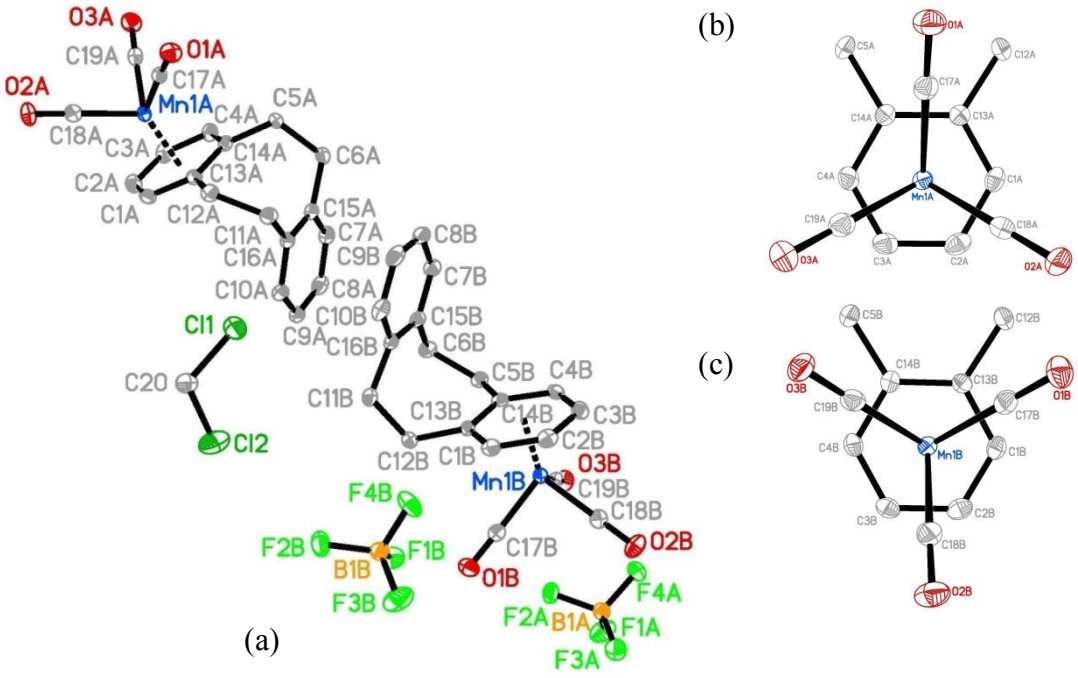

Figure 3.33 Two independent molecules of **38** (thermal ellipsoid with 50% probability) (a) side view (hydrogen atoms omitted for clarity); (b) *endo*-staggered $[Mn(CO)_3]^+$ moiety in molecule A; (c) *exo*-staggered $Mn(CO)_3]^+$ moiety in molecule B; (In (b) and (c) the view from below the Mn atom, orthogonal to the coordination plane was shown).

The two uncoordinated rings of the molecules A and B are arranged in a linear fashion. These were not considered as π-π interactions because the centroid-centroid distance is higher than 3.65 Å. Due to the presence of the BF_4^- counter anion several C-H···F hydrogen bond interactions were found (Figure 3.34a and b). There are only two C-H···O hydrogen bonds identified in **38**, and these were from O2B to H5E and O2B to H12F (Figure 3.34c). This was rather unexpected with the presence of the strong electron withdrawing Mn^+ moiety. All hydrogen bond interactions found in **38** are summarized in Table 3.6.

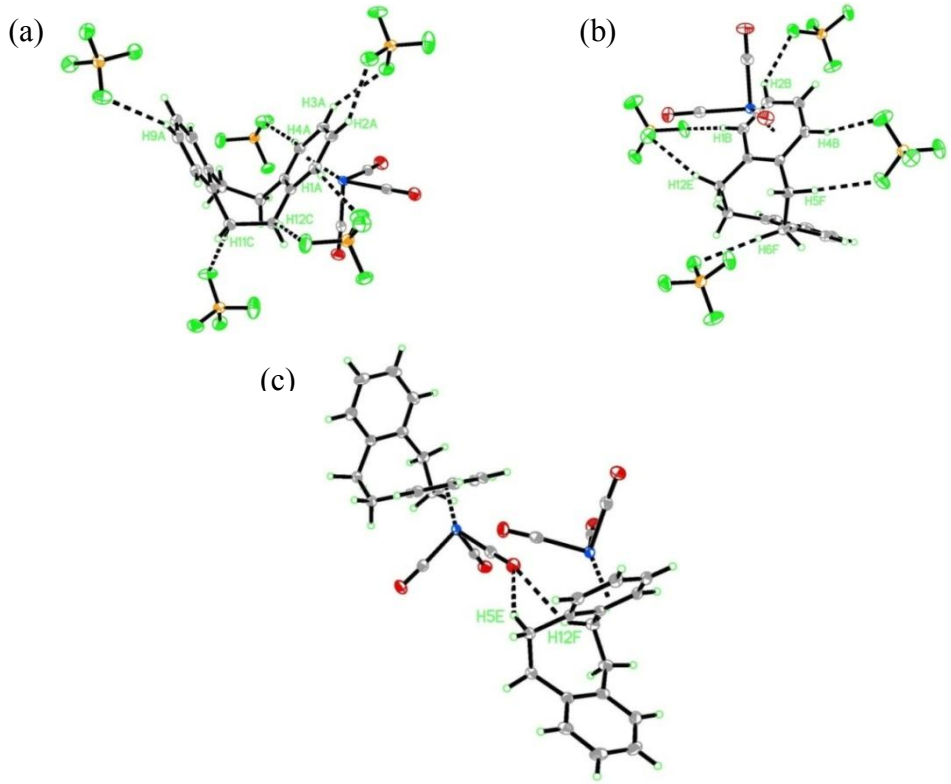

Figure 3.34 Hydrogen bonding interactions in **38** (a) C-H···F interactions in molecule A; (b) C-H···F interactions in molecule B; (c) C-H···O interactions from O2B with H5E and H12F in molecule A.

Table 3.6 Distances (Å) and angles (°) for C-H···X-Y (C-H···O-C and C-H···F-B) hydrogen bonds in **38** (All C-H bonds normalized to 1.08 Å).

H	X	Y	X···H	X···C	C-H···X	Y-X···H
H1A	F4A[1]	B1A	2.227	3.150(2)	142.0	125.5
H12C	F1A[1]	B1A	2.576	3.644(2)	169.8	109.7
H2A	F2B[2]	B1B	2.298	3.166(3)	136.1	122.6
H3A	F1B[2]	B1B	2.339	3.240(3)	139.9	115.4
H4A	F3A[3]	B1A	2.109	3.106(2)	152.3	126.7
H1B	F4B	B1B	2.101	3.173(2)	171.2	115.3
H2B	F2A[4]	B1A	2.363	3.185(3)	131.7	114.8
H4B	F3B[5]	B1B	2.381	3.435(3)	164.7	108.0
H11C	F4B[6]	B1B	2.266	3.332(2)	168.7	111.4
H6F	F3A[7]	B1A	2.475	3.539(2)	168.1	102.9
H12E	F1B	B1B	2.507	3.544(2)	160.6	119.4
H12F	O2B[7]	C18B	2.701	3.546(3)	134.8	152.1
H20A	F1A[1]	B1A	2.498	3.323(2)	132.3	138.8
H9A	F3A[7]	B1A	2.490	3.449(2)	147.5	103.1
H5E	O2B[7]	C18B	2.756	3.716(2)	147.9	134.2
H5F	F2B[5]	B1B	2.321	3.395(2)	172.9	132.8

[1] -x+1/2, y-1/2, z-1/2
[2] -x, -y+1, z+1/2
[3] -x+1/2, y-1/2, z+1/2
[4] x+1/2, -y+3/2, z
[5] x, y, z+1
[6] -x+1, -y+1, z+1/2
[7] x-1/2, -y+3/2, z

3.2.4 Heteronuclear complex with chromium and manganese

3.2.4.1 Synthesis attempts for 40

It was of interest to synthesize a mixed metal complex due to the unique differences shown by chromium and manganese tricarbonyl complexes. A blueprint for achieving a hetero complex is to have one metal moiety attached to the DBCOT framework and then attach the second metaltricarbonyl unit to the monometallic complex. After considering the conditions used to create monometallic complexes, it was determined that the best approach would be to create the $DBCOTCr(CO)_3$ first and then to coordinate a $Mn(CO)_3^+$ moiety. Several examples in the literature show that MTT agents were successful in creating a mixed-metal complex.[168-171, 332]

Several synthetic attempts were made to form **40**. In one attempt, a solid was isolated which has both chromium and manganese carbonyl peaks in the FTIR ATR data. Unfortunately, due to the low solubility of this solid, all attempts to obtain crystals failed.

3.2.4.2 The crystal structure of 41

During the attempts to make **40**, an unusual product was detected. According to the FTIR ATR spectra of the crude product, the reaction appeared incomplete. The product was not readily soluble as expected for **29** in dichloromethane or not insoluble as observed for **40**. The solids were dissolved in excess CH_2Cl_2 and were allowed to crystallize. Needle-like translucent crystals were obtained after slowly cooling the solution for several weeks.

Although the crystals were not high quality, due to the uniqueness of the product data was collected and processed. A disorder issue was detected but attempts to model this disorder were unsuccessful in lowering the R_1 value below 5%. [335] After final refinements, a goodness of fit (GOF) 0.959, and indices of 0.0854, 0.1812 for R_1, and wR_2 were achieved. The data clearly indicated that the structure of **41** is not only different from the starting materials, but it was a cocrystal of **29** and naphthalene, in a 2:1 ratio. The unit cell dimensions were significantly larger than for **29**. The total volume of the unit cell for **41** was 1954.86 $Å^3$ compared to 753.5 $Å^3$ for **29**. Many attempts were made to repeat the above synthesis. Unfortunately, these attempts were not successful.

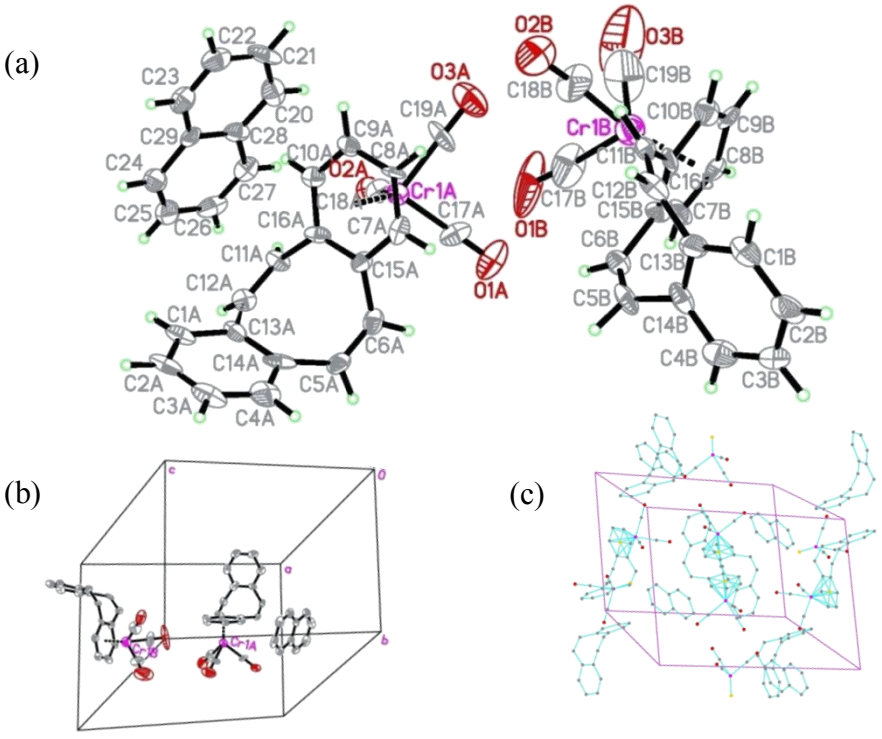

Figure 3.35 (a) Thermal ellipsoid (50% probability) drawing of **41**. The two $DBCOTCr(CO)_3$ molecules were named A and B; (b) triclinic unit cell of **41** (hydrogens are removed for clarity); (c) a packing diagram for **41**.

41 crystalized in the $P\bar{1}$ space group with two different molecules (named A and B) of DBCOTCr(CO)$_3$ and one molecule of naphthalene in the unit cell (Figure 3.35a and b). After a series of anisotropic refinements, some of the atomic positions had large thermal ellipsoids. Specifically, the three carbonyls of molecule B showed disorder. In both A and B, the Cr(CO)$_3$ moiety is in the *anti* configuration relative to the interior of the tub. When the molecules are viewed from below the Cr and orthogonal to the coordination plane both tricarbonyl units in A and B can be seen to be in the *exo*-staggered configuration (Figure 3.36a and b). The measured deviations from the ideally *exo*-staggered position were 3.0°, 1.7°, 0.2° and 11.2°, 10.1°, 11.8° for the A and B molecules, respectively. It is interesting to note that for DBCOTCr(CO)$_3$ alone (**29**), the tripod orientation is *endo* staggered, but with the inclusion of the naphthalene molecule in **41,** the conformation shifted to *exo*.

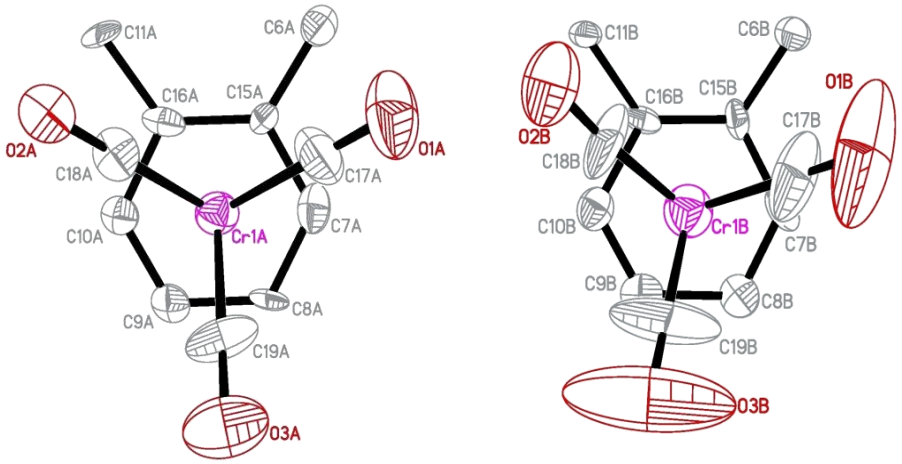

(a) (b)

Figure 3.36 (a) *exo* staggered Cr(CO)$_3$ moiety in molecule A; (b) *exo* staggered Cr(CO)$_3$ moiety in molecule B; (view from below of the Cr atom, orthogonal to the coordination plane).

The ϕ angles for A and B were close to the value of the free ligand and significantly different than in **29**. For molecule A, ϕ is 98.00 (0.36)^{o} and for B 97.32 (0.32)^{o}. The perpendicular angle of ϕ was observed in **29**, due to the unique dimeric packing behavior with C-H···π hydrogen bonding interactions. Although, the values for ϕ are relatively high in **41** compared to **29**, both A and B formed dimers with the adjacent molecules. In the dimer formed by molecule A with the adjacent molecule (1-x, 1-y, 1-z), the H9AA and arene centroid (C1A, C2A, C3A, C4A, C13A, C14A) distance is measured to be 2.600 Å (Figure 3.37a). Again, all C-H bonds are normalized to 1.08 Å prior to this analysis. The C9A-H9A···centroid angle is 150.2^{o} and the C-H vector angle to plane is 146.6^{o}. In the dimer formed by molecule B with the adjacent molecule (2-x, 1-y, 2-z), the H9B and arene centroid distance is 2.660 Å (Figure 3.37b). The C9B-H9B···centroid angle is 147.4^{o} and the C-H vector angle to plane is 151.6^{o}.

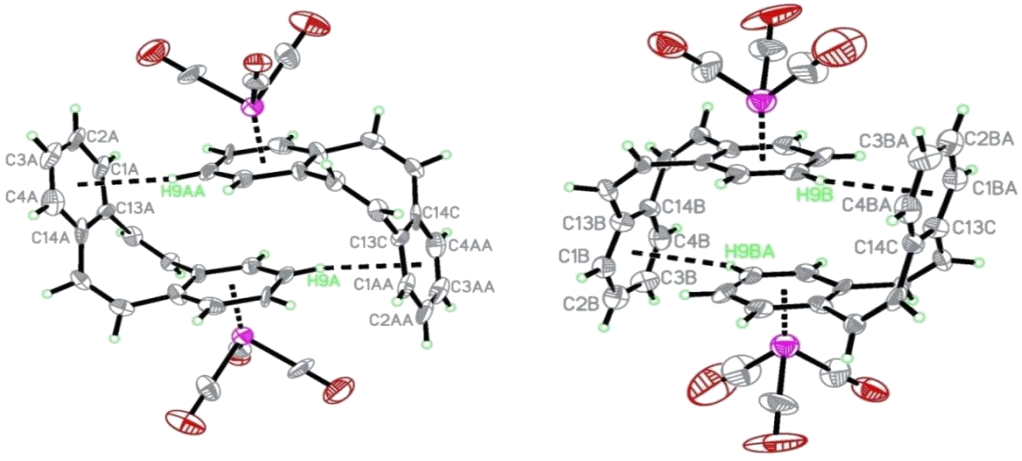

(a) (b)

Figure 3.37 Dimers formed in **41**. (a) molecule A with (1-x, 1-y, 1-z), and (b) molecule B with (2-x, 1-y, 2-z); C-H···π hydrogen bonds are indicated with dashed lines.

Not all of the C-H···π interactions found in the crystal were involved with forming dimers. One of the coordinated ring protons of molecule A (H10) interacts with the naphthalene molecule forming a C-H···π bond (Figure 3.38). All of the C-H···O hydrogen bonding interactions observed in **41** are summarized in Table 3.7. The strength of C-H···O interactions seemed to be similar to **29**, where the average C···O distance was 3.45 Å. For **29,** the average distance was 3.47 Å and for **36** it was 3.30 Å.

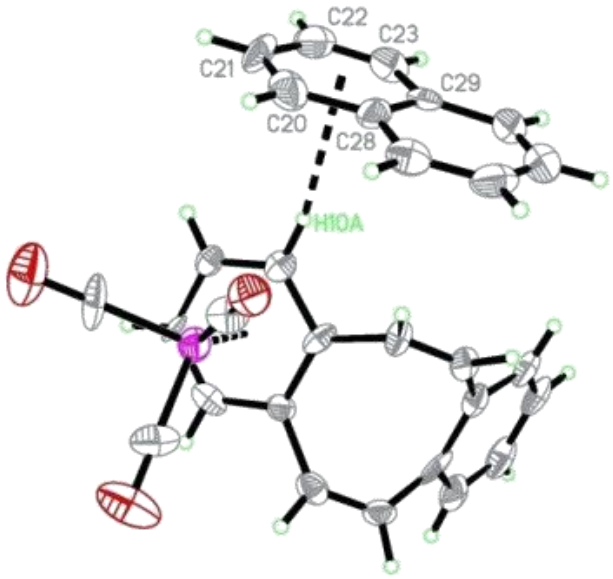

Figure 3.38 C-H···π hydrogen bond interaction in **41** with H10A and the naphthalene.

Table 3.7 C-H···O hydrogen bonding observed in **41**, distances (Å) and angles (°)

H	O	O···H	O···C	C-O···H	C-H···O
1A	2B[a]	2.64	3.643(16)	103.2	155.0
2A	2A[b]	2.65	3.448(15)	132.2	130.1
6A	1B[c]	2.68	3.685(16)	92.6	154.9
7A	1A[c]	2.52	3.557(16)	153.9	159.7
7A	1B[d]	2.75	3.332(18)	151.6	113.3
8A	1B[d]	2.61	3.257(17)	127.2	118.1
11B	2B[e]	2.33	3.240(16)	153.9	140.9

[a] 1-x, 1-y, 1-z
[b] x, -1+y, z
[c] 2-x, 1-y, 1-z
[d] x, y, z
[e] 1-x, 1-y, 2-z

3.3 NMR analysis for monometallic complexes

3.3.1 Interpretation of the NMR data for 29

In the ^{1}H-^{1}H COSY spectrum, the only cross coupling was observed between alkene protons. In the HMQC experiment, the direct C-H couplings were observed (Figure 3.39). ^{2}J and ^{3}J ^{13}C-^{1}H couplings were observed in the HMBC (Figure 3.40) spectrum. A magnified 2D spectrum for the non-coordinated arene and alkene carbon/proton peaks are shown in Figure 3.41. The carbons that fuse both rings are identified by their correlation with alkene protons. It is worth noting that C15 and C16 showed coupling only with the alkene protons, while C13 and C14 were also coupled with α protons (H1, H4) of the arene ring.

However, the carbon peaks at 130.14 (C1, C4), 130.04 (C6, C11) and 136. 36 (C5,C12), 136.19 ppm (C13, C14) are too close to determine assignments based solely on 2D experimental data. DFT calculations were performed to generate chemical shifts. The ^{1}H NMR chemical shifts were calculated as 8.29 (H2, H3), 8.07 (H1, H4), 7.80 (H5, H12), 7.50 (H6, H11), 6.16 (H8, H9), and 6.15 (H7, H10). Calculated ^{13}C NMR chemical shifts are 228.57 (C18, unique CO, *endo*), 227. 78 (C17, C19), 132.72 (C5, C12), 131.42 (C13, C14), 126.53 (C6, 11), 125.05 (C1, C4), 121.97 (C2, C3), 106.90 (C15, C16), 92.05 (C7, C10), and 89.58 (C8, C9). The assignments for the experimental ^{1}H and ^{13}C NMR are listed in Section 2.1.3.

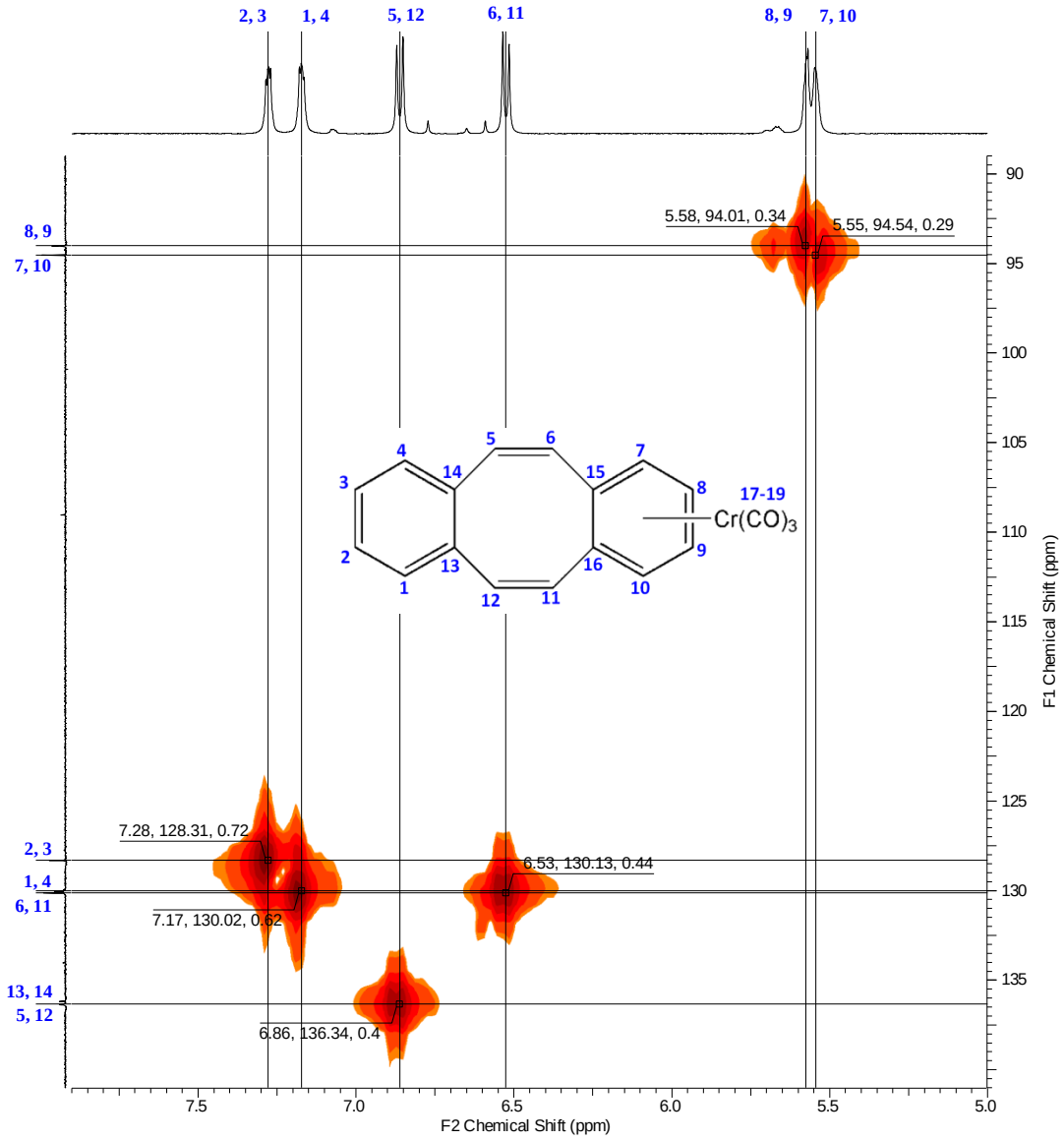

Figure 3.39 HMQC spectrum for **29**; 600 MHz, RT, acetone-d_6.

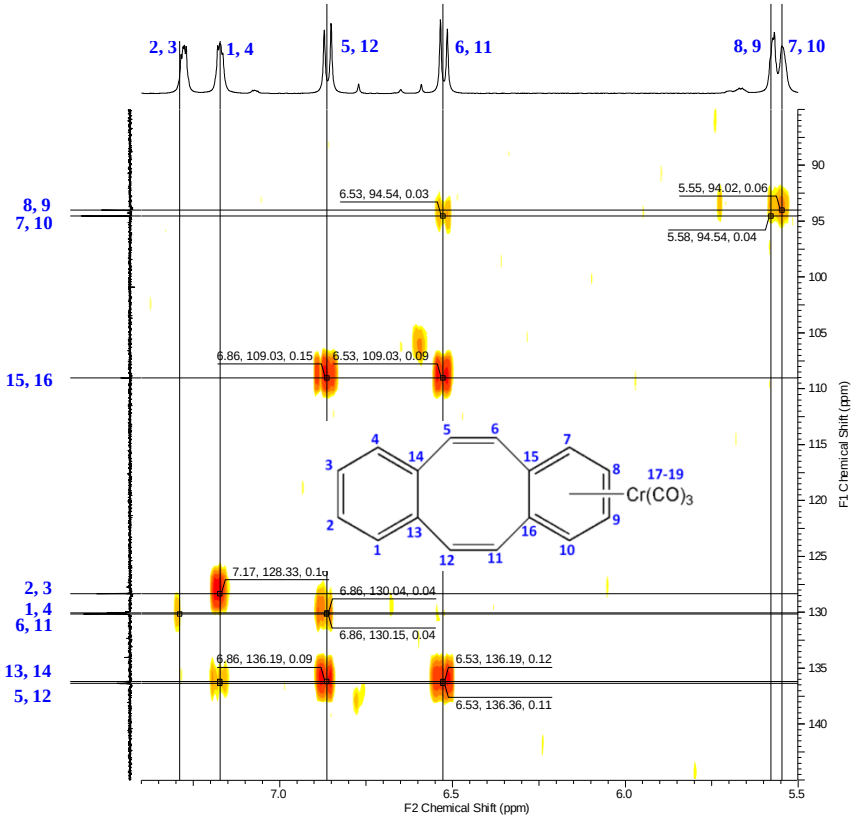

Figure 3.40 HMBC spectrum for **29**; 600 MHz, RT, acetone-d_6.

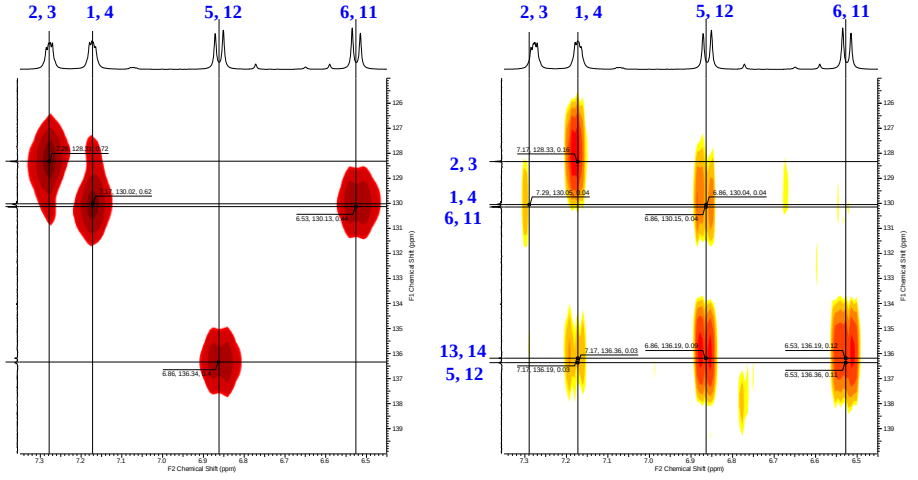

Figure 3.41 Enlarged view of 2D spectra for **29**, 600 MHz, RT, acetone-d_6; (a) HMQC, and (b) HMBC.

3.3.2 Characterization of 36

It was observed that the ^{1}H NMR spectrum of the manganese complexes in CD_2Cl_2 shows broad peaks at room temperature. The experimental spectrum for **28** and data reported by Sun *et al.* also confirm this behavior.[168] ^{1}H NMR spectra for the monometallic complexes of DBCOT are compared in Figure 3.42. Unlike for **29**, peaks in the spectrum of **36** are all within a 1.3 ppm window. All arene peaks are broad singlets. The doublet for H5, H12 is observed to overlap the coordinated ring β proton peaks. **36** showed greater separation of α and β proton peaks in both the coordinated and uncoordinated arene.

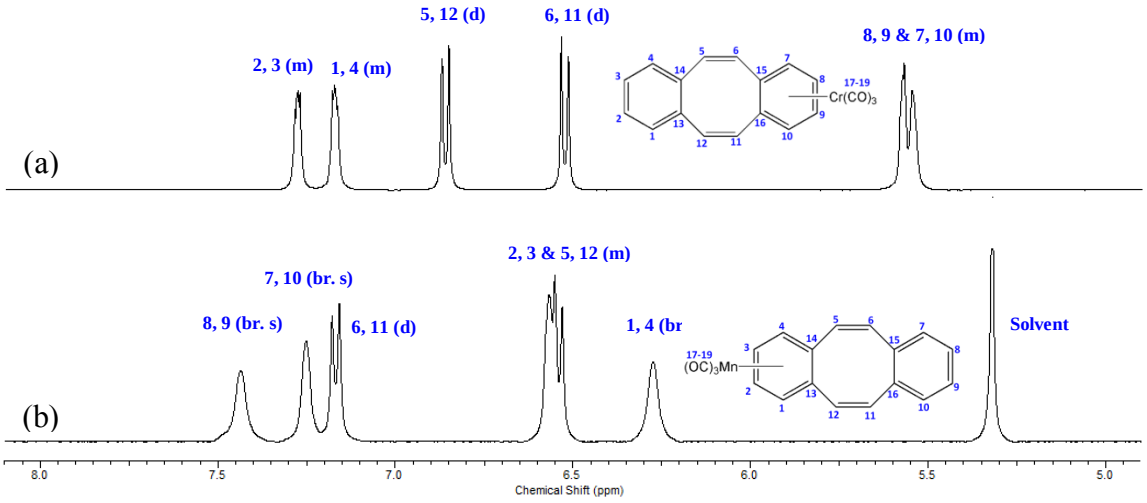

Figure 3.42 ^{1}H NMR spectra for the mono metallic complexes, 600 MHz, RT; (a) **29** in acetone-d_6, and (b) **36** in CD_2Cl_2.

In the ^{1}H-^{1}H COSY spectrum, cross coupling peaks were observed between alkene protons and coordinated arene protons. In the manganese complexes, clear cross peaks were observed for coordinated arene protons as opposed to their absence in the COSY spectrum of the chromium complex. Direct C-H couplings were observed in the HMQC spectrum (Figure 3.43). Long range ^{13}C-^{1}H couplings were observed in the HMBC spectrum (Figure 3.44). Interestingly, no couplings were present for protons H1, H4 and H8, H9 in the HMBC spectrum. The peak for the (C5, C12) and (H6, H11) correlation also appeared to be unusually weak. All other ^{13}C-^{1}H couplings appeared in expected positions.

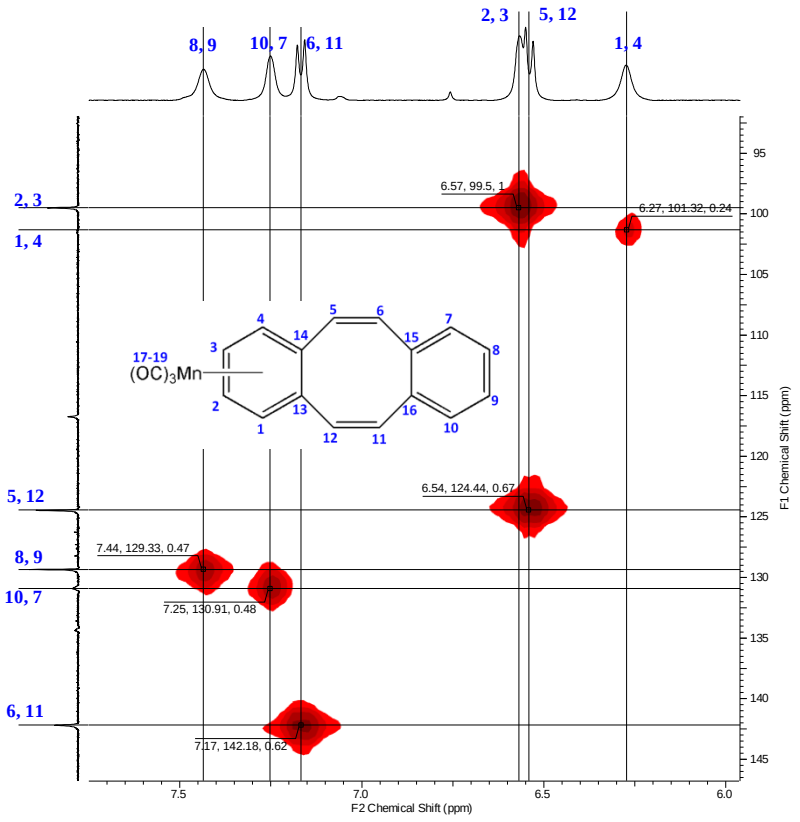

Figure 3.43 HMQC spectrum for **36**; 600 MHz, RT, CD_2Cl_2.

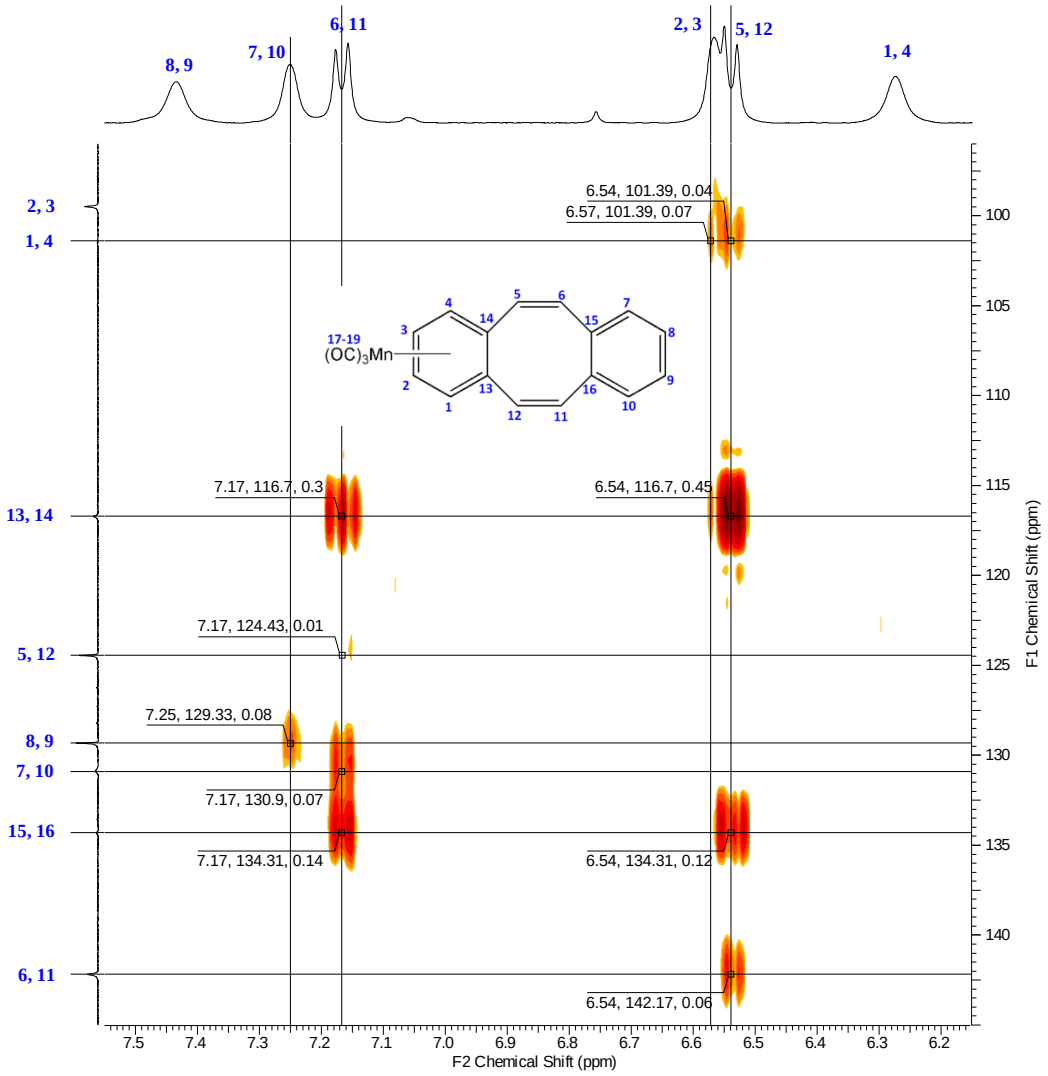

Figure 3.44 HMBC spectrum for **36**; 600 MHz, RT, CD_2Cl_2.

3.3.3 Characterization of 38

The free ligand **13** shows only two peaks for the arene and alkane protons (7.00 and 3.07 ppm). With the coordination to a manganesetricarbonyl moiety, six peaks are present for complex **38**. Apart from the separation of coordinated and non-coordinated arenes, the alkane protons also separate into three peaks. This separation of alkane protons depends on the relationship to the metal group. The metal moiety is coordinated to the C1, C2, C3, C4, C13 and C14 carbons in an *anti* conformation. The protons closer to the inside of the tub are assigned as 'C' and the protons placed away from the concave side are assigned as 'D'. The COSY spectrum for **38** is shown in Figure 3.45 and the HMQC spectrum in Figure 3.46. The HMBC spectrum is shown in Figure 2.11.

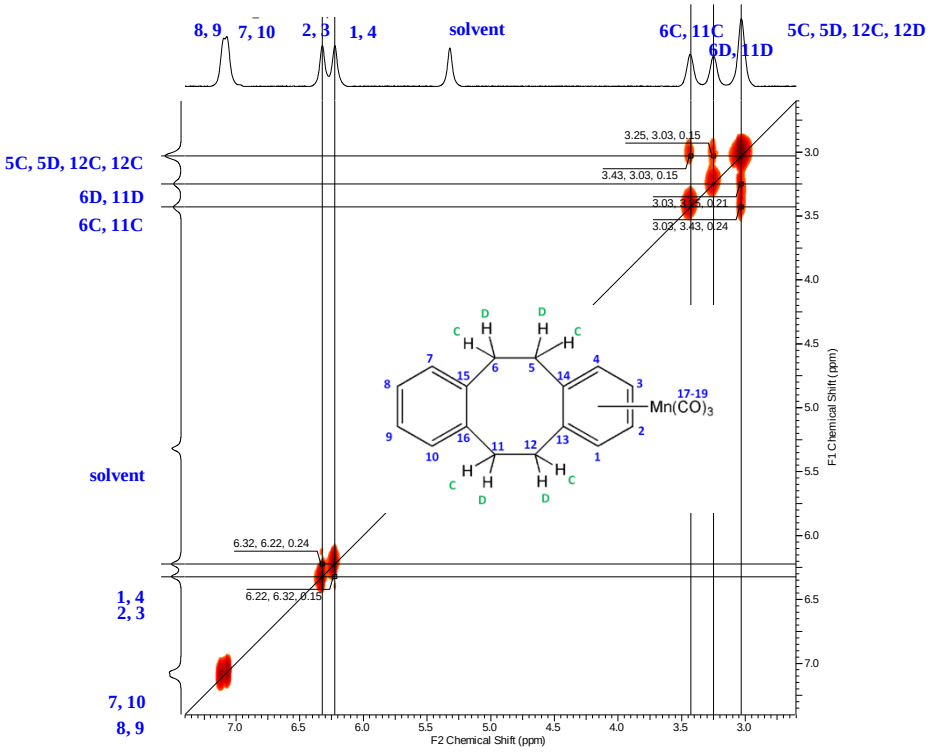

Figure 3.45 COSY spectrum for **38**; 600 MHz, RT, CD_2Cl_2.

In the ^{13}C NMR spectrum of **38**, all alkane carbons appear as one peak at 33.62 ppm. From Figure 3.46, direct C-H couplings can be observed. The carbon species at 33.62 ppm is shown to correlate with three separate proton signals at 3.43, 3.25 and 3.03 ppm. The H5C, H5D, H12C, and H12D protons were observed at the same chemical shift. The H6C and H11C protons are the least shielded and have a weak coupling from C1 and C4. The 6D and 11D protons are the furthest from the inside of the tub, and therefore, no coupling was observed with C7 and C10. **38** showed the highest number of cross peaks in all HMBC spectra during this study with 23 couplings (Figure 2.10).

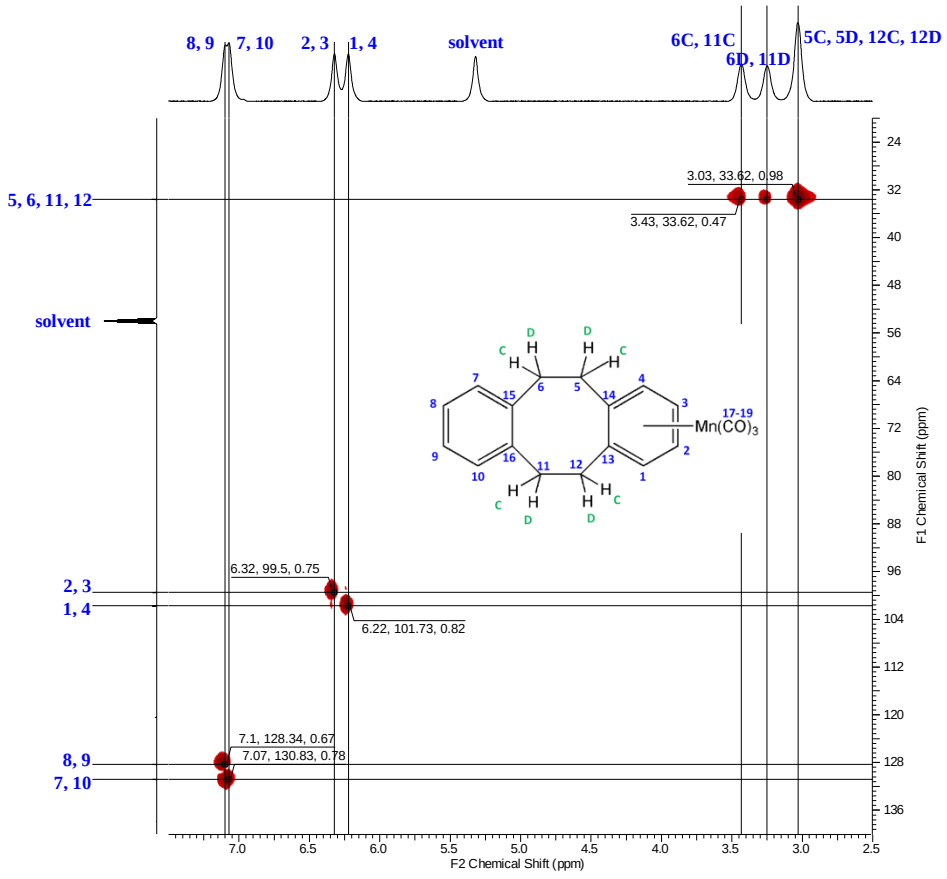

Figure 3.46 HMQC spectrum for **38**; 600 MHz, RT, CD_2Cl_2.

3.3.4 VT NMR analysis of monometallic complexes

3.3.4.1 Ring inversion of 29

Since the fluxionality of the DBCOT and the bischromium complex is already established, the monometallic complex **29** was also studied by VT NMR. Other than temperature dependent chemical shifts at low temperatures, no spectral changes are observed. As discussed earlier, complex **30** displays classical equal population equilibrium in its dynamic process with the associated change in alkenyl proton resonances. It was expected that complex **29** should also undergo a dynamic process (Scheme 3.4). The absence of spectral evidence suggests that either the fluxional process in **29** is too fast on the NMR time scale or the populations of the *anti* and *syn* species are highly unequal. Theoretical calculations were performed in search of an explanation.

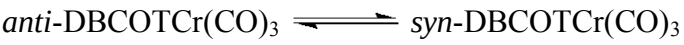

Scheme 3.4 The dynamic process in **29**

3.3.4.2 VT NMR analysis of complex 36

Unlike in the monochromium complex, **36** showed spectral changes with the decrease of temperature in the ^{1}H NMR experiment (Figure 3.47). Additional sharpened peaks were observed with the lowering of the temperature. The dynamic process for **36** should be similar to the one in Scheme 3.4, but it will not be in a 1:1 equilibrium as observed for **30**. With the overlapping of existing peaks, only a portion of emerging peaks were visible; a simulation of the dynamic process of **36** could not be achieved. As

such, the barrier to inversion could not be obtained experimentally. The ^{13}C NMR spectra taken at various temperatures are given in Figure 3.48.

The crystallographic data clearly indicated the manganese species in the solid state as *syn*-DBCOTMn(CO)$_3$. It can be assumed, even in solution, that *syn*-DBCOTMn(CO)$_3$ is preferred over *anti*-DBCOTMn(CO)$_3$ in the continuous dynamic process. The ^{1}H NMR spectra at low temperatures indicate the ratio between the two species is around 1:10. Theoretical calculations were conducted to further investigate the preference of the isomers.

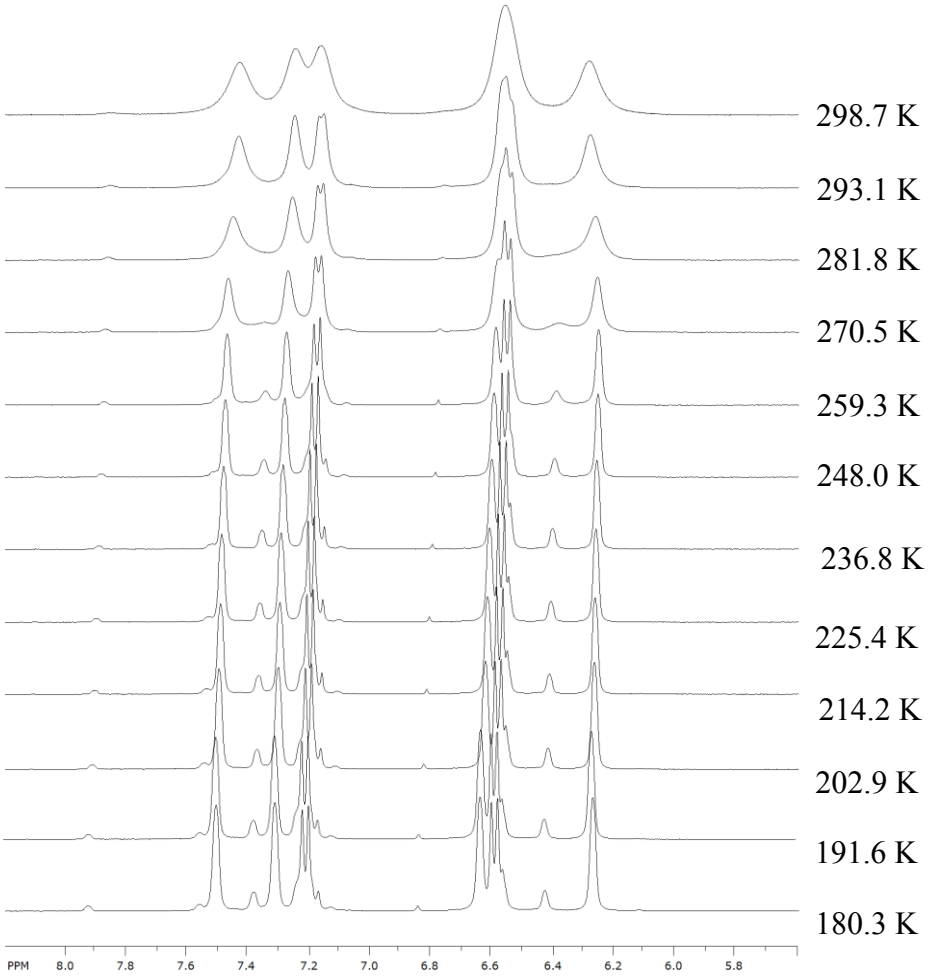

Figure 3.47 ^{1}H VT NMR spectra for **36**, 600 MHz, CD_2Cl_2.

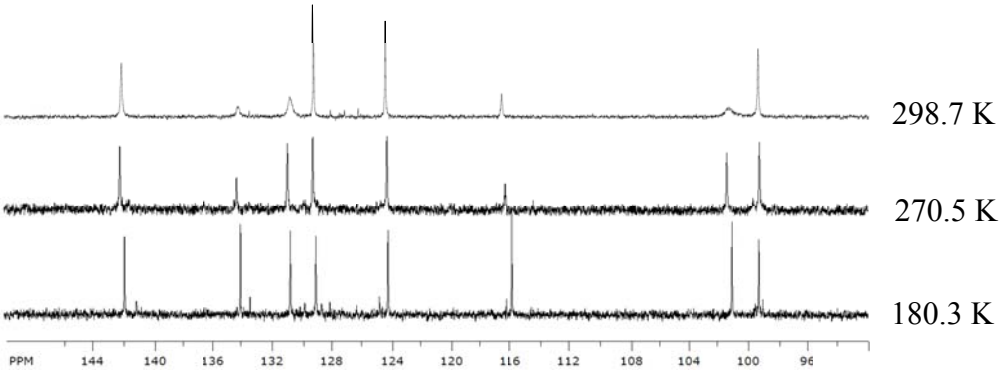

Figure 3.48 ^{13}C VT NMR spectra for **36**, 600 MHz, CD_2Cl_2.

3.4 Electrochemical analysis for chromium carbonyl complexes

Reike and coworkers studied the reduction chemistry of conjugated diarene bistricarbonylchromium complexes (Scheme 1.12).[155] Electrochemical analysis revealed that the naphthalenetricarbonylchromium dianion showed higher stability compared to the benzene dianion.[148, 152] The unusual stabilization in the naphthalene dianion resulted from a haptotropic rearrangement mechanism, where a reversible two-electron process was observed between **24** and **26** (Scheme 1.11).[148, 149]

In light of the above results, electrochemical studies for complexes **29** and **30** were conducted. Interestingly, the bischromiumtricarbonyl system showed reversibility in the CV. For complex **29** very little re-oxidation was observed (Figure 3.49). Both systems have similar reduction potentials with E_{pc}'s of -2.24 V vs. Fc/Fc^{+}. Several of the $E_{1/2}$ and E_{pc} values for related compounds are listed in Table 3.8. The CV of **30** shows similar shape to **24** indicating a rearrangement process stabilizes the reduced species. The DigiSim electrochemical simulation program was used to derive the mechanism of this reversible process. An acceptable fitting was not obtained. Having two arenes connected to the COT ring, **30** can rearrange into a conjugated complex. Conjugation is not achieved unless a planar geometry is obtained. Complex **30** was stirred with excess alkali metals under inert conditions to isolate a stable reduced species, but no change was detected in the IR.

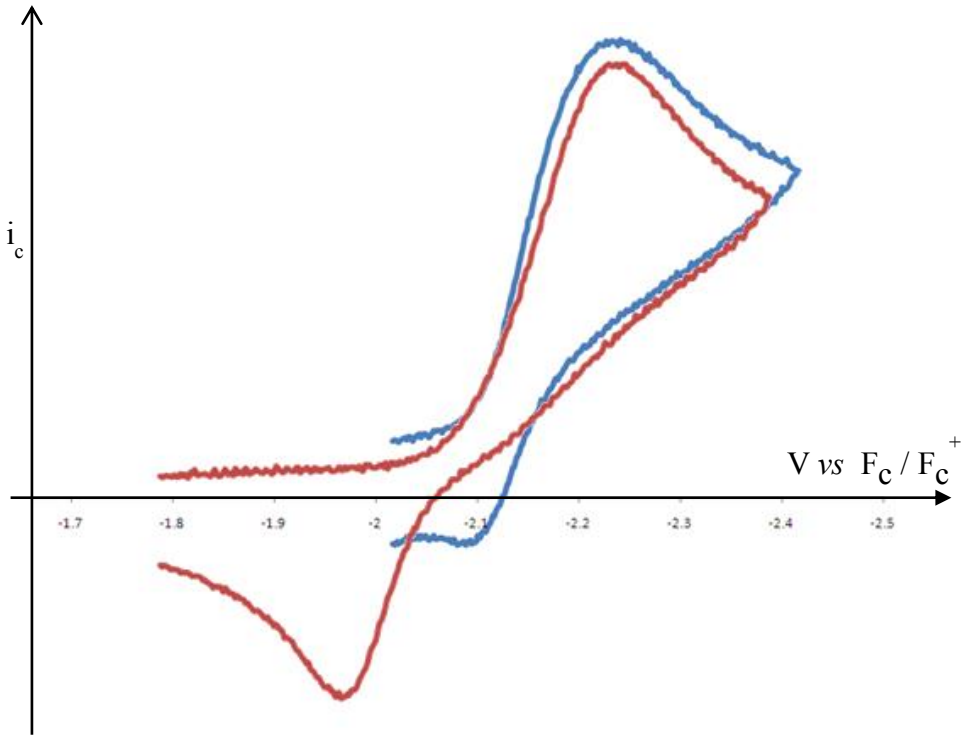

Figure 3.49 CV for **29** (blue) and **30** (red); Potentials were measured with respect to ferrocene internal standard.

Table 3.8 Selected reduction potential values from literature, Potential (V) adjusted to Fc/Fc^+ reference

Compound / Complex	Reduction potential/V
1	$E_{1/2}$ = -2.24[336]
1	$E_{1/2}(1)$ = -2.09 $E_{1/2}(2)$ = -2.17[337]
2	$E_{1/2}(1)$ = -2.26 $E_{1/2}(2)$ = -2.24[336]
10	$E_{1/2}$ = -2.28[336]
23	E_{pc} = -2.60[148]
24	E_{pc}= -1.98[152]

3.5 Theoretical calculations of DBCOT and its complexes

3.5.1 Ring inversion of DBCOT

Being symmetric molecules, neither COT, BCOT, nor DBCOT can be used alone in NMR studies to obtain the energy barrier for ring inversion. Therefore, all of the experimental values obtained are achieved with the introduction of (a) functional group(s) to break the symmetry of the molecule. Selected examples of mono substituted COT, BCOT, and DBCOT compounds, with their experimental energy barrier for ring inversion are listed in Figure 3.50.[3, 107] Using theoretical methods, activation parameters for the pure ligands can be calculated in the gas phase. In 2009, Bachrach reported the energy barriers to ring inversion for ligands **1**, **2**, and **10** using B3LYP/6-31G** and MP2/6-31G** basis sets.[108] In collaboration with Dr. Steven Gwaltney's research group, the barrier to ring inversion was calculated for DBCOT and **1b** using the B3LYP/6-31G** basis set. The energies were calculated at 298 K. These results are listed in Table 3.9 along with Bachrach's values.[108]

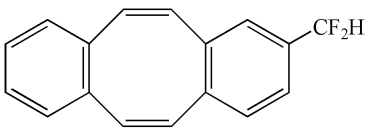

1b
12.3 ± 0.2 kcal mol^{-1}
-5°C

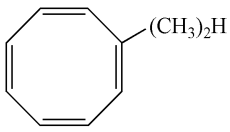

2f
14.8 ± 0.2 kcal mol^{-1}
-25°C

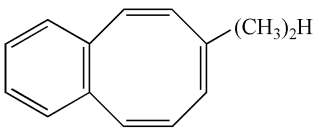

10a
13.4 ± 0.2 kcal mol^{-1}
-30°C

Figure 3.50 Selected examples of fused benzo derivatives and their $\Delta G^{\ddagger}$ obtained from VTNMR experiments; **1b**,[3] **2f**,[107] and **10a**.[107]

Table 3.9 Calculated energy barrier for ring inversion (electronic energies) of **1**, **2** and **10** using DFT and MP2 calculations.

Compound	Barrier heights (electronic energies) reported by Bachrach[108]		Barrier heights (electronic energies) calculated in this study
	B3LYP/6-31G** (kcal mol^{-1})	MP2/6-31G** (kcal mol^{-1})	B3LYP/6-31G** (kcal mol^{-1})
10	9.06	15.51	-
2	10.55	15.62	-
1	9.22	16.91	9.18
1b	-	-	9.44

The experimental values given in Figure 3.50 are $\Delta G^{\ddagger}$'s, while the calculated values listed in Table 3.9 are electronic energies. The total electronic energies were calculated independent of the temperature, while $\Delta G^{\ddagger}$ is temperature dependent. Therefore, the above results cannot be used in a direct comparison. The DFT/B3LYP calculations generally underestimate the true energy barrier. In contrast to this, the Møller-Plesset perturbation theory second order correction (MP2) approximations tend to overestimate the real value.[338] The average of these two methods generally provides a close approximation to the ring inversion barrier. Therefore, average of the two calculations may compare favorably with the experimental values. Furthermore, the relative energy differences of both calculated and experimental values should be comparable.

In this study, the electronic energies were calculated using B3LYP/6-31G**, and the values obtained for ligand **1** agree with Bachrach's DFT calculation.[108] The electronic

energy for compound **1b** was calculated, as it is the only experimentally determined DBCOT ring inversion barrier. According to DFT calculations, a slight barrier difference was observed between **1** and **1b**.

3.5.2 DFT calculations on monometallic tricarbonyl complexes

When two different but isoelectronic metal moieties were coordinated to ligand **1**, the resulting monometallic complexes showed opposite geometries in the crystal. The monochromium complex **29** favored the *anti* conformation, while manganese complex **36** favored *syn* with respect to the DBCOT tub. To understand the reasons behind these preferences, the above complexes were investigated by theoretical methods in the absence of packing forces. Using DFT/B3LYP calculations, the energy minimized structures for both chromium and manganese derivatives were determined. The *syn* and *anti* gas phase molecules of each metal were compared to determine the most stable conformers (Figure 3.51).

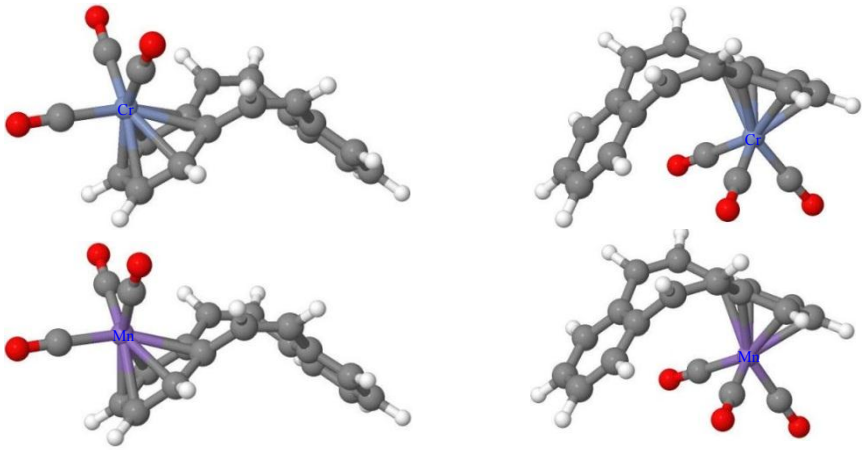

Figure 3.51 Minimum energy geometries for the *anti* (left) and *syn* (right) conformers of $DBCOTCr(CO)_3$ (top) and $[DBCOTMn(CO)_3]^+$ (bottom).

According to gas phase calculations for the DBCOTCr(CO)$_3$ complex, the internal energy of the *anti* conformation is lower than the *syn* conformation by 1.69 kcal mol^{-1}. The lowest energy was found when the carbonyls are in an *exo* staggered orientation. In the crystal structure, the *endo* staggered orientation was observed. However, the difference between *anti-exo* and *anti-endo* was only 0.59 kcal mol^{-1}. After an enthalpy correction, it was found that the enthalpy for the *anti* geometry is more stable by 1.70 kcal mol^{-1}. The entropy for the *anti* conformation is calculated to be slightly lower (by 0.50 cal mol^{-1} K^{-1}) than the *syn* conformation. At 298 K, the free energy for the *anti* conformer is favored by 2.11 kcal mol^{-1} compared to the *syn* conformation. Therefore, it can be stated that in **29**, the calculated gas phase structure agrees with the solid state crystal structure.

$$\Delta G = -RT \ln K \tag{3.16}$$

$$K_{anti/syn} = \frac{[anti\text{-DBCOTM(CO)}_3]}{[syn\text{-DBCOTM(CO)}_3]} \tag{3.17}$$

The relationship between the free energy and the equilibrium constant is found in Equation 3.16. The equilibrium constant for the different geometries in Scheme 3.4 can be defined as in Equation 3.17. Using the calculated free energy difference between the *syn* and *anti* species, $K_{anti/syn}$ can be calculated. From the equilibrium constant, the ratio between species can be estimated. The preference for *anti*-DBCOTCr(CO)$_3$ over *syn*-DBCOTCr(CO)$_3$ was calculated to be around 22:1. The high preference for *anti* species over *syn* may be the reason for not observing any spectral change in the NMR spectra at low temperatures. When temperature decreases, the τ increase, but if the species

population is too low, the chances of detecting the above species also become lower. Furthermore, when the temperature is lowered the K value also decreases, and the ratio between *anti* and *syn* increases.

In the manganesetricarbonyl derivative, the opposite geometry from **29** was calculated. The internal energy of the *syn* conformer is lower than the *anti* conformer by 0.94 kcal mol^{-1}. After correction, the enthalpy of the *syn* conformer is more stable by 0.96 kcal mol^{-1}. However, the entropy of the *anti* conformer is 3.2 cal mol^{-1} K^{-1} higher than for the *syn* conformer. According to theoretical calculations in the manganese derivative, the enthalpic and entropic contributions favor alternate conformers, *syn* and *anti*, respectively. The calculated free energy difference for the two species is merely 0.27 kcal mol^{-1} at 298 K favoring *syn*-$[DBCOTMn(CO)_3]^+$. The calculated minimum geometry agrees with the solid state crystal structure of **36**.

In complex **36**, a dynamic process occurs as in Scheme 3.4. Due to the internal energies being approximately equal, it can be assumed that both *anti* and *syn* species might give peaks in the slow exchange regime in the NMR experiment. It can be concluded the *anti*-$[DBCOTMn(CO)_3]^+$ species was observed in the low temperature NMR spectra as the emerging peaks. According to the calculations, the ratio of *syn* over *anti* was found to be 1.6:1.

The theoretical calculations can also be used to gain some insights about the packing forces in the crystal. In the geometry optimized gas phase structure of *anti*-$DBCOTCr(CO)_3$, the angle between the least squares planes was measured as 106.1°. This value is close to those values observed for the **30** and **36** complexes. The angle

determined in the crystal lattice for **29** was almost 90°. This observation clearly suggests that the extremely closed angle results from packing forces. In the monochromium complex, a dimer was formed having C-H$\cdots\pi$ interactions from the coordinated ring to the uncoordinated ring.

3.5.3 DFT calculations on bimetallic chromiumtricarbonyl complexes

During the synthesis and separation of the bimetallic chromium complex, it was observed that the major product was the *syn*,*anti*-DBCOT[$Cr(CO)_3$]$_2$. The crystal structure contained two chromium moieties attached on the opposite sides of the DBCOT tub.[190] However, it was also observed that the *anti*,*anti* product could be isolated in low yields. Fakhri *et al.* found that the *anti*,*anti* configuration was favored in the bischromium DBCOD complex.[193] Therefore, it was of interest to evaluate the favored conformations in bimetallic complexes of DBCOT. Theoretical calculations were conducted using the B3LYP/6-31G** basis set.

The calculated geometries are summarized in Figure 3.52 and Table 3.10. For ease of comparison, all energy values are compared relative to the energy of the lowest conformation found (the *syn*,*anti* isomer). Calculated results clearly indicate that the tricarbonyl orientation has a significant effect on the energies of these isomers. In the gas phase the *anti*,*anti* and *syn*,*anti* configurations were calculated to be essentially the same. However, from the crystal structure and the NMR spectrum the *syn*,*anti* configuration is preferred over the *anti*,*anti* configuration. From the NMR spectrum of the reaction mixture, the ratio of *syn*,*anti* to *anti*,*anti* were evaluated to be 20:1.

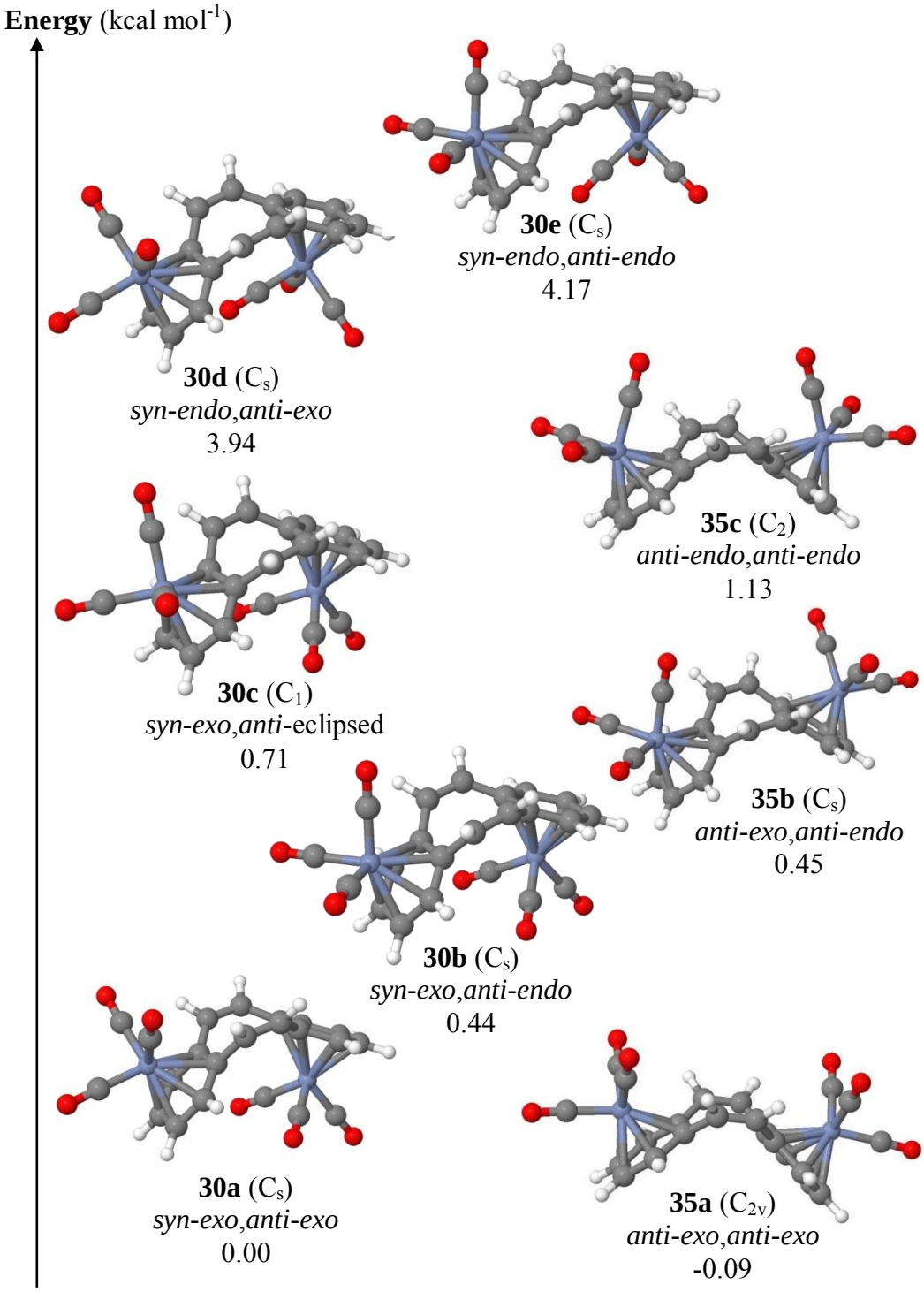

Figure 3.52 Energy diagram for possible geometries of *syn*,*anti* and *anti*,*anti*-isomers of DBCOT[Cr(CO)$_3$]$_2$; Electronic energies are compared relative to **30a**.

Table 3.10 Calculated structures and their thermodynamic parameters of *syn,anti* and *anti,anti*-isomers in DBCOT[$Cr(CO)_3$]$_2$; All energies compared relative to **30a**.

	Carbonyl orientation	Point group	Relative electronic energy kcal mol^{-1}	Relative ΔG kcal mol^{-1}	Relative ΔH kcal mol^{-1}	Relative ΔS kcal mol^{-1} K^{-1}
30a	*exo,exo*	C_s	0.00	0.00	0.00	0.00
30b	*exo,endo*	C_s	0.44	-0.09	0.50	2.56
30c	*exo*,eclipsed	C_1	0.71	1.79	0.20	-4.52
30d	*endo,exo*	C_s	3.94	4.79	3.43	-0.64
30e	*endo,endo*	C_s	4.17	4.65	3.70	0.97
30f	*endo,endo*	C_{2h}	9.49	-	-	-
30g	*exo,exo*	C_s	12.51	-	-	-
30h	*exo,endo*	C_s	10.62	-	-	-
30i	eclipsed,eclipsed	C_s	12.41	-	-	-
35a	*exo,exo*	C_{2v}	-0.09	-0.27	-0.08	0.46
35b	*exo,endo*	C_s	0.45	-0.96	0.55	5.64
35c	*endo,endo*	C_2	1.13	-0.151	1.28	6.13

In the crystal structure of **30**, four different carbonyl orientations were observed. The structures **30a**, **30b**, and **30c** are similar to the A, D and B independent molecules in the crystal lattice of **30**. Molecule A having the *exo,exo* carbonyl orientation is the lowest *syn,anti* isomer. The energy differences between A and D, and B and D are calculated to be 0.44 and 0.269 kcal mol^{-1}, respectively. From the packing diagrams, it was determined that these carbonyl orientations are controlled by C-H···O hydrogen bonding.

30a and **30b** are the two minimum energy orientations calculated for the *syn,anti* isomer (no imaginary frequencies present). Going from **30a** to **30b**, the rotation of the *anti* moiety takes place *via* the eclipsed transition state (**30c**). Therefore, the rotational barrier for the *anti* moiety is 0.71 kcal mol^{-1}. The rotational barrier for the *syn* moiety is

much higher in comparison to the *anti* moiety, as it experiences steric influences from the carbon skeleton. The energy difference between **30a** to **30d** is 3.94 kcal mol^{-1}. The larger energy gap seems to hinder the rotation of the *syn* moiety. This explains the crystal structure of **30**, where all four molecules (A-D) are in the *exo* orientation for the *syn* moiety.

The transition state for the ring inversion of **30** was evaluated using gas phase calculations. The resulting planar geometries are shown in Figure 3.53. Structure **30f** with the *endo*,*endo* configuration was the minimum energy geometry observed for the TS for the RI process. The calculated energy barrier to inversion is 9.48 kcal mol^{-1}. As discussed in Section 3.4.1, B3LYP/6-31G** generally underestimates the barrier.

The *exo*,*exo* orientation of a planar structure (**30g**) was also evaluated. Surprisingly, unlike in the boat conformation, the *exo*,*exo* was a highly unfavorable (12.51 kcal mol^{-1}) in the planar geometry. The *exo*,*endo* orientation (**30h**) of the planar structure is 10.62 kcal mol^{-1} higher than **30a**. The barrier for the tripod rotation in the planar transition state is determined as 1.14 kcal mol^{-1} from the difference between **30f** and **30h**.

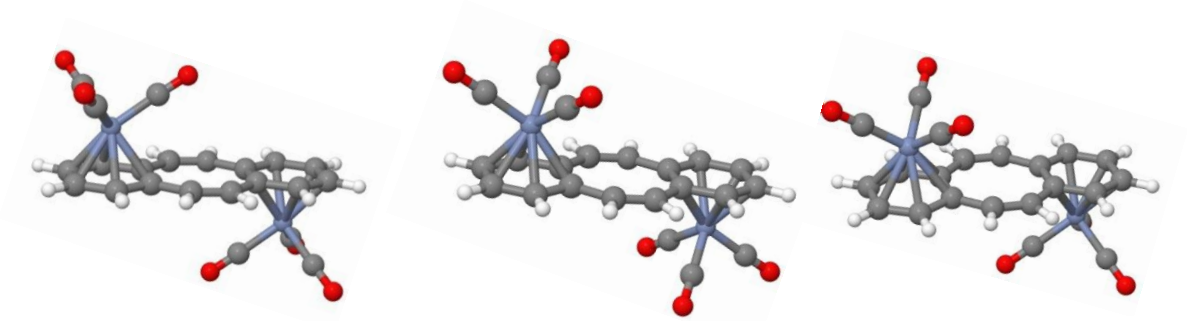

30f (C_{2h})
endo,*endo*
9.48 kcal mol^{-1}

30g (C_{2h})
exo,*exo*
12.51 kcal mol^{-1}

30h (C_s)
exo,*endo*
10.62 kcal mol^{-1}

Figure 3.53 Calculated planar transition states and the second order sadle points for *syn*,*anti*-DBCOT[$Cr(CO)_3$]$_2$. Energies are compared relative to **30a**.

3.5.4 Hindered rotor model for 30

The insight gained from theoretical calculations was beneficial to understanding the experimental results. According to line shape analysis for the ring inversion of **30**, $\Delta H^{\ddagger}$ and $\Delta S^{\ddagger}$ were determined to be 15.9 ± 0.4 kcal mol^{-1} and 12 ± 2 cal mol^{-1} K^{-1}, respectively. These values differ from the reported COT systems in the literature.[186, 269-277]

It is postulated that the large favorable entropy of activation is due to the free rotation of the carbonyl moieties achieved in the planar transition state. In the energy minima (**30a** and **30b**), only the *anti* moiety is able to rotate freely while the *syn*-$Cr(CO)_3$ group is hindered by the carbon skeleton. In the TS, both $Cr(CO)_3$ groups are unobstructed by the DBCOT framework. The calculated rotational barriers were 0.71 kcal mol^{-1} and 3.938 kcal mol^{-1} for *anti* and *syn* moieties in the ground state when compared to 1.14 kcal mol^{-1} in the transition state.

The large enthalpy of activation for **30** is due to the attractive interactions between carbonyls of the *syn*-chromiumtricarbonyl group with the arene ring. Similar to **36**, having a *syn* conformation is enthalpically favorable in the tub structure. The energy requirement and the overall RI process of **30** are summarized in Figure 3.54.

The main hypothesis is that the favorable $\Delta S^{\ddagger}$ is achieved by the ability of the tricarbonyl group to rotate freely in the TS. However, it should be noted that the solvent also plays a vital part in this process. The ring inversion process occurs in solution. There are molecule-solvent, and solvent-solvent interactions at play. Modeling with solvents is computationally expensive. Therefore, the solvent interactions are excluded in most theoretical studies. During the planarization of complex **30**, the previously hidden polar *syn* chromiumtricarbonyl unit will gain the ability to interact with the solvent molecules freely. These interactions should also contribute toward providing favorable conditions for the RI process.

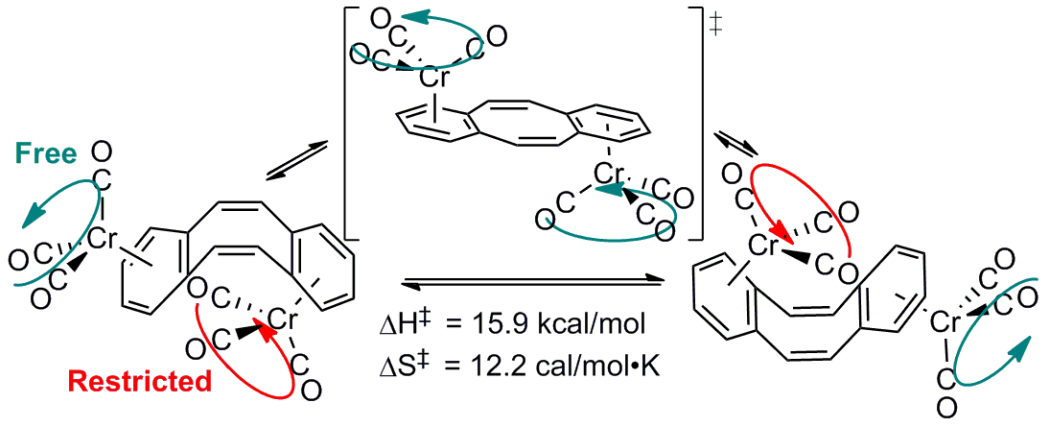

Figure 3.54 A schematic diagram displaying the hindered rotation of the ground state of **30**.

CHAPTER IV

CONCLUSIONS

Chromium and manganese "piano stool" type complexes of the organic ligand dibenzo[*a*,*e*]cyclooctatetraene have been studied. Prior to this work, eight membered ring inversions for compounds with a π-coordinated metal has not been studied. The main focus of the research was to evaluate the barrier to inversion in an η^6-arene COT derivative using NMR line shape analysis. The DBCOT alkenyl protons provided a straightforward system to study ring inversion in η^6,η^6-dibenzo[*a*,*e*]cyclooctatetraene-*syn*,*anti*-bis-(tricarbonylchromium). At room temperature, a singlet was observed at 6.65 ppm for all four alkene protons. When cooled to 180 K, two sets of sharp doublets appeared at 6.82 and 6.67 ppm with a coupling of 12 Hz. Accurate temperature determinations were made possible by calibrations using methanol-d_4.[212] The coalescence temperatures were found at 255.8 and 261.9 K for 300 and 600 MHz field strengths, respectively. The free energy of activation of the bistricarbonylchromium complex was determined to be 12.7 ± 0.1 kcal mol^{-1} at these two temperatures.

The activation parameters were obtained from Eyring plots (ln k/T vs 1/T) for the two different NMR field strengths. Surprisingly, coordination did not have a major effect on the overall free energy of activation. The $\Delta G^{\ddagger}$ found was similar to the value reported for 2-difluoromethyl derivative of DBCOT.[3] However, the enthalpy of activation and entropy of activation were significantly different from values found in the literature.[4, 6, 30]

The π-coordination results in an increase in the entropy of activation and a higher value for the enthalpy of activation. These are offsetting factors that leads to a similar $\Delta G^{\ddagger}$ as for the uncoordinated DBCOT. So far, all reported $\Delta S^{\ddagger}$ values for eight membered ring inversion were either negative or slightly positive.[186, 269-277] The highest reported $\Delta S^{\ddagger}$ was 2.2 cal mol^{-1} K^{-1}.[277] Therefore, the observed value of 12 ± 2 cal mol^{-1} K^{-1} is the highest favorable entropy of activation obtained for ring inversion in a cyclooctatetraene derivative. Because of the low absolute values for $\Delta S^{\ddagger}$, for COT derivatives $\Delta G^{\ddagger}$ is an approximation of the enthalpy of activation.[186, 269-277] The value of 15.9 ± 0.4 kcal mol^{-1} observed in this system is a high value for $\Delta H^{\ddagger}$ for a RI process.

According to density functional theory calculations using B3LYP/6-31G**, the favorable entropic term occurs because of the unrestricted chromiumtricarbonyl rotation in the planar transition state. The high enthalpic barrier is assumed to be the result of attractive interaction between the *endo* carbonyl groups of the *syn*-$Cr(CO)_3$ moiety and the remote arene ring. While in most nonmetallic systems $\Delta S^{\ddagger}$ is negligible, the huge enhancement of the favorability entropy of activation for ring inversion by coordinating a metal is demonstrated for the first time in this study.

With the bimetallic chromium complex favoring the *syn*,*anti*-configuration,[190] the question about the preferred configuration for monometallic complexes arose. Therefore, the cationic manganesetricarbonyl complex was synthesized for the first time using a manganesetricarbonyl transfer.[166] The crystal structures of this complex and the isoelectronic chromiumtricarbonyl derivative were obtained. Surprisingly, it was found that the orientations in the structures of the two compounds are different. In the $Cr(CO)_3$

complex, the metallic group is on the convex side of the DBCOT backbone. Conversely, the $Mn(CO)_3^+$ group is coordinated to the concave side of the organic backbone in the solid state. DFT calculations on the compounds confirmed that the observed metal orientations are the minimum energy geometries. In the case of manganese, an interaction of the carbonyls and the uncoordinated arene stabilizes the *syn* orientation.

In 1951, Cope and Fenton reported the constitutional isomer for the dibromo-5,6,11,12-tetrahydrodibenzo[*a,e*]cyclooctadiene.[78] However, previous to the current work the orientation of the two bromines was not known. Thaler and Yates predicted a *trans*-dibromo product.[44, 286] However, the crystal structure unequivocally shows a *cis* geometry for the dibromo product. The two bromine atoms were found *exo* to the interior of the DBCOD tub.

The reduction chemistry of mono- and bischromium DBCOT complexes was studied by cyclic voltammetry. No change was observed in the reduction potentials when either one or two chromiumtricarbonyl groups were coordinated to DBCOT. However, the reduced species for the bischromiumtricarbonyl shows enhanced stability compared to the monochromium derivative exhibiting some reversibility in the CV. It is postulated that the extra stability is due to haptotropic rearrangement in the π-arene coordinated system. Isolating a stable anionic species was not successful as the reduction was not observed even when excess sodium and potassium metal were added.

$DBCOTCr(CO)_3$ and $[DBCOTMn(CO)_3]^+$ were studied by variable temperature NMR. The chromium complex did not show any change with temperature, while the manganese showed additional peaks at low temperatures. According to DFT calculations,

the energy difference between *syn* and *anti*-$[DBCOTMn(CO)_3]^+$ is small. Therefore, it can be assumed that the emerging peaks in the low temperature NMR correspond to the *anti*-$[DBCOTMn(CO)_3]^+$.

All crystal structures discussed in this dissertation contained interesting hydrogen bonding interactions. In $DBCOTCr(CO)_3$, C-H···π interactions were observed and lead to formation of a dimeric arrangement in the crystal lattice. This is the first example of a COT derivative forming a dimer containing C-H···π hydrogen bonds. The dimeric packing was responsible for an extremely closed angle (91.70°) for the DBCOT backbone. These structural features may be used to developed tubular arrangements in supramolecular chemistry.

The angle between the two arene rings in $[DBCOTMn(CO)_3]BF_4$ is 106.7°. The higher angle in the manganese complex is the result of steric congestion introduced by the *syn*-moiety inside the tub. C-H···O hydrogen bonds in the manganese complex are stronger than in the isoelectronic chromium complex. The strong electron withdrawing effect of Mn^+ is the reason for this. Charge-assisted C-H···F hydrogen bonds were also observed due to the presence of the BF_4^- counter anions. The close arrangement of coordinated and non-coordinated arenes in $[DBCOTMn(CO)_3]^+$ resulted in linear continuous packing with π-π stacking interactions. This is the first arenetricarbonyl manganese complex having a linear arrangement with π-π stacking interactions in the crystal lattice. These might be useful in designing novel supramolecular organometallic layered materials.

The manganese complex of the 5,6,11,12-tetrahydrodibenzo[*a*,*e*]cyclooctadiene ligand was made for the first time. Interestingly, the $Mn(CO)_3^+$ moiety is observed in an *anti* position, compared to the *syn* isomer observed for $[DBCOTMn(CO)_3]^+$. Another striking difference is that $[DBCODMn(CO)_3]^+$ contains two independent molecules in the crystal lattice having *endo* and *exo*-staggered tripod orientations. Both C-H···F and C-H···O hydrogen bond interactions are observed in the crystal lattice. Synthesis of a heteronuclear bimetallic complex incorporating the DBCOT ligand was also attempted, but it was not successful. However, a novel co-crystal was isolated having $DBCOTCr(CO)_3$ and naphthalene in a 2:1 ratio. Unlike in $[DBCODMn(CO)_3]^+$, the independent molecules showed the same tripod orientations, but contained different angles for the DBCOT tub. Only one independent molecule is observed to interact with the naphthalene molecule by forming a C-H···π hydrogen bond.

In this dissertation, four new organometallic crystal structures were reported. They all show unique individual characteristics with different metal coordination, tripod rotation or the angle of the DBCOT tub. Now that these effects have been identified, they may be useful in development of other systems. These structural motifs might be important as synthons in organometallic supramolecular chemistry for generating desired structural arrangements having noncovalent interactions.

REFERENCES

1. Irngartinger, H.; Reibel, W. R. K. *Acta Crystallogr., Sect. B* **1981,** *37*, 1724-1728.

2. Mislow, K.; Perlmutter, H. D. *J. Am. Chem. Soc.* **1962,** *84*, 3591-3592.

3. Senkler, G. H., Jr.; Gust, D.; Riccobono, P. K.; Mislow, K. *J. Am. Chem. Soc.* **1972,** *94*, 8626-8627.

4. Oth, J. F. M. *Pure Appl. Chem.* **1971,** *25*, 573-622.

5. Anet, F. A. L.; Bourn, A. J. R.; Lin, Y. S. *J. Am. Chem. Soc.* **1964,** *86*, 3576-3577.

6. Paquette, L. A. *Pure Appl. Chem.* **1982,** *54*, 987-1004.

7. Lippincott, E. R.; Lord, R. C., Jr. *J. Am. Chem. Soc.* **1946,** *68*, 1868-1869.

8. Bastiansen, O.; Hassel, O.; Langseth, A. *Nature* **1947,** *160*, 128.

9. Kaufman, H. S.; Fankuchen, I.; Mark, H. *Nature* **1948,** *161*, 165.

10. Willstätter, R.; Waser, E. *Dtsch. Chem. Gest.* **1911,** *44*, 3423-3445.

11. Anet, F. A. L. *J. Am. Chem. Soc.* **1962,** *84*, 671-672.

12. Dickens, B.; Lipscomb, W. N. *J. Am. Chem. Soc.* **1961,** *83*, 489-490.

13. Streitwieser, A.; Mueller-Westerhoff, U. *J. Am. Chem. Soc.* **1968,** *90*, 7364-7364.

14. Kroon, P. A.; Helmholdt, R. B. *J. Organomet. Chem.* **1970,** *25*, 451-454.

15. Willstätter, R.; Heidelberger, M. *Dtsch. Chem. Gest.* **1913,** *46*, 517-527.

16. Hess, K. *Ber. Dtsch. Chem. Ges. B* **1919,** *52*, 1005-1013.

17. Fray, G. I.; Saxton, R. G. *The Chemistry of Cyclooctatetraene and Its Derivatives*. 1st ed.; Cambridge University Press: Cambridge, London, 1978.

18. Morrison, R. T.; Boyd, R. N. *Organic Chemistry*. 6th ed.; Pearson Education: New York, 1992.

19. Wang, C.; Xi, Z. *Chem. Commun.* **2007**, 5119-5133.

20. "The Nobel Prize in Chemistry 1915". Nobelprize.org. http://nobelprize.org/nobel_prizes/chemistry/laureates/1915/ (accessed 25 March 2011).

21. Wawzonek, S. *J. Am. Chem. Soc.* **1940,** *62*, 745-749.

22. Rapson, W. S.; Shuttleworth, R. G. *J. Chem. Soc.* **1941**, 487-90.

23. Bachman, G. B.; Hoaglin, R. I. *J. Org. Chem.* **1943,** *8*, 300-315.

24. Hurd, C. D.; Drake, L. R. *J. Am. Chem. Soc.* **1939,** *61*, 1943-1945.

25. Schopf, C.; Lehmann, G. *Ann.* **1935,** *518*, 1-37.

26. Cope, A. C.; Overberger, C. G. *J. Am. Chem. Soc.* **1947,** *69*, 976.

27. Reppe, W.; Schichting, O.; Klager, K.; Toepel, T. *Ann.* **1948,** *560*, 1-92.

28. Sondheimer, F.; Wolovsky, R. *J. Am. Chem. Soc.* **1962,** *84*, 260-269.

29. Paquette, L. A. *Tetrahedron* **1975,** *31*, 2855-2883.

30. Anet, F. A. L. *Top. Curr. Chem.* **1974,** *45*, 169-220.

31. Lippincott, E. R.; R. C. Lord, J.; McDonald, R. S. *J. Chem. Phys.* **1948,** *16*, 548-549.

32. Kaufman, H. S.; Fankuchen, I.; Mark, H. *J. Chem. Phys.* **1947,** *15*, 414-415.

33. Bastiansen, O.; Hassel, O. *Acta Chem. Scand.* **1949,** *3*, 209-210.

34. Traetteberg, M. *Acta Chem. Scand.* **1966,** *20*, 1724-6.

35. Lippincott, E. R.; Lord, R. C.; McDonald, R. S. *J. Am. Chem. Soc.* **1951,** *73*, 3370-3385.

36. Saksena, B. D.; Narain, H. *Nature* **1950,** *165*, 723-723.

37. Dewar, M. J. S.; Merz, K. M., Jr. *J. Chem. Soc., Chem. Commun.* **1985**, 343-344.

38. Bastiansen, O.; Hedberg, L.; Hedberg, K. *J. Chem. Phys.* **1957,** *27*, 1311-1317.

39. Person, W. B.; Pimentel, G. C.; Pitzer, K. S. *J. Am. Chem. Soc.* **1952,** *74*, 3437-3438.

40. Claus, K. H.; Krueger, C. *Acta Crystallogr. Sect. C* **1988,** *C44*, 1632-1634.

41. Nishinaga, T.; Ohmae, T.; Iyoda, M. *Symmetry* **2010,** *2*, 76-97.

42. Hückel, E. *Z. Phys.* **1931,** *70*, 204-286.

43. Hückel, E. *Z. Elektrochem.* **1937,** *43*, 752-788.

44. Yates, P.; Lewars, E. G.; McCabe, P. H. *Can. J. Chem.* **1970,** *48*, 788-795.

45. Carey, F. A.; Sundberg, R. J. *Advanced Organic Chemistry; Part A: Structure and Mechanisms*. 4th ed.; Plenum Publishing: New York, 2000.

46. Katz, T. J. *J. Am. Chem. Soc.* **1960,** *82*, 3784-3785.

47. Katz, T. J. *J. Am. Chem. Soc.* **1960,** *82*, 3785-3786.

48. Katz, T. J.; Strauss, H. L. *J. Chem. Phys.* **1960,** *32*, 1873-1875.

49. Bak, D. A.; Conrow, K. *J. Org. Chem.* **1966,** *31*, 3958-3965.

50. Goldberg, S. Z.; Raymond, K. N.; Harmon, C. A.; Templeton, D. H. *J. Amer. Chem. Soc.* **1974,** *96*, 1348-1351.

51. Olah, G. A.; Staral, J. S.; Paquette, L. A. *J. Am. Chem. Soc.* **1976,** *98*, 1267-1269.

52. Olah, G. A.; Staral, J. S.; Liang, G.; Paquette, L. A.; Melega, W. P.; Carmody, M. J. *J. Am. Chem. Soc.* **1977,** *99*, 3349-3355.

53. Nishinaga, T.; Komatsu, K.; Sugita, N. *J. Chem. Soc., Chem. Commun.* **1994**, 2319-2320.

54. Klärner, F.-G. *Angew. Chem. Int. Ed.* **2001,** *40*, 3977-3981.

55. Winstein, S. *J. Am. Chem. Soc.* **1959,** *81*, 6524-6525.

56. Keller, C. E.; Pettit, R. *J. Am. Chem. Soc.* **1966,** *88*, 604-606.

57. Keller, C. E.; Pettit, R. *J. Am. Chem. Soc.* **1966,** *88*, 606-607.

58. Schröder, G. *Angew. Chem.* **1963,** *75*, 722.

59. Avram, M.; Dinulescu, I. G.; Marica, E.; Mateescu, G.; Sliam, E.; Nenitzescu, C. D. *Chem. Ber.* **1964,** *97*, 382-389.

60. Zimmerman, H. E.; Paufler, R. M. *J. Am. Chem. Soc.* **1960,** *82*, 1514-1515.

61. Zimmerman, H. E.; Grunewald, G. L. *J. Am. Chem. Soc.* **1966,** *88*, 183-184.

62. Allred, E. L.; Beck, B. R. *J. Am. Chem. Soc.* **1973,** *95*, 2393-2394.

63. Paquette, L. A. *Acc. Chem. Res.* **1993,** *26*, 57-62.

64. Luz, Z.; Meiboom, S. *J. Chem. Phys.* **1973,** *59*, 1077-1091.

65. Cohen, A. D.; Sheppard, N.; Turner, J. J. *Proc. Chem. Soc.* **1958**, 118-119.

66. Staley, S. W.; Grimm, R. A.; Martin, G. S.; Sablosky, R. A. *Tetrahedron* **1997,** *53*, 10093-10102.

67. Altmann, S. L. *Proc. R. Soc. Ser. A* **1967,** *298*, 184-203.

68. Paik, D. H.; Yang, D.-S.; Lee, I. R.; Zewail, A. H. *Angew. Chem. Int. Ed.* **2004,** *43*, 2830-2834.

69. Huisgen, R.; Mietzsch, F.; Boche, G.; Seidl, H. *Chem. Soc. (London) Spec. Publ.* **1965,** *19*, 3-20.

70. Gilchrist, T. L. *Leicester Chem. Rev.* **1968,** *9*, 7-14.

71. Huisgen, R.; Mietzsch, F. *Angew. Chem. Int. Ed.* **1964,** *3*, 83-85.

72. Paquette, L. A.; Photis, J. M.; Ewing, G. D. *J. Am. Chem. Soc.* **1975,** *97*, 3538-3540.

73. Criegee, R.; Wirth, W. D.; Engel, W.; Brune, H. A.; Fischer, H. G.; Erikson, R. D. *Chem. Ber.* **1963,** *96*, 2230-2237.

74. Berno, P.; Ceccon, A.; Gambaro, A.; Venzo, A.; Ganis, P.; Valle, G. *J. Chem. Soc., Perkin Trans. 2* **1987**, 935-941.

75. Shuttleworth, R. G.; Rapson, W. S.; Stewart, E. T. *J. Chem. Soc.* **1944**, 71-73.

76. Rapson, W. S.; Shuttleworth, R. G.; van, N. J. N. *J. Chem. Soc.* **1943**, 326-327.

77. Fieser, L. F.; Pechet, M. M. *J. Am. Chem. Soc.* **1946,** *68*, 2577-2580.

78. Cope, A. C.; Fenton, S. W. *J. Am. Chem. Soc.* **1951,** *73*, 1668-1673.

79. Baker, W.; Banks, R.; Lyon, D. R.; Mann, F. G. *J. Chem. Soc.* **1945**, 27-30.

80. Boudjouk, P.; Sooriyakumaran, R.; Han, B. H. *J. Org. Chem.* **1986,** *51*, 2818-2819.

81. Domiano, P.; Cozzini, P.; Claramunt, R. M.; Lavandera, J. L.; Sanz, D.; Elguero, J. *J. Chem. Soc., Perkin Trans. 2* **1992**, 1609-1620.

82. Brickwood, D. J.; Ollis, W. D.; Stephanatou, J. S.; Stoddart, J. F. *J. Chem. Soc., Perkin Trans. 1* **1978**, 1398-1414.

83. Wittig, G.; Koenig, G.; Clauss, K. *Ann.* **1955,** *593*, 127-156.

84. Avram, M.; Dinu, D.; Mateescu, G.; Nenitzescu, C. D. *Chem. Ber.* **1960,** *93*, 1789-1794.

85. Schröder, G.; Martin, W.; Oth, J. F. M. *Angew. Chem. Int. Ed.* **1967,** *6*, 870-871.

86. Rabideau, P. W.; Hamilton, J. B.; Friedman, L. *J. Am. Chem. Soc.* **1968,** *90*, 4465-4466.

87. Wittig, G.; Eggers, H.; Duffner, P. *Ann.* **1958,** *619*, 10-27.

88. Griffin, C. E.; Peters, J. A. *J. Org. Chem.* **1963,** *28*, 1715-1716.

89. Avram, M.; Dinulescu, I. G.; Dinu, D.; Mateesen, G.; Nenitzesen, C. D. *Tetrahedron* **1963,** *19*, 309-317.

90. Nozaki, H.; Noyori, R. *Tetrahedron* **1966,** *22*, 2163-2166.

91. Cutshall, T. W.; Rabideau, P. W. *Can. J. Chem.* **1972,** *50*, 2364-2365.

92. Cope, A. C.; Fenton, S. W. *J. Am. Chem. Soc.* **1951,** *73*, 1673-1678.

93. Chaffins, S.; Brettreich, M.; Wudl, F. *Synthesis* **2002,** *9*, 1191-1194.

94. Läng, F.; Breher, F.; Stein, D.; Gruetzmacher, H. *Organometallics* **2005,** *24*, 2997-3007.

95. Stiles, M.; Burckhardt, U. *J. Am. Chem. Soc.* **1964,** *86*, 3396-3397.

96. Salisbury, L. E. *J. Org. Chem.* **1978,** *43*, 4991-4995.

97. Katz, T. J.; Yoshida, M.; Siew, L. C. *J. Am. Chem. Soc.* **1965,** *87*, 4516-4520.

98. Carnes, M.; Buccella, D.; Decatur, J.; Steigerwald, M. L.; Nuckolls, C. *Angew. Chem. Int. Ed.* **2008,** *47*, 2982-2985.

99. Crossley, R.; Downing, A. P.; Nogradi, M.; de Oliveira, A. B.; Ollis, W. D.; Sutherland, I. O. *J. Chem. Soc., Perkin Trans. 1* **1973**, 205-217.

100. Allinger, N. L.; Sprague, J. T. *Tetrahedron* **1975,** *31*, 21-24.

101. Jimeno, M. L.; Alkorta, I.; Elguero, J.; Anderson, J. E.; Claramunt, R. M.; Lavandera, J. L. *New J. Chem.* **1998,** *22*, 1079-1083.

102. Montecalvo, D.; St. Jacques, M.; Wasylishen, R. *J. Am. Chem. Soc.* **1973,** *95*, 2023-2024.

103. Sauriol-Lord, F.; St. Jacques, M. *Can. J. Chem.* **1975,** *53*, 3768-3776.

104. Figeys, H. P.; Dralants, A. *Tetrahedron Lett.* **1971**, 3901-3904.

105. Finder, C. J.; Chung, D.; Allinger, N. L. *Tetrahedron Lett.* **1972,** *13*, 4677-4680.

106. Huang, H.; Stewart, T.; Gutmann, M.; Ohhara, T.; Niimura, N.; Li, Y.-X.; Wen, J.-F.; Bau, R.; Wong, H. N. C. *J. Org. Chem.* **2009,** *74*, 359-369.

107. Buchanan, G. W. *Tetrahedron Lett.* **1972,** *13*, 665-668.

108. Bachrach, S. M. *J. Org. Chem.* **2009,** *74*, 3609-3611.

109. Nishiuchi, T.; Kuwatani, Y.; Nishinaga, T.; Iyoda, M. *Chem.-Eur. J.* **2009,** *15*, 6838-6847.

110. Zeise, W. C. *Ann. Phys.* **1827,** *9*, 932.

111. Zeise, W. C. *Ann. Phys.* **1831,** *97*, 497-541.

112. Collman, J. P.; Hegedus, L. S.; Norton, J. R.; Finke, R. G. *Principles and Applications of Organotransition Metal Chemistry*. 1st ed.; University Science Books: Mill Valley, CA, 1987.

113. Hunt, L. B. *Platinum Metals Rev.* **1984,** *28*, 76-83.

114. Douglas, B. E.; McDaniel, D. H.; Alexander, J. H. *Concepts and Models of Inorganic Chemistry*. 3rd ed.; John Wiley & Sons: New York, 2001.

115. Frankland, E. *Phil. Trans.* **1852,** *142*, 417-444.

116. Grignard, V. *C. R. Acad. Sci.* **1900,** *130*, 1322-1324.

117. Crabtree, R. H. *The Organometallic Chemistry of the Transition Metals*. 4th ed.; John Wiley & Sons: Hoboken, NJ, 2005.

118. Schutzenberger, M. P. *Ann.* **1868,** *15*, 10.

119. Werner, A. *Dtsch. Chem. Gest.* **1907,** *40*, 15-69.

120. Cotton, F. A.; Wilkinson, G. *Inorganic Chemistry*. 4th ed.; John Wiley & Sons: New York, 1980.

121. "The Nobel Prize in Chemistry 1913". Nobelprize.org. http://nobelprize.org/nobel_prizes/chemistry/laureates/1913/ (accessed 2 April 2011).

122. Wilkinson, G.; Rosenblum, M.; Whiting, M. C.; Woodward, R. B. *J. Am. Chem. Soc.* **1952,** *74*, 2125-2126.

123. Fischer, E. O.; Pfab, W. *Z. Naturforsch. B* **1952,** *7*, 377-379.

124. Hein, F. *Ber. Dtsch. Chem. Ges. B* **1919,** *52*, 195-196.

125. Uhlig, E. *Organometallics* **1993,** *12*, 4751-4756.

126. Kealy, T. J.; Pauson, P. L. *Nature* **1951,** *168*, 1039-1040.

127. Miller, S. A.; Tebboth, J. A.; Tremaine, J. F. *J. Chem. Soc.* **1952**, 632-635.

128. Fischer, E. O.; Fritz, H. P. *Adv. Inorg. Chem.* **1959,** *1*, 55-115.

129. "The Nobel Prize in Chemistry 1973". Nobelprize.org. http://nobelprize.org/nobel_prizes/chemistry/laureates/1973/ (accessed 2 April 2011).

130. Zeiss, H. H.; Herwig, W. *J. Am. Chem. Soc.* **1956,** *78*, 5959.

131. Zeiss, H. H.; Tsutsui, M. *J. Am. Chem. Soc.* **1957,** *79*, 3062-3066.

132. Fischer, E. O.; Hafner, W. *Z. Naturforsch. B* **1955,** *10*, 665-668.

133. Weiss, E.; Fischer, E. O. *Z. Anorg. Allg. Chem.* **1956,** *286*, 142-145.

134. Fischer, E. O.; Oefele, K. *Chem. Ber.* **1957,** *90*, 2532-2535.

135. Nicholls, B.; Whiting, M. C. *Proc. Chem. Soc.* **1958**, 152.

136. Natta, G.; Ercoli, R.; Calderazzo, F. *Chim. Ind. (Milan)* **1958,** *40*, 287-289.

137. Mahaffy, C. A. L.; Pauson, P. L. *Inorg. Synth.* **1979,** *19*, 154-158.

138. Kündig, E. P.; Perret, C.; Spichiger, S.; Bernardinelli, G. *J. Organomet. Chem.* **1985,** *286*, 183-200.

139. Fischer, E. O.; Oefele, K.; Essler, H.; Frohlich, W.; Mortensen, J. P.; Semmlinger, W. *Z. Naturforsch. B* **1958,** *13*, 458.

140. Wilkinson, G.; Cotton, F. A. *Prog. Inorg. Chem.* **1959,** *1*, 1-124.

141. Jiménez-Halla, J. O. C.; Robles, J.; Solà, M. *Chem. Phys. Lett.* **2008,** *465*, 181-189.

142. Semmelhack, M. F. In *Comprehensive Organometallic Chemistry II*, Abel, E. W.; Stone, F. G. A.; Wilkinson, G., Eds. Pergamon: Oxford, 1995; Vol. 12, pp 979-1016.

143. Semmelhack, M. F.; Hall, H. T. *J. Am. Chem. Soc.* **1974,** *96*, 7092-7094.

144. Semmelhack, M. F.; Hall, H. T., Jr.; Farina, R.; Yoshifuji, M.; Clark, G.; Bargar, T.; Hirotsu, K.; Clardy, J. *J. Am. Chem. Soc.* **1979,** *101*, 3535-3544.

145. Semmelhack, M. F.; Clark, G. R.; Farina, R.; Saeman, M. *J. Am. Chem. Soc.* **1979,** *101*, 217-218.

146. Senechal-Tocquer, M. C.; Senechal, D.; Le Bihan, J. Y.; Gentric, D.; Caro, B.; Gruselle, M.; Jaouen, G. *J. Organomet. Chem.* **1992,** *433*, 261-278.

147. Simonneaux, G.; Jaouen, G. *Tetrahedron* **1979,** *35*, 2249-2254.

148. Rieke, R. D.; Henry, W. P.; Arney, J. S. *Inorg. Chem.* **1987,** *26*, 420-427.

149. Henry, W. P. I. A Study of the Reductive Chemistry of Naphthalenetricarbonylchromium II. Other Exploratory Electrochemical Studies. Ph.D. Dissertation, University of Nebraska, Lincoln, August 1986.

150. Rieke, R. D.; Daruwala, K. P.; Forkner, M. W. *Organometallics* **1991,** *10*, 2946-2955.

151. Rieke, R. D.; Milligan, S. N.; Schulte, L. D. *Organometallics* **1987,** *6*, 699-705.

152. Henry, W. P.; Rieke, R. D. *J. Am. Chem. Soc.* **1983,** *105*, 6314-6316.

153. Nguyen Trong, A.; Elian, M.; Hoffmann, R. *J. Am. Chem. Soc.* **1978,** *100*, 110-116.

154. Semenov, M. E.; Voskoboinikov, D. B.; Gol'dshtein, L. Y. *Vestn. Vses. Nauchn.-Issled. Inst. Zheleznodor.-Transp.* **1961**, 42-43.

155. Milligan, S. N.; Rieke, R. D. *Organometallics* **1983,** *2*, 171-173.

156. Brimm, E. O.; Lynch, M. A.; Sesny, W. J. *J. Am. Chem. Soc.* **1954,** *76*, 3831-3835.

157. Wilson, W. E. *Z. Naturforsch. B* **1958,** *13*, 349-351.

158. Winkhaus, G.; Pratt, L.; Wilkinson, G. *J. Chem. Soc.* **1961**, 3807-3813.

159. Pauson, P. L.; Segal, J. A. *J. Chem. Soc., Dalton Trans.* **1975**, 1683-1686.

160. Kane-Maguire, L. A. P.; Sweigart, D. A. *Inorg. Chem.* **1979,** *18*, 700-706.

161. Jackson, J. D.; Villa, S. J.; Bacon, D. S.; Pike, R. D.; Carpenter, G. B. *Organometallics* **1994,** *13*, 3972-3980.

162. Astruc, D. *Top. Curr. Chem.* **1992,** *160*, 47-95.

163. Rybinskaya, M. I.; Kaganovich, V. S.; Kudinov, A. R. *Izv. Akad. Nauk SSSR, Ser. Khim.* **1984**, 885-888.

164. Mews, R. *Angew. Chem. Int. Ed.* **1975,** *14*, 640-640.

165. Uson, R.; Riera, V.; Gimeno, J.; Laguna, M.; Gamasa, M. P. *J. Chem. Soc., Dalton Trans.* **1979**, 996-1002.

166. Sun, S.; Yeung, L. K.; Sweigart, D. A.; Lee, T.-Y.; Lee, S. S.; Chung, Y. K.; Switzer, S. R.; Pike, R. D. *Organometallics* **1995,** *14*, 2613-2615.

167. Kim, S. B.; Lotz, S.; Sun, S.; Chung, Y. K.; Pike, R. D.; Sweigart, D. A.; Carroll, M. E.; Morvan, D.; Rauchfuss, T. B. *Inorg. Synth.* **2010,** *35*, 114-120.

168. Sun, S.; Dullaghan, C. A.; Carpenter, G. B.; Rieger, A. L.; Rieger, P. H.; Sweigart, D. A. *Angew. Chem. Int. Ed.* **1995,** *34*, 2540-2542.

169. Lee, S. S.; Lee, T.-Y.; Lee, J. E.; Lee, I.-S.; Chung, Y. K.; Lah, M. S. *Organometallics* **1996,** *15*, 3664-3669.

170. Kang, Y. K.; Lee, H.-K.; Lee, S. S.; Chung, Y. K.; Carpenter, G. *Inorg. Chim. Acta* **1997,** *261*, 37-44.

171. Kim, J. E.; Son, S. U.; Lee, S. S.; Chung, Y. K. *Inorg. Chim. Acta* **1998,** *281*, 229-234.

172. Son, S. U.; Park, K. H.; Lee, S. J.; Chung, Y. K.; Sweigart, D. A. *Chem. Commun.* **2001**, 1290-1291.

173. Rogers, R. D.; Atwood, J. L.; Albright, T. A.; Lee, W. A.; Rausch, M. D. *Organometallics* **1984,** *3*, 263-270.

174. Muetterties, E. L.; Bleeke, J. R.; Wucherer, E. J.; Albright, T. *Chem. Rev.* **1982,** *82*, 499-525.

175. Bailey, M. F.; Dahl, L. F. *Inorg. Chem.* **1965,** *4*, 1314-1319.

176. Carter, O. L.; McPhail, A. T.; Sim, G. A. *Chem. Commun.* **1966**, 212-213.

177. Price, J. T.; Sorensen, T. S. *Can. J. Chem.* **1968,** *46*, 515-522.

178. Schrauzer, G. N.; Glockner, P.; Eichler, S. *Angew. Chem. Int. Ed.* **1964,** *3*, 185-191.

179. Cope, A. C.; Hochstein, F. A. *J. Am. Chem. Soc.* **1950,** *72*, 2515-2520.

180. Mathews, F. S.; Lipscomb, W. N. *J. Am. Chem. Soc.* **1958,** *80*, 4745-4746.

181. Rausch, M. D.; Schrauzer, G. N. *Chem. Ind. (London)* **1959**, 957-958.

182. Manuel, T. A.; Stone, F. G. A. *Proc. Chem. Soc.* **1959**, 90.

183. Nakamura, A.; Hagihara, N. *Bull. Chem. Soc. Jpn.* **1959,** *32*, 880-881.

184. Dickens, B.; Lipscomb, W. N. *J. Chem. Phys.* **1962,** *37*, 2084-2093.

185. Fritz, H. P.; Keller, H. *Z. Naturforsch. B* **1961,** *16*, 348.

186. Hughes, R. P.; Carl, R. T.; Doig, S. J.; Hemond, R. C.; Samkoff, D. E.; Smith, W. L.; Stewart, L. C.; Davis, R. E.; Holland, K. D. *Organometallics* **1990,** *9*, 2732-2745.

187. Greenwood, N. N.; Earnshaw, A. *Chemistry of the Elements*. 2nd ed.; Pergamon Press: Elmsford, NY, 1997.

188. Templeton, L. K.; Templeton, D. H.; Walker, R. *Inorg. Chem.* **1976,** *15*, 3000-3003.

189. Müller, J.; Goeser, P.; Elian, M. *Angew. Chem. Int. Ed.* **1969,** *8*, 374-375.

190. Brown, M.; Zubkowski, J. D.; Valente, E. J.; Yang, G. Z.; Henry, W. P. *J. Organomet. Chem.* **2000,** *613*, 111-118.

191. Mak, T. C. W.; Ho, W. C.; Huang, N. Z. *J. Organomet. Chem.* **1983,** *251*, 413-421.

192. Benedikt, M.; Schlögl, K. *Monatsh. Chem.* **1978,** *109*, 805-822.

193. Fakhri, S. A.; Zenouz, A. M. *J. Organomet. Chem.* **2000,** *608*, 6-11.

194. Anton, D. R.; Crabtree, R. H. *Organometallics* **1983,** *2*, 621-627.

195. Anton, D. R.; Crabtree, R. H. *Organometallics* **1983,** *2*, 855-859.

196. Mak, T. C. W.; Wong, H. N. C.; Hung Sze, K.; Book, L. *J. Organomet. Chem.* **1983,** *255*, 123-134.

197. Sygula, A.; Fronczek, F. R.; Rabideau, P. W. *J. Organomet. Chem.* **1996,** *526*, 389-391.

198. Sharp, P. R. *J. Chem. Soc., Dalton Trans.* **2000**, 2647-2657.

199. Singh, A.; Sharp, P. R. *Organometallics* **2006,** *25*, 678-683.

200. Singh, A.; Sharp, P. R. *Inorg. Chim. Acta* **2008,** *361*, 3159-3164.

201. Carnes, M.; Buccella, D.; Chen, J. Y. C.; Ramirez, A. P.; Turro, N. J.; Nuckolls, C.; Steigerwald, M. *Angew. Chem. Int. Ed.* **2009,** *48*, 290-294.

202. Rabi, I. I.; Zacharias, J. R.; Millman, S.; Kusch, P. *Phys. Rev.* **1938,** *53*, 318.

203. Jackman, L. M.; Cotton, F. A.; Adams, R. D. *Dynamic Nuclear Magnetic Resonance Spectroscopy*. Academic Press: New York, 1975.

204. Bloch, F. *Phys. Rev.* **1946,** *70*, 460-74.

205. Bloch, F.; Hansen, W. W.; Packard, M. *Phys. Rev.* **1946,** *70*, 474-85.

206. "The Nobel Prize in Physics 1944". Nobelprize.org. http://nobelprize.org/nobel_prizes/physics/laureates/1944/ (accessed 20 July 2011).

207. "The Nobel Prize in Physics 1952". Nobelprize.org. http://nobelprize.org/nobel_prizes/physics/laureates/1952/ (accessed 20 July 2011).

208. Arnold, J. T.; Packard, M. E. *J. Chem. Phys.* **1951,** *19*, 1608-1609.

209. Liddel, U.; Ramsey, N. F. *J. Chem. Phys.* **1951,** *19*, 1608.

210. Van Geet, A. L. *Anal. Chem.* **1968,** *40*, 2227-2229.

211. Van Geet, A. L. *Anal. Chem.* **1970,** *42*, 679-680.

212. Findeisen, M.; Brand, T.; Berger, S. *Magn. Reson. Chem.* **2007,** *45*, 175-178.

213. Bloembergen, N.; Purcell, E. M.; Pound, R. V. *Phys. Rev.* **1948,** *73*, 679-712.

214. Gutowsky, H. S.; Pake, G. E. *J. Chem. Phys.* **1950,** *18*, 162-170.

215. Gutowsky, H. S.; Saika, A. *J. Chem. Phys.* **1953,** *21*, 1688-1694.

216. Gutowsky, H. S.; Holm, C. H. *J. Chem. Phys.* **1956,** *25*, 1228-1234.

217. Anet, F. A. L.; Bourn, A. J. R. *J. Am. Chem. Soc.* **1967,** *89*, 760-768.

218. Kessler, H.; Gusowski, V.; Hanack, M. *Tetrahedron Lett.* **1968**, 4665-4670.

219. Lambert, J. B.; Oliver, W. L., Jr. *Tetrahedron Lett.* **1968**, 6187-6190.

220. Harris, R. K. *Nuclear Magnetic Resonance Spectroscopy*. 2nd ed.; Longman Scientific & Technical: New York, 1986.

221. Becker, E. D. *High Resolution NMR: Theory and Chemical Applications*. 2nd ed.; Academic Press: Orlando, FL, 1980.

222. Kaplan, J. I.; Fraenkel, G. *NMR of Chemically Exchanging Systems*. 1st ed.; Academic Press: New York, 1980.

223. Shriver, D. F.; Drezdzon, M. A. *The Manipulation of Air-Sensitive Compounds*. 2nd ed.; John Wiley & Sons: New York, 1986.

224. Tiers, G. V. D. *J. Phys. Chem.* **1958,** *62*, 1151-152.

225. Aue, W. P.; Bartholdi, E.; Ernst, R. R. *J. Chem. Phys.* **1976,** *64*, 2229-2246.

226. Müller, L. *J. Am. Chem. Soc.* **1979,** *101*, 4481-4484.

227. Bax, A.; Summers, M. F. *J. Am. Chem. Soc.* **1986,** *108*, 2093-2094.

228. Budzelaar, P. H. M. *gNMR*, 4.1.0; Adept Scientific plc.: Herts, UK, 1999.

229. *Spartan'10*, 1.1.0; Wavefunction, Inc.: Irvine, CA, 2011.

230. Shao, Y.; Molnar, L. F.; Jung, Y.; Kussmann, J.; Ochsenfeld, C.; Brown, S. T.; Gilbert, A. T. B.; Slipchenko, L. V.; Levchenko, S. V.; O'Neill, D. P.; DiStasio Jr, R. A.; Lochan, R. C.; Wang, T.; Beran, G. J. O.; Besley, N. A.; Herbert, J. M.; Yeh Lin, C.; Van Voorhis, T.; Hung Chien, S.; Sodt, A.; Steele, R. P.; Rassolov, V. A.; Maslen, P. E.; Korambath, P. P.; Adamson, R. D.; Austin, B.; Baker, J.; Byrd, E. F. C.; Dachsel, H.; Doerksen, R. J.; Dreuw, A.; Dunietz, B. D.; Dutoi, A. D.; Furlani, T. R.; Gwaltney, S. R.; Heyden, A.; Hirata, S.; Hsu, C.-P.; Kedziora, G.; Khalliulin, R. Z.; Klunzinger, P.; Lee, A. M.; Lee, M. S.; Liang, W.; Lotan, I.; Nair, N.; Peters, B.; Proynov, E. I.; Pieniazek, P. A.; Min Rhee, Y.; Ritchie, J.; Rosta, E.; David Sherrill, C.; Simmonett, A. C.; Subotnik, J. E.; Lee Woodcock Iii, H.; Zhang, W.; Bell, A. T.; Chakraborty, A. K.; Chipman, D. M.; Keil, F. J.; Warshel, A.; Hehre, W. J.; Schaefer Iii, H. F.; Kong, J.; Krylov, A. I.; Gill, P. M. W.; Head-Gordon, M. *Phys. Chem. Chem. Phys.* **2006,** *8*, 3172-3191.

231. Lee, C.; Yang, W.; Parr, R. G. *Phys. Rev. B* **1988,** *37*, 785-789.

232. Becke, A. D. *J. Chem. Phys.* **1993,** *98*, 5648-5652.

233. Raghavachari, K.; Trucks, G. W. *J. Chem. Phys.* **1989,** *91*, 1062-1065.

234. *APEX*, 2; Bruker AXS Inc.: Madison, WI, 2009.

235. Sheldrick, G. *Acta Crystallogr. Sect. A* **2008,** *64*, 112-122.

236. *M270*, 4.30; Princeton Applied Research: Oak Ridge, TN, 1986.

237. Sawyer, D. T.; Sobkowiak, A.; Roberts, J. L. Electrochemistry for Chemists. 2nd ed.; John Wiley & Sons: New York, 1995.

238. Moore, J. A.; Mitchell, T. D. *Org. Prep. Proced. Int.* **1984,** *16*, 411-425.

239. Quick, M. H.; Angelici, R. J. *Inorg. Synth.* **1979,** *19*, 160-161.

240. *DigiSim*, 3; BASi: West Lafayette, IN, 2010.

241. Silverstein, R. M.; Webster, F. X.; Kiemie, D. *Spectrometric Identification of Organic Compounds*. 7th ed.; John Wiley & Sons: Hoboken, NJ, 2002.

242. Pople, J. A.; Schneider, W. G.; Bernstein, H. J. *High-Resolution Nuclear Magnetic Resonance*. McGraw-Hill: New York, 1959.

243. Brown, D. A.; Raju, J. R. *J. Chem. Soc. A* **1966**, 1617-1620.

244. Fritz, H. P.; Kreiter, C. G. *J. Organomet. Chem.* **1967,** *7*, 427-440.

245. Leonard, S. K. *Tetrahedron Lett.* **1978,** *19*, 2361-2362.

246. Langer, E.; Lehner, H. *J. Organomet. Chem.* **1979,** *173*, 47-52.

247. Wagner, G. W.; Hanson, B. E. *Inorg. Chem.* **1987,** *26*, 2019-2022.

248. Braga, D.; Grepioni, F. *Polyhedron* **1990,** *9*, 53-61.

249. McGlinchey, M. J.; Bougeard, P.; Sayer, B. G.; Hofer, R.; Lock, C. J. L. *J. Chem. Soc., Chem. Commun.* **1984**, 789-790.

250. Glaros, G.; Cromwell, N. H. *J. Chem. Educ.* **1971,** *48*, 202-203.

251. Ammann, C.; Meier, P.; Merbach, A. E. *J. Magn. Reson.* **1982,** *46*, 319-321.

252. Harris, R. K.; Becker, E. D.; Cabral De Menezes, S. M.; Goodfellow, R.; Granger, P. *Pure Appl. Chem.* **2001,** *73*, 1795-1818.

253. Jameson, C. J.; Rehder, D.; Hoch, M. *J. Am. Chem. Soc.* **1987,** *109*, 2589-2594.

254. Jameson, A. K.; Jameson, C. J. *J. Am. Chem. Soc.* **1973,** *95*, 8559-8561.

255. Jameson, C. J.; Jameson, A. K.; Cohen, S. M. *J. Magn. Reson.* **1975,** *19*, 385-392.

256. Morin, F. G.; Solum, M. S.; Withers, J. D.; Grant, D. M.; Dalling, D. K. *J. Magn. Reson.* **1982,** *48*, 138-142.

257. Hoffman, R. E.; Becker, E. D. *J. Magn. Reson.* **2005,** *176*, 87-98.

258. Hoffman, R. E. *Magn. Reson. Chem.* **2006,** *44*, 606-616.

259. Sandström, J. *Dynamic NMR Spectroscopy*. Academic Press: London, 1982.

260. Tabushi, I.; Yamada, H. *Tetrahedron* **1977,** *33*, 1101-1104.

261. Baxter, N. J.; Williamson, M. P. *J. Biomol. NMR* **1997,** *9*, 359-369.

262. Ludwig, R.; Weinhold, F.; Farrar, T. C. *J. Phys. Chem. A* **1997,** *101*, 8861-8870.

263. Gung, B. W.; Zhu, Z.; Zou, D.; Everingham, B.; Oyeamalu, A.; Crist, R. M.; Baudlier, J. *J. Org. Chem.* **1998,** *63*, 5750-5761.

264. Daley, M. E.; Graether, S. P.; Sykes, B. D. *Biochemistry* **2004,** *43*, 13012-13017.

265. Atkins, P. W. *Physical Chemistry*. 6th ed.; Oxford University Press: Oxford, 1998.

266. Harris, D. C. *Quantitative Chemical Analysis*. 5th ed.; W. H. Freeman: New York, 1999.

267. Mendaham, J.; Denny, R. C.; Barnes, J. D.; Thomas, M. *Vogle's Textbook of Quantitative Chemical Analysis*. 6th ed.; Pearson Education: Singapore, 2004.

268. Karadakov, P. B. *J. Phys. Chem. A* **2008,** *112*, 12707-12713.

269. Gardlik, J. M.; Paquette, L. A.; Gleiter, R. *J. Am. Chem. Soc.* **1979,** *101*, 1617-1620.

270. Paquette, L. A.; Gardlik, J. M. *J. Am. Chem. Soc.* **1980,** *102*, 5016-5025.

271. Paquette, L. A.; Gardlik, J. M.; Johnson, L. K.; McCullough, K. J. *J. Am. Chem. Soc.* **1980,** *102*, 5026-5032.

272. Paquette, L. A.; Hanzawa, Y.; McCullough, K. J.; Tagle, B.; Swenson, W.; Clardy, J. *J. Am. Chem. Soc.* **1981,** *103*, 2262-2269.

273. Paquette, L. A.; Hanzawa, Y.; Hefferon, G. J.; Blount, J. F. *J. Org. Chem.* **1982,** *47*, 265-2672.

274. Paquette, L. A.; Gardlik, J. M.; McCullough, K. J.; Hanzawa, Y. *J. Am. Chem. Soc.* **1983,** *105*, 7644-7648.

275. Paquette, L. A.; Gardlik, J. M.; McCullough, K. J.; Samodral, R.; DeLucca, G.; Ouellette, R. J. *J. Am. Chem. Soc.* **1983,** *105*, 7649-7655.

276. Paquette, L. A.; Wang, T. Z. *J. Am. Chem. Soc.* **1988,** *110*, 8192-8197.

277. Paquette, L. A.; Wang, T. Z.; Luo, J.; Cottrell, C. E.; Clough, A. E.; Anderson, L. B. *J. Am. Chem. Soc.* **1990,** *112*, 239-253.

278. Oth, J. F. M.; Merényi, R.; Martini, T.; Schröder, G. *Tetrahedron Lett.* **1966,** *7*, 3087-3093.

279. Gwynn, D. E.; Whitesides, G. M.; Roberts, J. D. *J. Am. Chem. Soc.* **1965,** *87*, 2862-2864.

280. Stevenson, C. D.; Brown, E. C.; Hrovat, D. A.; Borden, W. T. *J. Am. Chem. Soc.* **1998,** *120*, 8864-8867.

281. Staley, S. W.; Kehlbeck, J. D. *Org. Lett.* **1999,** *1*, 565-568.
282. Staley, S. W.; Vignon, S. A.; Eliasson, B. *J. Org. Chem.* **2001,** *66*, 3871-3877.

283. Wender, P. A.; Christy, J. P.; Lesser, A. B.; Gieseler, M. T. *Angew. Chem. Int. Ed.* **2009,** *48*, 7687-7690.

284. Paquette, L. A.; Gardlik, J. M.; Photis, J. M. *J. Am. Chem. Soc.* **1976,** *98*, 7096-7098.

285. Anderson, J. E.; Kirsch, P. A. *J. Chem. Soc., Perkin Trans. 2* **1992**, 1951-1957.

286. Thaler, W. *J. Am. Chem. Soc.* **1963,** *85*, 2607-2613.

287. Albright, T. A. *Acc. Chem. Res.* **1982,** *15*, 149-155.

288. Albright, T. A.; Hofmann, P.; Hoffmann, R.; Lillya, C. P.; Dobosh, P. A. *J. Am. Chem. Soc.* **1983,** *105*, 3396-3411.

289. Hughes, S. J.; Moss, J. R.; Naidoo, K. J.; Kelly, J. F.; Batsanov, A. S. *J. Organomet. Chem.* **1999,** *588*, 176-185.

290. Peitz, D. J.; Palmer, R. T.; Radonovich, L. J.; Woolsey, N. F. *Organometallics* **1993,** *12*, 4580-4584.

291. Traylor, T. G.; Goldberg, M. J.; Miksztal, A. R.; Strouse, C. E. *Organometallics* **1989,** *8*, 1101-1105.

292. Sardone, N.; Seresini, P.; Zecchi, G. *Acta Crystallogr. Sect. C* **1996,** *52*, 613-615.

293. Braga, D.; Grepioni, F.; Biradha, K.; Pedireddi, V. R.; Desiraju, G. R. *J. Am. Chem. Soc.* **1995,** *117*, 3156-3166.

294. Bürgi, H.-B.; Dunitz, J. D. *Structure Correlation*. Wiley-VCH: New York, 1994; Vol. 2.

295. Braga, D.; Dyson, P. J.; Grepioni, F.; Johnson, B. F. G.; Calhorda, M. J. *Inorg. Chem.* **1994,** *33*, 3218-3228.

296. Braga, D.; Grepioni, F.; Calhorda, M. J.; Veiros, L. F. *Organometallics* **1995,** *14*, 1992-2001.

297. Braga, D.; Byrne, J. J.; Grepioni, F.; Parisini, E.; Dyson, P. J.; Gaede, P. E.; Johnson, B. F. G.; Reed, D. *Organometallics* **1995,** *14*, 4892-4898.

298. Braga, D.; Grepioni, F. *Acc. Chem. Res.* **1997,** *30*, 81-87.

299. Perjéssy, A.; Hrnciar, P.; Susteková, Z.; Bowden, K.; Ranson, R. J.; Hritzová, O.; Prónayová, N. a. *J. Organomet. Chem.* **1998,** *552*, 1-8.

300. Grepioni, F.; Braga, D.; Dyson, P. J.; Johnson, B. F. G.; Sanderson, F. M.; Calhorda, M. J.; Veiros, L. F. *Organometallics* **1995,** *14*, 121-130.

301. Semmelhack, M. F.; Clark, G. R.; Garcia, J. L.; Harrison, J. J.; Thebtaranonth, Y.; Wulff, W.; Yamashita, A. *Tetrahedron* **1981,** *37*, 3957-3965.

302. Desiraju, G. R. *J. Chem. Soc., Chem. Commun.* **1989**, 179-180.

303. Desiraju, G. R. *J. Chem. Soc., Chem. Commun.* **1990**, 454-455.

304. Pedireddi, V. R.; Desiraju, G. R. *J. Chem. Soc., Chem. Commun.* **1992**, 988-990.

305. Braga, D.; Grepioni, F.; Tedesco, E. *Organometallics* **1998,** *17*, 2669-2672.

306. Brisdon, A. K.; Crossley, I. R.; Pritchard, R. G.; Warren, J. E. *Acta Crystallogr. Sect. C* **2003,** *59*, m322-m324.

307. Allen, F. *Acta Crystallogr., Sect. B* **2002,** *58*, 380-388.

308. Gancarz, R. A.; Blount, J. F.; Mislow, K. *Organometallics* **1985,** *4*, 2028-2032.

309. Toyota, S.; Okuhara, H.; Ōki, M. *Organometallics* **1997,** *16*, 4012-4015.

310. Harrington, L. E.; Cahill, L. S.; McGlinchey, M. J. *Organometallics* **2004,** *23*, 2884-2891.

311. Parfitt, D. S.; Jordan, J. D.; Keister, J. B. *Organometallics* **1992,** *11*, 4009-4015.

312. E. Bitterwolf, T.; Ceccon, A.; Gambaro, A.; Ganis, P.; Kuck, D.; Manoli, F.; L. Rheingold, A.; Valle, G.; Venzo, A. *J. Chem. Soc., Perkin Trans. 2* **1997**, 735-742.

313. Pike, R. D.; Sweigart, D. A. *Coord. Chem. Rev.* **1999,** *187*, 183-222.

314. Grepioni, F.; Cojazzi, G.; Draper, S. M.; Scully, N.; Braga, D. *Organometallics* **1998,** *17*, 296-307.

315. Stanghellini, P. L.; Diana, E.; Arrais, A.; Rossin, A.; Kettle, S. F. A. *Organometallics* **2006,** *25*, 5024-5030.

316. Ceccon, A.; Giacometti, G.; Venzo, A.; Ganis, P.; Zanotti, G. *J. Organomet. Chem.* **1981,** *205*, 61-69.

317. Gommans, L. H. P.; Main, L.; Nicholson, B. K. *J. Organomet. Chem.* **1985,** *284*, 345-351.

318. Mailvaganam, B.; Frampton, C. S.; Top, S.; Sayer, B. G.; McGlinchey, M. J. *J. Am. Chem. Soc.* **1991,** *113*, 1177-1185.

319. Behrens, U.; Heck, J.; Maters, M.; Frenzen, G.; Roelofsen, A.; Sommerdijk, H. T. *J. Organomet. Chem.* **1994,** *475*, 233-240.

320. Brammer, L.; Klooster, W. T.; Lemke, F. R. *Organometallics* **1996,** *15*, 1721-1727.

321. Tamm, M.; Grzegorzewski, A.; Steiner, T.; Jentzsch, T.; Werncke, W. *Organometallics* **1996,** *15*, 4984-4990.

322. Moussa, J.; Chamoreau, L. M.; Boubekeur, K.; Amouri, H.; Rager, M. N.; Grotjahn, D. B. *Organometallics* **2007,** *27*, 67-71.

323. Hanson, A. W. *Cryst. Struct. Commun.* **1982,** *11*, 937-942.

324. Braga, D.; Scaccianoce, L.; Grepioni, F.; Draper, S. M. *Organometallics* **1996,** *15*, 4675-4677.

325. Grepioni, F.; Cojazzi, G.; Braga, D.; Marseglia, E.; Scaccianoce, L.; F. G. Johnson, B. *J. Chem. Soc., Dalton Trans.* **1999**, 553-558.

326. Braga, D.; Maini, L.; Grepioni, F.; Elschenbroich, C.; Paganelli, F.; Schiemann, O. *Organometallics* **2001,** *20*, 1875-1881.

327. Marchetti, F.; Pettinari, C.; Cerquetella, A.; Cingolani, A.; Pettinari, R.; Monari, M.; Wanke, R.; Kuznetsov, M. L.; Pombeiro, A. J. L. *Inorg. Chem.* **2009,** *48*, 6096-6108.

328. Hunter, C. A.; Sanders, J. K. M. *J. Am. Chem. Soc.* **1990,** *112*, 5525-5534.

329. Curtis, M. D.; Cao, J.; Kampf, J. W. *J. Am. Chem. Soc.* **2004,** *126*, 4318-4328.

330. Sygula, A.; Saebø, S. *Int. J. Quantum Chem.* **2009,** *109*, 65-72.

331. Treichel, P. M.; Fivizzani, K. P.; Haller, K. J. *Organometallics* **1982,** *1*, 931-934.

332. Reingold, J. A.; Virkaitis, K. L.; Carpenter, G. B.; Sun, S.; Sweigart, D. A.; Czech, P. T.; Overly, K. R. *J. Am. Chem. Soc.* **2005,** *127*, 11146-11158.

333. Dullaghan, C. A.; Carpenter, G. B.; Sweigart, D. A. *Chem.-Eur. J.* **1997,** *3*, 75-78.

334. Dullaghan, C. A.; Zhang, X.; Walther, D.; Carpenter, G. B.; Sweigart, D. A.; Meng, Q. *Organometallics* **1997,** *16*, 5604-5606.

335. Ed: Müller, P. *Crystal Structure Refinement: A Crystallographer's Guide to SHELXL*. Oxford University Press: Oxford, UK, 2006.

336. Anderson, L. B.; Paquette, L. A. *J. Am. Chem. Soc.* **1972,** *94*, 4915-4919.

337. Kojima, H.; Bard, A. J.; Wong, H. N. C.; Sondheimer, F. *J. Am. Chem. Soc.* **1976,** *98*, 5560-5565.

338. Cramer, C. J. *Essentials of Computational Chemistry; Theories and Models*. 2nd ed.; John Wiley & Sons: Sussex, UK, 2004.

APPENDIX A

BOND LENGTHS AND BOND ANGLES

Bond lengths (Å) for **17**

Br(1)-C(6)	1.992(3)	C(7)-C(13)	1.403(5)
Br(2)-C(11)	1.999(3)	C(8)-C(9)	1.392(5)
C(1)-C(10)	1.385(6)	C(8)-H(8)	0.9300
C(1)-C(2)	1.385(6)	C(9)-C(15)	1.382(6)
C(1)-H(1)	0.9300	C(9)-H(9)	0.9300
C(2)-C(3)	1.404(5)	C(10)-C(14)	1.385(5)
C(2)-H(2)	0.9300	C(10)-H(10)	0.9300
C(3)-C(4)	1.397(5)	C(11)-C(12)	1.532(5)
C(3)-C(11)	1.514(5)	C(11)-H(11)	0.9800
C(4)-C(14)	1.406(5)	C(12)-C(13)	1.514(5)
C(4)-C(5)	1.515(5)	C(12)-H(12A)	0.9700
C(5)-C(6)	1.542(5)	C(12)-H(12B)	0.9700
C(5)-H(5A)	0.9700	C(13)-C(16)	1.396(5)
C(5)-H(5B)	0.9700	C(14)-H(14)	0.9300
C(6)-C(7)	1.509(5)	C(15)-C(16)	1.384(5)
C(6)-H(6)	0.9800	C(15)-H(15)	0.9300
C(7)-C(8)	1.394(5)	C(16)-H(16)	0.9300

Bond angles (^{o}) for **17**

C(10)-C(1)-C(2)	119.6(4)	C(15)-C(9)-C(8)	120.3(3)
C(10)-C(1)-H(1)	120.2	C(15)-C(9)-H(9)	119.9
C(2)-C(1)-H(1)	120.2	C(8)-C(9)-H(9)	119.9
C(1)-C(2)-C(3)	121.2(4)	C(14)-C(10)-C(1)	120.0(4)
C(1)-C(2)-H(2)	119.4	C(14)-C(10)-H(10)	120.0
C(3)-C(2)-H(2)	119.4	C(1)-C(10)-H(10)	120.0
C(4)-C(3)-C(2)	119.4(3)	C(3)-C(11)-C(12)	119.6(3)
C(4)-C(3)-C(11)	125.4(3)	C(3)-C(11)-Br(2)	108.8(2)
C(2)-C(3)-C(11)	115.2(3)	C(12)-C(11)-Br(2)	108.3(2)
C(3)-C(4)-C(14)	118.7(3)	C(3)-C(11)-H(11)	106.5
C(3)-C(4)-C(5)	122.6(3)	C(12)-C(11)-H(11)	106.5
C(14)-C(4)-C(5)	118.7(3)	Br(2)-C(11)-H(11)	106.5
C(4)-C(5)-C(6)	112.0(3)	C(13)-C(12)-C(11)	109.9(3)
C(4)-C(5)-H(5A)	109.2	C(13)-C(12)-H(12A)	109.7
C(6)-C(5)-H(5A)	109.2	C(11)-C(12)-H(12A)	109.7
C(4)-C(5)-H(5B)	109.2	C(13)-C(12)-H(12B)	109.7
C(6)-C(5)-H(5B)	109.2	C(11)-C(12)-H(12B)	109.7
H(5A)-C(5)-H(5B)	107.9	H(12A)-C(12)-H(12B)	108.2
C(7)-C(6)-C(5)	119.3(3)	C(16)-C(13)-C(7)	119.4(3)
C(7)-C(6)-Br(1)	108.9(2)	C(16)-C(13)-C(12)	119.2(3)

C(5)-C(6)-Br(1)	107.8(2)	C(7)-C(13)-C(12)	121.4(3)
C(7)-C(6)-H(6)	106.7	C(10)-C(14)-C(4)	121.2(3)
C(5)-C(6)-H(6)	106.7	C(10)-C(14)-H(14)	119.4
Br(1)-C(6)-H(6)	106.7	C(4)-C(14)-H(14)	119.4
C(8)-C(7)-C(13)	118.9(3)	C(9)-C(15)-C(16)	119.2(3)
C(8)-C(7)-C(6)	117.1(3)	C(9)-C(15)-H(15)	120.4
C(13)-C(7)-C(6)	124.0(3)	C(16)-C(15)-H(15)	120.4
C(9)-C(8)-C(7)	120.9(4)	C(15)-C(16)-C(13)	121.4(4)
C(9)-C(8)-H(8)	119.5	C(15)-C(16)-H(16)	119.3
C(7)-C(8)-H(8)	119.5	C(13)-C(16)-H(16)	119.3

Bond lengths (Å) for **29**

Cr(1)-C(1)	1.839(2)	C(6)-C(7)	1.428(3)
Cr(1)-C(19)	1.843(2)	C(6)-C(13)	1.486(2)
Cr(1)-C(18)	1.847(2)	C(7)-C(8)	1.484(2)
Cr(1)-C(2)	2.2079(19)	C(8)-C(9)	1.331(3)
Cr(1)-C(3)	2.2125(18)	C(8)-H(8)	0.9300
Cr(1)-C(4)	2.2149(18)	C(9)-C(10)	1.480(3)
Cr(1)-C(5)	2.2151(19)	C(9)-H(9)	0.9300
Cr(1)-C(7)	2.2457(18)	C(10)-C(11)	1.402(3)
Cr(1)-C(6)	2.2511(18)	C(10)-C(17)	1.403(3)
O(1)-C(1)	1.158(2)	C(11)-C(14)	1.400(3)
O(2)-C(18)	1.158(2)	C(11)-C(12)	1.484(3)
O(3)-C(19)	1.156(2)	C(12)-C(13)	1.329(3)
C(2)-C(7)	1.412(3)	C(12)-H(12)	0.9300
C(2)-C(3)	1.414(3)	C(13)-H(13)	0.9300
C(2)-H(2)	0.9300	C(14)-C(15)	1.382(3)
C(3)-C(4)	1.397(3)	C(14)-H(14)	0.9300
C(3)-H(3)	0.9300	C(15)-C(16)	1.392(3)
C(4)-C(5)	1.415(3)	C(15)-H(15)	0.9300
C(4)-H(4)	0.9300	C(16)-C(17)	1.384(3)
C(5)-C(6)	1.410(2)	C(16)-H(16)	0.9300
C(5)-H(5)	0.9300	C(17)-H(17)	0.9300

Bond angles (°) for **29**

C(1)-Cr(1)-C(19)	88.47(8)	C(5)-C(4)-H(4)	120.1
C(1)-Cr(1)-C(18)	89.70(8)	Cr(1)-C(4)-H(4)	129.4
C(19)-Cr(1)-C(18)	87.21(8)	C(6)-C(5)-C(4)	121.27(17)
C(1)-Cr(1)-C(2)	152.66(8)	C(6)-C(5)-Cr(1)	72.99(10)
C(19)-Cr(1)-C(2)	90.50(8)	C(4)-C(5)-Cr(1)	71.37(11)
C(18)-Cr(1)-C(2)	117.55(8)	C(6)-C(5)-H(5)	119.4
C(1)-Cr(1)-C(3)	115.34(8)	C(4)-C(5)-H(5)	119.4
C(19)-Cr(1)-C(3)	89.54(8)	Cr(1)-C(5)-H(5)	128.6
C(18)-Cr(1)-C(3)	154.66(8)	C(5)-C(6)-C(7)	118.82(16)
C(2)-Cr(1)-C(3)	37.32(7)	C(5)-C(6)-C(13)	118.54(16)
C(1)-Cr(1)-C(4)	89.27(8)	C(7)-C(6)-C(13)	122.64(16)
C(19)-Cr(1)-C(4)	115.58(8)	C(5)-C(6)-Cr(1)	70.21(10)
C(18)-Cr(1)-C(4)	157.14(8)	C(7)-C(6)-Cr(1)	71.29(10)
C(2)-Cr(1)-C(4)	66.66(7)	C(13)-C(6)-Cr(1)	130.27(13)
C(3)-Cr(1)-C(4)	36.79(7)	C(2)-C(7)-C(6)	119.39(16)
C(1)-Cr(1)-C(5)	90.14(8)	C(2)-C(7)-C(8)	117.77(16)
C(19)-Cr(1)-C(5)	152.83(8)	C(6)-C(7)-C(8)	122.84(16)
C(18)-Cr(1)-C(5)	119.92(8)	C(2)-C(7)-Cr(1)	70.06(10)
C(2)-Cr(1)-C(5)	78.57(7)	C(6)-C(7)-Cr(1)	71.69(10)
C(3)-Cr(1)-C(5)	66.68(7)	C(8)-C(7)-Cr(1)	129.75(12)
C(4)-Cr(1)-C(5)	37.25(7)	C(9)-C(8)-C(7)	125.30(17)
C(1)-Cr(1)-C(7)	153.95(8)	C(9)-C(8)-H(8)	117.4
C(19)-Cr(1)-C(7)	117.56(8)	C(7)-C(8)-H(8)	117.4
C(18)-Cr(1)-C(7)	92.43(7)	C(8)-C(9)-C(10)	127.03(17)
C(2)-Cr(1)-C(7)	36.97(7)	C(8)-C(9)-H(9)	116.5
C(3)-Cr(1)-C(7)	66.99(7)	C(10)-C(9)-H(9)	116.5
C(4)-Cr(1)-C(7)	78.86(7)	C(11)-C(10)-C(17)	119.00(17)
C(5)-Cr(1)-C(7)	66.40(7)	C(11)-C(10)-C(9)	123.62(16)
C(1)-Cr(1)-C(6)	116.94(8)	C(17)-C(10)-C(9)	117.32(17)
C(19)-Cr(1)-C(6)	154.58(8)	C(14)-C(11)-C(10)	118.60(17)
C(18)-Cr(1)-C(6)	93.41(7)	C(14)-C(11)-C(12)	118.19(17)
C(2)-Cr(1)-C(6)	66.71(7)	C(10)-C(11)-C(12)	123.10(17)
C(3)-Cr(1)-C(6)	79.10(7)	C(13)-C(12)-C(11)	127.03(17)
C(4)-Cr(1)-C(6)	66.91(7)	C(13)-C(12)-H(12)	116.5
C(5)-Cr(1)-C(6)	36.80(6)	C(11)-C(12)-H(12)	116.5
C(7)-Cr(1)-C(6)	37.02(6)	C(12)-C(13)-C(6)	124.99(17)
O(1)-C(1)-Cr(1)	178.64(17)	C(12)-C(13)-H(13)	117.5
C(7)-C(2)-C(3)	121.02(17)	C(6)-C(13)-H(13)	117.5
C(7)-C(2)-Cr(1)	72.97(10)	C(15)-C(14)-C(11)	121.91(18)
C(3)-C(2)-Cr(1)	71.52(11)	C(15)-C(14)-H(14)	119.0
C(7)-C(2)-H(2)	119.5	C(11)-C(14)-H(14)	119.0
C(3)-C(2)-H(2)	119.5	C(14)-C(15)-C(16)	119.47(18)

Cr(1)-C(2)-H(2)	128.3	C(14)-C(15)-H(15)	120.3
C(4)-C(3)-C(2)	119.63(17)	C(16)-C(15)-H(15)	120.3
C(4)-C(3)-Cr(1)	71.70(11)	C(17)-C(16)-C(15)	119.42(18)
C(2)-C(3)-Cr(1)	71.17(10)	C(17)-C(16)-H(16)	120.3
C(4)-C(3)-H(3)	120.2	C(15)-C(16)-H(16)	120.3
C(2)-C(3)-H(3)	120.2	C(16)-C(17)-C(10)	121.53(18)
Cr(1)-C(3)-H(3)	129.3	C(16)-C(17)-H(17)	119.2
C(3)-C(4)-C(5)	119.85(17)	C(10)-C(17)-H(17)	119.2
C(3)-C(4)-Cr(1)	71.51(10)	O(2)-C(18)-Cr(1)	177.31(18)
C(5)-C(4)-Cr(1)	71.38(10)	O(3)-C(19)-Cr(1)	179.9(2)
C(3)-C(4)-H(4)	120.1		

Bond lengths (Å) for **36**

Mn(1)-C(17)	1.8188(12)	C(4)-C(5)	1.3975(17)
Mn(1)-C(16)	1.8272(13)	C(4)-H(4)	0.9300
Mn(1)-C(21)	1.8294(12)	C(5)-C(20)	1.4165(17)
Mn(1)-C(20)	2.1762(12)	C(5)-H(5)	0.9300
Mn(1)-C(5)	2.1807(12)	C(6)-C(7)	1.3323(17)
Mn(1)-C(1)	2.1834(12)	C(6)-H(6)	0.9300
Mn(1)-C(4)	2.1874(12)	C(7)-C(8)	1.4779(17)
Mn(1)-C(3)	2.2372(11)	C(7)-H(7)	0.9300
Mn(1)-C(2)	2.2492(11)	C(8)-C(13)	1.4032(17)
O(6)-C(21)	1.1334(14)	C(8)-C(9)	1.4043(17)
O(5)-C(17)	1.1385(15)	C(9)-C(10)	1.4023(18)
F(3)-B(2)	1.3827(17)	C(9)-C(14)	1.4802(17)
F(4)-B(2)	1.3928(18)	C(10)-C(11)	1.3863(19)
F(5)-B(2)	1.3870(19)	C(10)-H(10)	0.9300
F(6)-B(2)	1.3849(18)	C(11)-C(12)	1.3921(19)
O(2)-C(16)	1.1376(16)	C(11)-H(11)	0.9300
C(1)-C(20)	1.3955(17)	C(12)-C(13)	1.3862(18)
C(1)-C(2)	1.4309(17)	C(12)-H(12)	0.9300
C(1)-H(1)	0.9300	C(13)-H(13)	0.9300
C(2)-C(3)	1.4071(17)	C(14)-C(15)	1.3327(19)
C(2)-C(15)	1.4811(16)	C(14)-H(14)	0.9300
C(3)-C(4)	1.4325(16)	C(15)-H(15)	0.9300
C(3)-C(6)	1.4809(17)	C(20)-H(1A)	0.9300

Bond angles (°) for **36**

C(17)-Mn(1)-C(16)	90.54(6)	C(5)-C(4)-Mn(1)	71.08(7)
C(17)-Mn(1)-C(21)	88.39(5)	C(3)-C(4)-Mn(1)	73.01(7)
C(16)-Mn(1)-C(21)	91.67(5)	C(5)-C(4)-H(4)	119.3
C(17)-Mn(1)-C(20)	156.57(5)	C(3)-C(4)-H(4)	119.3
C(16)-Mn(1)-C(20)	112.79(5)	Mn(1)-C(4)-H(4)	129.0
C(21)-Mn(1)-C(20)	88.71(5)	C(4)-C(5)-C(20)	119.53(11)
C(17)-Mn(1)-C(5)	118.62(5)	C(4)-C(5)-Mn(1)	71.60(7)
C(16)-Mn(1)-C(5)	150.44(5)	C(20)-C(5)-Mn(1)	70.86(7)
C(21)-Mn(1)-C(5)	84.87(5)	C(4)-C(5)-H(5)	120.2
C(20)-Mn(1)-C(5)	37.95(5)	C(20)-C(5)-H(5)	120.2
C(17)-Mn(1)-C(1)	152.88(5)	Mn(1)-C(5)-H(5)	129.7
C(16)-Mn(1)-C(1)	88.83(5)	C(7)-C(6)-C(3)	128.46(11)
C(21)-Mn(1)-C(1)	118.73(5)	C(7)-C(6)-H(6)	115.8
C(20)-Mn(1)-C(1)	37.34(5)	C(3)-C(6)-H(6)	115.8
C(5)-Mn(1)-C(1)	67.64(5)	C(6)-C(7)-C(8)	129.76(11)
C(17)-Mn(1)-C(4)	91.60(5)	C(6)-C(7)-H(7)	115.1
C(16)-Mn(1)-C(4)	157.98(5)	C(8)-C(7)-H(7)	115.1
C(21)-Mn(1)-C(4)	110.30(5)	C(13)-C(8)-C(9)	119.01(12)
C(20)-Mn(1)-C(4)	67.72(5)	C(13)-C(8)-C(7)	116.37(11)
C(5)-Mn(1)-C(4)	37.32(4)	C(9)-C(8)-C(7)	124.48(11)
C(1)-Mn(1)-C(4)	79.41(5)	C(10)-C(9)-C(8)	118.87(11)
C(17)-Mn(1)-C(3)	90.23(5)	C(10)-C(9)-C(14)	117.08(11)
C(16)-Mn(1)-C(3)	120.33(5)	C(8)-C(9)-C(14)	123.79(12)
C(21)-Mn(1)-C(3)	147.98(5)	C(11)-C(10)-C(9)	121.59(12)
C(20)-Mn(1)-C(3)	80.11(4)	C(11)-C(10)-H(10)	119.2
C(5)-Mn(1)-C(3)	67.88(4)	C(9)-C(10)-H(10)	119.2
C(1)-Mn(1)-C(3)	67.00(5)	C(10)-C(11)-C(12)	119.38(12)
C(4)-Mn(1)-C(3)	37.76(4)	C(10)-C(11)-H(11)	120.3
C(17)-Mn(1)-C(2)	115.36(5)	C(12)-C(11)-H(11)	120.3
C(16)-Mn(1)-C(2)	92.34(5)	C(13)-C(12)-C(11)	119.83(12)
C(21)-Mn(1)-C(2)	155.85(5)	C(13)-C(12)-H(12)	120.1
C(20)-Mn(1)-C(2)	67.82(4)	C(11)-C(12)-H(12)	120.1
C(5)-Mn(1)-C(2)	79.96(4)	C(12)-C(13)-C(8)	121.26(12)
C(1)-Mn(1)-C(2)	37.63(4)	C(12)-C(13)-H(13)	119.4
C(4)-Mn(1)-C(2)	67.02(4)	C(8)-C(13)-H(13)	119.4
C(3)-Mn(1)-C(2)	36.56(4)	C(15)-C(14)-C(9)	128.67(11)
O(6)-C(21)-Mn(1)	177.18(11)	C(15)-C(14)-H(14)	115.7
C(20)-C(1)-C(2)	121.80(11)	C(9)-C(14)-H(14)	115.7
C(20)-C(1)-Mn(1)	71.05(7)	C(14)-C(15)-C(2)	128.25(11)
C(2)-C(1)-Mn(1)	73.68(6)	C(14)-C(15)-H(15)	115.9
C(20)-C(1)-H(1)	119.1	C(2)-C(15)-H(15)	115.9
C(2)-C(1)-H(1)	119.1	O(2)-C(16)-Mn(1)	179.10(12)

Mn(1)-C(1)-H(1)	128.5	O(5)-C(17)-Mn(1)	178.38(10)
C(3)-C(2)-C(1)	118.59(11)	C(1)-C(20)-C(5)	119.48(11)
C(3)-C(2)-C(15)	123.82(11)	C(1)-C(20)-Mn(1)	71.61(7)
C(1)-C(2)-C(15)	117.43(11)	C(5)-C(20)-Mn(1)	71.20(7)
C(3)-C(2)-Mn(1)	71.26(6)	C(1)-C(20)-H(1A)	120.3
C(1)-C(2)-Mn(1)	68.69(6)	C(5)-C(20)-H(1A)	120.3
C(15)-C(2)-Mn(1)	135.77(8)	Mn(1)-C(20)-H(1A)	129.3
C(2)-C(3)-C(4)	119.26(11)	F(3)-B(2)-F(6)	111.18(12)
C(2)-C(3)-C(6)	124.71(11)	F(3)-B(2)-F(5)	109.23(13)
C(4)-C(3)-C(6)	115.98(11)	F(6)-B(2)-F(5)	109.36(12)
C(2)-C(3)-Mn(1)	72.19(7)	F(3)-B(2)-F(4)	108.84(12)
C(4)-C(3)-Mn(1)	69.23(6)	F(6)-B(2)-F(4)	108.78(12)
C(6)-C(3)-Mn(1)	132.52(8)	F(5)-B(2)-F(4)	109.42(12)
C(5)-C(4)-C(3)	121.31(11)		

Bond lengths (Å) for **38**

Cl(2)-C(20)	1.762(2)	C(7A)-C(8A)	1.383(3)
Mn(1A)-C(17A)	1.8248(18)	C(7A)-H(7A)	0.9500
Mn(1A)-C(19A)	1.829(2)	C(2B)-C(3B)	1.406(3)
Mn(1A)-C(18A)	1.829(2)	C(2B)-H(2B)	0.9500
Mn(1A)-C(2A)	2.178(2)	C(8A)-H(8A)	0.9500
Mn(1A)-C(4A)	2.1787(19)	C(10A)-C(16A)	1.399(3)
Mn(1A)-C(3A)	2.179(2)	C(10A)-H(10A)	0.9500
Mn(1A)-C(1A)	2.1950(19)	C(12B)-C(13B)	1.508(3)
Mn(1A)-C(14A)	2.2038(19)	C(12B)-C(11B)	1.554(3)
Mn(1A)-C(13A)	2.233(2)	C(12B)-H(12E)	0.9900
Mn(1B)-C(18B)	1.8256(18)	C(12B)-H(12F)	0.9900
Mn(1B)-C(19B)	1.827(2)	C(3A)-C(4A)	1.425(3)
Mn(1B)-C(17B)	1.832(2)	C(3A)-H(3A)	0.9500
Mn(1B)-C(1B)	2.180(2)	C(3B)-C(4B)	1.403(3)
Mn(1B)-C(3B)	2.183(2)	C(3B)-H(3B)	0.9500
Mn(1B)-C(2B)	2.188(2)	C(7B)-C(8B)	1.390(3)
Mn(1B)-C(4B)	2.193(2)	C(7B)-C(15B)	1.398(3)
Mn(1B)-C(13B)	2.2026(19)	C(7B)-H(7B)	0.9500
Mn(1B)-C(14B)	2.236(2)	C(15B)-C(16B)	1.404(3)
F(4A)-B(1A)	1.396(3)	C(15B)-C(6B)	1.506(3)
Cl(1)-C(20)	1.749(2)	C(6B)-C(5B)	1.554(3)
F(4B)-B(1B)	1.389(2)	C(6B)-H(6E)	0.9900
F(3B)-B(1B)	1.386(2)	C(6B)-H(6F)	0.9900
F(2A)-B(1A)	1.397(2)	C(10B)-C(9B)	1.385(3)

O(1B)-C(17B)	1.134(3)	C(10B)-C(16B)	1.403(3)
F(2B)-B(1B)	1.391(2)	C(10B)-H(10B)	0.9500
F(1B)-B(1B)	1.397(2)	C(13A)-C(14A)	1.428(3)
F(1A)-B(1A)	1.386(2)	C(13A)-C(12A)	1.518(3)
F(3A)-B(1A)	1.391(3)	C(5B)-C(14B)	1.515(3)
O(3A)-C(19A)	1.136(2)	C(5B)-H(5E)	0.9900
O(2A)-C(18A)	1.136(2)	C(5B)-H(5F)	0.9900
C(1B)-C(2B)	1.396(3)	C(16B)-C(11B)	1.513(3)
C(1B)-C(13B)	1.431(3)	C(20)-H(20A)	0.9900
C(1B)-H(1B)	0.9500	C(20)-H(20B)	0.9900
C(17A)-O(1A)	1.132(2)	C(5A)-C(14A)	1.512(3)
C(19B)-O(3B)	1.137(3)	C(5A)-C(6A)	1.556(3)
C(11A)-C(16A)	1.512(3)	C(5A)-H(5C)	0.9900
C(11A)-C(12A)	1.562(3)	C(5A)-H(5D)	0.9900
C(11A)-H(11C)	0.9900	C(8B)-C(9B)	1.387(4)
C(11A)-H(11D)	0.9900	C(8B)-H(8B)	0.9500
O(2B)-C(18B)	1.135(2)	C(6A)-H(6C)	0.9900
C(9A)-C(10A)	1.387(3)	C(6A)-H(6D)	0.9900
C(9A)-C(8A)	1.392(3)	C(14A)-C(4A)	1.405(3)
C(9A)-H(9A)	0.9500	C(4A)-H(4A)	0.9500
C(2A)-C(3A)	1.387(3)	C(9B)-H(9B)	0.9500
C(2A)-C(1A)	1.419(3)	C(4B)-C(14B)	1.433(3)
C(2A)-H(2A)	0.9500	C(4B)-H(4B)	0.9500
C(15A)-C(7A)	1.395(3)	C(11B)-H(11E)	0.9900
C(15A)-C(16A)	1.403(3)	C(11B)-H(11F)	0.9900
C(15A)-C(6A)	1.518(3)	C(12A)-H(12C)	0.9900
C(1A)-C(13A)	1.404(3)	C(12A)-H(12D)	0.9900
C(1A)-H(1A)	0.9500	C(13B)-C(14B)	1.408(3)

Bond angles (^{o}) for **38**

C(17A)-Mn(1A)-C(19A)	91.25(9)	C(13B)-C(12B)-H(12F)	109.3
C(17A)-Mn(1A)-C(18A)	90.33(8)	C(11B)-C(12B)-H(12F)	109.3
C(19A)-Mn(1A)-C(18A)	90.58(9)	H(12E)-C(12B)-H(12F)	107.9
C(17A)-Mn(1A)-C(2A)	152.37(8)	C(2A)-C(3A)-C(4A)	119.7(2)
C(19A)-Mn(1A)-C(2A)	116.38(9)	C(2A)-C(3A)-Mn(1A)	71.41(13)
C(18A)-Mn(1A)-C(2A)	89.28(8)	C(4A)-C(3A)-Mn(1A)	70.90(11)
C(17A)-Mn(1A)-C(4A)	115.80(8)	C(2A)-C(3A)-H(3A)	120.1
C(19A)-Mn(1A)-C(4A)	88.65(8)	C(4A)-C(3A)-H(3A)	120.1
C(18A)-Mn(1A)-C(4A)	153.86(8)	Mn(1A)-C(3A)-H(3A)	130.0
C(2A)-Mn(1A)-C(4A)	67.87(8)	C(4B)-C(3B)-C(2B)	119.8(2)
C(17A)-Mn(1A)-C(3A)	153.96(8)	C(4B)-C(3B)-Mn(1B)	71.69(12)

C(19A)-Mn(1A)-C(3A)	89.16(9)	C(2B)-C(3B)-Mn(1B)	71.44(13)
C(18A)-Mn(1A)-C(3A)	115.70(8)	C(4B)-C(3B)-H(3B)	120.1
C(2A)-Mn(1A)-C(3A)	37.13(8)	C(2B)-C(3B)-H(3B)	120.1
C(4A)-Mn(1A)-C(3A)	38.18(7)	Mn(1B)-C(3B)-H(3B)	129.1
C(17A)-Mn(1A)-C(1A)	114.52(8)	C(10A)-C(16A)-C(15A)	119.06(17)
C(19A)-Mn(1A)-C(1A)	154.22(8)	C(10A)-C(16A)-C(11A)	119.56(19)
C(18A)-Mn(1A)-C(1A)	90.11(8)	C(15A)-C(16A)-C(11A)	121.38(16)
C(2A)-Mn(1A)-C(1A)	37.86(8)	C(8B)-C(7B)-C(15B)	121.92(19)
C(4A)-Mn(1A)-C(1A)	79.63(8)	C(8B)-C(7B)-H(7B)	119.0
C(3A)-Mn(1A)-C(1A)	67.45(8)	C(15B)-C(7B)-H(7B)	119.0
C(17A)-Mn(1A)-C(14A)	88.18(8)	C(7B)-C(15B)-C(16B)	118.56(18)
C(19A)-Mn(1A)-C(14A)	115.19(8)	C(7B)-C(15B)-C(6B)	119.71(18)
C(18A)-Mn(1A)-C(14A)	154.20(8)	C(16B)-C(15B)-C(6B)	121.68(18)
C(2A)-Mn(1A)-C(14A)	80.41(8)	C(15B)-C(6B)-C(5B)	114.99(16)
C(4A)-Mn(1A)-C(14A)	37.40(7)	C(15B)-C(6B)-H(6E)	108.5
C(3A)-Mn(1A)-C(14A)	68.25(8)	C(5B)-C(6B)-H(6E)	108.5
C(1A)-Mn(1A)-C(14A)	67.31(7)	C(15B)-C(6B)-H(6F)	108.5
C(17A)-Mn(1A)-C(13A)	87.88(7)	C(5B)-C(6B)-H(6F)	108.5
C(19A)-Mn(1A)-C(13A)	152.74(8)	H(6E)-C(6B)-H(6F)	107.5
C(18A)-Mn(1A)-C(13A)	116.66(8)	C(9B)-C(10B)-C(16B)	121.7(2)
C(2A)-Mn(1A)-C(13A)	67.79(8)	C(9B)-C(10B)-H(10B)	119.2
C(4A)-Mn(1A)-C(13A)	67.46(7)	C(16B)-C(10B)-H(10B)	119.2
C(3A)-Mn(1A)-C(13A)	80.10(8)	C(1A)-C(13A)-C(14A)	118.75(19)
C(1A)-Mn(1A)-C(13A)	36.97(7)	C(1A)-C(13A)-C(12A)	119.16(17)
C(14A)-Mn(1A)-C(13A)	37.55(7)	C(14A)-C(13A)-C(12A)	122.09(18)
C(18B)-Mn(1B)-C(19B)	91.00(9)	C(1A)-C(13A)-Mn(1A)	70.04(11)
C(18B)-Mn(1B)-C(17B)	89.72(9)	C(14A)-C(13A)-Mn(1A)	70.11(12)
C(19B)-Mn(1B)-C(17B)	90.31(8)	C(12A)-C(13A)-Mn(1A)	131.62(13)
C(18B)-Mn(1B)-C(1B)	115.66(8)	C(14B)-C(5B)-C(6B)	115.44(16)
C(19B)-Mn(1B)-C(1B)	153.34(8)	C(14B)-C(5B)-H(5E)	108.4
C(17B)-Mn(1B)-C(1B)	89.51(9)	C(6B)-C(5B)-H(5E)	108.4
C(18B)-Mn(1B)-C(3B)	89.87(8)	C(14B)-C(5B)-H(5F)	108.4
C(19B)-Mn(1B)-C(3B)	115.53(9)	C(6B)-C(5B)-H(5F)	108.4
C(17B)-Mn(1B)-C(3B)	154.16(9)	H(5E)-C(5B)-H(5F)	107.5
C(1B)-Mn(1B)-C(3B)	67.53(8)	C(10B)-C(16B)-C(15B)	118.90(18)
C(18B)-Mn(1B)-C(2B)	89.34(8)	C(10B)-C(16B)-C(11B)	118.10(18)
C(19B)-Mn(1B)-C(2B)	153.05(9)	C(15B)-C(16B)-C(11B)	122.91(18)
C(17B)-Mn(1B)-C(2B)	116.63(9)	Cl(1)-C(20)-Cl(2)	111.82(13)
C(1B)-Mn(1B)-C(2B)	37.27(8)	Cl(1)-C(20)-H(20A)	109.3
C(3B)-Mn(1B)-C(2B)	37.53(8)	Cl(2)-C(20)-H(20A)	109.3
C(18B)-Mn(1B)-C(4B)	117.31(9)	Cl(1)-C(20)-H(20B)	109.3
C(19B)-Mn(1B)-C(4B)	88.73(8)	Cl(2)-C(20)-H(20B)	109.3
C(17B)-Mn(1B)-C(4B)	152.96(8)	H(20A)-C(20)-H(20B)	107.9
C(1B)-Mn(1B)-C(4B)	79.59(8)	C(14A)-C(5A)-C(6A)	110.23(15)

C(3B)-Mn(1B)-C(4B)	37.39(8)	C(14A)-C(5A)-H(5C)	109.6
C(2B)-Mn(1B)-C(4B)	67.38(8)	C(6A)-C(5A)-H(5C)	109.6
C(18B)-Mn(1B)-C(13B)	153.71(8)	C(14A)-C(5A)-H(5D)	109.6
C(19B)-Mn(1B)-C(13B)	115.24(8)	C(6A)-C(5A)-H(5D)	109.6
C(17B)-Mn(1B)-C(13B)	88.60(8)	H(5C)-C(5A)-H(5D)	108.1
C(1B)-Mn(1B)-C(13B)	38.11(7)	C(9B)-C(8B)-C(7B)	119.39(19)
C(3B)-Mn(1B)-C(13B)	80.52(8)	C(9B)-C(8B)-H(8B)	120.3
C(2B)-Mn(1B)-C(13B)	68.18(8)	C(7B)-C(8B)-H(8B)	120.3
C(4B)-Mn(1B)-C(13B)	67.56(7)	C(15A)-C(6A)-C(5A)	116.58(15)
C(18B)-Mn(1B)-C(14B)	155.05(8)	C(15A)-C(6A)-H(6C)	108.1
C(19B)-Mn(1B)-C(14B)	88.73(8)	C(5A)-C(6A)-H(6C)	108.1
C(17B)-Mn(1B)-C(14B)	115.23(8)	C(15A)-C(6A)-H(6D)	108.1
C(1B)-Mn(1B)-C(14B)	67.39(7)	C(5A)-C(6A)-H(6D)	108.1
C(3B)-Mn(1B)-C(14B)	67.93(8)	H(6C)-C(6A)-H(6D)	107.3
C(2B)-Mn(1B)-C(14B)	79.92(8)	C(4A)-C(14A)-C(13A)	119.71(19)
C(4B)-Mn(1B)-C(14B)	37.74(7)	C(4A)-C(14A)-C(5A)	119.40(17)
C(13B)-Mn(1B)-C(14B)	36.97(7)	C(13A)-C(14A)-C(5A)	120.88(18)
C(2B)-C(1B)-C(13B)	121.05(18)	C(4A)-C(14A)-Mn(1A)	70.33(11)
C(2B)-C(1B)-Mn(1B)	71.67(12)	C(13A)-C(14A)-Mn(1A)	72.34(12)
C(13B)-C(1B)-Mn(1B)	71.80(11)	C(5A)-C(14A)-Mn(1A)	130.66(13)
C(2B)-C(1B)-H(1B)	119.5	C(14A)-C(4A)-C(3A)	120.64(18)
C(13B)-C(1B)-H(1B)	119.5	C(14A)-C(4A)-Mn(1A)	72.27(11)
Mn(1B)-C(1B)-H(1B)	129.6	C(3A)-C(4A)-Mn(1A)	70.92(11)
O(1A)-C(17A)-Mn(1A)	176.22(16)	C(14A)-C(4A)-H(4A)	119.7
O(1B)-C(17B)-Mn(1B)	178.21(18)	C(3A)-C(4A)-H(4A)	119.7
O(3B)-C(19B)-Mn(1B)	177.41(18)	Mn(1A)-C(4A)-H(4A)	129.6
C(16A)-C(11A)-C(12A)	114.46(15)	C(10B)-C(9B)-C(8B)	119.51(18)
C(16A)-C(11A)-H(11C)	108.6	C(10B)-C(9B)-H(9B)	120.2
C(12A)-C(11A)-H(11C)	108.6	C(8B)-C(9B)-H(9B)	120.2
C(16A)-C(11A)-H(11D)	108.6	C(3B)-C(4B)-C(14B)	121.10(18)
C(12A)-C(11A)-H(11D)	108.6	C(3B)-C(4B)-Mn(1B)	70.92(12)
H(11C)-C(11A)-H(11D)	107.6	C(14B)-C(4B)-Mn(1B)	72.78(11)
O(2A)-C(18A)-Mn(1A)	178.67(18)	C(3B)-C(4B)-H(4B)	119.4
C(10A)-C(9A)-C(8A)	119.33(18)	C(14B)-C(4B)-H(4B)	119.4
C(10A)-C(9A)-H(9A)	120.3	Mn(1B)-C(4B)-H(4B)	129.3
C(8A)-C(9A)-H(9A)	120.3	C(16B)-C(11B)-C(12B)	116.99(16)
O(2B)-C(18B)-Mn(1B)	178.12(18)	C(16B)-C(11B)-H(11E)	108.0
C(3A)-C(2A)-C(1A)	119.9(2)	C(12B)-C(11B)-H(11E)	108.0
C(3A)-C(2A)-Mn(1A)	71.46(13)	C(16B)-C(11B)-H(11F)	108.0
C(1A)-C(2A)-Mn(1A)	71.71(11)	C(12B)-C(11B)-H(11F)	108.0
C(3A)-C(2A)-H(2A)	120.1	H(11E)-C(11B)-H(11F)	107.3
C(1A)-C(2A)-H(2A)	120.1	C(13A)-C(12A)-C(11A)	113.87(15)
Mn(1A)-C(2A)-H(2A)	129.1	C(13A)-C(12A)-H(12C)	108.8
C(7A)-C(15A)-C(16A)	119.01(17)	C(11A)-C(12A)-H(12C)	108.8

C(7A)-C(15A)-C(6A)	118.70(18)	C(13A)-C(12A)-H(12D)	108.8
C(16A)-C(15A)-C(6A)	122.24(16)	C(11A)-C(12A)-H(12D)	108.8
O(3A)-C(19A)-Mn(1A)	177.04(18)	H(12C)-C(12A)-H(12D)	107.7
C(13A)-C(1A)-C(2A)	121.30(18)	C(14B)-C(13B)-C(1B)	119.38(19)
C(13A)-C(1A)-Mn(1A)	72.99(11)	C(14B)-C(13B)-C(12B)	121.31(19)
C(2A)-C(1A)-Mn(1A)	70.44(11)	C(1B)-C(13B)-C(12B)	119.30(17)
C(13A)-C(1A)-H(1A)	119.4	C(14B)-C(13B)-Mn(1B)	72.82(12)
C(2A)-C(1A)-H(1A)	119.4	C(1B)-C(13B)-Mn(1B)	70.09(11)
Mn(1A)-C(1A)-H(1A)	129.8	C(12B)-C(13B)-Mn(1B)	128.89(13)
C(8A)-C(7A)-C(15A)	121.44(19)	C(13B)-C(14B)-C(4B)	118.71(19)
C(8A)-C(7A)-H(7A)	119.3	C(13B)-C(14B)-C(5B)	123.10(19)
C(15A)-C(7A)-H(7A)	119.3	C(4B)-C(14B)-C(5B)	118.16(17)
C(1B)-C(2B)-C(3B)	119.9(2)	C(13B)-C(14B)-Mn(1B)	70.21(12)
C(1B)-C(2B)-Mn(1B)	71.06(12)	C(4B)-C(14B)-Mn(1B)	69.48(11)
C(3B)-C(2B)-Mn(1B)	71.04(13)	C(5B)-C(14B)-Mn(1B)	130.76(13)
C(1B)-C(2B)-H(2B)	120.1	F(1A)-B(1A)-F(3A)	109.86(16)
C(3B)-C(2B)-H(2B)	120.1	F(1A)-B(1A)-F(4A)	109.99(18)
Mn(1B)-C(2B)-H(2B)	130.4	F(3A)-B(1A)-F(4A)	109.27(16)
C(7A)-C(8A)-C(9A)	119.79(18)	F(1A)-B(1A)-F(2A)	108.99(16)
C(7A)-C(8A)-H(8A)	120.1	F(3A)-B(1A)-F(2A)	109.41(17)
C(9A)-C(8A)-H(8A)	120.1	F(4A)-B(1A)-F(2A)	109.30(16)
C(9A)-C(10A)-C(16A)	121.36(19)	F(3B)-B(1B)-F(4B)	109.73(17)
C(9A)-C(10A)-H(10A)	119.3	F(3B)-B(1B)-F(2B)	109.23(17)
C(16A)-C(10A)-H(10A)	119.3	F(4B)-B(1B)-F(2B)	109.57(16)
C(13B)-C(12B)-C(11B)	111.82(16)	F(3B)-B(1B)-F(1B)	110.20(16)
C(13B)-C(12B)-H(12E)	109.3	F(4B)-B(1B)-F(1B)	108.20(16)
C(11B)-C(12B)-H(12E)	109.3	F(2B)-B(1B)-F(1B)	109.89(16)

Bond lengths (Å) for **41**

Cr(1A)-C(19A)	1.827(14)	C(3A)-C(4A)	1.382(17)
Cr(1A)-C(17A)	1.835(15)	C(3A)-H(3A)	0.9500
Cr(1A)-C(18A)	1.849(14)	C(4A)-C(14A)	1.431(17)
Cr(1A)-C(10A)	2.213(11)	C(4A)-H(4A)	0.9500
Cr(1A)-C(7A)	2.218(12)	C(14A)-C(5A)	1.490(16)
Cr(1A)-C(8A)	2.221(12)	C(5A)-C(6A)	1.342(15)
Cr(1A)-C(9A)	2.240(12)	C(5A)-H(5A)	0.9500
Cr(1A)-C(15A)	2.261(12)	C(6A)-H(6A)	0.9500
Cr(1A)-C(16A)	2.279(11)	C(18A)-O(2A)	1.166(12)
O(1A)-C(17A)	1.189(14)	C(8B)-C(7B)	1.392(15)
O(3A)-C(19A)	1.194(14)	C(8B)-C(9B)	1.459(15)
C(21)-C(20)	1.400(17)	C(8B)-Cr(1B)	2.258(11)

C(21)-C(22)	1.453(18)	C(8B)-H(8B)	0.9500
C(21)-H(21)	0.9500	C(7B)-C(15B)	1.450(15)
C(20)-C(28)	1.429(17)	C(7B)-Cr(1B)	2.210(13)
C(20)-H(20)	0.9500	C(7B)-H(7B)	0.9500
C(28)-C(29)	1.420(16)	C(15B)-C(16B)	1.408(15)
C(28)-C(27)	1.446(16)	C(15B)-C(6B)	1.469(15)
C(29)-C(23)	1.414(16)	C(15B)-Cr(1B)	2.298(12)
C(29)-C(24)	1.465(16)	C(6B)-C(5B)	1.340(16)
C(24)-C(25)	1.364(17)	C(6B)-H(6B)	0.9500
C(24)-H(24)	0.9500	C(5B)-C(14B)	1.522(16)
C(25)-C(26)	1.392(17)	C(5B)-H(5B)	0.9500
C(25)-H(25)	0.9500	C(14B)-C(4B)	1.405(17)
C(26)-C(27)	1.373(17)	C(14B)-C(13B)	1.409(16)
C(26)-H(26)	0.9500	C(4B)-C(3B)	1.400(17)
C(27)-H(27)	0.9500	C(4B)-H(4B)	0.9500
C(22)-C(23)	1.331(17)	C(3B)-C(2B)	1.379(17)
C(22)-H(22)	0.9500	C(3B)-H(3B)	0.9500
C(23)-H(23)	0.9500	C(2B)-C(1B)	1.423(17)
C(7A)-C(8A)	1.408(15)	C(2B)-H(2B)	0.9500
C(7A)-C(15A)	1.429(15)	C(1B)-C(13B)	1.403(16)
C(7A)-H(7A)	0.9500	C(1B)-H(1B)	0.9500
C(15A)-C(16A)	1.443(15)	C(13B)-C(12B)	1.486(16)
C(15A)-C(6A)	1.494(16)	C(12B)-C(11B)	1.367(15)
C(16A)-C(10A)	1.434(15)	C(12B)-H(12B)	0.9500
C(16A)-C(11A)	1.496(15)	C(11B)-C(16B)	1.486(15)
C(10A)-C(9A)	1.410(15)	C(11B)-H(11B)	0.9500
C(10A)-H(10A)	0.9500	C(16B)-C(10B)	1.456(15)
C(9A)-C(8A)	1.418(15)	C(16B)-Cr(1B)	2.267(12)
C(9A)-H(9A)	0.9500	C(10B)-C(9B)	1.399(15)
C(8A)-H(8A)	0.9500	C(10B)-Cr(1B)	2.223(12)
C(11A)-C(12A)	1.320(15)	C(10B)-H(10B)	0.9500
C(11A)-H(11A)	0.9500	C(9B)-Cr(1B)	2.224(12)
C(12A)-C(13A)	1.484(15)	C(9B)-H(9B)	0.9500
C(12A)-H(12A)	0.9500	O(2B)-C(18B)	1.186(14)
C(13A)-C(1A)	1.392(15)	C(18B)-Cr(1B)	1.812(15)
C(13A)-C(14A)	1.459(17)	Cr(1B)-C(19B)	1.807(17)
C(1A)-C(2A)	1.396(16)	Cr(1B)-C(17B)	1.844(17)
C(1A)-H(1A)	0.9500	C(17B)-O(1B)	1.159(16)
C(2A)-C(3A)	1.403(17)	C(19B)-O(3B)	1.143(17)
C(2A)-H(2A)	0.9500		

Bond angles (°) for **41**

C(19A)-Cr(1A)-C(17A)	86.4(6)	C(3A)-C(4A)-C(14A)	122.8(13)
C(19A)-Cr(1A)-C(18A)	89.0(6)	C(3A)-C(4A)-H(4A)	118.6
C(17A)-Cr(1A)-C(18A)	87.3(6)	C(14A)-C(4A)-H(4A)	118.6
C(19A)-Cr(1A)-C(10A)	116.8(5)	C(4A)-C(14A)-C(13A)	117.9(12)
C(17A)-Cr(1A)-C(10A)	156.8(5)	C(4A)-C(14A)-C(5A)	117.5(12)
C(18A)-Cr(1A)-C(10A)	93.0(5)	C(13A)-C(14A)-C(5A)	124.6(11)
C(19A)-Cr(1A)-C(7A)	116.5(6)	C(6A)-C(5A)-C(14A)	127.8(11)
C(17A)-Cr(1A)-C(7A)	91.5(5)	C(6A)-C(5A)-H(5A)	116.1
C(18A)-Cr(1A)-C(7A)	154.4(5)	C(14A)-C(5A)-H(5A)	116.1
C(10A)-Cr(1A)-C(7A)	78.2(4)	C(5A)-C(6A)-C(15A)	126.8(11)
C(19A)-Cr(1A)-C(8A)	89.6(5)	C(5A)-C(6A)-H(6A)	116.6
C(17A)-Cr(1A)-C(8A)	116.1(5)	C(15A)-C(6A)-H(6A)	116.6
C(18A)-Cr(1A)-C(8A)	156.3(5)	O(1A)-C(17A)-Cr(1A)	179.6(14)
C(10A)-Cr(1A)-C(8A)	66.7(4)	O(2A)-C(18A)-Cr(1A)	178.8(11)
C(7A)-Cr(1A)-C(8A)	37.0(4)	O(3A)-C(19A)-Cr(1A)	178.7(12)
C(19A)-Cr(1A)-C(9A)	90.0(5)	C(7B)-C(8B)-C(9B)	116.3(11)
C(17A)-Cr(1A)-C(9A)	153.1(5)	C(7B)-C(8B)-Cr(1B)	70.0(7)
C(18A)-Cr(1A)-C(9A)	119.3(5)	C(9B)-C(8B)-Cr(1B)	69.7(6)
C(10A)-Cr(1A)-C(9A)	36.9(4)	C(7B)-C(8B)-H(8B)	121.8
C(7A)-Cr(1A)-C(9A)	66.4(4)	C(9B)-C(8B)-H(8B)	121.8
C(8A)-Cr(1A)-C(9A)	37.1(4)	Cr(1B)-C(8B)-H(8B)	130.7
C(19A)-Cr(1A)-C(15A)	153.7(5)	C(8B)-C(7B)-C(15B)	124.8(11)
C(17A)-Cr(1A)-C(15A)	92.5(5)	C(8B)-C(7B)-Cr(1B)	73.7(7)
C(18A)-Cr(1A)-C(15A)	117.3(5)	C(15B)-C(7B)-Cr(1B)	74.5(7)
C(10A)-Cr(1A)-C(15A)	66.8(4)	C(8B)-C(7B)-H(7B)	117.6
C(7A)-Cr(1A)-C(15A)	37.2(4)	C(15B)-C(7B)-H(7B)	117.6
C(8A)-Cr(1A)-C(15A)	67.4(4)	Cr(1B)-C(7B)-H(7B)	126.2
C(9A)-Cr(1A)-C(15A)	79.2(4)	C(16B)-C(15B)-C(7B)	117.3(10)
C(19A)-Cr(1A)-C(16A)	153.9(5)	C(16B)-C(15B)-C(6B)	124.7(11)
C(17A)-Cr(1A)-C(16A)	119.6(5)	C(7B)-C(15B)-C(6B)	117.8(10)
C(18A)-Cr(1A)-C(16A)	91.9(5)	C(16B)-C(15B)-Cr(1B)	70.8(7)
C(10A)-Cr(1A)-C(16A)	37.2(4)	C(7B)-C(15B)-Cr(1B)	68.0(7)
C(7A)-Cr(1A)-C(16A)	66.6(4)	C(6B)-C(15B)-Cr(1B)	127.8(8)
C(8A)-Cr(1A)-C(16A)	79.4(4)	C(5B)-C(6B)-C(15B)	125.3(11)
C(9A)-Cr(1A)-C(16A)	67.0(4)	C(5B)-C(6B)-H(6B)	117.4
C(15A)-Cr(1A)-C(16A)	37.1(4)	C(15B)-C(6B)-H(6B)	117.4
C(20)-C(21)-C(22)	118.3(12)	C(6B)-C(5B)-C(14B)	127.6(11)
C(20)-C(21)-H(21)	120.9	C(6B)-C(5B)-H(5B)	116.2
C(22)-C(21)-H(21)	120.9	C(14B)-C(5B)-H(5B)	116.2
C(21)-C(20)-C(28)	120.6(13)	C(4B)-C(14B)-C(13B)	120.7(12)
C(21)-C(20)-H(20)	119.7	C(4B)-C(14B)-C(5B)	116.6(12)
C(28)-C(20)-H(20)	119.7	C(13B)-C(14B)-C(5B)	122.5(12)

C(29)-C(28)-C(20)	119.6(12)	C(3B)-C(4B)-C(14B)	119.4(12)
C(29)-C(28)-C(27)	119.4(12)	C(3B)-C(4B)-H(4B)	120.3
C(20)-C(28)-C(27)	121.0(13)	C(14B)-C(4B)-H(4B)	120.3
C(23)-C(29)-C(28)	117.7(12)	C(2B)-C(3B)-C(4B)	121.8(13)
C(23)-C(29)-C(24)	124.5(12)	C(2B)-C(3B)-H(3B)	119.1
C(28)-C(29)-C(24)	117.7(12)	C(4B)-C(3B)-H(3B)	119.1
C(25)-C(24)-C(29)	120.0(13)	C(3B)-C(2B)-C(1B)	118.0(13)
C(25)-C(24)-H(24)	120.0	C(3B)-C(2B)-H(2B)	121.0
C(29)-C(24)-H(24)	120.0	C(1B)-C(2B)-H(2B)	121.0
C(24)-C(25)-C(26)	122.2(14)	C(13B)-C(1B)-C(2B)	121.9(12)
C(24)-C(25)-H(25)	118.9	C(13B)-C(1B)-H(1B)	119.1
C(26)-C(25)-H(25)	118.9	C(2B)-C(1B)-H(1B)	119.1
C(27)-C(26)-C(25)	120.2(13)	C(1B)-C(13B)-C(14B)	118.0(12)
C(27)-C(26)-H(26)	119.9	C(1B)-C(13B)-C(12B)	118.1(11)
C(25)-C(26)-H(26)	119.9	C(14B)-C(13B)-C(12B)	123.8(12)
C(26)-C(27)-C(28)	120.5(12)	C(11B)-C(12B)-C(13B)	126.4(11)
C(26)-C(27)-H(27)	119.8	C(11B)-C(12B)-H(12B)	116.8
C(28)-C(27)-H(27)	119.8	C(13B)-C(12B)-H(12B)	116.8
C(23)-C(22)-C(21)	120.0(13)	C(12B)-C(11B)-C(16B)	127.3(11)
C(23)-C(22)-H(22)	120.0	C(12B)-C(11B)-H(11B)	116.4
C(21)-C(22)-H(22)	120.0	C(16B)-C(11B)-H(11B)	116.4
C(22)-C(23)-C(29)	123.7(13)	C(15B)-C(16B)-C(10B)	119.8(11)
C(22)-C(23)-H(23)	118.2	C(15B)-C(16B)-C(11B)	124.9(10)
C(29)-C(23)-H(23)	118.2	C(10B)-C(16B)-C(11B)	115.3(10)
C(8A)-C(7A)-C(15A)	122.4(12)	C(15B)-C(16B)-Cr(1B)	73.2(7)
C(8A)-C(7A)-Cr(1A)	71.6(7)	C(10B)-C(16B)-Cr(1B)	69.4(7)
C(15A)-C(7A)-Cr(1A)	73.1(7)	C(11B)-C(16B)-Cr(1B)	127.5(8)
C(8A)-C(7A)-H(7A)	118.8	C(9B)-C(10B)-C(16B)	120.7(11)
C(15A)-C(7A)-H(7A)	118.8	C(9B)-C(10B)-Cr(1B)	71.7(7)
Cr(1A)-C(7A)-H(7A)	129.0	C(16B)-C(10B)-Cr(1B)	72.7(7)
C(7A)-C(15A)-C(16A)	118.6(11)	C(9B)-C(10B)-H(10B)	119.6
C(7A)-C(15A)-C(6A)	117.6(11)	C(16B)-C(10B)-H(10B)	119.6
C(16A)-C(15A)-C(6A)	123.8(10)	Cr(1B)-C(10B)-H(10B)	128.1
C(7A)-C(15A)-Cr(1A)	69.8(7)	C(10B)-C(9B)-C(8B)	121.0(11)
C(16A)-C(15A)-Cr(1A)	72.2(7)	C(10B)-C(9B)-Cr(1B)	71.6(7)
C(6A)-C(15A)-Cr(1A)	127.9(8)	C(8B)-C(9B)-Cr(1B)	72.3(7)
C(10A)-C(16A)-C(15A)	117.8(11)	C(10B)-C(9B)-H(9B)	119.5
C(10A)-C(16A)-C(11A)	116.9(11)	C(8B)-C(9B)-H(9B)	119.5
C(15A)-C(16A)-C(11A)	125.2(10)	Cr(1B)-C(9B)-H(9B)	129.0
C(10A)-C(16A)-Cr(1A)	68.9(6)	O(2B)-C(18B)-Cr(1B)	174.6(16)
C(15A)-C(16A)-Cr(1A)	70.8(7)	C(19B)-Cr(1B)-C(18B)	82.4(9)
C(11A)-C(16A)-Cr(1A)	129.2(8)	C(19B)-Cr(1B)-C(17B)	86.1(9)
C(9A)-C(10A)-C(16A)	122.6(12)	C(18B)-Cr(1B)-C(17B)	87.4(7)
C(9A)-C(10A)-Cr(1A)	72.6(7)	C(19B)-Cr(1B)-C(7B)	126.5(8)

C(16A)-C(10A)-Cr(1A)	73.9(7)	C(18B)-Cr(1B)-C(7B)	150.5(7)
C(9A)-C(10A)-H(10A)	118.7	C(17B)-Cr(1B)-C(7B)	88.7(6)
C(16A)-C(10A)-H(10A)	118.7	C(19B)-Cr(1B)-C(10B)	113.1(7)
Cr(1A)-C(10A)-H(10A)	126.9	C(18B)-Cr(1B)-C(10B)	97.0(6)
C(10A)-C(9A)-C(8A)	119.1(11)	C(17B)-Cr(1B)-C(10B)	160.7(7)
C(10A)-C(9A)-Cr(1A)	70.5(7)	C(7B)-Cr(1B)-C(10B)	78.2(4)
C(8A)-C(9A)-Cr(1A)	70.7(7)	C(19B)-Cr(1B)-C(9B)	91.8(7)
C(10A)-C(9A)-H(9A)	120.5	C(18B)-Cr(1B)-C(9B)	125.2(6)
C(8A)-C(9A)-H(9A)	120.5	C(17B)-Cr(1B)-C(9B)	146.9(6)
Cr(1A)-C(9A)-H(9A)	130.9	C(7B)-Cr(1B)-C(9B)	66.2(4)
C(7A)-C(8A)-C(9A)	119.4(11)	C(10B)-Cr(1B)-C(9B)	36.7(4)
C(7A)-C(8A)-Cr(1A)	71.4(7)	C(19B)-Cr(1B)-C(8B)	97.4(7)
C(9A)-C(8A)-Cr(1A)	72.2(7)	C(18B)-Cr(1B)-C(8B)	163.1(6)
C(7A)-C(8A)-H(8A)	120.3	C(17B)-Cr(1B)-C(8B)	109.5(6)
C(9A)-C(8A)-H(8A)	120.3	C(7B)-Cr(1B)-C(8B)	36.3(4)
Cr(1A)-C(8A)-H(8A)	128.3	C(10B)-Cr(1B)-C(8B)	67.4(5)
C(12A)-C(11A)-C(16A)	126.1(11)	C(9B)-Cr(1B)-C(8B)	38.0(4)
C(12A)-C(11A)-H(11A)	116.9	C(19B)-Cr(1B)-C(16B)	149.7(8)
C(16A)-C(11A)-H(11A)	116.9	C(18B)-Cr(1B)-C(16B)	92.2(6)
C(11A)-C(12A)-C(13A)	129.7(11)	C(17B)-Cr(1B)-C(16B)	123.5(7)
C(11A)-C(12A)-H(12A)	115.2	C(7B)-Cr(1B)-C(16B)	66.1(4)
C(13A)-C(12A)-H(12A)	115.2	C(10B)-Cr(1B)-C(16B)	37.8(4)
C(1A)-C(13A)-C(14A)	117.3(12)	C(9B)-Cr(1B)-C(16B)	67.1(4)
C(1A)-C(13A)-C(12A)	119.0(12)	C(8B)-Cr(1B)-C(16B)	79.5(4)
C(14A)-C(13A)-C(12A)	123.6(11)	C(19B)-Cr(1B)-C(15B)	163.8(8)
C(13A)-C(1A)-C(2A)	123.1(13)	C(18B)-Cr(1B)-C(15B)	113.8(6)
C(13A)-C(1A)-H(1A)	118.5	C(17B)-Cr(1B)-C(15B)	94.5(7)
C(2A)-C(1A)-H(1A)	118.5	C(7B)-Cr(1B)-C(15B)	37.5(4)
C(1A)-C(2A)-C(3A)	120.3(13)	C(10B)-Cr(1B)-C(15B)	66.4(4)
C(1A)-C(2A)-H(2A)	119.9	C(9B)-Cr(1B)-C(15B)	78.8(4)
C(3A)-C(2A)-H(2A)	119.9	C(8B)-Cr(1B)-C(15B)	67.1(4)
C(4A)-C(3A)-C(2A)	118.6(13)	C(16B)-Cr(1B)-C(15B)	35.9(4)
C(4A)-C(3A)-H(3A)	120.7	O(1B)-C(17B)-Cr(1B)	175.4(17)
C(2A)-C(3A)-H(3A)	120.7	O(3B)-C(19B)-Cr(1B)	177.9(18)